To the Graduate Council:

I am submitting herewith a thesis written by Sherrell R. Greene entitled "The Design, Implementation and Cost-Benefit Analysis of a Dynamic Testing Program in the Experimental Breeder Reactor-II." I recommend that it be accepted in partial fulfillment of the requirements for the degree of Master of Science, with a major in Nuclear Engineering.

T. W. Kerlin, Major Professor

We have read this thesis
and recommend its acceptance:

Accepted for the Council:

Vice Chancellor
Graduate Studies and Research

THE DESIGN, IMPLEMENTATION AND COST-BENEFIT ANALYSIS OF A DYNAMIC TESTING PROGRAM IN THE EXPERIMENTAL BREEDER REACTOR-II

A Thesis

Presented for The

Master of Science

Degree

The University of Tennessee, Knoxville

Sherrell R. Greene

March, 1979

1390850

DEDICATION

This work is dedicated to my parents, Bill and Melba Greene.

ACKNOWLEDGEMENTS

I wish to express my appreciation to Dr. Pietro Pasqua and Dr. Tom Kerlin for making this work possible. Appreciation is also expressed to Dr. Marcia Katz and fellow students Mike Poore and Jim Freels for their many helpful comments and discussions during the preparation of this thesis. I am also grateful to Mrs. Gail Colson for her patience and effort in preparing the final manuscript.

I would like to acknowledge the help of my wife, Becky, who prepared most of the original figures for this thesis, and whose love and encouragement have been an inspiration to me throughout this project.

Finally, and most importantly, I would like to acknowledge the constant daily guidance of my Lord and Savior, Jesus Christ, who "was delivered over to death for our sins and raised to life for our justification."

ABSTRACT

Dynamic tests have been performed for many years in commercial pressurized and boiling water reactors. The purpose of this study was to evaluate the technological and economical feasibility of extending the current light water reactor testing procedures to both present and future liquid metal fast breeder reactors.

A 38 node linearized, lumped parameter, EBR-II system model was developed. This model was analyzed to obtain the predicted system time and frequency response for reactivity perturbations, intermediate heat exchanger secondary inlet sodium temperature perturbation frequency response, and various system nodal frequency response sensitivities. The results of this analysis indicate that the sodium pot residence time, IHX primary and secondary heat transfer coefficients and reactor core, inner reflector and out blanket heat transfer coefficient-area products can be identified through dynamic testing in EBR-II.

A dynamic test employing a pseudo random binary sequency (PRBS) was designed for EBR-II and a qualitative cost/benefit analysis performed to determine the economic feasibility of implementing a testing program. The results of this analysis indicate that the PRBS method offers a substantial economic advantage over both the rod drop and oscillator rod dynamic testing procedures.

TABLE OF CONTENTS

CHAPTER		PAGE
1.	INTRODUCTION	1
	Purpose of Study	1
	Benefits of Dynamic Testing	1
	Methods of Dynamic Testing	2
	Previous Dynamic Testing Experiments in Nuclear Reactors	4
	Scope and Intent of Thesis	5
2.	A DESCRIPTION OF THE EBR-II	8
	Introduction	8
	A General Description	8
	Reactor	12
	Active Core	16
	Axial Blankets	16
	Inner Radial Reflector	16
	Outer Blanket	21
	Control Assemblies	21
	Safety Assemblies	26
	Control Rod Drive Mechanisms	26
	Reactivity Control System	26
	Intermediate Heat Exchanger	31
3.	THEORETICAL MODEL	34
	Introduction	34
	Kinetics	37
	Active Core Model	43
	Reflector and Blanket Regions Model	49
	Piping, Plenums, and Pot Models	51
	Intermediate Heat Exchanger Model	56
4.	MATHEMATICAL METHODS FOR TIME, FREQUENCY RESPONSE, AND SENSITIVITY ANALYSIS	59
	Introduction	59
	System Time Response	59
	Prompt Jump Model	60
	System Frequency Response	64
	Frequency Response Sensitivity	65
	Stability Margin Assessment	66
5.	SIMULATION RESULTS	70
	Introduction	70
	Experimental and Theoretical Rod Drop Response	70
	Prompt Jump Models	72

CHAPTER PAGE

System Stability 91
System Time Response to Ten Cent Reactivity Step 94
System Frequency Response for Reactivity Perturbations 107
System Frequency Response for IHX Secondary Inlet Sodium Temperature Perturbations 110

6. PARAMETER IDENTIFICATION 113

Introduction 113
Uniqueness 114
Frequency Response Sensitivities 117
Separability of Parameters 119

7. TEST DESIGN 137

Introduction 137
Planning the Test 137
Role of Theoretical Analysis 138
Evaluation of Input Equipment Capabilities 138
Effects of Imperfect Test Signals on Test Planning 141
Evaluation of Sensor Capabilities 141
Selection of Test Signal 143
An Alternate Test Procedure 147

8. TEST IMPLEMENTATION 153

Introduction 153
Method of Inputting Test Signal 153
Data Acquisition and Analysis 154
Interpreting Results 161

9. COST/BENEFIT ANALYSIS 163

Introduction 163
Costs of Testing in EBR-II 163
Approximate Man Power Costs 165
Summary of EBR-II Test Costs 167
Costs of Rod Drop Testing 170
Costs of Oscillator Rod Testing 172
The Economic Impact of Dynamic Testing on LMFBR Design and Operation 172

10. CONCLUSIONS AND RECOMMENDATIONS FOR FUTURE WORK 175

Conclusions 175
Future Work and Study 176

LIST OF REFERENCES 178

CHAPTER PAGE

APPENDIXES 181

APPENDIX A 182

APPENDIX B 184

APPENDIX C 217

APPENDIX D 250

VITA 264

LIST OF TABLES

TABLE		PAGE
2.1.	Reactor Coolant System Data	11
2.2.	EBR-II Lattice Data for Run 25	15
2.3.	EBR-II Neutronics Parameters	17
2.4.	EBR-II Operational Parameters	19
2.5.	Intermediate Heat Exchanger Design and Performance Data	33
3.1.	Known EBR-II Feedback Mechanisms	40
3.2.	Feedback Mechanisms Employed in EBR-II Model	41
3.3.	Core Model Parameter Data	50
3.4.	Reflectors and Blanket Model Parameter Data	52
3.5.	Piping, Plenums, and Pot Model Parameter Data	55
3.6.	Heat Exchanger Model Parameter Data	58
4.1.	38 Node A Matrix Elements	61
5.1.	38 Node Model Eigenvalues	92
5.2.	37 Node Prompt Jump Model Eigenvalues	93
5.3.	38 Node Steady State Model Response to $\delta\tau$ = + 10 cents	112
6.1.	Parameters of Interest in Sensitivity Analysis	116
6.2.	EBR-II Identifiable Parameters	136
7.1.	Test Sensors	142
7.2.	Predicted Nodal Response to 1.6 Cent Test Signal	151
8.1.	Modulo-2 Addition Rules	156
8.2.	Test Signal Generation	157

TABLE PAGE

9.1. Test Hardware Costs 164

9.2. Hardware Installation Manpower Costs 166

9.3. Incremental Test Costs 168

9.4. EBR-II Testing Program Costs 169

LIST OF FIGURES

FIGURE		PAGE
1.1.	Dynamic Testing Critical Path Planning Chart	7
2.1.	EBR-II System Schematic	9
2.2.	EBR-II Primary Vessel and Internals	10
2.3.	The Experimental Breeder Reactor - II	13
2.4.	EBR-II Lattice Face	14
2.5.	Run 25 Reactor Loading	18
2.6.	EBR-II Driver Fuel Assembly	20
2.7.	EBR-II Reflector Assembly	22
2.8.	EBR-II Blanket Assembly	23
2.9.	Mark I Control Rod Assembly	24
2.10.	Mark I Control Rod Worth Curve	25
2.11.	Mark I Safety Rod Assembly	27
2.12.	Nominal Safety Rod Positions	28
2.13.	Control Rod Drive Mechanism	29
2.14.	EBR-II Intermediate Heat Exchanger	32
3.1.	EBR-II 38 Node Model Schematic	38
3.2.	EBR-II Fuel Pin Cross Section	44
3.3.	38 Node Model's Fuel Pin Representation	45
3.4.	Mann's Model	47
4.1.	EBR-II Feedback System	67
5.1.	Comparison of Experimental and Model Response to -5 Cents Rod Drop	71
5.2.	Response of the 37 Node Prompt Jump and 38 Node Models to $\delta\tau$ = -5 Cents	74
5.3.	Response of Reduced Prompt Jump and 38 Node Models to $\delta\tau$ = 5 Cents	83

FIGURE PAGE

5.4. Predicted EBR-II Stability Margin 95

5.5. EBR-II 38 Node Model Response to $\delta\rho = +10¢$ 96

5.6. Frequency Response of Reactor Power for Reactivity Perturbations 108

5.7. EBR-II Zero Power Frequency Response for Reactivity Perturbations 109

5.8. Frequency Response of Reactor Power for IHX Secondary Inlet Sodium Temperature Perturbations 111

6.1. Power Frequency Response Sensitivity 118

6.2. Upper Core Sodium Temperature Frequency Response Sensitivity 122

6.3. Sensitivity of the Upper Reflector Upper Sodium Temperature Frequency Response to the Upper Reflector Sodium Void Coefficient 124

6.4. Sensitivity of Upper Plenum Sodium Temperature Frequency Response to the Upper Reflector Sodium Void Coefficient 125

6.5. Sensitivity of Inner Reflector Upper Coolant Temperature Frequency Response to the Inner Reflector Sodium Void Coefficient 126

6.6. Sensitivity of the Upper Plenum Sodium Temperature Frequency Response to the Inner Reflector Sodium Void Coefficient 127

6.7. Sensitivity of the Inner Reflector Upper Sodium Temperature Frequency Response to UA_{inner} 128

6.8. Sensitivity of the Upper Plenum Sodium Temperature Frequency Response to UA_{inner} 129

6.9. Sensitivity of the Outer Blanket Upper Sodium Temperature Frequency Response to UA_{outer} 130

6.10. Sensitivity of the Upper Plenum Sodium Temperature Frequency Response to UA_{outer} 131

FIGURE PAGE

6.11. Sensitivity of the High Pressure Plenum Sodium Temperature Frequency Response to U_p and U_s 132

6.12. Sensitivity of the IHX Primary Outlet Sodium Temperature Frequency Response to U_p and U_s 133

6.13. Sensitivity of the IHX Secondary Outlet Sodium Temperature Frequency Response to U_p and U_s 134

7.1. Desired and Actual Input Test Signals 140

7.2. Bandwidth of 2047 Bit and Two 127 Bit Test Signals . . . 149

8.1. Seven Stage Modulo-2 Shift Register With Feedback From Stages One and Seven 155

8.2. EBR-II Input Test Signal 159

8.3. Data Acquisition Equipment Arrangement 160

B.1. Frequency Response of Reactor Power for Reactivity Perturbations 185

B.2. Frequency Response of Fuel Temperature for Reactivity Perturbations 186

B.3. Frequency Response of Fuel Pin Sodium Bond Temperature for Reactivity Perturbations 187

B.4. Frequency Response of Fuel Cladding Temperature for Reactivity Perturbations 188

B.5. Frequency Response of Lower Core Sodium Temperature for Reactivity Perturbations 189

B.6. Frequency Response of Upper Core Sodium Temperature for Reactivity Perturbations 190

B.7. Frequency Response of Low Pressure Inlet Sodium Temperature for Reactivity Perturbations 191

B.8. Frequency Response of Low Pressure Plenum Sodium Temperature for Reactivity Perturbations 192

B.9. Frequency Response of High Pressure Inlet Sodium Temperature for Reactivity Perturbations 193

FIGURE PAGE

B.10. Frequency Response of High Pressure Plenum Sodium Temperature for Reactivity Perturbations 194

B.11. Frequency Response of Lower Reflector Metal Temperature for Reactivity Perturbations 195

B.12. Frequency Response of Lower Reflector Lower Sodium Temperature for Reactivity Perturbations 196

B.13. Frequency Response of Lower Reflector Upper Sodium Temperature for Reactivity Perturbations 197

B.14. Frequency Response of Upper Reflector Metal Temperature for Reactivity Perturbations 198

B.15. Frequency Response of Upper Reflector Lower Sodium Temperature for Reactivity Perturbations 199

B.16. Frequency Response of Upper Reflector Upper Sodium Temperature for Reactivity Perturbations 200

B.17. Frequency Response of Inner Reflector Metal Temperature for Reactivity Perturbations 201

B.18. Frequency Response of Inner Reflector Lower Sodium Temperature for Reactivity Perturbations 202

B.19. Frequency Response of Inner Reflector Upper Sodium Temperature for Reactivity Perturbations 203

B.20. Frequency Response of Blanket Metal Temperature for Reactivity Perturbations 204

B.21. Frequency Response of Blanket Lower Sodium Temperature for Reactivity Perturbations 205

B.22. Frequency Response of Blanket Upper Sodium Temperature for Reactivity Perturbations 206

B.23. Frequency Response of Upper Plenum Sodium Temperature for Reactivity Perturbations 207

B.24. Frequency Response of Reactor Outlet Sodium Temperature for Reactivity Perturbations 208

B.25. Frequency Response of IHX Inlet Sodium Temperature for Reactivity Perturbations 209

B.26. Frequency Response of IHX Primary Node 1 Sodium Temperature for Reactivity Perturbations 210

FIGURE PAGE

B.27. Frequency Response of IHX Primary Node 2 Sodium Temperature for Reactivity Perturbations 211

B.28. Frequency Response of Pot Sodium Temperature for Reactivity Perturbations 212

B.29. Frequency Response of IHX Tube Bundle Temperature for Reactivity Perturbations 213

B.30. Frequency Response of IHX Secondary Node 1 Sodium Temperature for Reactivity Perturbations 214

B.31. Frequency Response of IHX Secondary Node 2 Sodium Temperature for Reactivity Perturbations 215

B.32. Frequency Response of IHX Secondary Outlet Sodium Temperature for Reactivity Perturbations 216

C.1. Frequency Response of Reactor Power for IHX Secondary Inlet Sodium Temperature Perturbations 218

C.2. Frequency Response of Fuel Temperature for IHX Secondary Inlet Sodium Temperature Perturbations 219

C.3. Frequency Response of Sodium Bond Temperature for IHX Secondary Inlet Sodium Temperature Perturbations . . 220

C.4. Frequency Response of Clad Temperature for IHX Secondary Inlet Sodium Temperature Perturbations 221

C.5. Frequency Response of Lower Core Sodium Temperature for IHX Secondary Inlet Sodium Temperature Perturbations 222

C.6. Frequency Response of Upper Core Sodium Temperature for IHX Secondary Inlet Sodium Temperature Perturbations 223

C.7. Frequency Response of Low Pressure Inlet Sodium Temperature for IHX Secondary Inlet Sodium Temperature Perturbations 224

C.8. Frequency Response of Low Pressure Plenum Sodium Temperature for IHX Secondary Inlet Sodium Temperature Perturbations 225

C.9. Frequency Response of High Pressure Inlet Sodium Temperature for IHX Secondary Inlet Sodium Temperature Perturbations 226

FIGURE PAGE

C.10. Frequency Response of High Pressure Plenum Sodium Temperature for IHX Secondary Inlet Sodium Temperature Perturbations 227

C.11. Frequency Response of Lower Reflector Metal Temperature for IHX Secondary Inlet Sodium Temperature Perturbations 228

C.12. Frequency Response of Lower Reflector Lower Sodium Temperature for IHX Secondary Inlet Sodium Temperature Perturbations 229

C.13. Frequency Response of Lower Reflector Upper Sodium Temperature for IHX Secondary Inlet Sodium Temperature Perturbations 230

C.14. Frequency Response of Upper Reflector Metal Temperature for IHX Secondary Inlet Sodium Temperature Perturbations 231

C.15. Frequency Response of Upper Reflector Lower Sodium Temperature for IHX Secondary Inlet Sodium Temperature Perturbations 232

C.16. Frequency Response of Upper Reflector Upper Sodium Temperature for IHX Secondary Inlet Sodium Temperature Perturbations 233

C.17. Frequency Response of Inner Reflector Metal Temperature for IHX Secondary Inlet Sodium Temperature Perturbations 234

C.18. Frequency Response of Inner Reflector Lower Sodium Temperature for IHX Secondary Inlet Sodium Temperature Perturbations 235

C.19. Frequency Response of Inner Reflector Upper Sodium Temperature for IHX Secondary Inlet Sodium Temperature Perturbations 236

C.20. Frequency Response of Blanket Metal Temperature for IHX Secondary Inlet Sodium Temperature Perturbations 237

C.21. Frequency Response of Blanket Lower Sodium Temperature for IHX Secondary Inlet Sodium Temperature Perturbations 238

C.22. Frequency Response of Blanket Upper Sodium Temperature for IHX Secondary Inlet Sodium Temperature Perturbations 239

FIGURE PAGE

C.23. Frequency Response of Upper Plenum Sodium Temperature for IHX Secondary Inlet Sodium Temperature Perturbations 240

C.24. Frequency Response of Reactor Outlet Sodium Temperature for IHX Secondary Inlet Sodium Temperature Perturbations 241

C.25. Frequency Response of IHX Primary Inlet Sodium Temperature for IHX Secondary Inlet Sodium Temperature Perturbations 242

C.26. Frequency Response of IHX Primary Node 1 Sodium Temperature for IHX Secondary Inlet Sodium Temperature Perturbations 243

C.27. Frequency Response of IHX Primary Node 2 Sodium Temperature for IHX Secondary Inlet Sodium Temperature Perturbations 244

C.28. Frequency Response of Primary Pot Sodium Temperature for IHX Secondary Inlet Sodium Temperature Perturbations 245

C.29. Frequency Response of IHX Tube Bundle Temperature for IHX Secondary Inlet Sodium Temperature Perturbations 246

C.30. Frequency Response of IHX Secondary Node 1 Temperature for IHX Secondary Inlet Sodium Temperature Perturbations 247

C.31. Frequency Response of IHX Secondary Node 2 Sodium Temperature for IHX Secondary Inlet Sodium Temperature Perturbations 248

C.32. Frequency Response of IHX Secondary Outlet Sodium Temperature for IHX Secondary Inlet Sodium Temperature Perturbations 249

D.1. Reactor Power Frequency Response Sensitivity to α_{steel} 251

D.2. Reactor Power Frequency Response Sensitivity to $\alpha_{core\ sodium}$ 252

D.3. Reactor Power Frequency Response Sensitivity to $\alpha_{lower\ ref.\ sodium}$ 253

D.4. Reactor Power Frequency Response Sensitivity to $\alpha_{upper\ ref.\ sodium}$ 254

FIGURE PAGE

D.5. Reactor Power Frequency Response Sensitivity to $\alpha_{\text{inner ref. sodium}}$ 255

D.6. Reactor Power Frequency Response Sensitivity to UA_{core} 256

D.7. Reactor Power Frequency Response Sensitivity to UA_{lower} 257

D.8. Reactor Power Frequency Response Sensitivity to $UA_{\text{inner reflector}}$ 258

D.9. Reactor Power Frequency Response Sensitivity to τ_{pot} 259

D.10. Reactor Power Frequency Response Sensitivity to U_p 260

D.11. Reactor Power Frequency Response Sensitivity to U_s 261

D.12. Pot Sodium Temperature Frequency Response Sensitivity to U_p 262

D.13. Pot Sodium Temperature Frequency Response Sensitivity to U_s 263

CHAPTER 1

INTRODUCTION

1.1 Purpose of Study

This work represents the second phase of a three part study aimed at evaluating the costs and benefits of dynamic testing in liquid metal fast breeder reactors (LMFBR's). One of the primary goals of the study is an assessment of the feasibility of extending current light water reactor testing procedures to LMFBR's. Previous work by Huynh[1] dealt with such applications for the Fast Flux Test Facility (FFTF). The subject of this thesis is the analysis of such procedures for use in the Experimental Breeder Reactor II (EBR-II), located at Idaho Falls, Idaho. The topics of this thesis are the synthesis of a mathematical model, frequency response sensitivity studies, planning of the tests, and evaluation of the costs and benefits of the tests.

1.2 Benefits of Dynamic Testing

Dynamic testing can yield four primary benefits for LMFBR applications:

1. Determination of stability margins. The most common index of stability is the phase margin. Determination of the phase margin of a system necessitates knowledge of the open loop system frequency response.
2. Identification of safety and performance related parameters. Certain basic system parameters such as reactivity feedback coefficients and heat transfer coefficients have a dominant role in determining the safety and performance characteristics

of the reactor. Methods exist today for determining these parameters by interpreting dynamic test data. The basic principle involved exploits the difference in the time constants of the processes occurring in the reactor during operation.

3. Plant surveillance and trouble shooting. Dynamic tests may be performed at regular intervals during plant operation to provide an indication of changing plant parameters. Any abrupt change in the system frequency response over a given frequency range might indicate a change in some basic system parameter whose associated time constant would correspond to the frequency range of interest.
4. Verification of theoretical models. Much money and effort has been devoted to the development of fairly sophisticated reactor modeling techniques. If the models are to be of any practical use, they must at least be capable of predicting the response of the system to small perturbations. Dynamic testing provides the data to which these theoretical model responses may be compared for evaluation of their ability to accurately predict the true system response.

1.3 Methods of Dynamic Testing

Dynamic tests need not require elaborate test procedures, if one is interested only in transient behavior during scram or plant behavior characteristics over a limited frequency range. Tests can be designed which use simple inputs such as a step or ramp. The familiar rod drop test has been used for many years to simulate a step reactivity insertion. The disadvantages of the step and ramp are that

they normally lack signal power over much of the frequency range for which information is desired. An additional problem associated with the step and ramp is that signals of sufficient magnitude to yield useful results often demand extreme perturbations in normal plant operational procedure.

Dynamic tests have also been designed which employ periodic input signals such as sine waves. Tests of this type are very attractive from the data analysis standpoint, since the frequency response of a system is defined as the response of the system to a sinusodial input. The attractiveness of this procedure is overshadowed by the mechanical problems associated with the production of the test signal. The production of a sinusodial input with standard plant hardware is an extremely difficult process, and the associated test times are very long.[2]

Binary periodic test signals[3] were developed as an efficient substitute for sinusodial signals. This method employs an input consisting of a sequence of small bilevel perturbations. The input sequence may be a pseudo-random binary sequence[3], (PRBS), or a multi-frequency binary sequence[3], (MFBS). The important advantages of these signals are:

1. The signals will require very small perturbations in normal plant operating procedure.
2. The signals are normally easily implemented with standard plant hardware.
3. The system frequency response can be measured over a broad frequency range since the signal contains significant power over broad frequency ranges.

4. The time required to implement the test is significantly less than that which would be required by classical test procedures.

1.4 Previous Dynamic Testing Experiments in Nuclear Reactors

Dynamic tests have been performed in many reactors using binary input signals such as the PRBS and MFBS as well as sinusodial signals.[4] Reactors which have been tested in this way are:

Research Reactors

High Flux Isotope Reactor (HFIR)

Molten Salt Reactor (MSR)

Rocket Vehicle Application (NERVA)

Sodium Reactor Experiment

Pressurized Water Reactors

Saxton Plant (20 MWt Experimental)

Yankee (600 MWt)

Trino (825 MWt)

H. B. Robinson Unit 2 (2200 MWt)

Oconee I (2568 MWt)

Millstone 2

Boiling Water Reactors

Big Rock Point

Garigliano (Italy)

Grundermmingen (Germany)

Heavy Water Reactors

Halden Heavy Water Boiling Reactor (20 MWt)

Agesta (55 MWt)

Fast Reactors

Enrico Fermi (200 MWt)

EBR I

SEFOR (Germany)

1.5 Scope and Intent of Thesis

The subject of this thesis is the design, implementation and cost/benefit analysis of a dynamic testing program in EBR-II. After the goals of the testing program are defined, the test design process can begin. An integral part of the test design process is the formulation and analysis of a system model. This model is necessary in order to estimate approximate system responses to various system perturbations. These system responses are in turn needed to estimate the identifiability of the various system parameters of interest.

This thesis deals first with a description of the overall EBR-II system. A rather detailed description of each major EBR-II primary system component is given. Chapter 3 deals with the formulation of a system model based on the conservation laws of neutrons, mass, and energy. It is a linearized, lumped parameter state variable model, which includes representations of the reactor core and plenums, primary loop piping, and the intermediate heat exchanger. The various analysis techniques which were used with the model are described in Chapter 4. Chapter 5 deals with results of the analysis performed on the model. The predicted model time response for a -5 and a +10 cent reactivity perturbation and frequency response to reactivity and IHX, (intermediate heat exchanger), secondary inlet sodium temperature

perturbations are discussed. Chapter 6 deals with the parameter identifiability analysis and discusses which parameters may be identified from test data. Chapter 7 discusses the basis for test signal design and goes through the test design process. Successful test signal design requires knowledge of the model analysis results, as well as a familiarity with the reactor control system and sensor capabilities.

Finally, the cost/benefit ratio of dynamic testing in EBR-II in particular and LMFBR's in general is examined. Figure 1.1 is a general critical path planning chart for the dynamic testing process.

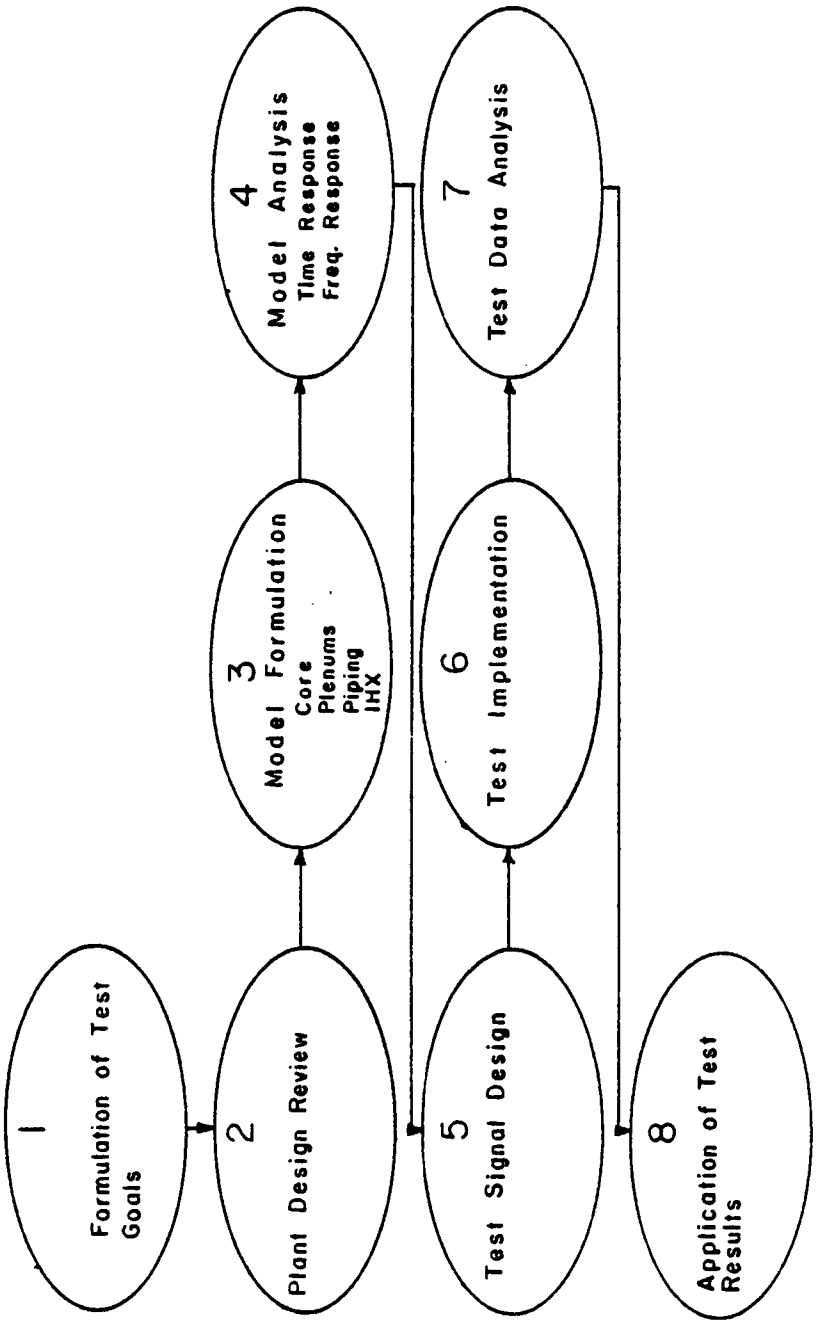


Figure 1.1 Dynamic Testing Critical Path Planning Chart.

CHAPTER 2

A DESCRIPTION OF THE EBR-II

2.1 Introduction

This chapter presents a brief description of the EBR-II and a tabulation of pertinent design data employed in the mathematical model. A complete system description can be found in Reference 5.

2.2 A General Description

The Experimental Breeder Reactor II is a pool type, sodium cooled, unmoderated fast reactor. The reactor is fueled with a uranium-molybdenum-ruthenium alloy known as "Fissium." Driver fuel enrichment varies from approximately 52 to 64 atom percent. The reactor provides a maximum neutron flux of 3.55×10^{15} n/cm^2 sec and a maximum power level of 62.5 MWt. A schematic of the EBR-II system is shown in Figure 2.1.

The reactor lattice, primary coolant pumps, and intermediate heat exchanger are all submerged in the primary tank or "pot" (Fig. 2.2). The pot contains approximately 86000 gallons of sodium at a nominal temperature of 700°F. The primary system uses two sodium supply loops, each containing a single stage centrifugal pump which provides 4700 gal/min. of sodium (at 50 psig) at full power. Pertinent primary coolant system flow data is given in Table 2.1. The intermediate heat exchanger is a shell and tube type, with the primary sodium flowing on the shell side. Heat from the secondary sodium is transferred to the steam supply loop via an arrangement of eight parallel connected natural circulation evaporators and two parallel once

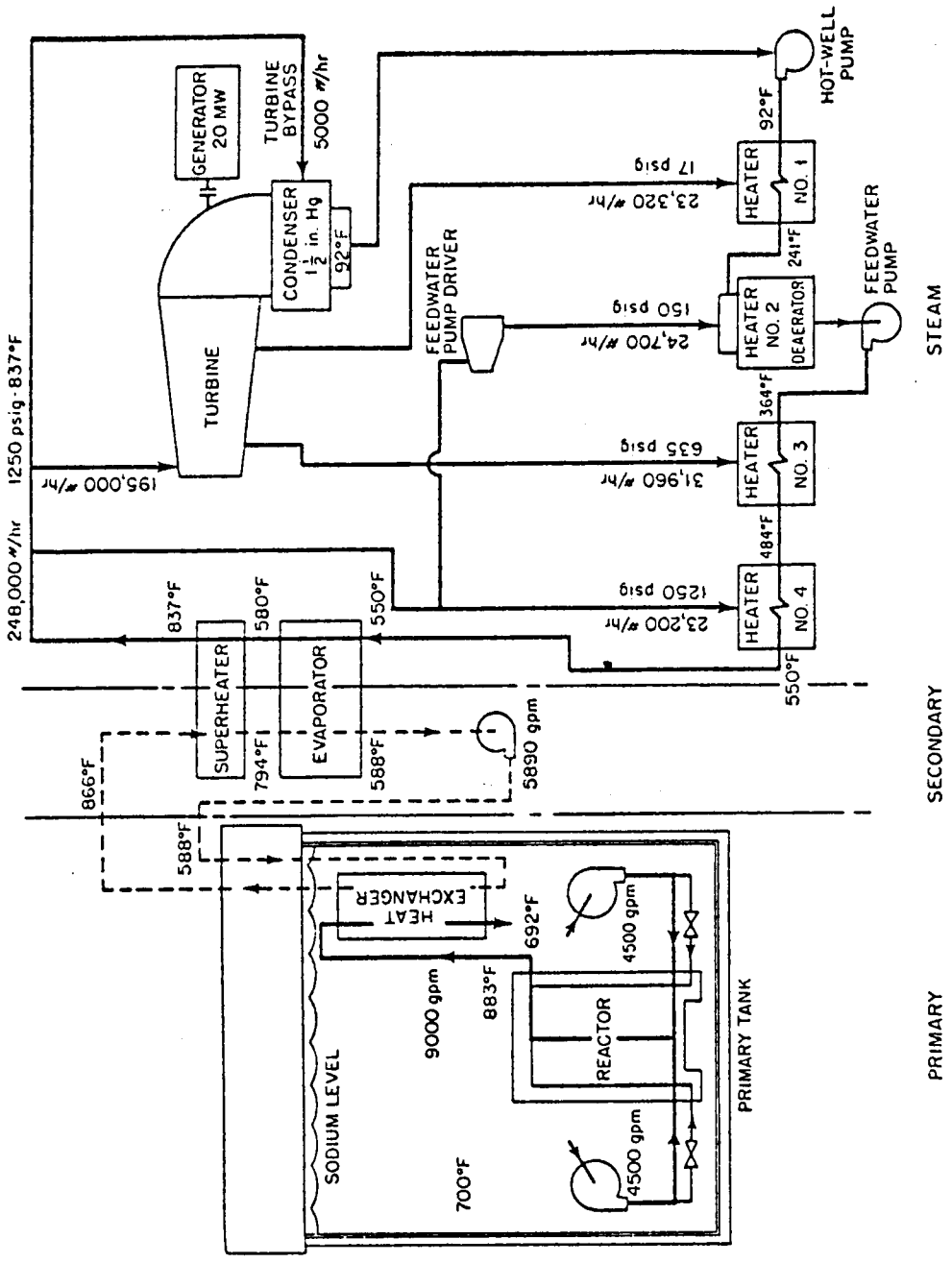


Figure 2.1 EBR-II System Schematic.

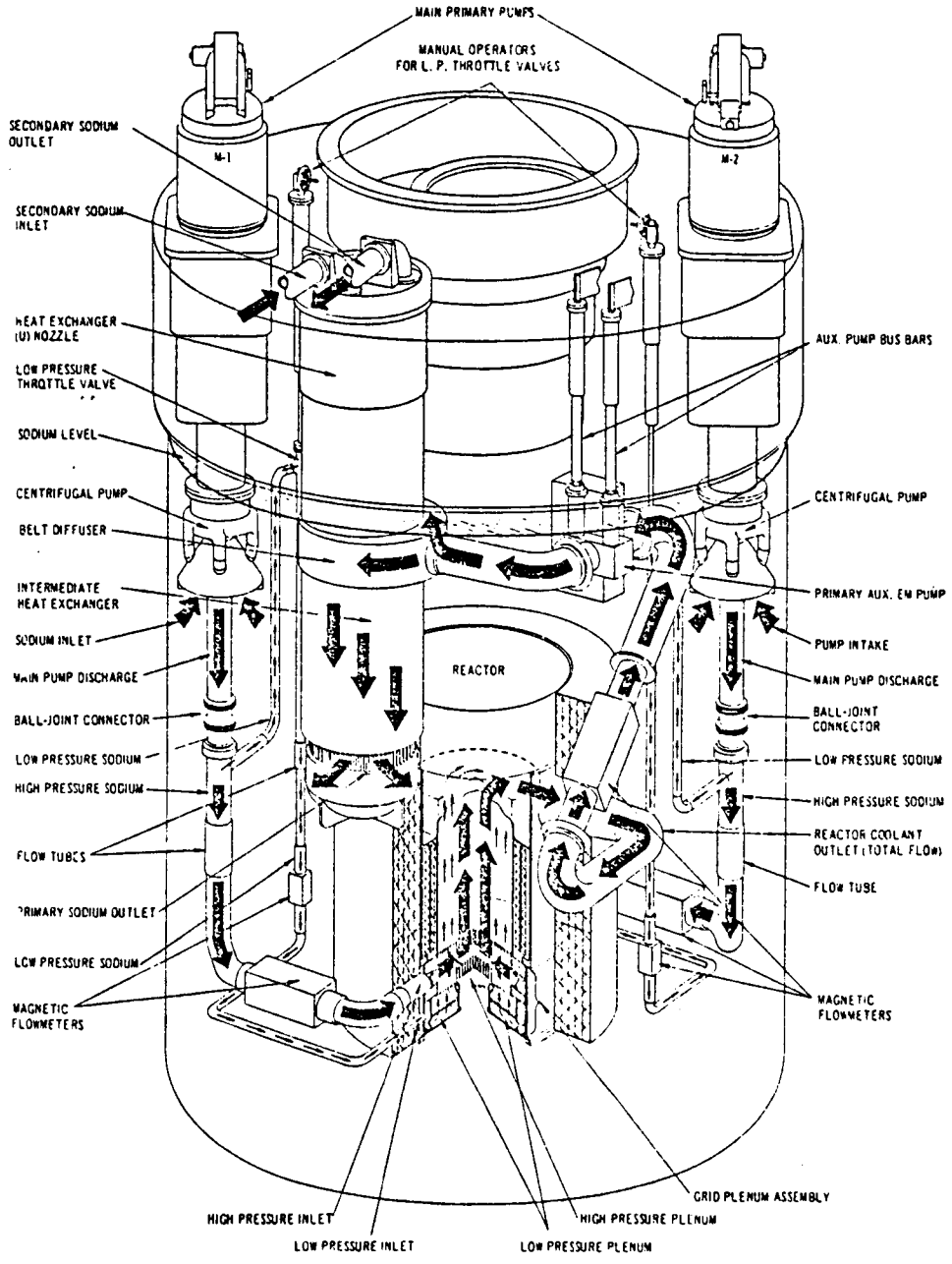


Figure 2.2 EBR-II Primary Vessel and Internals.

TABLE 2.1

REACTOR COOLANT SYSTEM DATA

Sodium Flow Into Reactor Plenums	9305 GPM
Sodium Flow Through Core	6145 GPM
Sodium Flow Through Inner Reflector	1475 GPM
Sodium Flow Through Outer Blanket	1260 GPM
Sodium Flow Into Heat Exchanger	8865 GPM

through superheaters. This arrangement produces superheated (582°F) steam which drives a General Electric type AT B-2 generator, producing approximately 19 MWe. Turbine exhaust steam flows into a shell and tube type condenser. The condenser cooling water absorbs the heat from the steam and conveys it to either of two forced draft, counter flow cooling towers, which dumps the heat to the atmosphere. The condensed steam ultimately returns to the evaporators, thus completing the steam cycle.

The EBR-II was designed and is operated by the Argonne National Laboratory. The reactor has been operating since 1964 as an experimental, base loaded LMFBR power station. In the early 1970's, the primary operating emphasis of the EBR-II was shifted from experimental power generation to experimental irradiation of LMFBR fuels and structural materials. The reactor is located on the National Reactor Test Site near Idaho Falls, Idaho.

2.3 Reactor

The reactor lattice accomodates 637 hexagonal shaped subassemblies, each 2.29 in. across flats and 91 53/64 in. long (Fig. 2.3). The subassemblies are spaced on a triangular pitch of 2.320 in. center to center (Fig. 2.4). The lattice is composed of four distinct regions: 1) active core, 2) lower and upper axial reflectors, 3) inner radial reflector, 4) outer blanket.

Due to its experimental nature, several different core loadings have been used in the EBR-II. The core loading employed in run 25 (6/29/67 to 7/20/67) was chosen as the standard core for analysis purposes. Pertinent lattice data for run 25 are given in Table 2.2. The

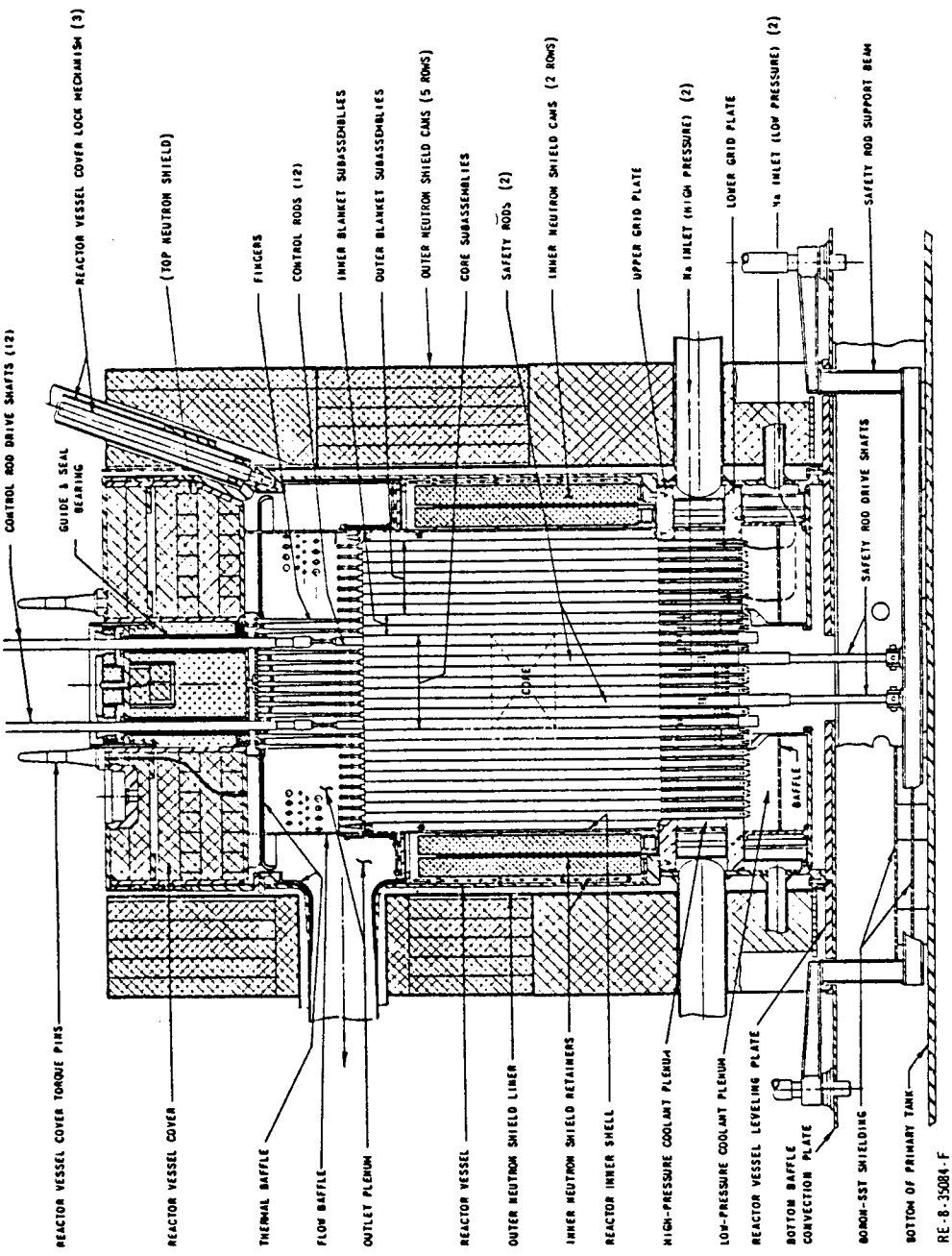


Figure 2.3 The Experimental Breeder Reactor-II.

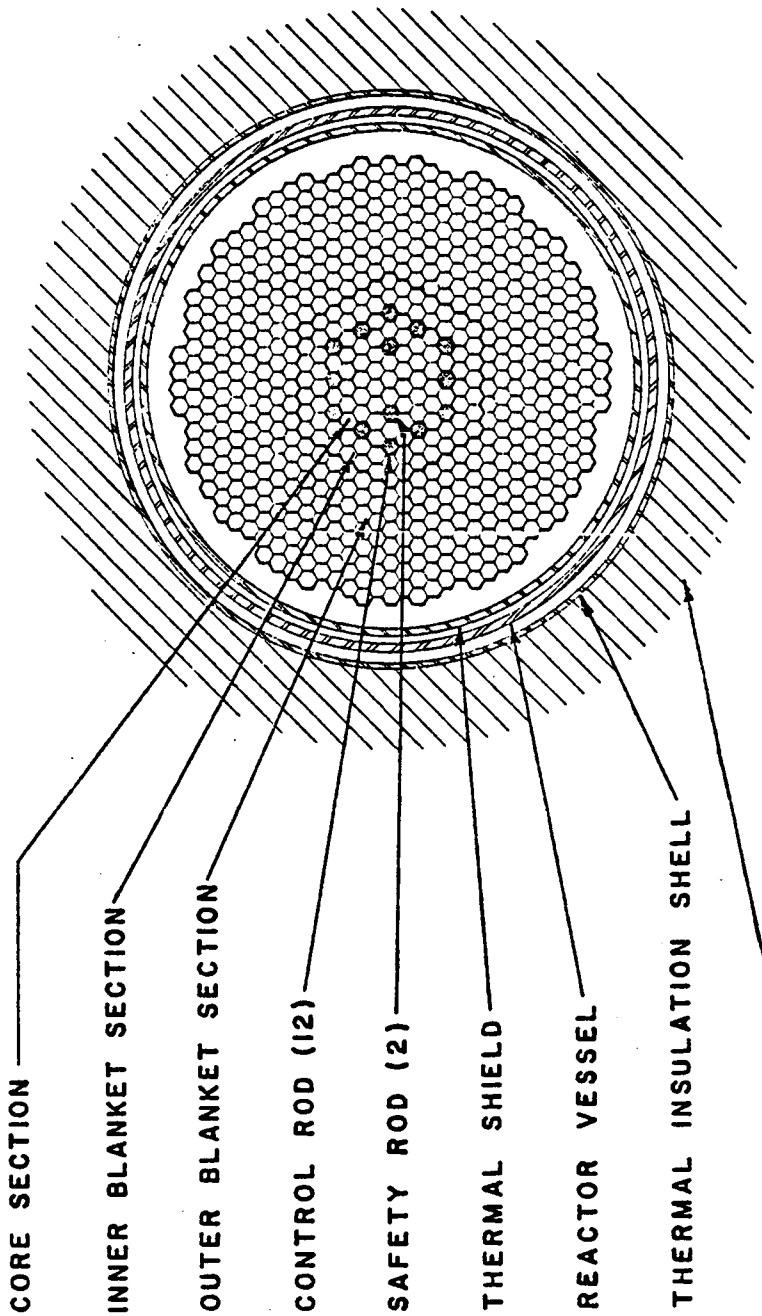


Figure 2.4 EBR-II Lattice Face.

TABLE 2.2

EBR-II LATTICE DATA FOR RUN 25

Number of Assemblies	637
Number of Control Rods	12
Number of Safety Rods	2
Lattice Pitch	2.320 in. (Triangular)
Assembly Shape	Hexagonal
Dimension Across Flats	2.290 in.
Height	91.83 in.
Active Core	
Height	13.5 in.
Volume	72.8 liters
U-235 Content	206.34 Kg.
U-238 Content	183.37 Kg.
Pu-239 Content	2.86 Kg.
Axial Reflector Material	304 Stainless
Axial Reflector Mass	460 lbm.
Inner Reflector Material	304 Stainless
Inner Reflector Mass	3150 lbm.
Blanket Material	Depleted U
Blanket Mass	50200 lbm.

choice of the run 25 loading as the standard core was dictated by two primary considerations: precise data for run 25 reactivity feedback coefficients were readily available, and the composition of the axial reflector regions has remained relatively unchanged through the present time. EBR-II neutronics data are given in Table 2.3. A schematic of the run 25 loading is shown in Fig. 2.5. Typical reactor operational temperatures are listed in Table 2.4.

2.4 Active Core

The active core contained 62 type Mark 1A SRB (Fig. 2.6) fuel bearing assemblies, along with 26 experimental and control assemblies. The height of the active core in this run was 13.5 inches, with a core volume of 72.79 liters. The total amount of uranium (U-235 & U-238) in the core was 389 Kg.

2.5 Axial Blankets

The original EBR-II core loadings included a depleted uranium blanket. After plutonium breeding was proven feasible, the uranium blanket elements were replaced with stainless steel rods in order to speed fabrication and reduce loading cost. The axial reflector elements in the SRB (Stainless Rod Blanket) type assemblies in run 25 were each composed of type 304-L stainless steel rods. The height of each reflector region was 18 inches (Fig. 2.6). The total amount of stainless steel in each blanket region was approximately 460 lbm.

2.6 Inner Radial Reflector

The original EBR-II loadings contained depleted uranium assemblies in rows 7 and 8. Prior to run 25, 76 stainless steel

TABLE 2.3

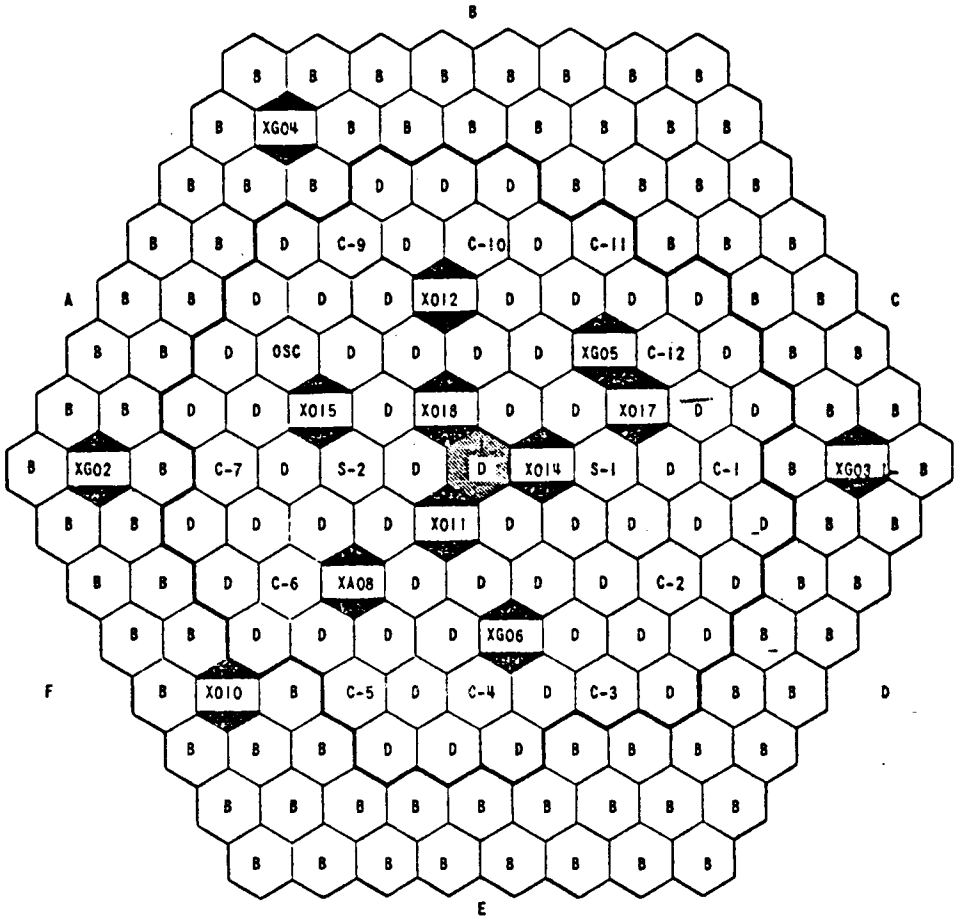
EBR-II NEUTRONICS PARAMETERS*

Group	β_i	$\lambda_i (Sec)^{-1}$
1	0.000252	0.0127
2	0.001480	0.0317
3	0.001344	0.1150
4	0.002941	0.3110
5	0.001024	1.4000
6	0.000237	3.7800

$\beta_{Total} = 0.007278$

$\ell_p = 1.55 \times 10^{-7}$ sec.

*From ANL 7664



KEY

D - Driver fuel (Fissium)

C - Control

X - Experimental

B - Inner Reflector (stainless steel)

Figure 2.5 Run 25 Reactor Loading.

TABLE 2.4

EBR-II OPERATIONAL PARAMETERS

Reactor Power	45MWt
Reactor Inlet Sodium Temp.	700°F
Reactor Outlet Sodium Temp.	831°F
Lower Reflector Temp.	700°F
Core Fuel Temp.	912°F
Clad Temp.	823°F
Sodium Temp.	785°F
Upper Reflector Temp.	870°F
Inner Reflector Temp.	763°F
Outer Reflector Temp.	724°F

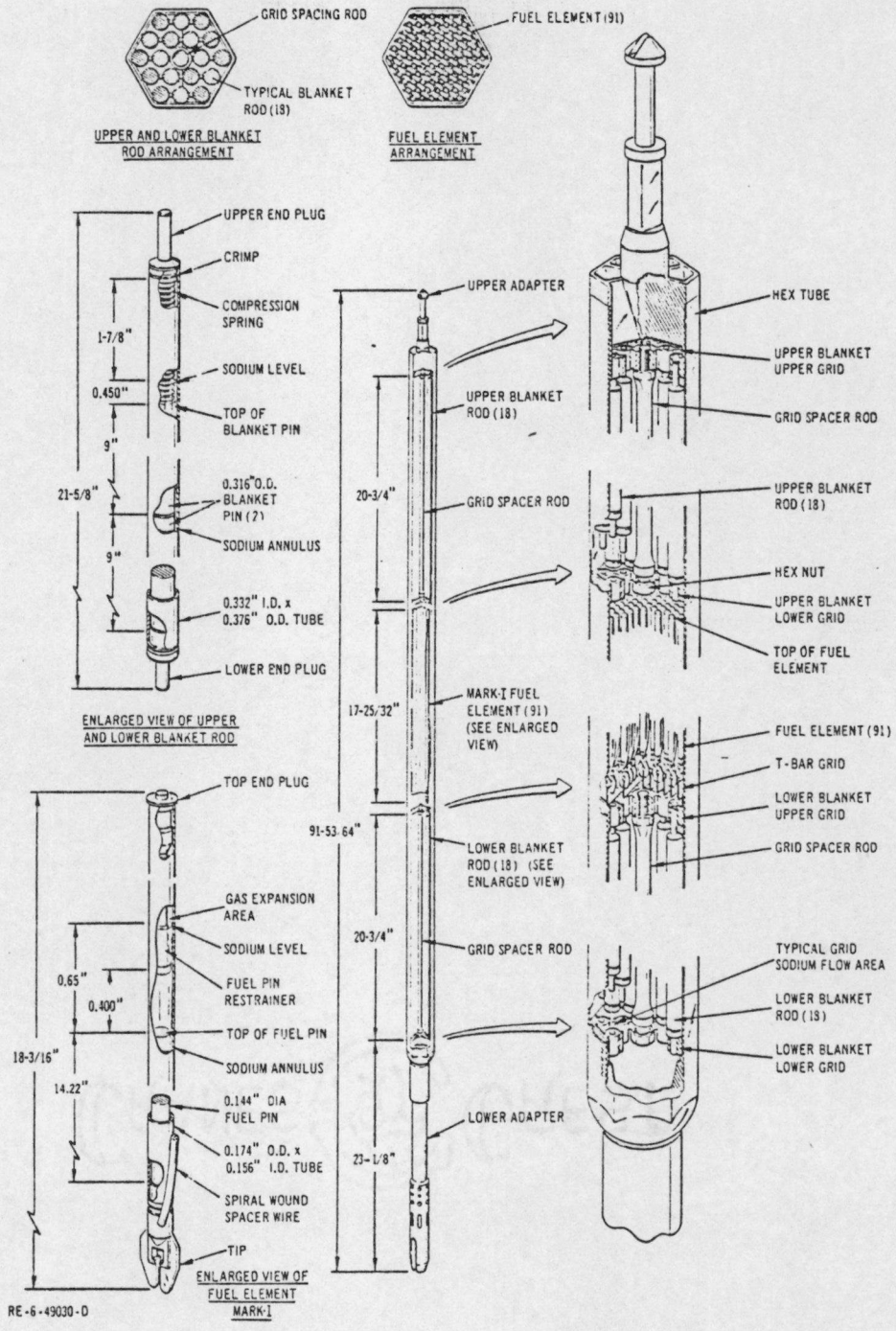


Figure 2.6 EBR-II Driver Fuel Assembly.

subassemblies were inserted in these positions. A reflector assembly typical of the type used in run 25 is shown in Fig. 2.7. The assembly consists of a cluster of 12 stainless steel rods. Each rod is 16 7/16 in. long and 0.493 in. in diameter. Total inner reflector stainless steel loading for this run was approximately 3150 lbm.

2.7 Outer Blanket

The remainder of the lattice in run 25 was composed of depleted uranium subassemblies. Fig. 2.8 is a schematic representation of one of these assemblies. The fillers for the outer blanket subassemblies are 61 7/16 in. long, 0.146 in. wide, and approximately 0.108 in. thick. Total mass of depleted uranium in the outer blanket was approximately 50200 lbm.

2.8 Control Assemblies

The EBR-II is designed to accomodate 12 control assemblies located in row 5 of the lattice. The control rods move vertically inside of hexagonal tubes of "guide thimbles". The control rods utilize the same type of fuel elements as the fuel assemblies except that each assembly contains 61 fuel pins, rather than 91. A typical Mark I control rod assembly is shown in Figure 2.9. The reactivity worth of each control rod varies sightly with each reactor run. The reactivity worth of a rod as a function of distance of insertion of the rod into the core is shown in Figure 2.10. Although the total worth of a control rod may vary from run to run, the shape of the curve should remain unchanged. It is apparent from Figure 2.10, that the maximum reactivity insertion rate for a single control rod banked at the midcore position is approximately 6.56 ¢/inch.

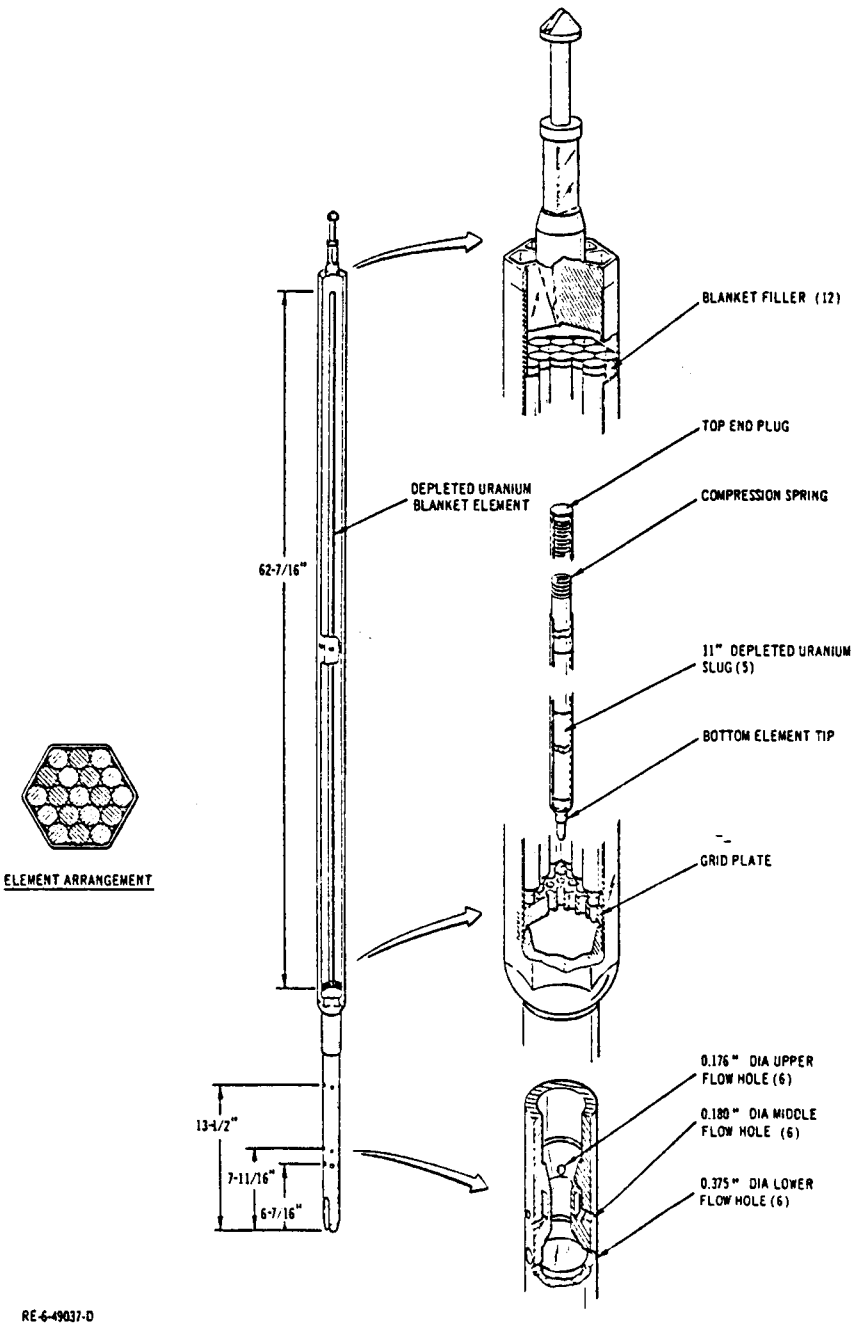


Figure 2.7 EBR-II Reflector Assembly.

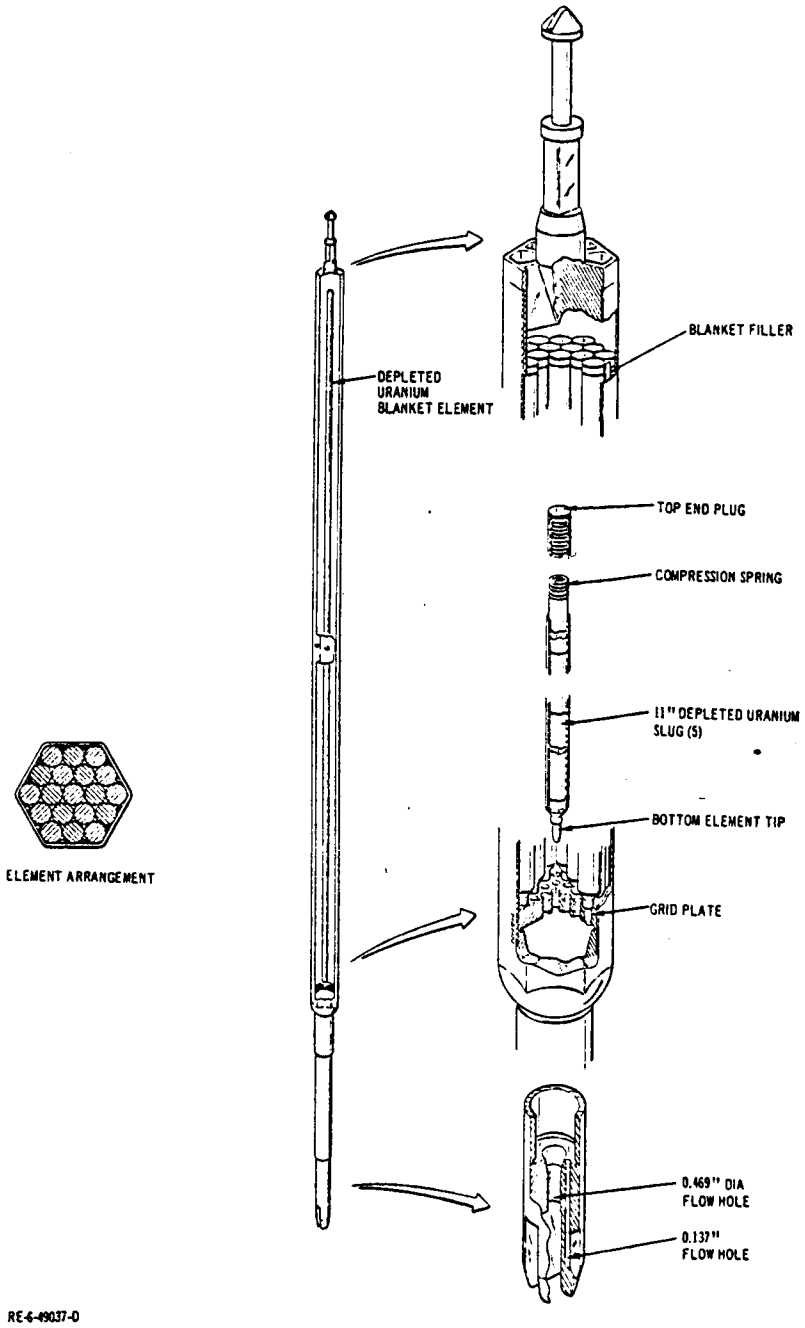


Figure 2.8 EBR-II Blanket Assembly.

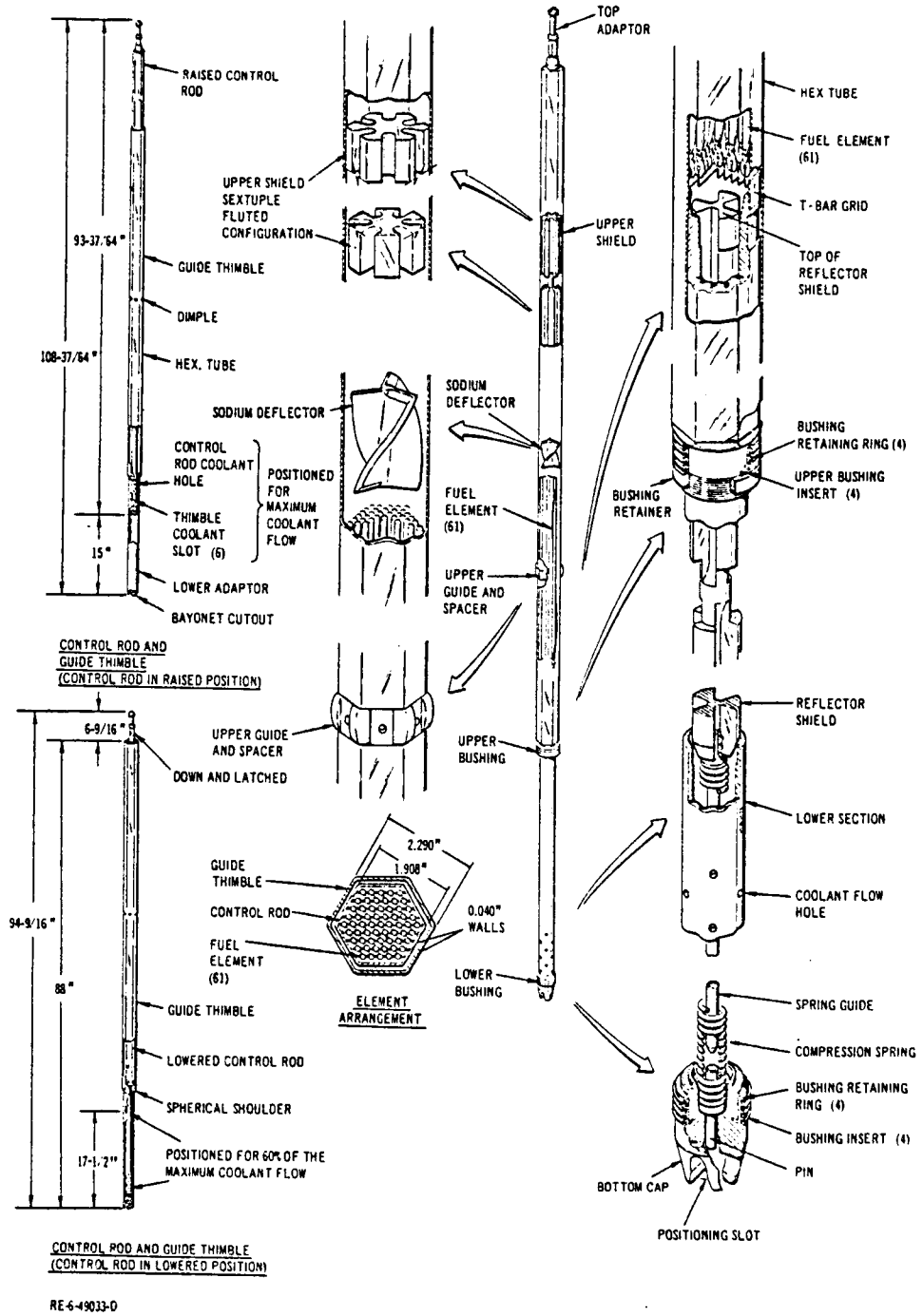


Figure 2.9 Mark I Control Rod Assembly.

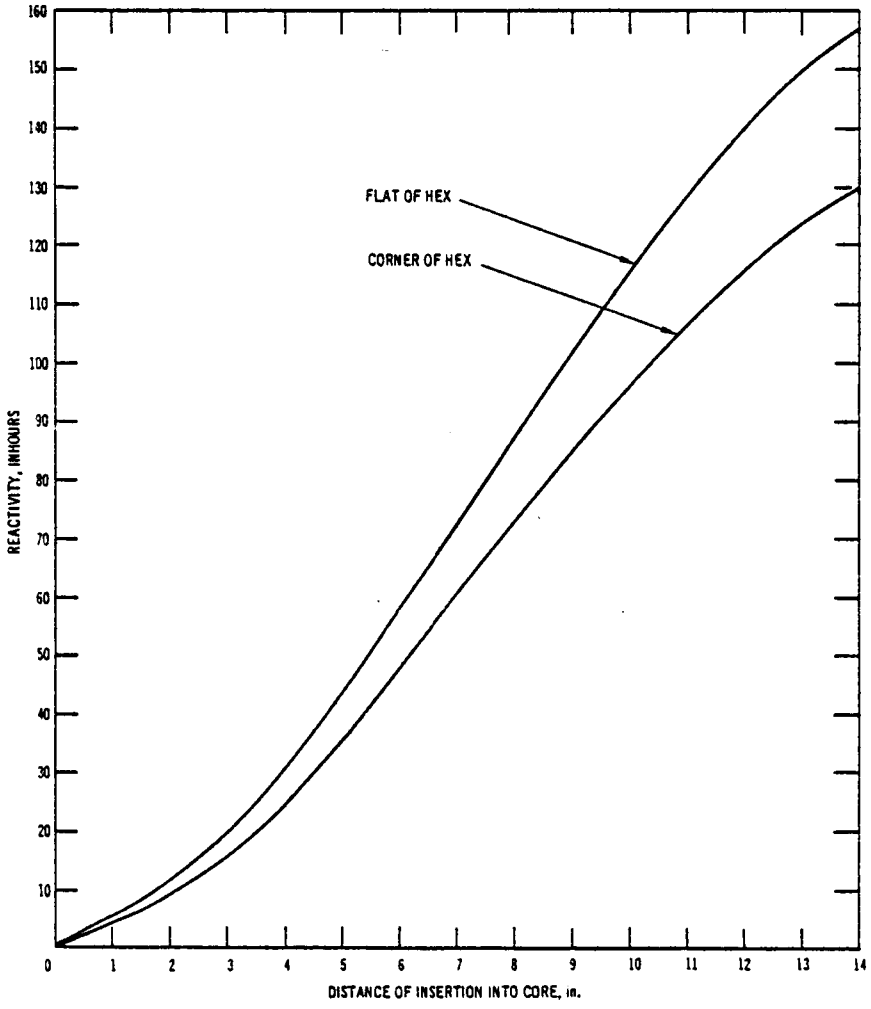


Figure 2.10 Mark I Control Rod Worth Curve.

2.9 Safety Assemblies

The EBR-II contains two safety assemblies, located in row 3 of the lattice. The rod consists of a modified fuel assembly with the core section composed of 61, type Mark IA fuel pins. The safety rods are positioned with the fuel in the core region, or lowered 14 inches to remove the fuel from the core. A typical Mark I safety assembly is shown in Figure 2.11. Typical safety rod positions are shown in Figure 2.12.

2.10 Control Rod Drive Mechanisms

The control rod drive mechanisms (CRDM), in the EBR-II are of the rack and pinion type. The drives can raise or lower each control rod individually at a speed of 4.76 inches per minute over the entire 14 inches of travel. From Section 2.8, with a maximum rod worth of 6.56 ¢/inch, the maximum reactivity insertion rate for one rod is approximately 0.52 ¢/second. Figure 2.13 shows the control rod drive mechanism. Each control rod drive mechanism consists of a control rod drive, gripper operating mechanism, scram mechanism, a guide tube and a main shaft which contains the drive shaft assembly, the gripper shaft assembly, and the sensing shaft assembly. The drive shaft assembly is used to control the vertical position of the control rod in the reactor core. Operation of the drive shaft assembly is controlled by a control rod drive mechanism for normal operation or by the scram mechanism for accelerated downward travel.

2.11 Reactivity Control System

The EBR-II is controlled by movement of the driver fuel bearing control and safety rod assemblies. Reactor control both for steady

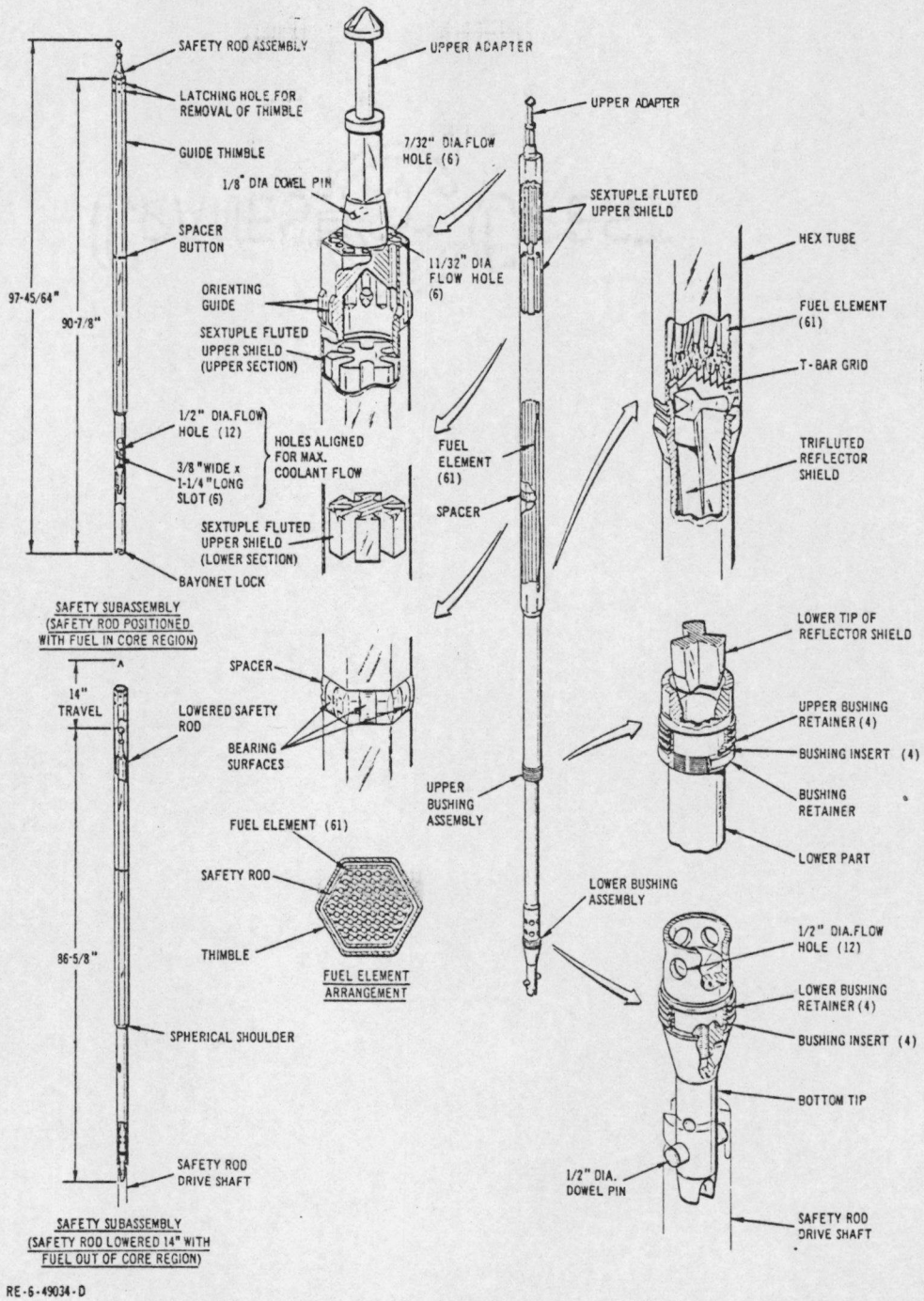


Figure 2.11 Mark I Safety Rod Assembly.

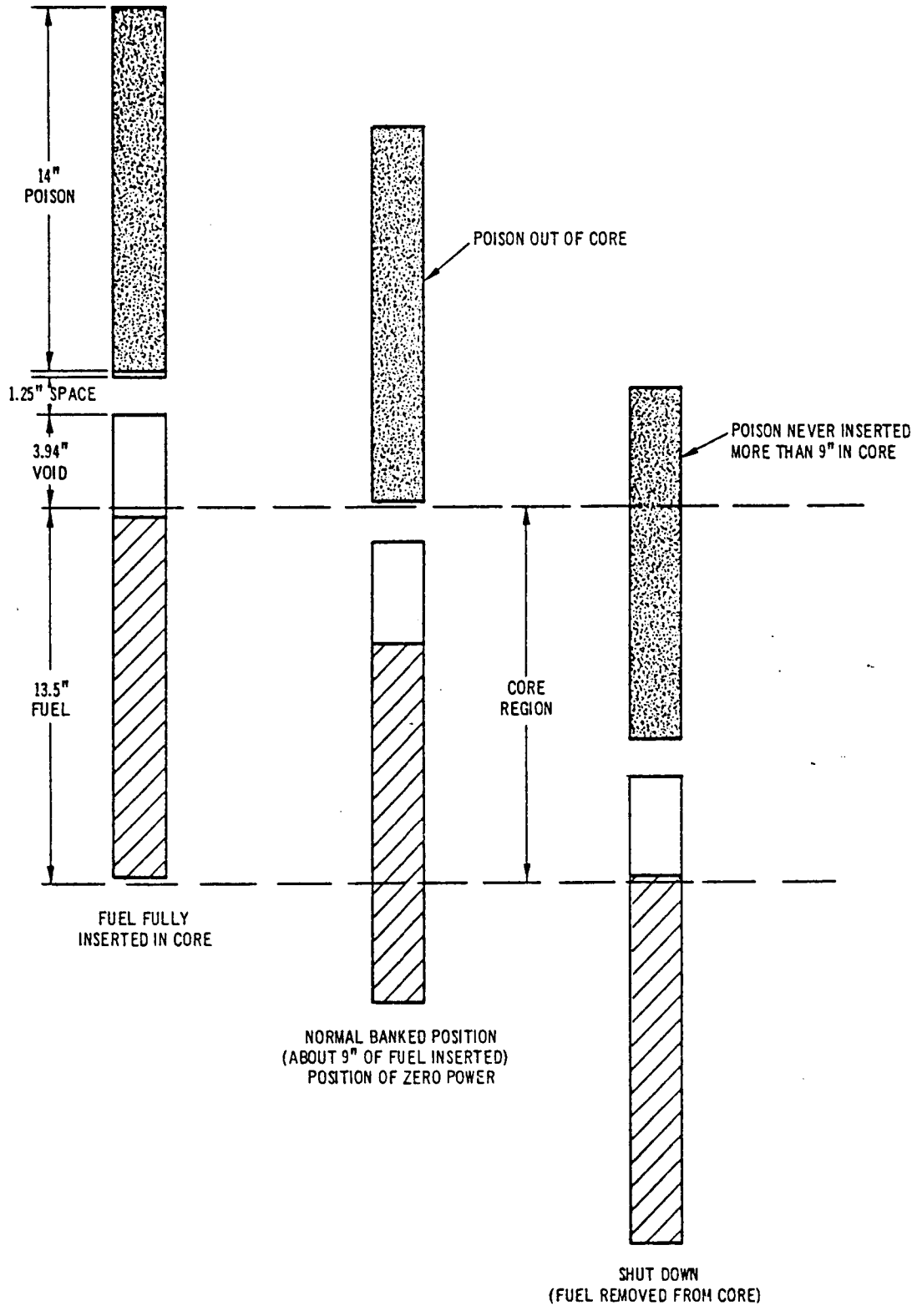


Figure 2.12 Nominal Safety Rod Positions.

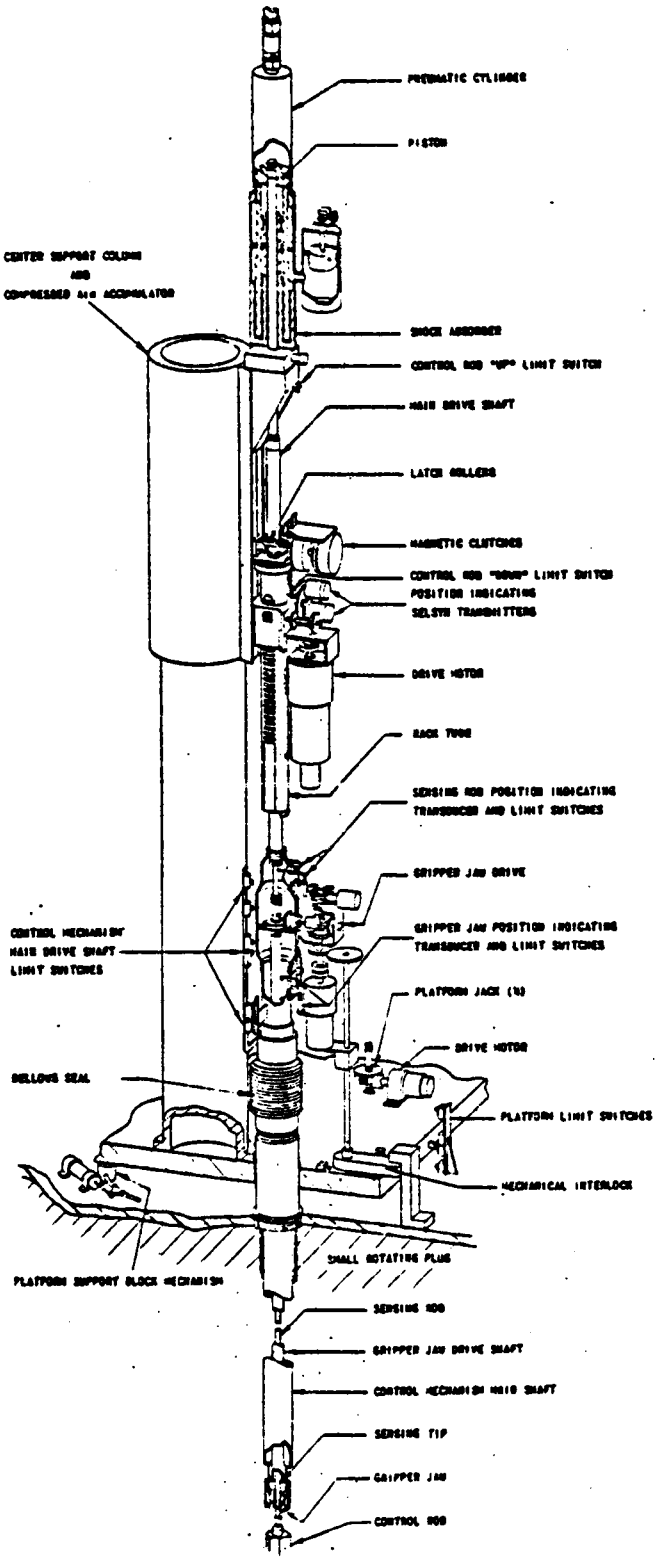


Figure 2.13 Control Rod Drive Mechanism.

state operations and power level changes is accomplished manually. No automatic control system of any type is provided for this purpose. Each of the twelve control rods are operated individually from switches and push buttons on the control console in the main control room. The control rod drive to be operated is selected by a twelve position manual control rod selector switch and actuated by operating the manual rod control switch to raise or lower a rod. The reactor is brought to power by raising the control rods into the core one at a time in small increments, until criticality is obtained. The reactor is then brought to power by continuing to raise a single control rod in small increments and allowing the power to stabilize after each incremental power increase. Reactor power is decreased by slowly driving the control rods downward out of the core or by pneumatic ejection in the case of a scram. As noted in Section 2.10, the maximum reactivity insertion rate for a single control rod is approximately 0.52 ¢/second.

The EBR-II nuclear instrumentation consists of three identical and independent wide range channels A, B, and C. Each channel is comprised of a fission counter/chamber detector assembly, preamplifier, 10 decade log power indicator, linear power indicator, and various recorders, trip relays and annuciators. The linear level channel equipment consists of two identical and independent channels, each comprised of a compensated ion chamber detector assembly, a high voltage power supply, automatic picoammeter, two recorders, a percent range meter and trip relays and annunciators.

2.12 Intermediate Heat Exchanger

The intermediate heat exchanger, (IHX), transfers heat from the radioactive primary sodium to the non-radioactive secondary sodium. The heat exchanger is a shell and tube type, counter flow, single tube wall unit. Fig. 2.14 shows a detailed view of the intermediate heat exchanger. The well casing is approximately 18 5/8 ft. long and 6 ft. in diameter, and is composed of type 304 stainless. The tube bundle consists of 3248, 5/8 in., type 304 stainless steel tubes. Each tube has a minimum wall thickness of 0.049 in. The tubes are arranged on a 13/16 in. triangular pitch. Primary sodium entrance and secondary sodium entrance and exit pipes are schedule 20 type 304 stainless steel. Pertinent IHX physical and operational data are given in Table 2.5.

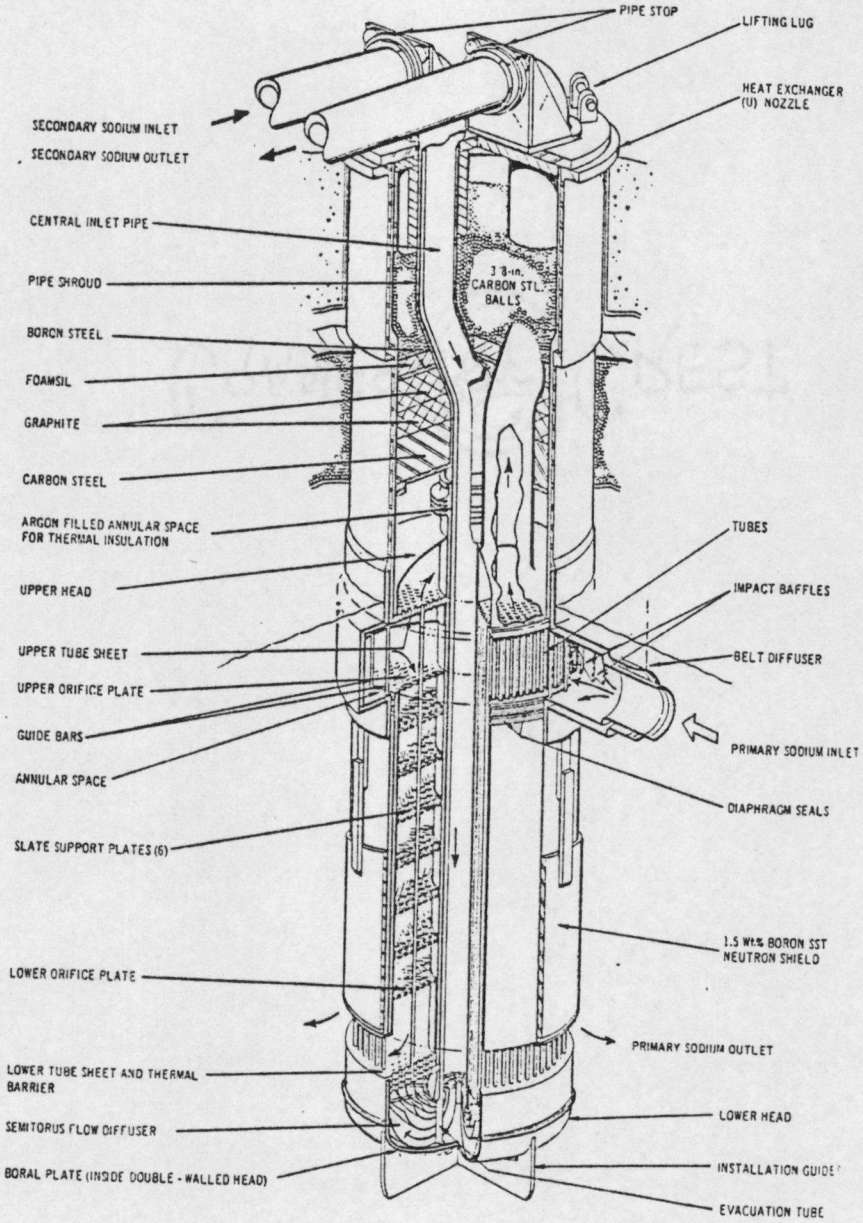


Figure 2.14 EBR-II Intermediate Heat Exchanger.

TABLE 2.5

INTERMEDIATE HEAT EXCHANGER DESIGN
AND PERFORMANCE DATA

Primary Flow Rate (lbm/hr)	3,810,000
Primary Sodium Inlet Temp.	883°F
Primary Sodium Outlet Temp.	700°F
Secondary Flow Rate (lbm/hr)	2,360,000
Secondary Sodium Inlet Temperature	586°F
Secondary Sodium Outlet Temperature	872°F
Number of Tubes	3248
Effective Surface Area ($ft.^2$)	4900
Overall Tube Length (ft.)	10.29
Empty Weight (lbs)	56,000
Flooded Weight (lbs)	62,000

CHAPTER 3

THEORETICAL MODEL

3.1 Introduction

The modeling technique employed in this thesis is known as the state variable approach. Large regions of material are represented by a single node which is characterized by region averaged parameters. The linearization process can be illustrated by examining the one group point kinetics power equation,

$$\frac{dP}{dt} = \frac{\rho - B}{\Lambda} P + \lambda C \tag{3.1}$$

or

$$\frac{dP}{dt} = -\frac{\beta}{\Lambda} P + \lambda C + \frac{\rho P}{\Lambda} \tag{3.2}$$

where

P = Power (or neutron density)

β = Total delayed neutron fraction

Λ = Neutron generation time

λ = Neutron decay constant

C = Precursor Concentration

ρ = Total Reactivity

Equations 3.1 and 3.2 are nonlinear due to the dependence of the total reactivity (ρ) on reactor power (P):

$$\rho = \rho_{ext} + \Sigma \alpha_i T_i \tag{3.3}$$

where

ρ_{ext} = externally induced reactivity changes such as control rod movements

α_i = temperature dependent reactivity feedback coefficients such as Doppler, fuel expansion, etc.

T_i = material temperatures (such as fuel and coolant temperatures).

But, the temperatures of the various materials in the reactor are themselves functions of reactor power,

$$T_i = F_i(P) \tag{3.4}$$

so that

$$\rho = \rho_{ext} + \Sigma\alpha_i F_i(P) \tag{3.5}$$

and more precisely,

$$\frac{dP}{dt} = \frac{-\beta}{\Lambda} P + \lambda C + \frac{P\Sigma\alpha_i F_i(P)}{\Lambda} + \frac{\rho_{ext} P}{\Lambda} \quad . \tag{3.6}$$

Equation 3.6 illustrates in a more precise manner, the nonlinearity of Equations 3.1 and 3.2.

The next step in the linearization process involves representing reactor power, neutron concentration, and reactivity in the perturbation form, $X_o + \delta X$, where X_o represents the original or steady state value of the variable, and δX represents the deviation of the value from steady state. Therefore,

$$P \rightarrow P_o + \delta P$$

$$C \rightarrow C_o + \delta C$$

$$\rho \rightarrow \rho_o + \delta\rho$$

Since the reactor is assumed to be initially at steady state, ρ_o equals zero, and

$$\rho \rightarrow \delta\rho \, .$$

Making the substitution and rewriting equation 3.1,

$$\frac{dP_o}{dt} + \frac{d\delta P}{dt} = \frac{-\beta}{\Lambda} P_o - \frac{\beta}{\Lambda} \delta P + \lambda C_o + \lambda \delta C + \frac{P_o \delta\rho}{\Lambda} + \frac{\delta P \delta\rho}{\Lambda} \qquad (3.7)$$

or

$$\frac{dP_o}{dt} + \frac{\beta}{\Lambda} P_o + \lambda C_o + \frac{d\delta P}{dt} = \frac{-\beta \delta P}{\Lambda} + \lambda \delta C + \frac{P_o \delta\rho}{\Lambda} + \frac{\delta P \delta\rho}{\Lambda} . \qquad (3.8)$$

But from equation 3.2, at steady state,

$$\frac{dP_o}{dt} = \frac{\beta}{\Lambda} P_o + C_o = 0 \qquad (3.9)$$

Therefore,

$$\frac{d\delta P}{dt} = \frac{-\beta}{\Lambda} \delta P + \lambda \delta C + \frac{\delta\rho P_o}{\Lambda} + \frac{\delta\rho \delta_P}{\Lambda} . \qquad (3.10)$$

Now, if one assumes that the magnitude of the perturbation will be small, $\delta\rho$ is small, and

$$\delta\rho\delta P \to 0.$$

Therefore, if one limits himself to small perturbations about steady state, the linearized perturbation form of the point kinetics equation is

$$\frac{d\delta P}{dt} = -\frac{\beta}{\Lambda} \delta P + \lambda \delta C + \frac{P_o}{\Lambda} \delta\rho \qquad (3.11)$$

or

$$\frac{d}{dt} \frac{\delta P}{P_o} = \frac{-\beta}{\Lambda} \frac{\delta P}{P_o} + \lambda \frac{\delta C}{P_o} + \frac{\delta\rho}{\Lambda} . \qquad (3.12)$$

A similar linearization process was employed in deriving the remainder of the equations which were used in the model. This formulation yields a set of linearized, coupled, first order, ordinary differential equations. The model includes representations of point kinetics, heat transfer models for the active core, lower, upper, and inner reflectors, outer blanket, piping and plenums, and the intermediate heat exchanger. A schematic representation of the system model is shown in Figure 3.1.

3.2 Kinetics

The reactor power is modeled by the point kinetics equations, with 6 delayed neutron groups. The linearized equations are:

$$\frac{d}{dt}\left(\frac{\delta P}{P_o}\right) = \frac{-\beta_T}{\Lambda}\frac{\delta P}{P_o} + \sum_1^6 \lambda_i \frac{\delta C_i}{P_o} + \sum_j \frac{\alpha_j}{\Lambda}\delta T_j + \frac{\beta_T}{\Lambda}\delta\rho_{ext} \quad (3.13)$$

$$\frac{d}{dt}\left(\frac{\delta C_i}{P_o}\right) = \frac{\beta_i}{\Lambda}\frac{\delta C_i}{P_o} - \lambda_i \frac{\delta C_i}{P_o} \quad (3.14)$$

where

δP = the deviation of reactor power from initial steady state value

P_o = initial steady state power

β_T = total delayed neutron fraction

Λ = neutron generation time (assumed equal to prompt neutron lifetime, ℓ_p, in Table 2.3, page 17)

λ_i = decay constant for ith delayed neutron group

δC_i = deviation of ith precursor concentration from steady state value

α_j = jth reactivity feedback coefficient

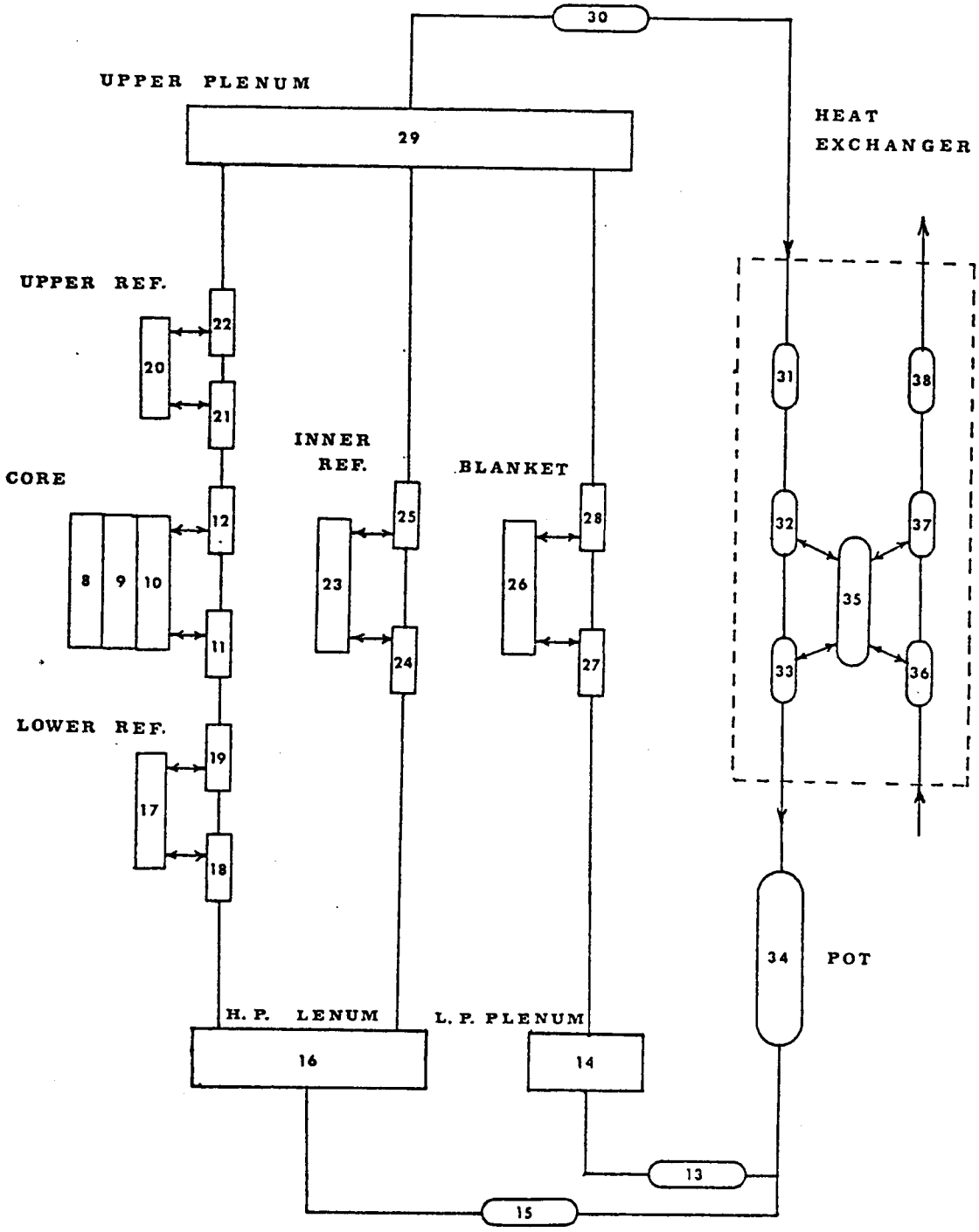


Figure 3.1 EBR-II 38 Node Model Schematic.

δT_j = deviation of jth material temperature from steady state value

$\delta \rho_{ext}$ = reactivity due to control rod movement.

The nine feedback mechanisms known to exist in EBR-II are listed in Table 3.1, along with the system parameters to which they are coupled. The steel expansion coefficient reflects changes in reactivity due to expansion of clad, reflector, and structural steel within the lattice. All of the steel is assumed to have the same temperature as that of the fuel cladding in the active core.

Seven of the nine reactivity coefficients from run 25 were well identified. However, the function and value of the core bowing and control expansion coefficients are not well understood. Core bowing is thought to be a function of sodium temperature gradiants. The bowing feedback function is known to be positive and nonlinear with respect to temperature, but there is no direct means of measuring subassembly deflections. Control rod expansion is assumed to be proportional to sodium temperature, and the worth of a control rod is not linear with respect to core insertion length. Thermal expansion effects will, therefore, contribute different reactivities depending upon the extent of rod insertion. This situation is complicated even further by the fact that the values of each of the seven identified feedback coefficients have been observed to vary by up to 20% from run to run[6]. This variation is due to modifications in the subassembly composition and loading patterns.

Table 3.2 lists the seven identified feedback coefficients, their values, and the fraction of the run 25 calculated total isothermal

TABLE 3.1

KNOWN EBR-II FEEDBACK MECHANISMS

Mechanism	Coupled Parameter
Doppler	Fuel Temp.
Steel Expansion	Clad Temp.
Core. Na. Exp.	Core Na
Upper Ref. Na. Exp.	Upper Ref. Na. Temp.
Lower Ref. Na. Exp.	Lower Ref. Na. Temp.
Fuel Exp.	Fuel Temp.
Inner Ref. Na. Exp.	Inner Ref. Na. Temp.
Core Bowing	(Sodium Temp.)
Control Rod Exp.	Local Na. Temp.

TABLE 3.2

FEEDBACK MECHANISMS EMPLOYED IN EBR-II MODEL

Mechanism	($\Delta k/k/°F$)	% of TIFC*
Doppler	$+0.222 \times 10^{-6}$	1.1
Steel Exp.	-0.720×10^{-5}	28
Core Na	-0.481×10^{-5}	19
Upper Ref. Na	-0.223×10^{-5}	9
Lower Ref. Na	-0.223×10^{-5}	9
Fuel Exp.	-0.200×10^{-5}	8
In. Ref. Na	-0.120×10^{-5}	4.5
	TOTAL	78

*TIFC = -2.53×10^{-5} $\Delta k/k/°F$ (From ANL 5719)

feedback coefficient (TIFC) represented by each. This TIFC was calculated by Argonne National Lab personnel, and assumes an isothermal reactor temperature distribution and no core bowing. The seven identified feedback coefficients constitute 77% of the TIFC.

Two alternative model formulations must now be considered: (1) the model can be formulated to employ only the seven identified feedback coefficients, or (2) one or some combination of the seven identified feedback coefficients could be increased to reflect the missing 23% of the TIFC, and a new imaginery feedback coefficient (which would be some function of the radial temperature gradient within the reactor) added to represent the unknown bowing coefficient. In making the decision as to which formulation will be followed, one must consider the impact of the different formulations upon the goals of this investigation. As stated in Chapter 1, the goals of this study are to develop the methodology for dynamic testing in EBR-II and to evaluate the cost/benefit ratio of such a testing program. These goals do not include the development of the actual model to be employed in a given test. Before the actual test is conducted, and the parameter identification performed, the model would have to be modified to incorporate the actual feedback coefficients from the run in question. Available information regarding the core bowing and control rod expansion could easily be incorporated at that time. Additionally, it is very probable that the number of system parameters which would be identifiable with the seven coefficient model will represent the minimum number one could expect to identify with methods discussed in this thesis. This model would yield a worst case or conservative limit for the value of the cost/benefit ratio.

Conversely, if one chooses the option of adjusting the seven known coefficients, and creating an eighth to account for core bowing, the possibility exists of biasing the parameter identification analysis in favor of the identification of a larger number of parameters. The crux of the problem is that while choosing this second option for model formulation does result in an increase in the amount of information contained in the model, this information is in a highly speculative form and could easily result in an overly optimistic estimate of the number of identifiable parameters and therefore an unrealistically low cost/benefit ratio. Because of these considerations, it was decided to include only the seven identified feedback coefficients in the model.

A final comment is that due to the small sodium temperature rise through the outer blanket (20°F) and the low reactivity importance of the blanket region, there is no reactivity feedback associated with the outer blanket sodium.

3.3 Active Core Model

Fig. 3.2 shows a cross-sectional view of an EBR-II fuel pin. The corresponding pin model is shown in Fig. 3.3. An average fuel pin is represented by 3 nodes: one in each of the fuel, sodium bond and steel cladding regions (Fig. 3.3). The expressions for the heat transfer resistance formulas are derived in Reference 1, and listed in Appendix A. Two coolant nodes are coupled to the pin model. The representation of the clad to coolant heat transfer with one metal and two coolant nodes is known as Mann's model[7]. Each of the two coolant nodes is based on a well mixed approximation. The driving

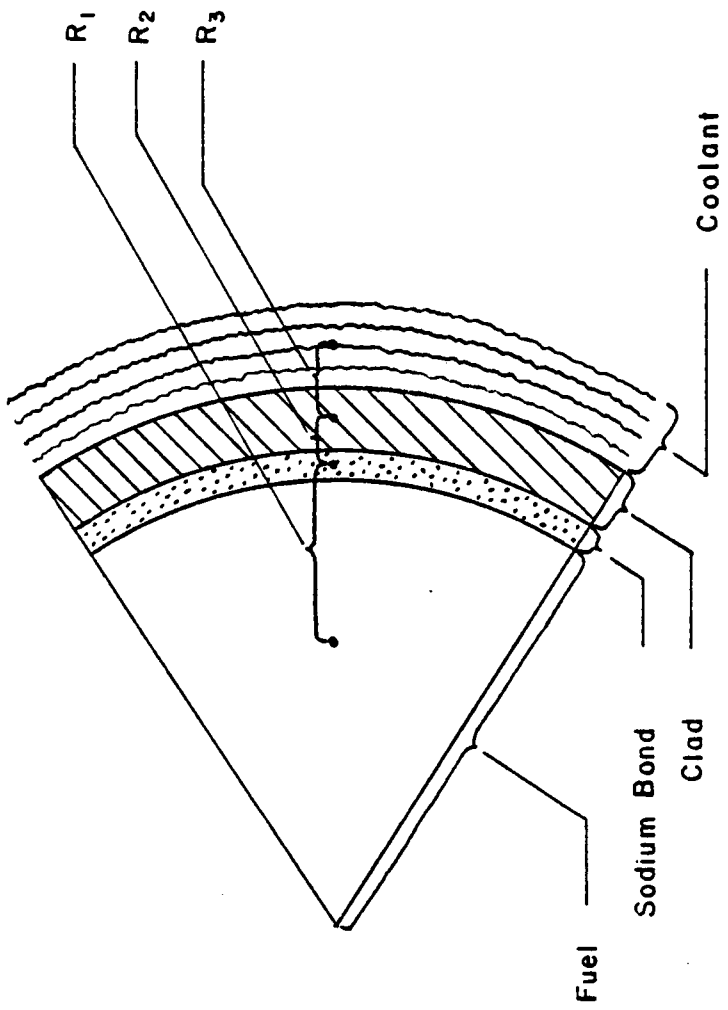


Figure 3.2 EBR-II Fuel Pin Cross Section.

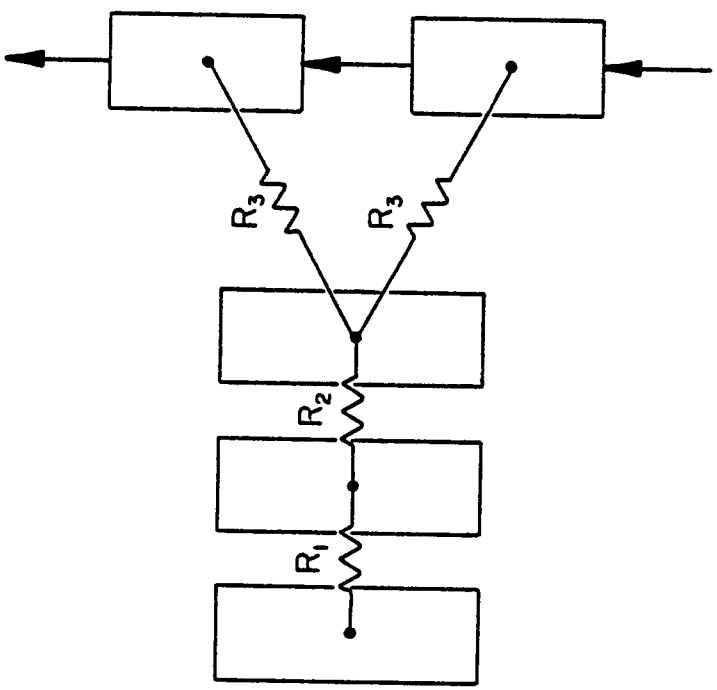


Figure 3.3 38 Node Model's Fuel Pin Representation.

force for heat transfer is taken as the difference in temperature between the clad and the average temperature of the first coolant node (Fig. 3.4). Two other fuel to coolant heat transfer models sometimes used in dynamics work are the single well mixed node approach ($\theta_{out} = \bar{\theta}$), and the arithmatic average approximation, ($\theta_{out} = 2\bar{\theta} - \theta_{in}$). Mann's model is actually a more detailed representation of the well mixed node approximation and is therefore a more desirable model for serious work.

The arithmatic average approach yields a rapid decrease in outlet temperature for a rapid increase in inlet temperature. Since any fluid has a finite heat capacity, its temperature cannot change instantly following an inlet temperature perturbation. The arithmatic average approximation therefore yields a nonphysical response for rapid inlet temperature perturbations. This error becomes more and more pronounced as the frequency of the perturbation increases. The equations for the pin model are:

$$\frac{d}{dt}\ \delta T_F = \frac{P_f}{(MC_p)_f}\ \frac{\delta P}{P_o} - \frac{1}{R_1(MCP)_F}\ (\delta T_F - \delta T_B) \tag{3.15}$$

$$\frac{d\delta T_B}{dt} = \frac{1}{R_1(MC_p)_B}\ (\delta T_F - \delta T_B) - \frac{1}{R_2(MC_p)_B}\ (\delta T_B - \delta T_C) \tag{3.16}$$

$$\frac{d\delta T_C}{dt} = \frac{1}{R_2(MC_p)_C}\ (\delta T_B - \delta T_C) - \frac{1}{R_3(MC_p)_C}\ (\delta T_C - \delta \theta_1) \tag{3.17}$$

$$\frac{d\delta \theta_1}{dt} = \frac{1}{R_3(MC_p)_\theta}\ (\delta T_C - \delta \theta_1) + \frac{2}{\tau}\ (\delta \gamma_2 - \delta \theta_1) \tag{3.18}$$

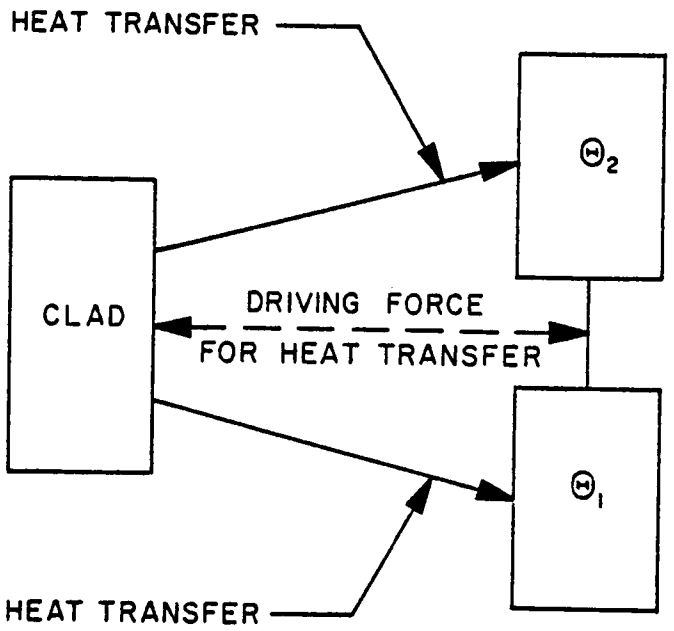


Figure 3.4 Mann's Model.

$$\frac{d\delta\theta_2}{dt} = \frac{1}{R_3(MC_p)_\theta}(\delta T_C - \delta\theta_1) + \frac{2}{\tau}(\delta\theta_1 - \delta\theta_2) \qquad (3.19)$$

where:

δT_F = Deviation of the fuel temperature from steady state

P_F = Fraction of reactor power generated in the fuel

$(MC_p)_F$ = Total fuel heat capacity

P_o = Initial reactor power

R_1 = Fuel node average to bond node average heat transfer resistance

δT_B = Deviation of sodium bond temperature from equilibrium

$(MC_p)_B$ = Sodium bond heat capacity

R_2 = Sodium bond node average to clad node average heat transfer resistance

δT_C = Deviation of stainless steel clad temperature from equilibrium

$(MC_p)_C$ = Clad heat capacity

R_3 = Clad node average to coolant node average heat transfer resistance

$\delta\theta_1$ = Deviation of core sodium coolant node 1 temperature from equilibrium

$\delta\theta_2$ = Deviation of sodium coolant node 2 temperature from equilibrium

$(MC_p)_\theta$ = Sodium coolant nodal heat capacity for the active core region

τ = Residence time of the coolant in the active core

$\delta\gamma_2$ = Deviation of the temperature of the upper coolant node in the lower axial reflector region from equilibrium.

Table 3.3 lists pertinent core model parameter data.

3.4 Reflector and Blanket Regions Model

The lower, upper, and inner reflectors and the outer blanket regions are each represented by one metal and two coolant nodes. Mann's model is employed in each case. The three equations for each region are:

$$\frac{d\delta T_M}{dt} = \frac{P_i}{(MC_p)_M}\frac{\delta P}{P_o} - \frac{UA}{(MC_p)_M}(\delta T_M - \delta\Gamma_1) \tag{3.20}$$

$$\frac{d\delta\Gamma_1}{dt} = \frac{UA}{(MC_p)_\Gamma}(\delta T_M - \delta\Gamma_1) + \frac{2}{\tau}(\delta\theta_{in} - \delta\Gamma_1) \tag{3.21}$$

$$\frac{d\delta\Gamma_1}{dt} = \frac{UA}{(MC_p)_\Gamma}(\delta T_M - \delta\Gamma_1) + \frac{2}{\tau}(\delta\Gamma_1 - \delta\Gamma_2) \tag{3.22}$$

where:

δT_M = Deviation of region metal temperature from equilibrium

P_i = Fraction of power generated in the core region

$(MC_p)_M$ = Heat capacity of the metal in the region

U = Metal to coolant heat transfer coefficient

A = Metal to coolant heat transfer area

$\delta\Gamma_i$ = Deviation of first regional coolant node temperature from equilibrium

$(MC_p)_\Gamma$ = Regional coolant node heat capacity

τ = Residence time of coolant in the region

$\delta\Gamma_2$ = Deviation of second regional coolant node temperature from equilibrium.

TABLE 3.3

CORE MODEL PARAMETER DATA

Power Fraction, P_f	.836
Total Fuel Heat Capacity, MC_f	34.80 Btu/°F
Total Sodium Bond Heat Capacity, MC_B	2.03 Btu/°F
Total Cladding Heat Capacity, MC_C	13.33 Btu/°F
Total Coolant Heat Capacity, MC_S	16.69 Btu/°F
Fuel to Sodium Bond Thermal Resistance, R1	6.585 sec°F/Btu
Sodium Bond to Cladding Thermal Resistance, R2	7.0973 sec°F/Btu
Cladding to Coolant Thermal Resistance, R3	12.5879 sec°F/Btu
Coolant Residence Time in Active Core, τ	0.075 sec

The reflector and blanket region model data are given in Table 3.4.

3.5 Piping, Plenums, and Pot Models

The transport of the coolant through the plenums, from the upper plenum to the heat exchanger inlet, through the pot, and from the pot to the reactor inlet plenums is represented by first order lag approximations. This approximation involves several basic assumptions. These assumptions are:

1) The pipe and plenum sections can be treated as well mixed volumes.
2) There is no axial heat conduction.
3) There are no heat gains or losses to the piping.
4) The coolant density in the pipe is constant.

With these assumptions, the equations describing heat transport in the piping, pot, and plenums are:

$$\frac{d\delta U}{dt} = \frac{\dot{M}_1 C_{p1}}{(MC_p)_U}(\delta\gamma_4 - \delta U) + \frac{\dot{M}_2 C_{p2}}{(MC_p)_U}(\delta\gamma_6 - \delta U) + \frac{\dot{M}_3 C_{p3}}{(MC_p)_U}(\delta\gamma_8 - \delta U) \quad (3.23)$$

$$\frac{d\delta P_o}{dt} = \frac{1}{\tau_1}(\delta U - \delta P_o) \quad (3.24)$$

$$\frac{d\delta\theta_p}{dt} = \frac{1}{\tau_2}(\delta P_{out} - \delta\theta_p) \quad (3.25)$$

$$\frac{d\delta P_{LI}}{dt} = \frac{1}{\tau_3}(\delta\theta_p - \delta P_{LI}) \quad (3.26)$$

$$\frac{d\delta P_{HI}}{dt} = \frac{1}{\tau_4}(\delta\theta_p - \delta P_{HI}) \quad (3.27)$$

TABLE 3.4

REFLECTORS AND BLANKET MODEL PARAMETER DATA

Axial Reflectors	
Power Fraction, P_f	.012
Metal Heat Capacity, MC_p	54.70 Btu/°F
Coolant Heat Capacity, MC_p	27.10 Btu/°F
Coolant Residence Time, τ	.106 Sec.
Lower Reflector, UA	71.08 Btu/sec°F
Upper Reflector, UA	4.62
Inner Reflector	
Power Fraction, P_f	.098
Metal Heat Capacity, MC_p	378.18 Btu/°F
Coolant Heat Capacity, MC_p	14.26 Btu/°F
Coolant Residence Time in the, UA	0.27 sec.
Inner Reflector UA	32.03 Btu/sec°F
Outer Blanket	
Power Fraction, P_f	.022
Metal Heat Capacity, MC_p	1797.85 Btu/°F
Coolant Heat Capacity, MC_p	217.36 Btu/°F
Coolant Residence Time, τ	1.09 sec
Outer Blanket UA	14.89 Btu/sec°F

$$d\delta H = \frac{1}{\tau_5} (\delta P_I - \delta H) \tag{3.28}$$

$$d\delta L = \frac{1}{\tau_6} (\delta P_I - \delta L) \tag{3.29}$$

where:

δU = Deviation of upper plenum sodium temperature from equilibrium

$\dot{M}_1$ = Coolant mass flow rate through active core and axial reflectors

C_{p1} = Specific heat of sodium in the active core and axial reflector regions

$\dot{M}_2$ = Coolant mass flow rate through inner reflector region

C_{p2} = Specific heat of sodium in the inner reflector region

$\dot{M}_3$ = Coolant mass flow rate through the outer blanket

C_{p3} = Specific heat of sodium in the outer blanket region

$(MC_p)_U$ = Heat capacity of the sodium in the upper plenum region

$\delta\gamma_4$ = Deviation of the temperature of the sodium in the upper coolant node of the upper axial reflector from steady state

$\delta\gamma_6$ = Deviation of the temperature of the sodium in the upper coolant node of the inner reflector from steady state

$\delta\gamma_8$ = Deviation of the temperature of the sodium in the upper coolant node of the outer blanket from steady state

δP_o = Deviation of the temperature of the sodium in the outlet piping from steady state

τ_1 = Residence time of the sodium in the reactor outlet piping

$\delta \Theta_p$ = Deviation of the temperature of the sodium in the pot from steady state

τ_2 = Residence time of the sodium in the pot

δP_2 = Deviation of the sodium temperature in the second primary coolant node of the intermediate heat exchanger from steady state

δP_{LI} = Deviation of the sodium temperature in the pot-to-reactor low pressure piping from steady state

δP_{HI} = Deviation of the sodium temperature in the pot-to-reactor high pressure piping from steady state

τ_3 = Residence time of the sodium in the pot-to-reactor low pressure piping

τ_4 = Residence time of the sodium in the pot-to-reactor high pressure piping

δH = Deviation of the high pressure plenum sodium temperature from equilibrium

τ_5 = High pressure plenum sodium residence time

δL = Deviation of the low pressure plenum sodium temperature from equilibrium

τ_6 = Low pressure plenum sodium residence time.

Table 3.5 lists the parameter values used in the piping, plenum, and pot models.

TABLE 3.5

PIPING, PLENUMS, AND POT MODEL PARAMETER DATA

Upper Plenum	
$\dot{M}_{core}/M_u$	.1198 sec^{-1}
$\dot{M}_{IR}/M_u$	.0288 sec^{-1}
$\dot{M}_B/M_u$	.0246 sec^{-1}
Coolant Residence Time in Reactor Outlet Piping	1.54 sec
Coolant Residence Time in Low Pressure Reactor Inlet Piping	1.80 sec
Coolant Residence Time in High Pressure Reactor Inlet Piping	1.78 sec
Coolant Residence Time in Low Pressure Plenum	16.28 sec
Coolant Residence Time in High Pressure Plenum	1.49 sec
Coolant Residence Time in Pot	552.6 sec

3.6 Intermediate Heat Exchanger Model

The intermediate heat exchanger is represented by a seven node model. The primary inlet and secondary outlet plenums are represented by first order lag approximations. The tube wall is represented by a single node. Heat transfer from both the primary sodium to the tubes and from the tube wall to the secondary sodium is represented by Mann's model formulations. The equations for the heat exchanger model are:

$$\frac{d\delta P_{in}}{dt} = \frac{1}{\tau_7}\,\delta P_{out} - \frac{1}{\tau_7}\,\delta P_{in} \tag{3.30}$$

$$\frac{d\delta P_1}{dt} = \frac{2}{\tau_8}\,\delta P_{in} - \left[\frac{(UA)_P}{(MC_p)_P} + \frac{2}{\tau_8}\right]\delta P_1 + \frac{(UA)_P}{(MC_p)_P}\,\delta M \tag{3.31}$$

$$\frac{d\delta P_2}{dt} = \left[\frac{2}{\tau_8} - \frac{(UA)_P}{(MC_p)_P}\right]\delta P_1 - \frac{2}{\tau_8}\,\delta P_2 + \frac{(UA)_P}{(MC_p)_P}\,\delta M \tag{3.32}$$

$$\frac{d\delta M}{dt} = \frac{(UA)_P}{(MC_p)_M}\,\delta P_1 - \left[\frac{(UA)_P + (UA)_S}{(MC_p)_M}\right]\delta M + \frac{(UA)_S}{(MC_p)_M}\,\delta S_1 \tag{3.33}$$

$$\frac{d\delta S_1}{dt} = \frac{(UA)_S}{(MC_p)_S}\,\delta M - \left[\frac{(UA)_S}{(MC_p)_S} + \frac{2}{\tau_9}\right]\delta S_1 + \frac{2}{\tau_9}\,\delta S_{in} \tag{3.34}$$

$$\frac{d\delta S_2}{dt} = \frac{(UA)_S}{(MC_p)_S}\,\delta M - \left[\frac{(UA)_S}{(MC_p)_S} - \frac{2}{\tau_9}\right]\delta S_1 - \frac{2}{\tau_9}\,\delta S_2 \tag{3.35}$$

$$\frac{d\delta S_o}{dt} = \frac{1}{\tau_{10}}\,\delta S_2 - \frac{1}{\tau_{10}}\,\delta S_o \tag{3.36}$$

where:

δP_{in} = Deviation of primary inlet plenum sodium temperature from equilibrium

τ_7 = Sodium residence time in the primary outlet plenum

δP_{out} = Deviation of reactor outlet sodium temperature from equilibrium

δP_1 = Deviation of the temperature of the sodium in the first primary node from equilibrium

τ_8 = Sodium residence time in both primary nodes

$(UA)_P$ = Product of primary sodium to tube wall heat transfer coefficient and total primary heat transfer area

$(MC_P)_P$ = Total primary sodium heat capacity (both nodes)

δM = Deviation of tube wall temperature from steady state

δP_2 = Deviation of the second primary sodium node temperature from equilibrium

$(MC_P)_M$ = Total heat capacity of the tube bundle metal

$(UA)_S$ = Product of secondary sodium to tube wall heat transfer coefficient and total secondary heat transfer area

δS_1 = Deviation of the first secondary sodium node temperature from equilibrium

τ_9 = Sodium residence time in both secondary nodes

δS_{in} = Deviation of secondary sodium inlet temperature from equilibrium

δS_o = Deviation of secondary outlet plenum sodium temperature from equilibrium

τ_{10} = Sodium residence time in secondary outlet plenum.

Table 3.6 lists heat exchanger model parameter values of interest.

TABLE 3.6

HEAT EXCHANGER MODEL PARAMETER DATA

Primary Inlet Plenum Sodium Residence Time τ_7	1.91 sec
Primary Sodium Residence Time in Heat Exchanger, τ_8	7.29 sec
Primary UA	505.03 Btu/sec°F
Primary Sodium Heat Capacity, MC_p	2336.26 Btu/°F
Tube Bundle Heat Capacity, MC_p	841.66 Btu/°F
Secondary UA	598.94 Btu/sec°F
Secondary Sodium Heat Capacity, MC_p	564.25 Btu/°F
Secondary Sodium Residence Time in Heat Exchanger, τ_9	2.86 sec
Secondary Sodium Residence Time in Outlet Plenum, τ_{10}	0.25 sec

CHAPTER 4

MATHEMATICAL METHODS FOR TIME, FREQUENCY RESPONSE, AND SENSITIVITY ANALYSIS

4.1 Introduction

The mathematical techniques employed in the analysis of the system model are discussed in this chapter. Topics covered include methods for obtaining the system time response to any perturbation, the prompt jump model, system frequency response and frequency response sensitivity, and finally, methods for assessing the stability of the system.

4.2 System Time Response

The 38 linearized ordinary differential equations which comprise the system model, can be cast in the following matrix form:

$$\frac{d\bar{X}}{dt} = A\bar{X} + \bar{f}(t) \tag{4.1}$$

where:

$\bar{X}$ = the solution vector

A = the matrix of constant coefficients

$\bar{f}(t)$ = the vector of time varying forcing functions.

The time response of the system represented by equation 4.1 was computed by the MATEXP[8] code. MATEXP employs the matrix exponential method of solution. The system response at time $t + \Delta t$ is given by:

$$X(t + \Delta t) = e^{A\Delta t}\ \bar{X}(t) + e^{A(t + \Delta t)} \int_{t}^{t + \Delta t} e^{-A\Delta t}\ \bar{f}(t)\ dt \tag{4.2}$$

If the forcing function f(t) is constant over the interval t, to t + Δt, the exact solution from Eq. 4.2 is:

$$X(t + \Delta t) = e^{A\Delta t}\ \bar{X}(t) + (e^{A\Delta t} - I)\ A^{-1}\ \bar{f}(t) \tag{4.3}$$

where,

$$e^{A\Delta t} = I + A\Delta t + \frac{(A\Delta t)^2}{2!} + \frac{(A\Delta t)^3}{3!} + \ldots \tag{4.4}$$

and,

$$(e^{A\Delta t} - I)\ A^{-1} = \Delta t \left[I + \frac{A\Delta t}{2!} + \frac{(A\Delta t)^2}{3!} + \frac{(A\Delta t)^3}{4!} + \ldots \right]. \tag{4.5}$$

Note that due to Eq. 4.5, the inverse A matrix need not be calculated. Table 4.1 lists the nonzero A matrix elements for the EBR-II model.

4.3 Prompt Jump Model

A problem which is sometimes encountered in the use of the point kinetics equations with the matrix exponential method is the occurrence of numerical problems that arise because of an extremely large eigenvalue. Consider the power equation, Eq. 3.1,

$$\frac{d\delta P/P_o}{dt} = \frac{-\beta}{\Lambda}\ \frac{\delta P}{P_o} + \Sigma\lambda_i\ \delta C_i + \frac{\Sigma\alpha_i \delta T_i}{\Lambda} + \frac{\delta\rho_{ext}}{\Lambda}\ . \tag{4.6}$$

In the EBR-II, $\beta/\Lambda = 46954.8$. This diagonal element is much larger than the remaining terms in the equations, and strongly influences the magnitude of the largest eigenvalue. Eigenvalues with large magnitudes correspond to short time constants in the physical system, and

TABLE 4.1

38 NODE A MATRIX ELEMENTS

I	J	a_{IJ}	I	J	a_{IJ}
1	1	-46954.80	18	18	-21.556
1	2	.0127	19	17	2.62270
1	3	.0317	19	18	16.3106
1	4	.1150	19	19	-18.9333
1	5	.3110	20	1	10.3966
1	6	1.400	20	20	-.084524
1	7	3.7800	20	21	.084524
1	8	-9.8179	21	12	18.9333
1	10	-39.7626	21	20	.170612
1	11	-13.2818	21	21	-19.1039
1	12	-13.2818	22	20	.17062
1	18	-.08632	22	21	18.7627
1	19	-.08632	22	22	-18.9333
1	21	-.08632	23	1	.17068
1	22	-.08632	23	23	-.0847
1	24	-.37935	23	24	.0847
1	25	-.37935	24	16	7.4186
2	1	1625.81	24	23	2.2452
2	2	-.0127	24	24	-9.6638
3	1	9548.39	25	23	2.2452
3	3	-.03170	25	24	5.1734
4	1	8670.96	25	25	-7.4186
4	4	-.1150	26	1	.5799
5	1	18974.2	26	26	-.00830
5	5	-.31100	26	27	.00830
6	1	6606.45	27	14	1.8327
6	6	-1.4000	27	26	.0685
7	1	1529.03	27	27	-1.9012
7	7	-3.7800	28	26	.0685
8	1	1165.66	28	27	1.7642
8	8	-24.6124	28	28	-1.8327
8	9	24.6124	29	22	.11980
9	8	422.290	29	25	.02880
9	9	-814.12	29	28	.02460
9	10	391.822	29	29	-.1732
10	9	59.652	30	29	.6510
10	10	-93.285	30	30	-.6510
10	11	33.633	31	30	.5240
11	10	26.838	31	31	-.5240
11	11	-53.505	32	31	.2740
11	19	26.667	32	32	-.4902

TABLE 4.1 (continued)

I	J	a_{IJ}	I	J	a_{IJ}
12	10	26.838	32	35	.2162
12	11	-.1710	33	32	.0580
12	12	-26.667	33	33	-.2740
13	13	-.5549	33	35	.2162
13	34	-.5549	34	33	.00180
14	13	.0614	34	34	-.00180
14	14	-.0614	35	32	.6000
15	15	-.5630	35	35	-1.3116
15	34	.5630	35	36	.7116
16	15	.6700	36	35	1.0614
16	16	-.6700	36	36	-1.7713
17	1	10.396	37	35	1.0614
17	17	-1.2995	37	36	.3516
17	18	1.2995	37	37	-.7098
18	16	18.9333	38	37	4.000
18	17	2.6227	38	38	-4.000

therefore necessitate very small time increments in the matrix exponential solution. The analyst would like to use the largest time increment possible in order to reduce computer costs. A solution to this dilemma is the so-called "prompt jump approximation."[9]

Rearranging Equation 4.6, one obtains,

$$\Lambda \frac{d\delta P/P_o}{dt} = -\beta \frac{\delta P}{P_o} + \Lambda\Sigma\lambda_i \delta C_i + \Sigma\alpha_i \delta T_i + \delta\rho_{ext}$$

Since Λ is so small (10^{-7}), and with the assumption of small perturbations, one obtains

$$\Lambda \frac{d\delta P/P_o}{dt} \simeq 0 \tag{4.8}$$

and

$$-\beta \frac{\delta P}{P_o} + \Lambda\Sigma\lambda_i \delta C_i + \Sigma\alpha_i \delta T_i + \delta\rho_{ext} = 0 \tag{4.9}$$

or

$$\frac{\delta P}{P_o} = \frac{\Lambda}{\beta} \Sigma\lambda_i \delta C_i + \frac{\Sigma\alpha_i \delta T_i}{\beta} + \frac{\delta\rho_{ext}}{\beta} = 0 . \tag{4.10}$$

This expression for $\frac{\delta P}{P_o}$ is substituted into the six precursor equations and the equations for the fuel, axial reflectors, inner reflector, and outer blanket metal temperature equations. This substitution results in the elimination of the large eigenvalue (and the associated need for using very small time steps) and the reduction in the order of the matrix from 38th order to 37th order. Due to the fact that the derivative term in Eq. 3.1 is eliminated, a step in reactivity results in a direct or prompt jump in reactor power. For

this reason, the model described above is often called the "prompt jump model."

4.4 System Frequency Response

The system frequency response was calculated by the SFR-III[10] code. The linear, constant coefficient system represented by Eq. 4.1, can be written as

$$\frac{d\bar{X}}{dt} = A\bar{X} + \bar{g}f \tag{4.11}$$

where

f = a scalar which represents the disturbance to the system

$\bar{g}$ = a vector of coefficients of f (the complete system disturbance vector is $\bar{g}f$)

Equation 4.11 is Laplace transformed to obtain

$$s\bar{X}(s) = A\bar{X}(s) + \bar{g}f(s) \tag{4.12}$$

where

s = the Laplace transform variable

$\bar{X}(s)$ = Laplace transform of $\bar{X}$

$\bar{f}(s)$ = Laplace transform of f

Equation 4.12 can be written as

$$\frac{\bar{X}(s)}{f(s)} = -[A - sI]^{-1}\ \bar{g} \tag{4.13}$$

The term $\bar{X}(s)/f(s)$ is recognized as the vector of transfer functions, $\bar{G}(s)$, and so

$$\bar{G}(s) = -[A - sI]^{-1}\ \bar{g} \tag{4.14}$$

The frequency response of the system at some angular frequency, ω, is obtained by replacing the Laplace transform variable s with $j\omega$:

$$\bar{G}(j\omega) = -[A - j\omega I]^{-1} \bar{g} \tag{4.15}$$

where

$\bar{G}(j\omega)$ = the system frequency vector

$j = (-1)^{1/2}$

ω = angular frequency

4.5 Frequency Response Sensitivity

The sensitivity of the system frequency response vector eq. 4.15 to changes in system matrix elements a_{ij} can also calculated by SFR-III. Equation 4.15 is differentiated with respect to matrix element a_{ij} to obtain

$$\Delta_{ij} \bar{G} + [A - sI] \frac{\partial \bar{G}}{\partial a_{ij}} = 0 \tag{4.16}$$

where

$\Delta_{ij} = \partial A / \partial a_{ij}$ is a column with unity in row i, and column j, and zeros elsewhere

$\partial G / \partial a_{ij}$ = the desired response sensitivity.

Equation 4.16 can be rearranged to give:

$$\frac{\partial \bar{G}}{\partial a_{ij}} = -[A - sI]^{-1} \Delta_{ij} \bar{G} \tag{4.17}$$

It is observed that:

1) The same matrix, $[A-sI]^{-1}$, appears in each equation. Since this matrix is required for determining the frequency response in Eq. (4.14), no additional computation is required to furnish this operator for the sensitivity calculations.
2) Δ_{ij} is a known quantity.
3) $\overline{G}(s)$ is already known from the basic frequency response calculation.

The net conclusion from these observations is that the system frequency response sensitivities may be obtained by simply multiplying known quantities together.

4.6 Stability Margin Assessment

The block diagram of the EBR-II system is shown in Figure 4.1. The overall closed loop transfer function, G_c, can be written as

$$G_c = \frac{G}{1+GH} \tag{4.18}$$

where

G = The EBR-II zero power transfer function

H = The transfer function for all system feedback mechanisms.

Equation 4.18 can be rearranged to yield

$$GH = \frac{G}{G_c} - 1 . \tag{4.19}$$

Equation 4.19 is useful for calculating the system open loop transfer function, GH, since the system zero power transfer function, G, is easily calculated from methods discussed in Section 4.3 (if sufficiently

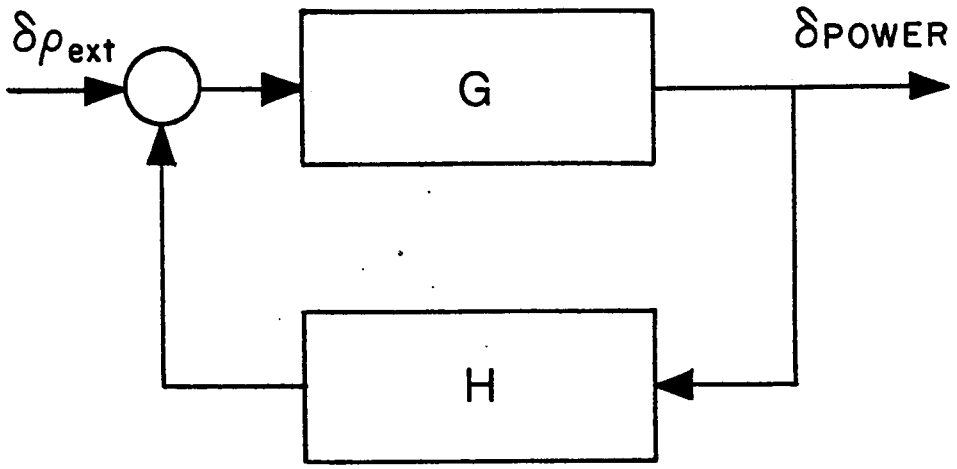


Figure 4.1 EBR-II Feedback System.

accurate neutron precursor data is available), and the system closed loop gain, G_c, can be measured experimentally. These values are substituted into Equation 4.19, to yield a numerical value for the system open loop frequency response. This open loop frequency response is used in conjunction with the Nyquist stability criterion to determine the stability of the closed loop system. For the vast majority of nuclear reactor applications, the transfer functions, G, and H, have no poles with positive real parts. The Nyquist stability criterion for this case is[3]:

> The closed loop system whose open loop transfer function has no poles with positive real parts is stable if and only if there are no clockwise encirclements of the (-1,j0) point by the locus of $GH(j\omega)$, as ω varies from $-\infty$ to $+\infty$.

The most common stability index for Nyquist plots is the phase margin. The phase margin is defined as the angle between the negative real axis and the line from the origin through the point where the Nyquist locus has a magnitude of unity. A phase margin of at least 20 degrees has been shown to be desirable for pressurized water reactor systems[3] and should also be desirable in LMFBR applications.

A second method of determining the stability of the system may be employed once the accuracy of the system model has been verified. This method makes use of standard computational routines to calculate the eigenvalues of the system A matrix. The classical way of solving linear, constant coefficient equations is given by Equation 4.20,

$$\overline{X}(t) = \sum_{i=1}^{N} y_i e^{\lambda_i t} \qquad (4.20)$$

where

$\overline{X}$ = The solution vector

$\overline{Y}$ = eigenvector "i"

λ_i = eigenvalue "i".

The time behavior of the system is, therefore, controlled by the exponential terms in the following manner:

1) If the real parts of all the eigenvalues are negative, a transient will return to equilibrium, and the system is therefore, stable.

2) If the real part of any eigenvalue is positive, the transient will grow indefinitely, and the system is unstable.

3) If any pair of distinct, complex conjugate eigenvalues has a zero real part, then the transient will have an undamped oscillation. From a practical standpoint, this is an undesirable condition.

From these considerations, it is apparent that one need only calculate the eigenvalues of the verified system A matrix to determine the stability of the system.

CHAPTER 5

SIMULATION RESULTS

5.1 Introduction

The computer programs MATEXP and SFR-III were used to obtain the system time and frequency response for several different cases. The first step in the simulation process was to examine the accuracy of the system model. The accuracy of the model was verified by comparison of actual experimental rod drop data with the model's predicted response to the same perturbation. The model was then used to predict the system time response to a reactivity step of 10 cents, the system frequency response to reactivity perturbation, and the system frequency response for intermediate heat exchanger secondary inlet sodium temperature perturbations.

5.2 Experimental and Theoretical Rod Drop Response

If a system model is to be of any use in dynamic studies, it must accurately predict the response of the system to the various perturbations of interest. For an operational plant, experimental data may be used in the model verification process. Considerable data are available on the stability characteristics of the EBR-II. Experimental data were taken at the beginning of every reactor run for most core loadings that were run at significant power from run 26 through the present time[5]. Both rod oscillation and rod drop tests were performed. The rod drop tests were performed with a stainless steel rod in place of a standard control rod. Figure 5.1 shows the 38 node model's predicted response to a -5 cent reactivity step

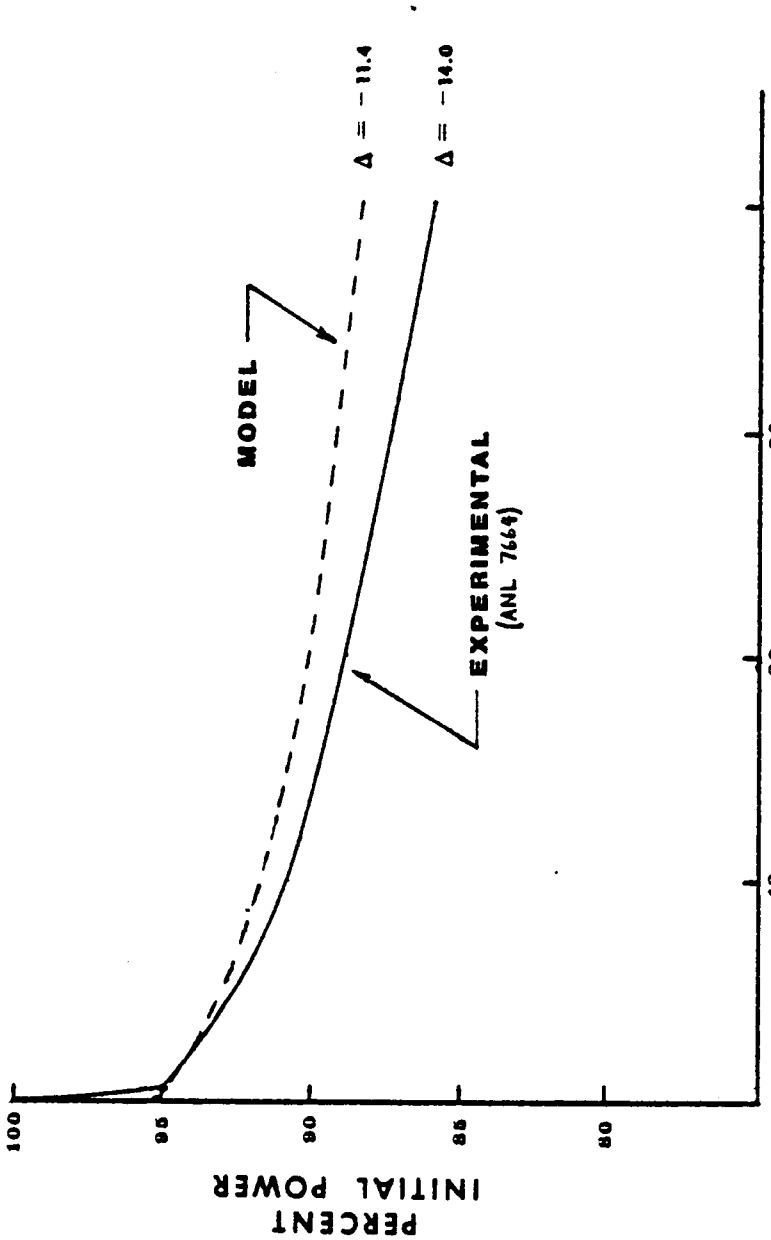


Figure 5.1 Comparison of Experimental & Model Response to -5¢ Rod Drop.

insertion and the experimental data for a -5 cent rod drop test conducted during run 33a. Data from this test were chosen due to the similarity between run 25 and 33a core loadings[11].

Differences in the experimental and predicted response during the first second are due to the difference between the actual rod insertion time of .28 seconds and the zero rod insertion time assumed by the model. Differences in the predicted and experimental responses over the remaining time can be attributed to slight differences between the actual feedback coefficients in run 33a and those (from run 25) employed in the model and to the absence of any control rod expansion or core bowing feedback mechanism in the model. The EBR-II sodium and fuel temperature coefficients of reactivity can vary by several percent from run to run[12], so that exact agreement between run 33a experimental and predicted model power response should not be expected. The significance of Figure 5.1 is to verify the general rod drop time response of the model for various core loadings. The difference between the predicted and experimental response is approximately 18.5 percent at 40 seconds after the rod drop. The MATEXP execution which generated the 38 node model response shown in Figure 5.1 employed a computational time step of 2×10^{-5} sec., and used 7.85 minutes of CPU time on an IBM 360/65 computer.

5.3 Prompt Jump Models

The development of the prompt jump model as a means of reducing computer costs was discussed in Section 4.3. A comparison of the response of the 37 node prompt jump model and the 38 order model to a

-5 cent step reactivity insertion is shown in Figures 5.2 through 5.9 Examination of the figures reveals the high degree of agreement between the predicted system response of the full 38 order and prompt jump models. The largest difference (.06°F) occurs in the predicted response of the upper reflector metal temperature. Not only does the response of the two models agree well at 40 seconds into the transient, but an examination of Figure 5.2 illustrates the extremely close agreement of the two models.

The prompt jump results shown in Figure 5.2 were generated on a Digital Equipment Corporation System 10 computer. Two problems were encountered when the IBM 360 was used for analysis of this model. The first problem involves the relative magnitudes of the A matrix elements in the prompt jump model. The ratio of the maximum-to-minimum elements is on the order of 1×10^{10}. The IBM 360/65 utilizes 32 bits to represent a real number, while the DEC 10 uses 36 bits to represent the same number. In the series representation of the $e^{A t}$ term, round-off error becomes very important, and the IBM 360/65 is not capable of maintaining the precision of the results. The IBM 360, therefore, yields an erroneous system time response for the prompt jump model. The second problem encountered with the IBM 360 analysis of the prompt jump model is related to the increase in the number of nonzero A matrix elements produced by this model. The 38 node model has only 44 nonzero A matrix elements, while the prompt jump model has 97 nonzero elements. The IBM 360/65 requires a significantly longer time to evaluate the product of two nonzero floating-point numbers than it requires to multiply by zero. In the case of the EBR-II model,

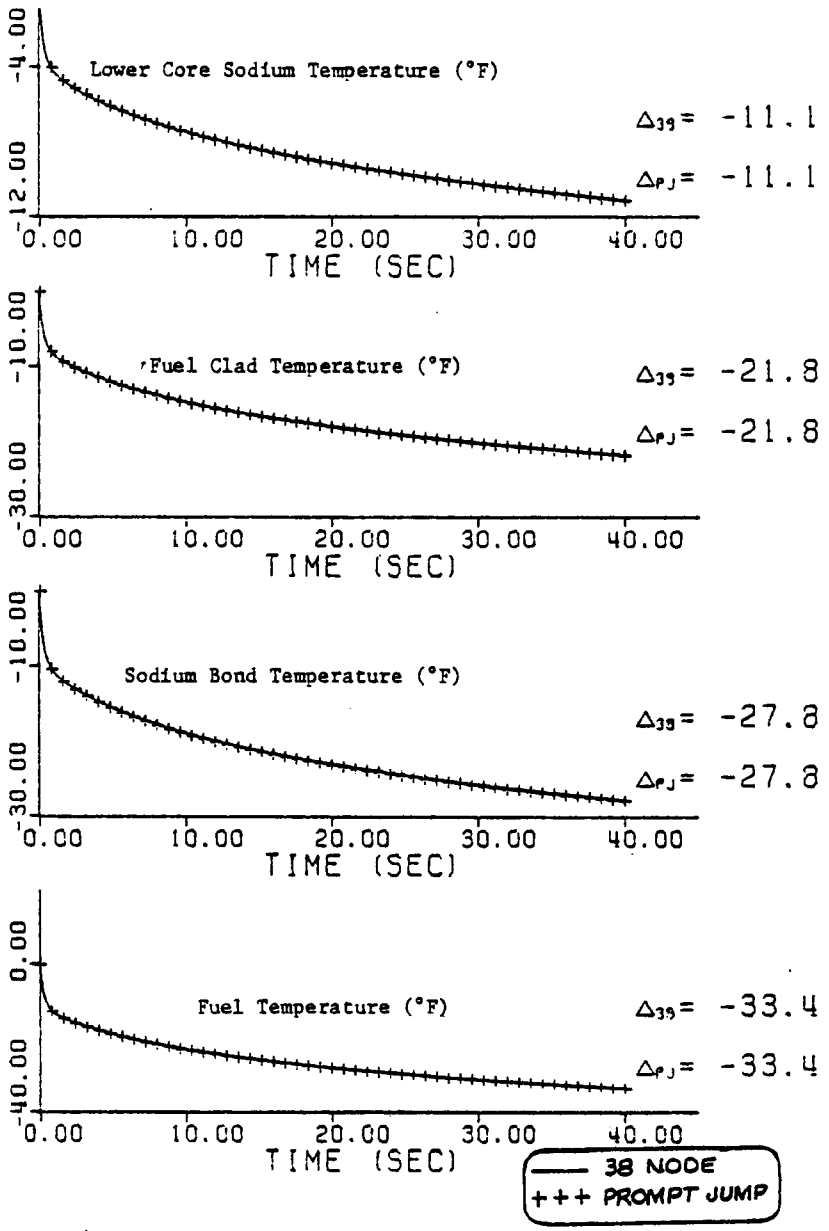


Figure 5.2 Response of the 37 Node Prompt Jump and 38 Node Models To $\delta\rho$ = -5 cents.

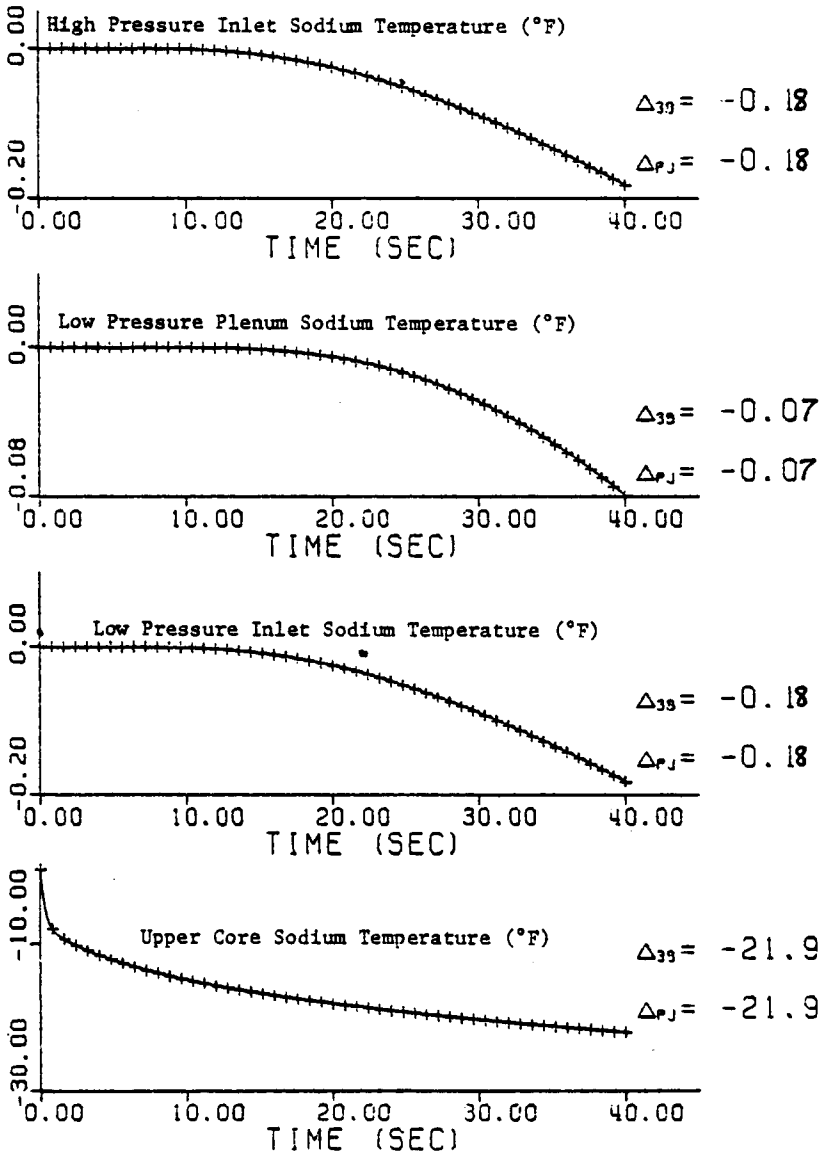


Figure 5.2 (continued)

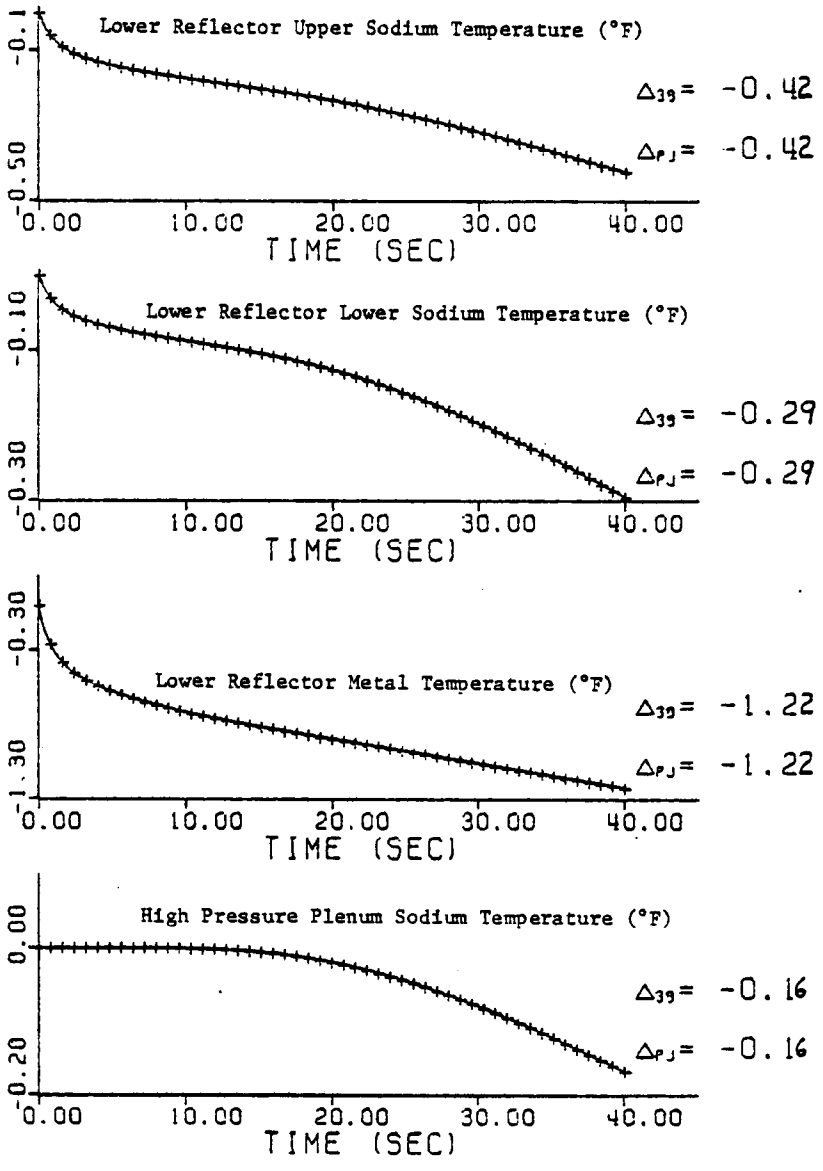


Figure 5.2 (continued)

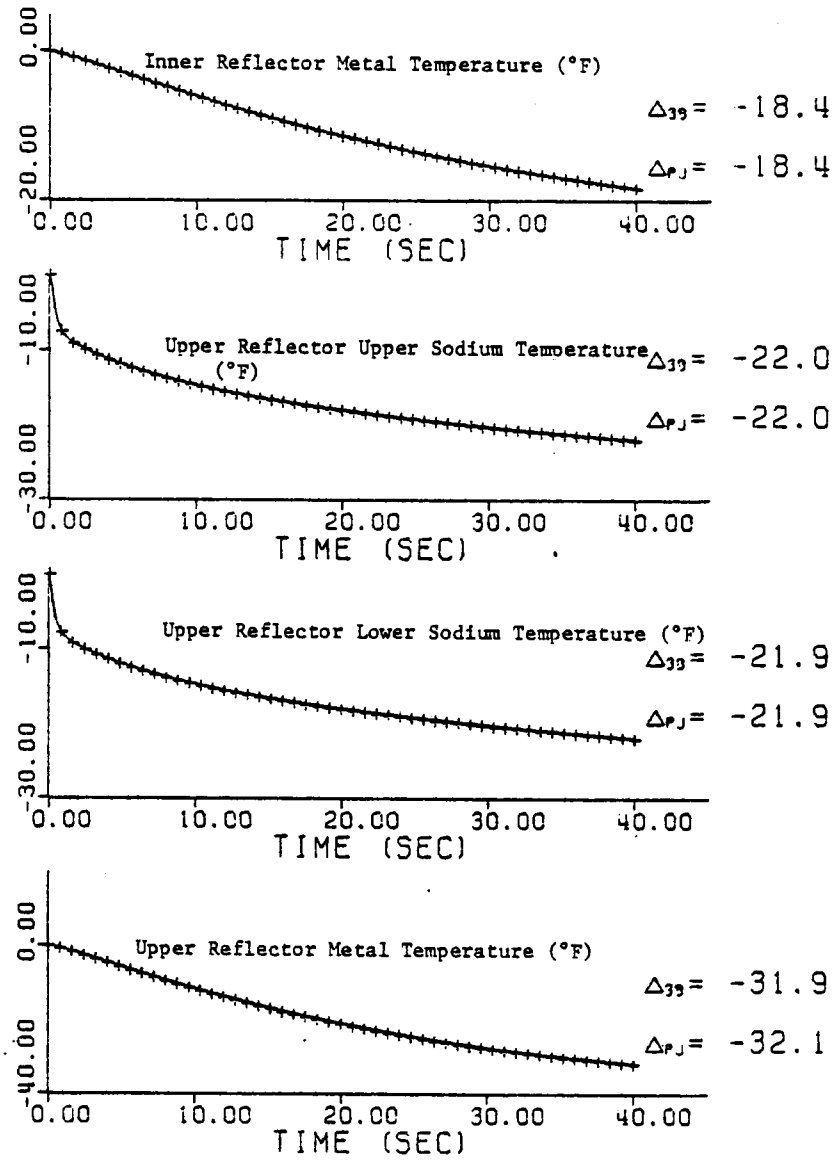


Figure 5.2 (continued)

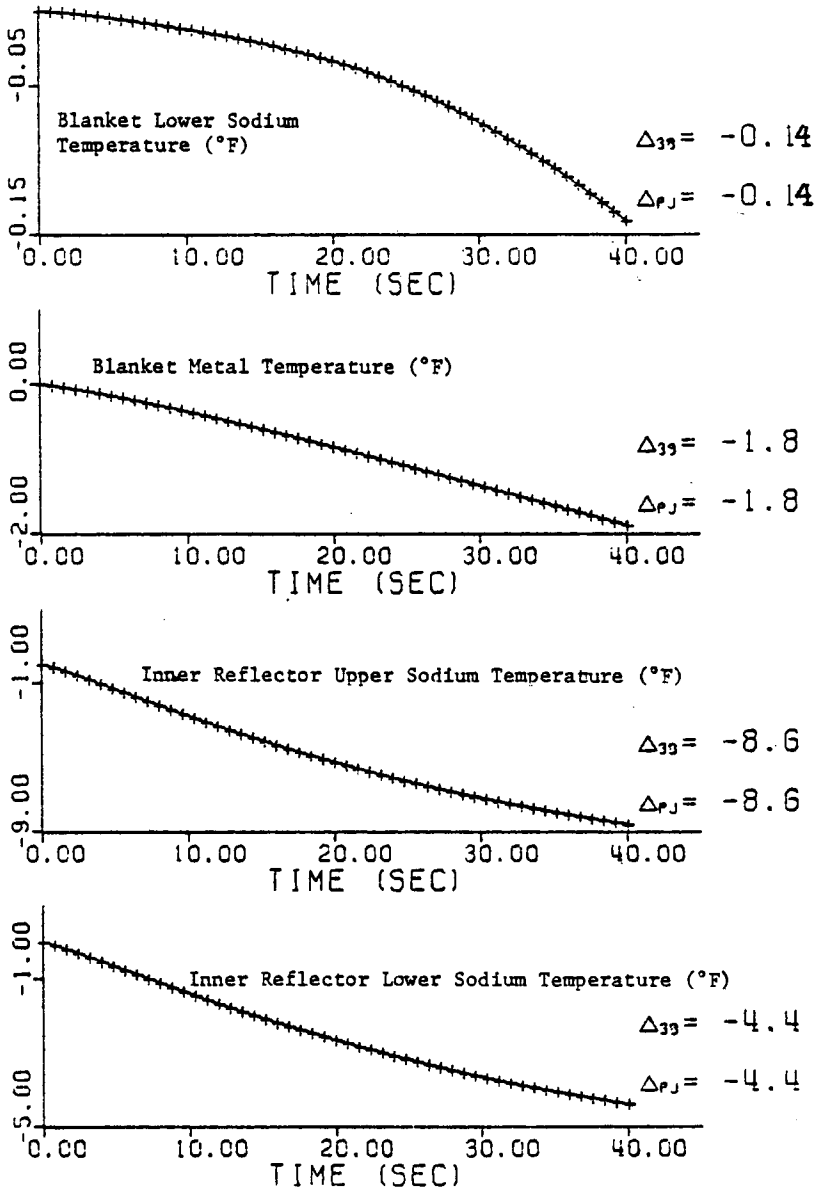


Figure 5.2 (continued)

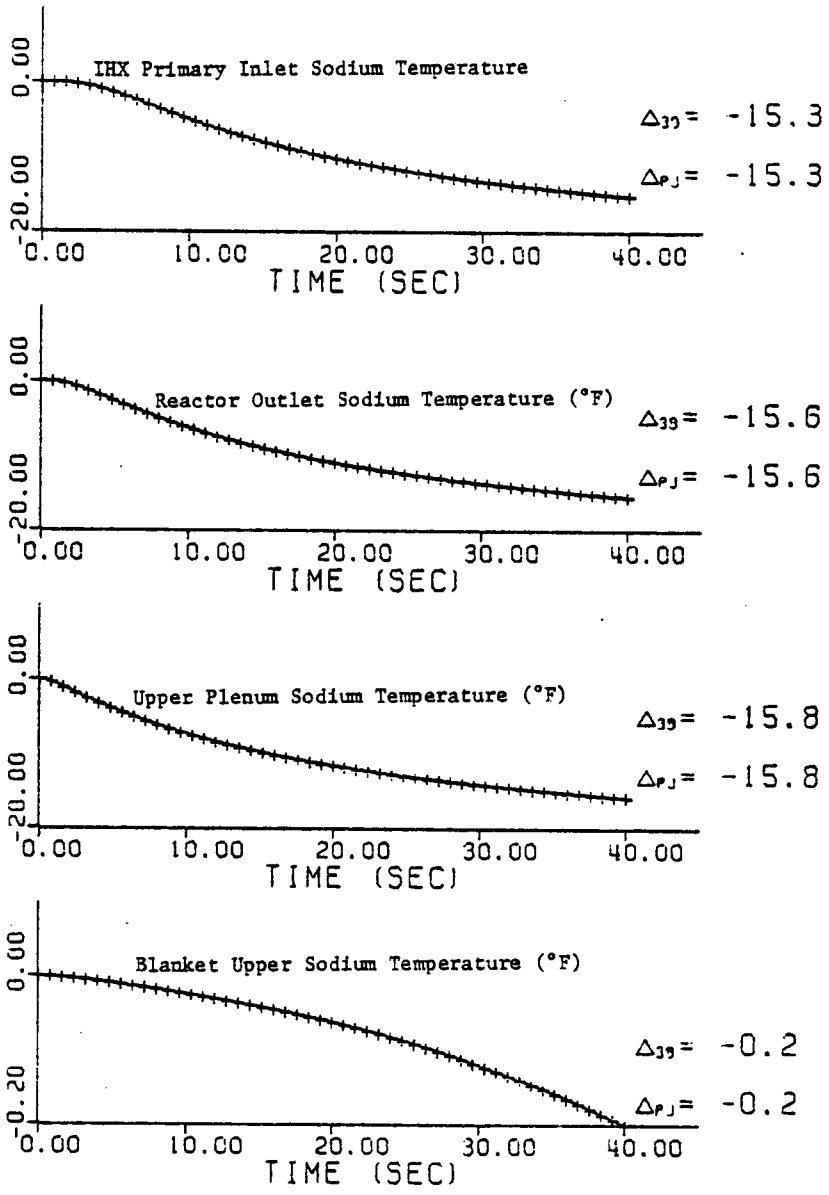


Figure 5.2 (continued)

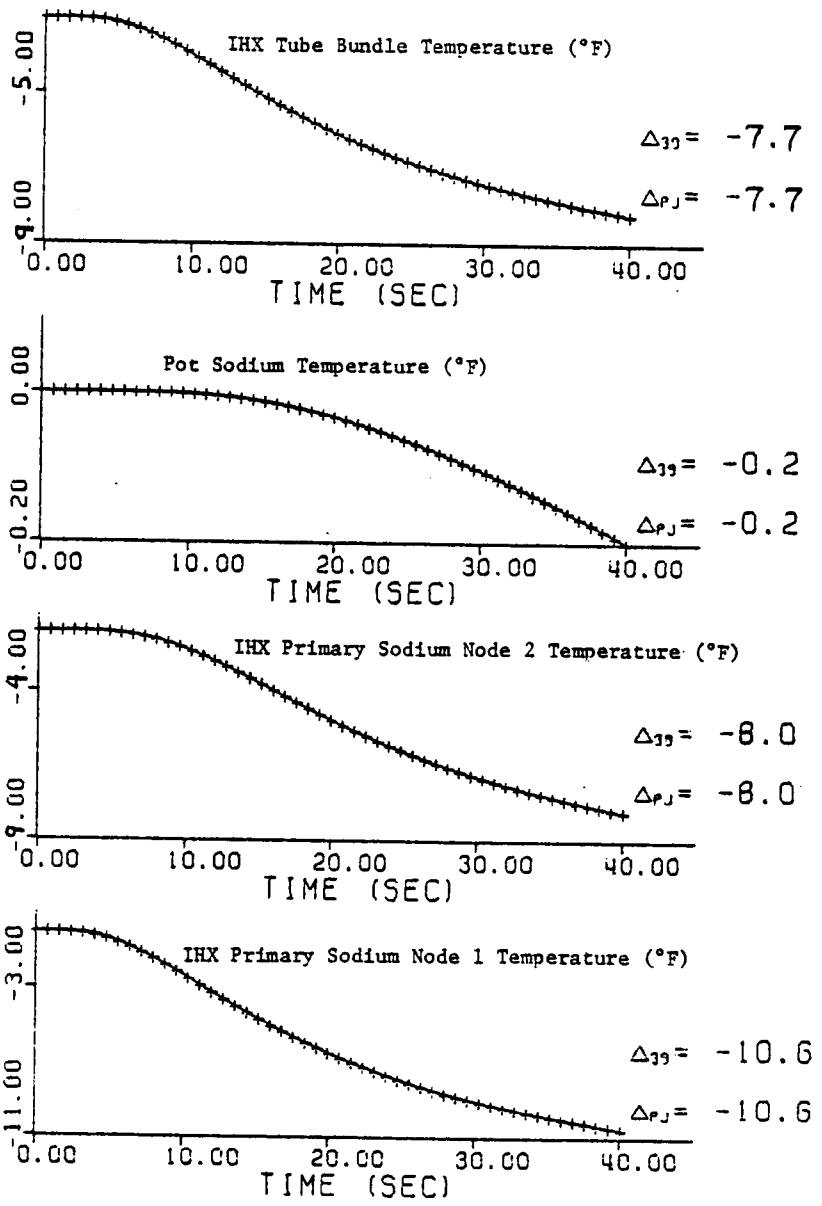


Figure 5.2 (continued)

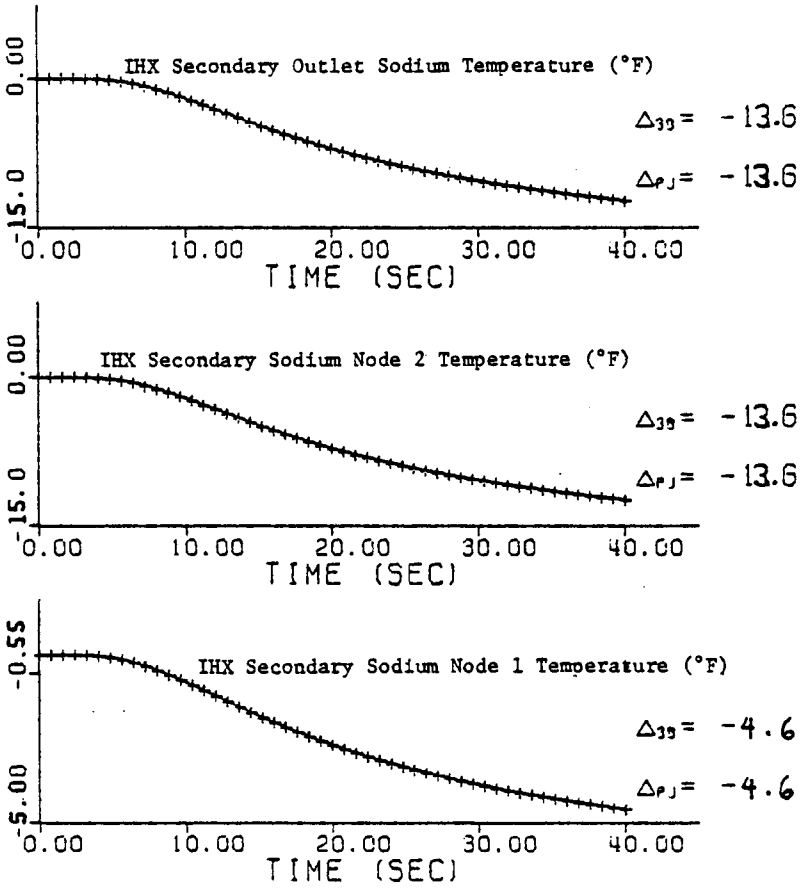


Figure 5.2 (continued)

it is apparent that the increased computational time increment of .0012 seconds does not compensate for the increased amount of time required for matrix multiplication.

After the results of the 37th order prompt jump model were obtained, it was decided to attempt to improve the results of the IBM 360/65 prompt jump analysis by depopulating the A matrix. This was accomplished by simply zeroing out any positive matrix element whose magnitude was less than 10^{-4}. Depopulating the system A matrix reduces the computer time requirement in two ways: (1) by reducing the amount of time required to read the input data, (2) by reducing the amount of time required to calculate the $e^{A\,t}$ term (Section 4.2). The precision problem is overcome by reducing the ratio of the maximum-to-minimum A matrix element to approximately 2×10^{7}. The time response of this "reduced" prompt jump model to a -5 cent reactivity step is shown in Figure 5.3 along with the full 38th order model response. A careful examination of these figures indicates that almost all of the predicted reduced prompt jump model temperatures are within 2°F of their companion 38 node response. The notable exceptions to this behavior are the response of the inner reflector and GAM5 and GAM6 coolant temperatures, which differ from the 38 node response by approximately 15°F, 3.5°F and 7°F, respectively. The difference in these responses can be explained by the fact that in the depopulating procedure, the terms in the inner reflector metal temperature equation which couple it to the precursor equations (and therefore the reactivity perturbation) were deleted due to their low magnitude. The inner reflector produces approximately

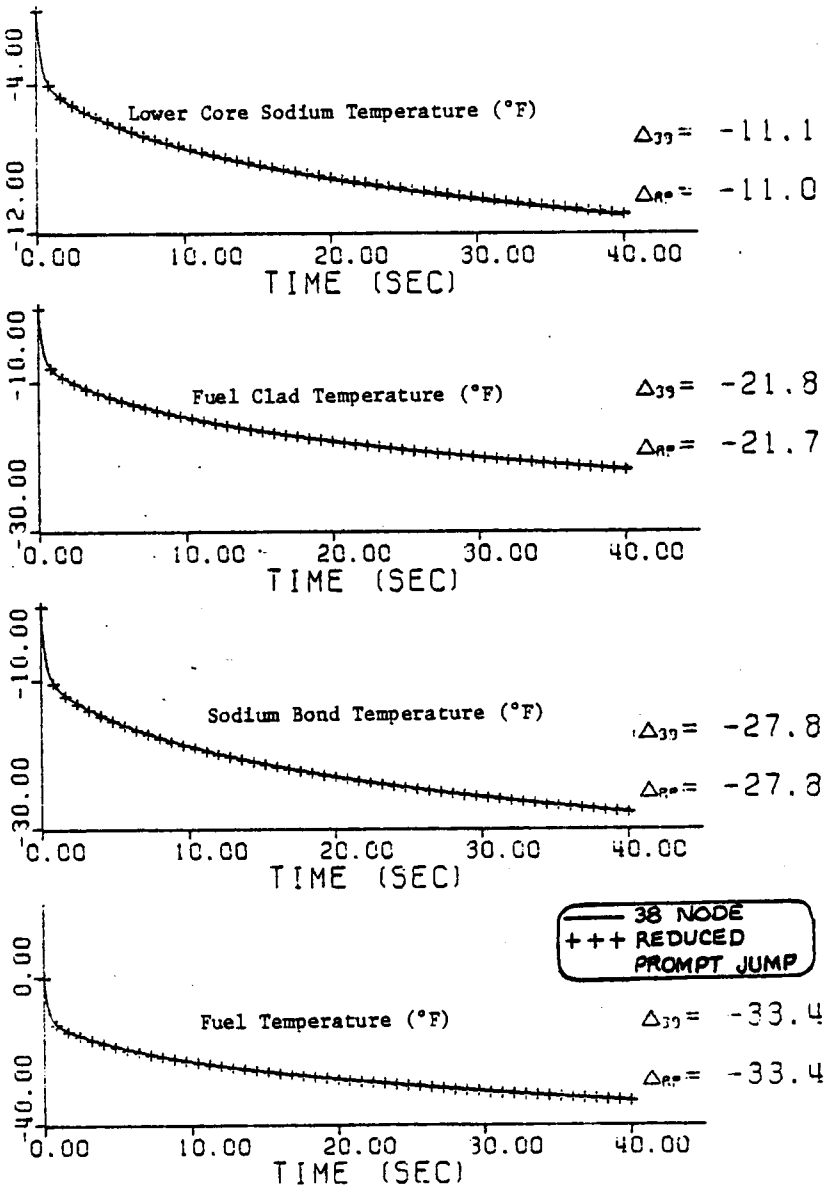


Figure 5.3 Response of Reduced Prompt Jump and 38 Node Models to $\delta\rho$ = -5 cents.

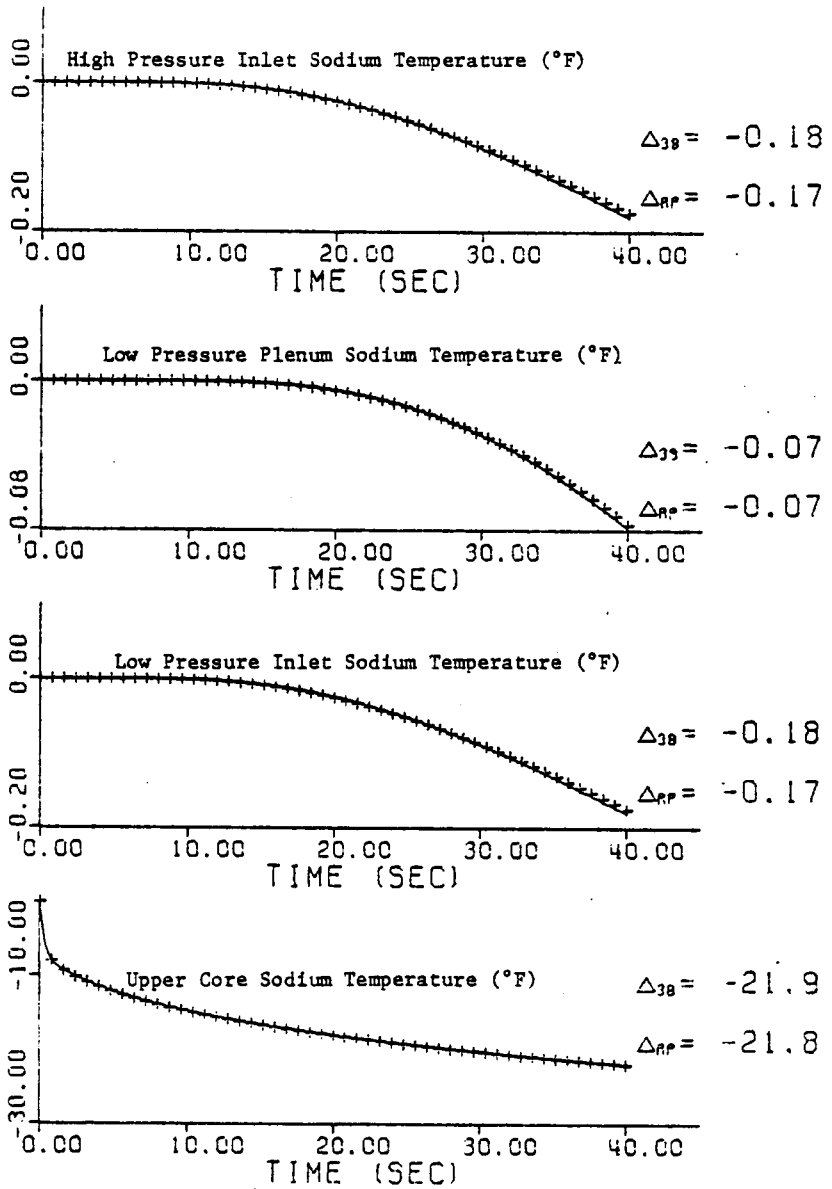


Figure 5.3 (continued)

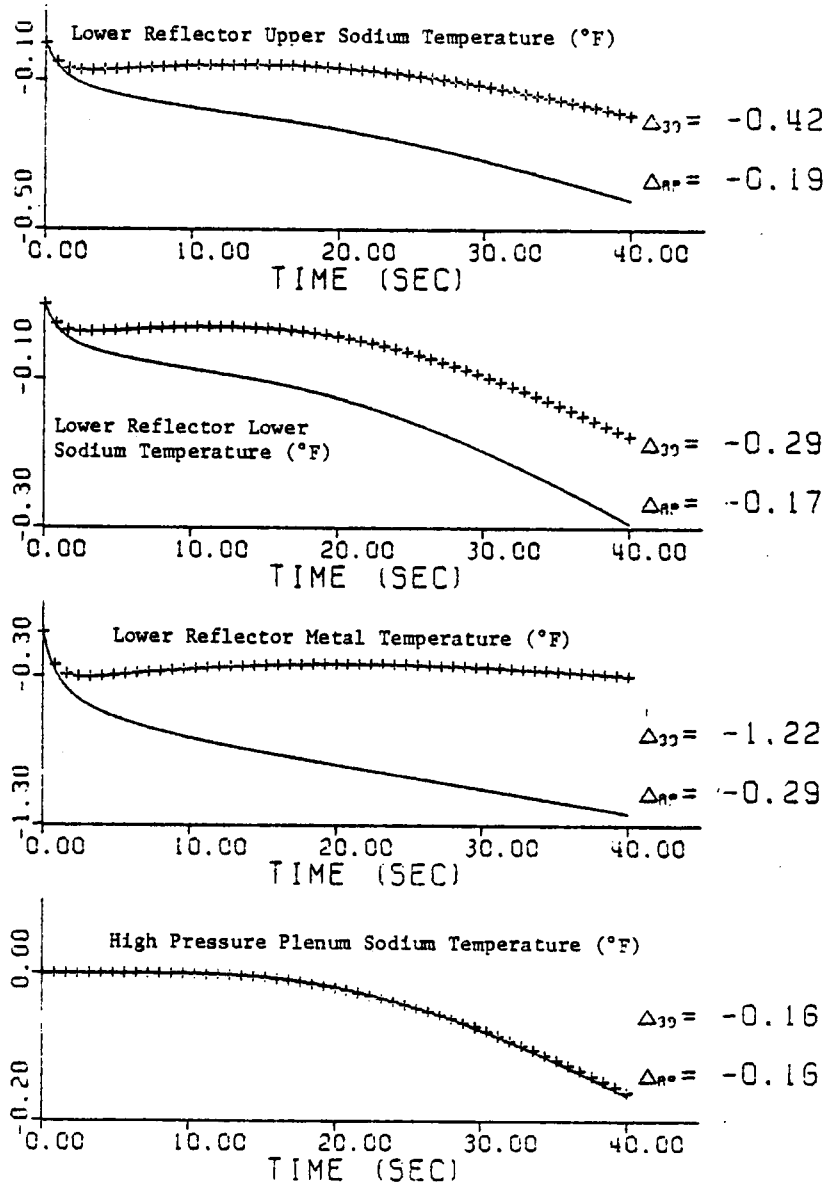
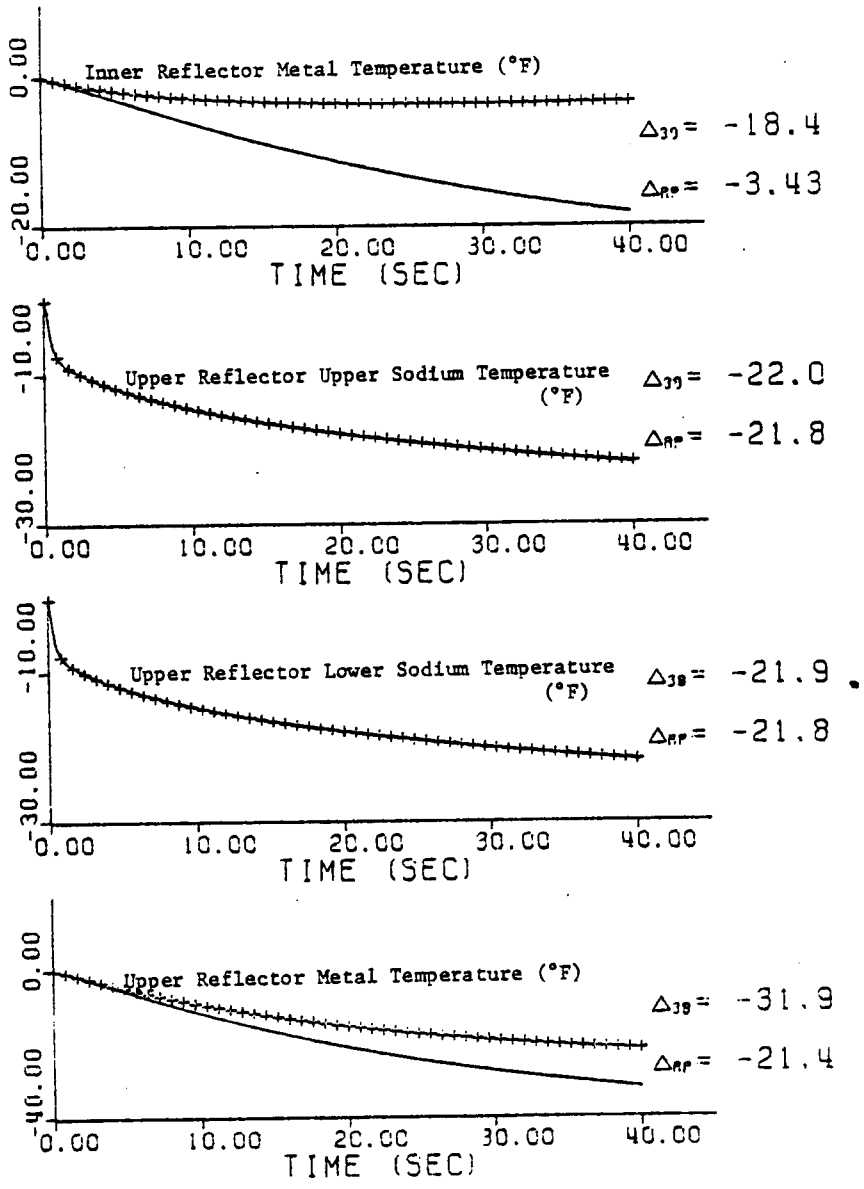


Figure 5.3 (continued)



Δ_{33} = -18.4

Δ_{RR} = -3.43

Δ_{33} = -22.0

Δ_{RR} = -21.8

Δ_{33} = -21.9

Δ_{RR} = -21.8

Δ_{33} = -31.9

Δ_{RR} = -21.4

Figure 5.3 (continued)

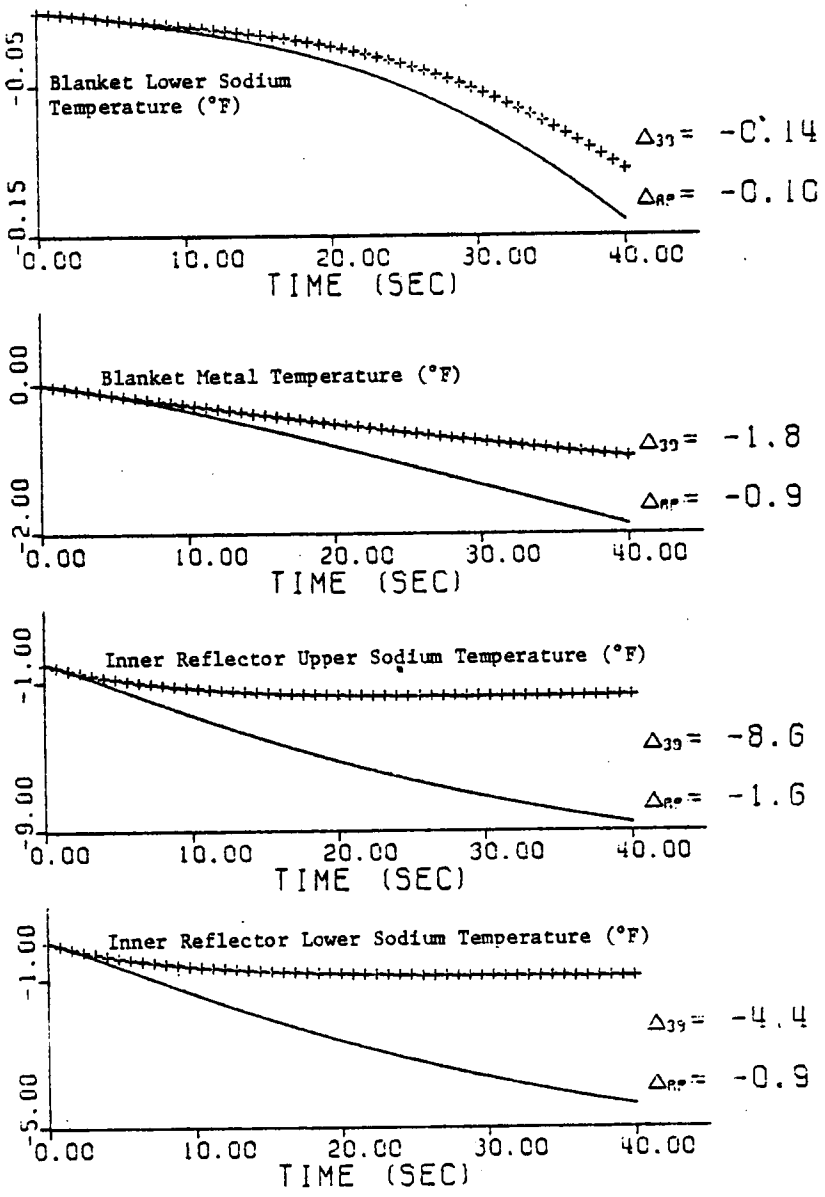


Figure 5.3 (continued)

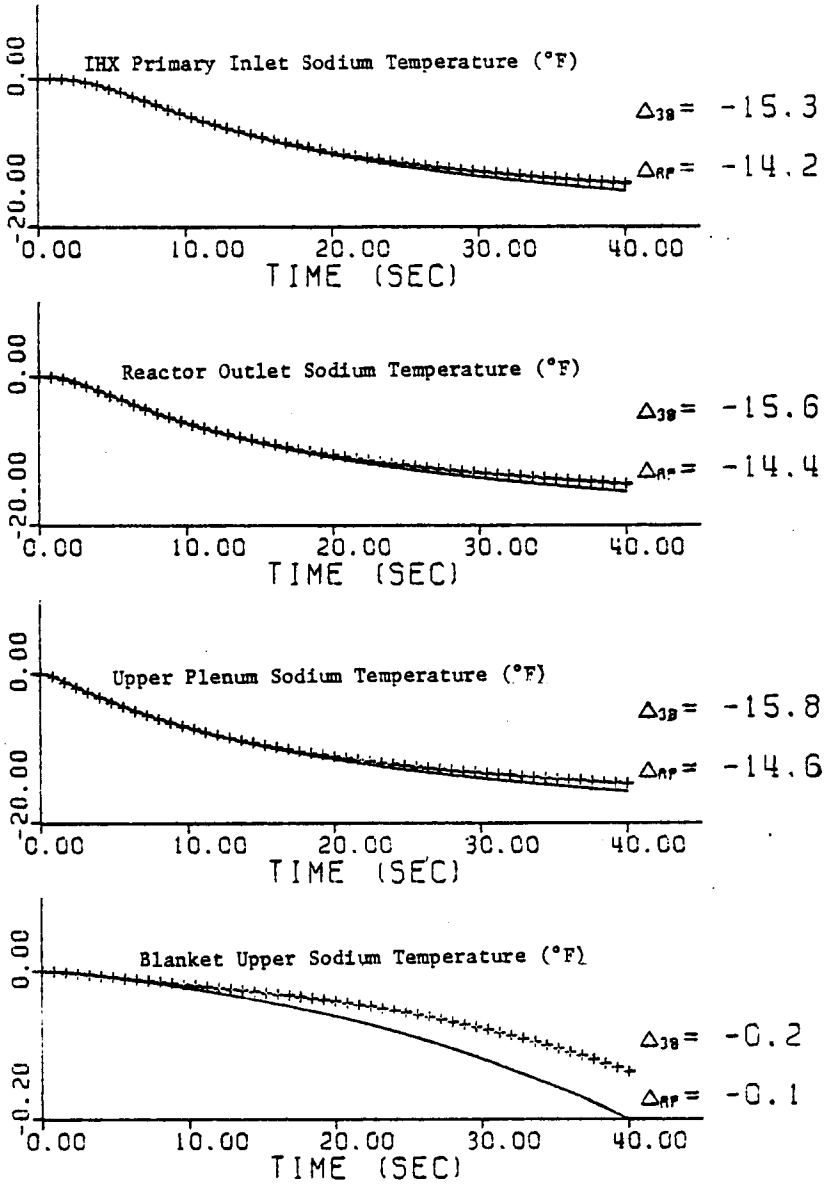


Figure 5.3 (continued)

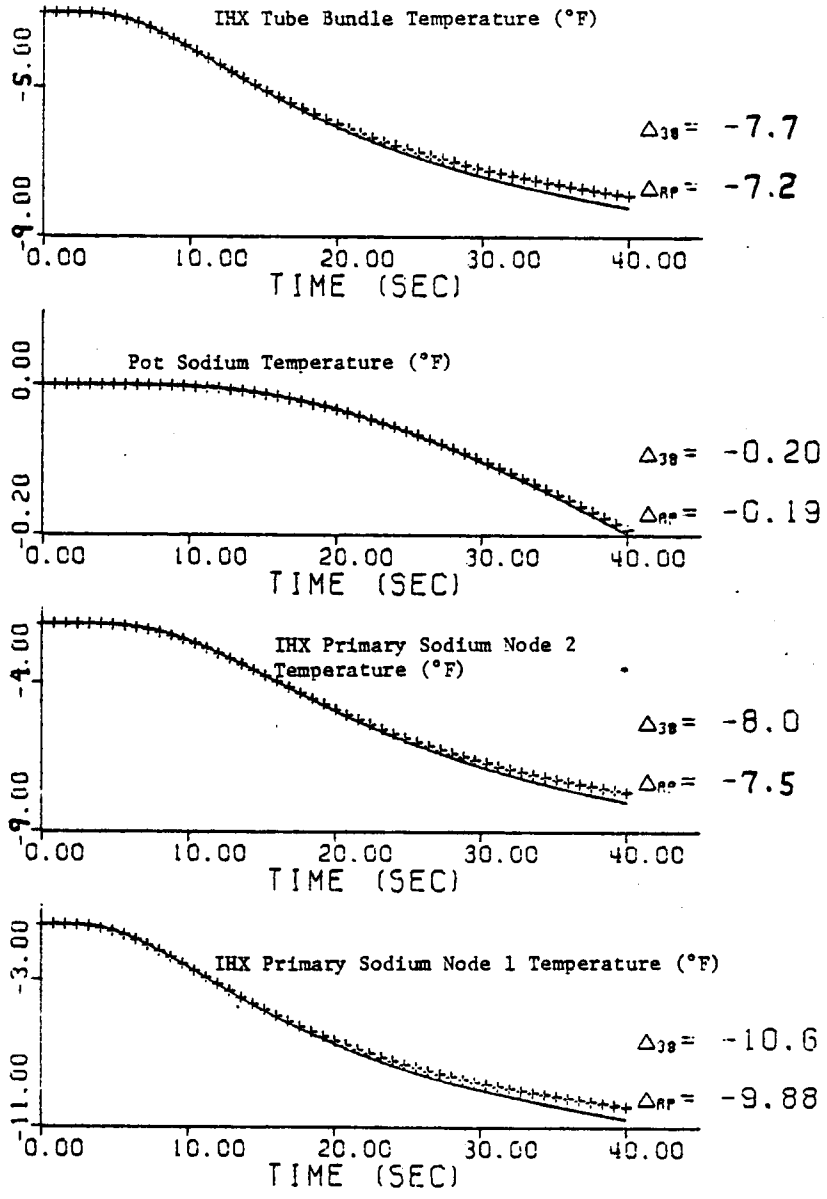


Figure 5.3 (continued)

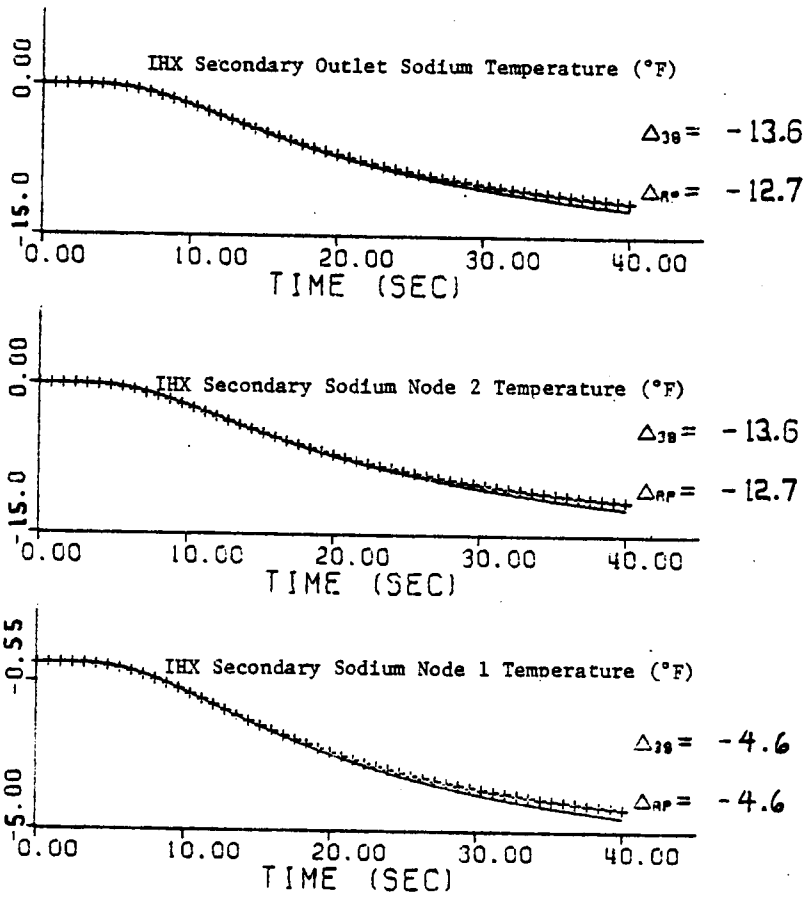


Figure 5.3 (continued)

9% of the total EBR-II thermal power, and it is evident that the precursor coupling terms in the inner reflector metal temperature equation cannot be deleted (regardless of their magnitude) if one hopes to simulate the time response of this core region accurately. It is worth noting that even though the predicted inner reflector metal temperature of the full and prompt jump models differ by as much as 15°F, their predicted reactor coolant outlet temperature differs by only approximately 1.2°F. The IBM 360/65 execution for this reduced prompt jump model used only 3.6 minutes of cpu time - a 46% savings compared to that needed for the full 38 order model.

5.4 System Stability

As discussed in Section 4.6, the stability of a given physical system can be determined once the eigenvalues of the system A matrix are known. The stability of a system model is assured if the real parts of all of the eigenvalues of the system A matrix are negative. When used with a verified system model, this procedure is very helpful in determining the stability of the system. Table 5.1 lists the calculated eigenvalues of the 38 node model. The real parts of all the eigenvalues are negative, thus indicating that the unoptimized 38 node model represents a stable system. Table 5.2 lists the calculated eigenvalues of the prompt jump model. The real part of each of the eigenvalues is negative. It is also apparent that the large negative eigenvalue (-46955.03) is eliminated by the prompt jump formulation, thereby enabling one to use a much larger time increment in the MATEXP analysis.

TABLE 5.1

38 NODE MODEL EIGENVALUES

	Eigenvalues	
No.	Real	Imaginery
1	-857.2801	
2	-46955.0302	
3	-34.1164	
4	-90.7431	
5	-21.7477	
6	-25.9863	
7	-18.5649	
8	-19.4388	
9	-18.9861	
10	-7.4223	
11	-9.6871	
12	-5.6379	
13	-6.8315	
14	-3.9355	-.1960
15	-3.9355	+.1960
16	-4.0001	
17	-1.8333	
18	-1.9011	
19	-1.2776	
20	-1.3319	
21	-1.1447	
22	-.7061	
23	-.6210	-.0753
24	-.6210	.0753
25	-.5551	
26	-.4169	-.0559
27	-.4169	.0559
28	-.2261	-.0294
29	-.2261	.0294
30	-.1806	
31	-.0827	
32	-.0850	
33	-.0618	
34	-.0651	
35	-.0102	
36	-.0193	
37	-.0017	
38	-.0080	

TABLE 5.2

37 NODE PROMPT JUMP MODEL EIGENVALUES

	Eigenvalues	
No.	Real	Imaginery
1	-391.0711	
2	-845.2506	
3	-875.9375	
4	-26.6455	
5	-28.0800	
6	-21.7716	
7	-19.1397	-.2741
8	-19.1397	.2741
9	-18.6718	
10	-7.1821	
11	-9.6809	
12	-5.6313	
13	-6.8361	
14	-3.6775	
15	-4.0089	
16	-1.8392	
17	-1.9018	
18	-1.2200	
19	-1.1373	
20	-1.3261	
21	-.6159	-.0553
22	-.6159	.0553
24	-.5548	
25	-.4565	
26	-.3806	
27	-.2512	
28	-.1962	
29	-.1789	
30	-.0149	
31	-.0838	
32	-.0080	
33	-.0697	
34	-.0008	-.0006
35	-.0008	.0006
36	-.0656	
37	-.0618	

Stability margins were discussed in Section 4.6. The most common stability margin is the phase margin. A phase margin of at least 20 degrees is desirable. Figure 5.4 is a Nyquist plot of the quantity (1+GH) for the 38 node model. From the definition of the phase margin (Section 4.6), it is apparent that the expected phase margin of the EBR-II is approximately 180 degrees. This large phase margin implies that a substantial amount of prompt, negative feedback is present in EBR-II. The actual EBR-II phase margin will probably be somewhat smaller than this value, since it is probable that the empirical value is significantly influenced by the structural steel feedback component (Table 3.2). The model assumes that all the structural steel within the core has the same temperature as that of the fuel cladding, and therefore probably over estimates the actual amount of negative feedback from structural steel expansion.

5.5 System Time Response to Ten Cent Reactivity Step

The time response of the system variables to a reactivity step of 10 cents is given in Figure 5.5. From the time response of reactor power one can see the prompt jump in power at time t=0. The model response shows the reactor power jumping by a factor of 1.099 within the first two seconds after the perturbation. The remainder of the power transient is very smooth and well behaved due to successive inputs of fuel expansion, structural steel expansion, core coolant, upper reflector coolant, inner reflector coolant, and lower reflector coolant negative reactivity feedbacks. As the various materials within the reactor undergo temperature transients, their size and density also change, thus altering their neutron transport

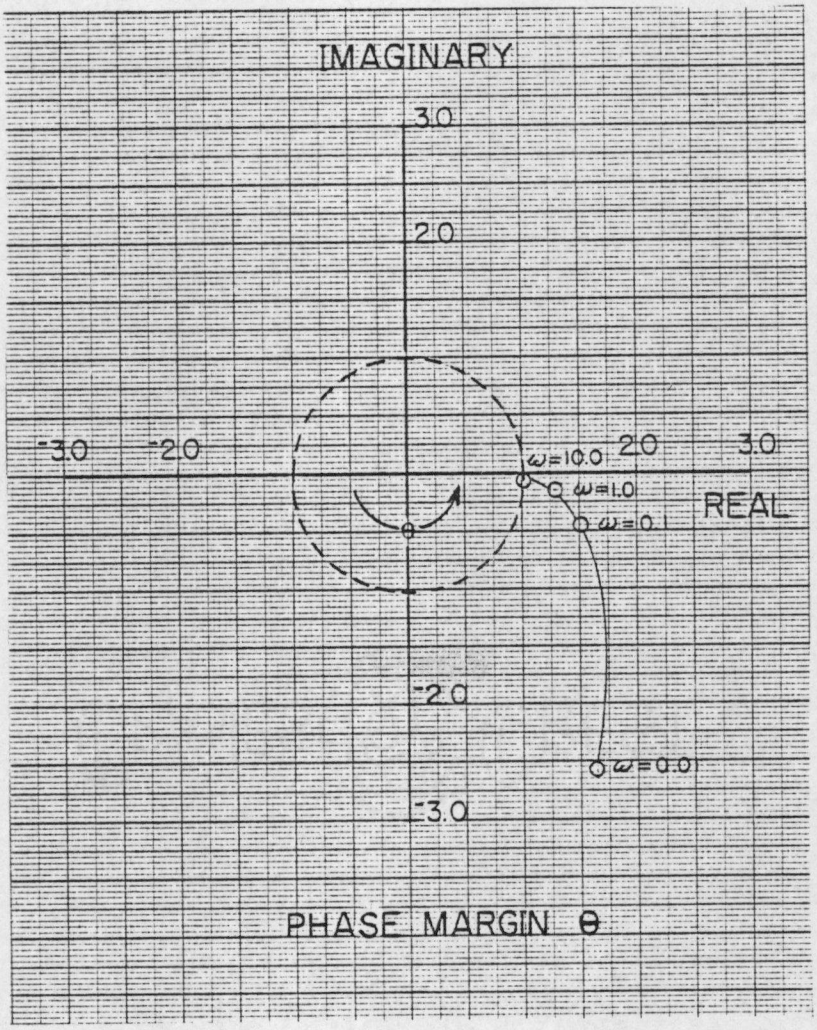


Figure 5.4 Predicted EBR-II Stability Margin.

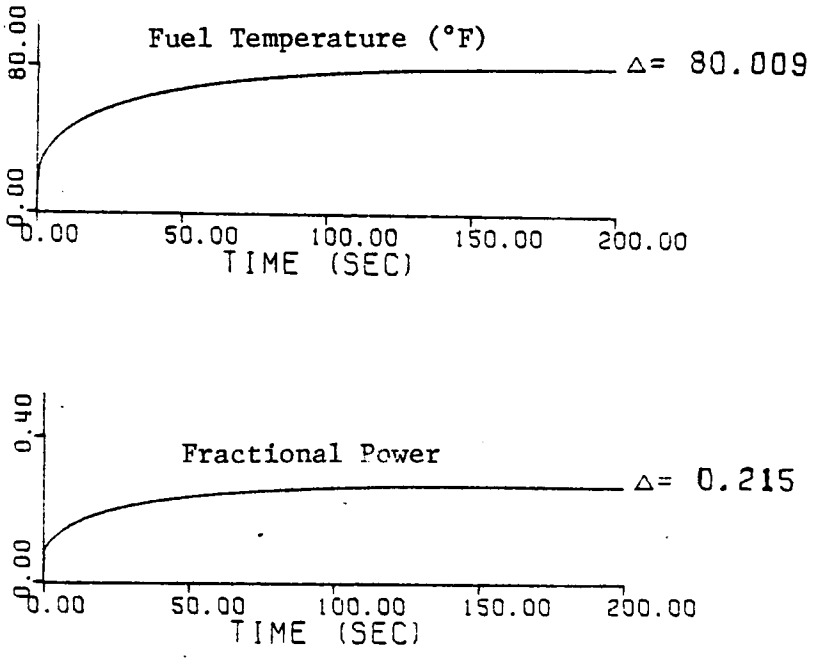


Figure 5.5 EBR-II 38 Node Model Response to $\delta\rho$ = +10¢.

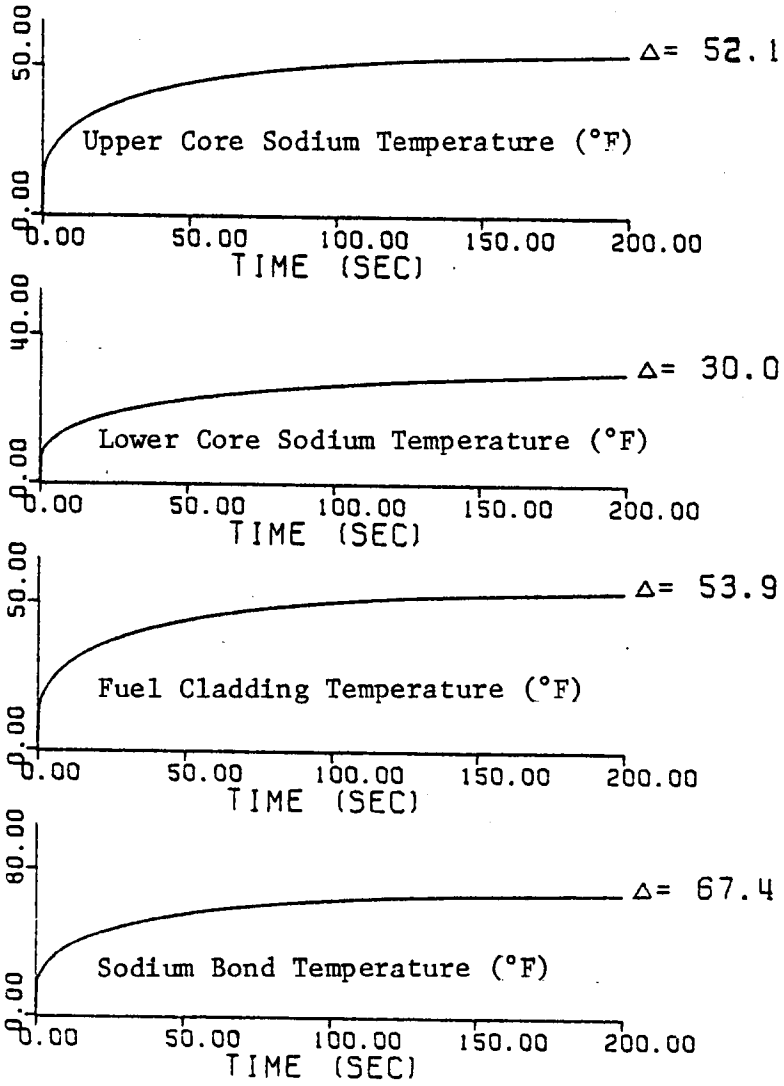


Figure 5.5 (continued)

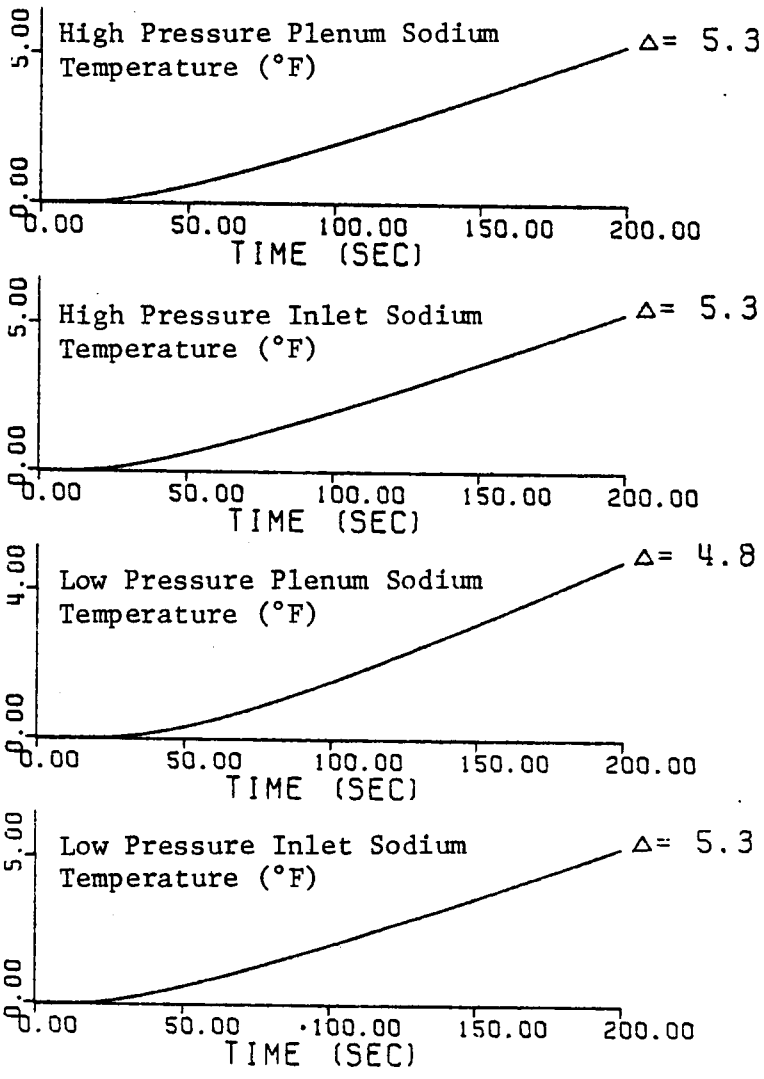


Figure 5.5 (continued)

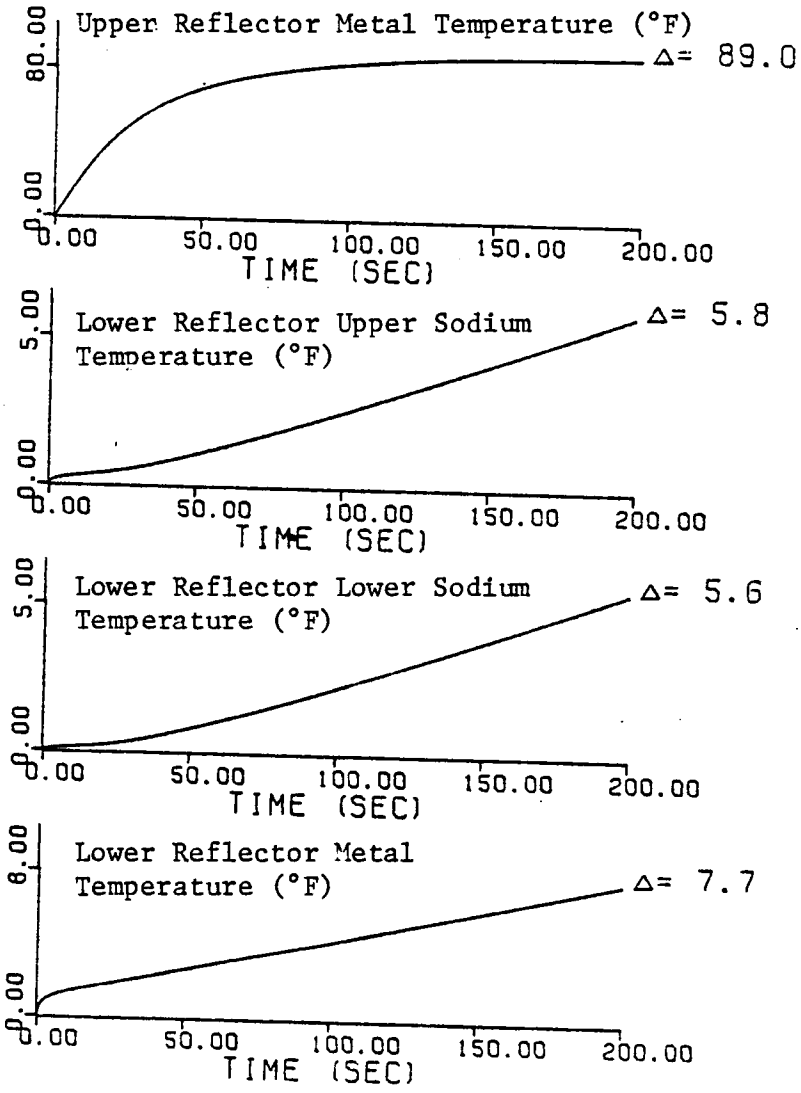


Figure 5.5 (continued)

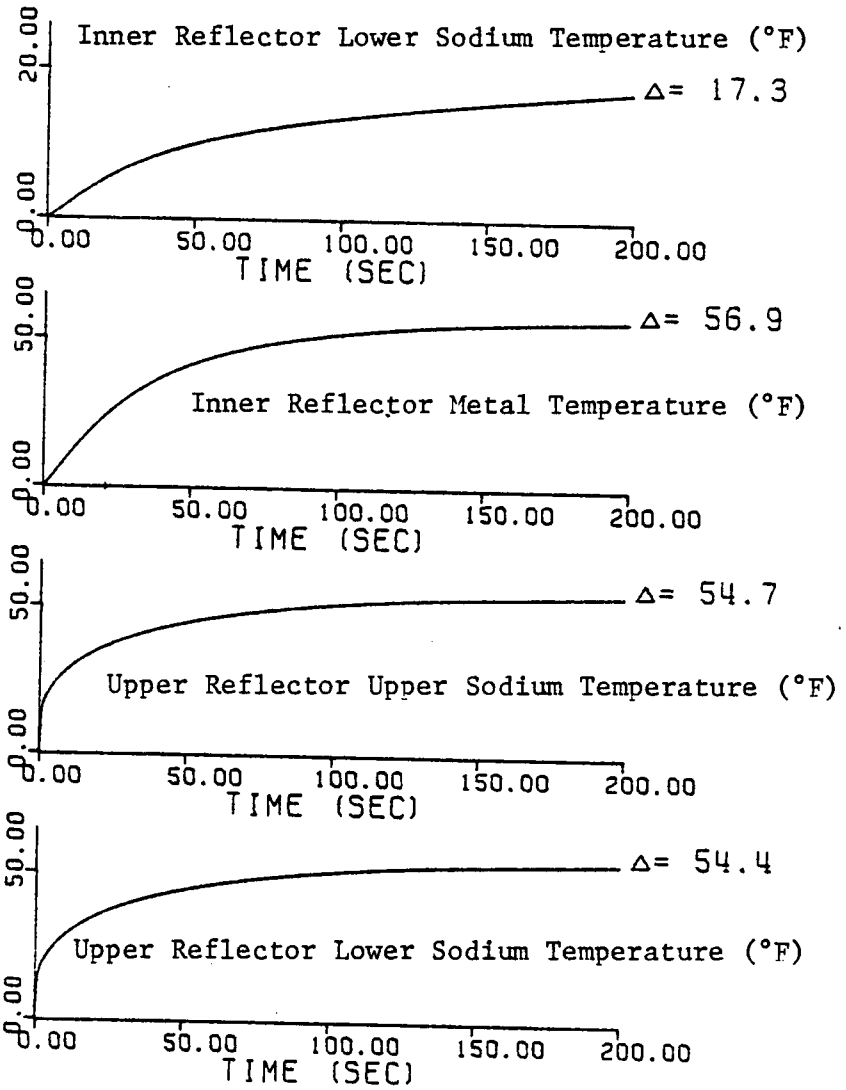


Figure 5.5 (continued)

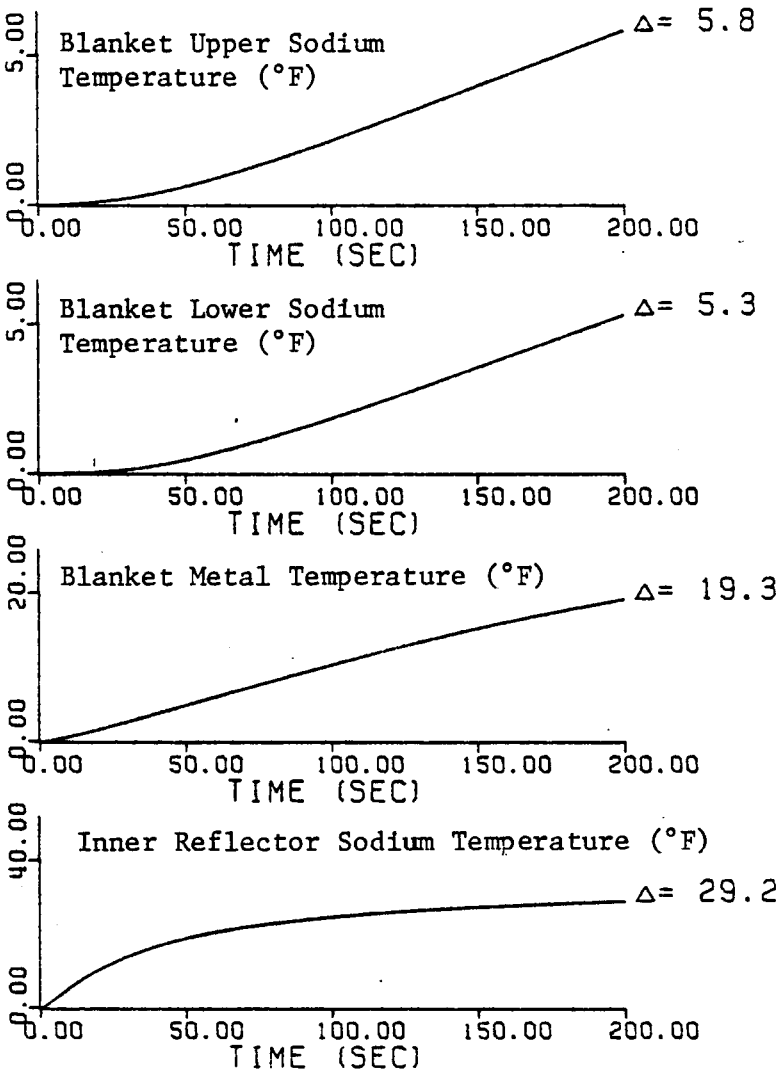


Figure 5.5 (continued)

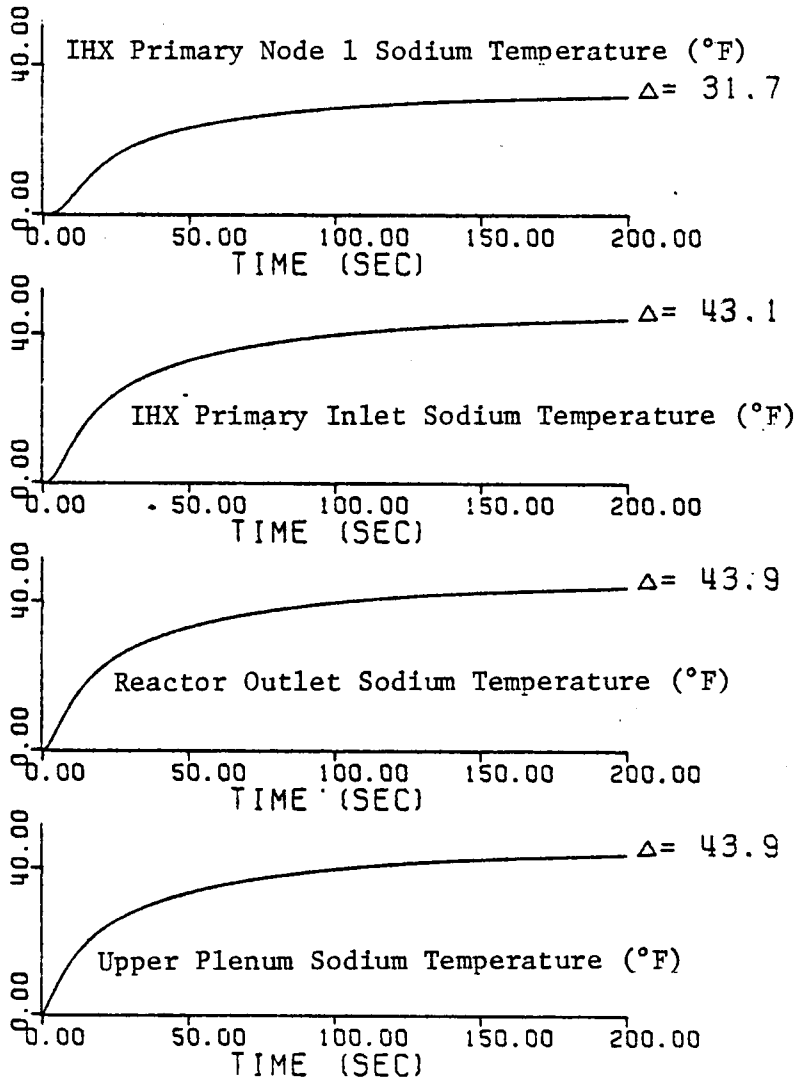


Figure 5.5 (continued)

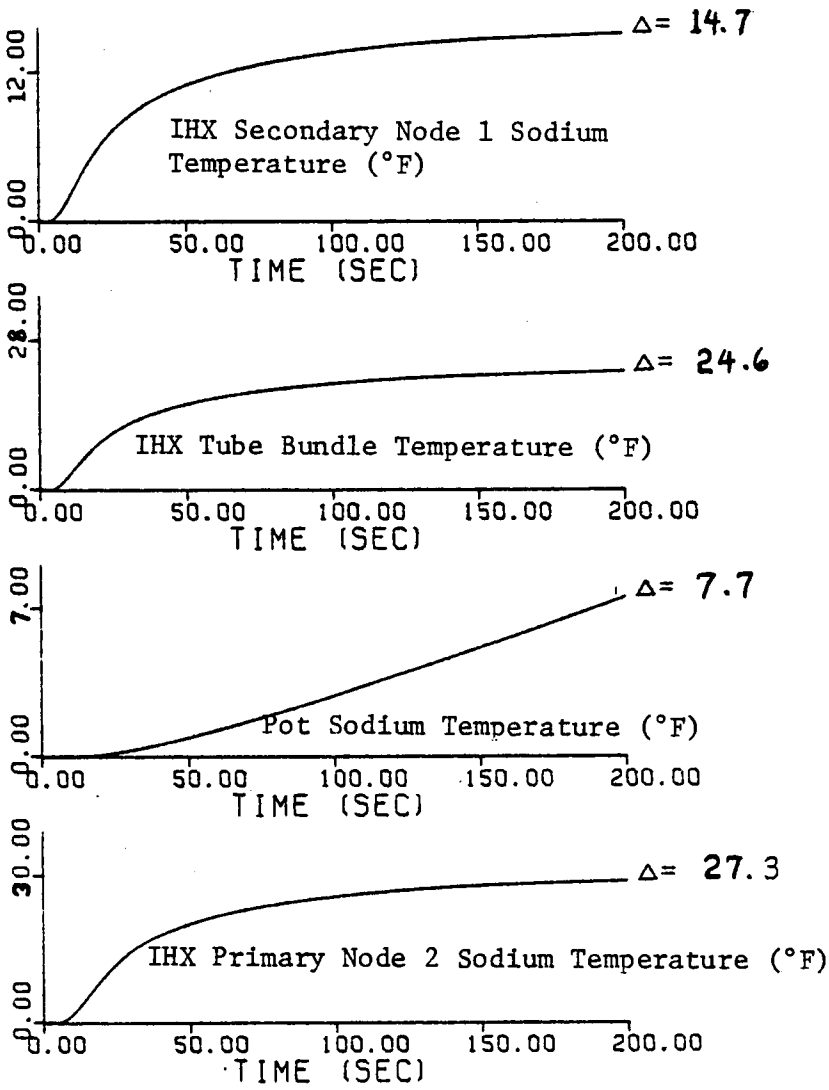


Figure 5.5 (continued)

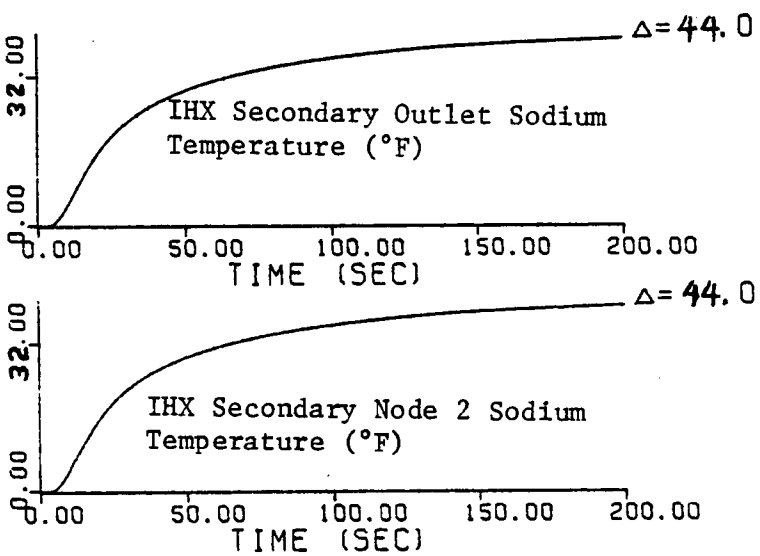


Figure 5.5 (continued)

properties, and introducing reactivity. The new steady state power level is therefore determined by both the reactivity input and the negative temperature coefficients of reactivity. The power level shown at t=200 seconds ($\frac{\partial P}{P_o}$ =.265) is not the steady state value. Because of the high computing cost involved with calculating steady state responses in the time domain, an alternate method is used to obtain these new steady state values. One can obtain an accurate estimate of the new steady state value of power (or any other state variable) following a step input, by simply observing the zero frequency gain of the state variable for the same perturbation.

The step response of a state variable at infinite time is numerically equivalent to the product of the magnitude of the gain of the state variable for the same perturbation at zero frequency, and the value of the forcing function in dollars. This can be proven with the aid of the final value theorem. The final value theorem states that for any function of time, F(t),

$$\lim_{t \to \infty} F(t) = \lim_{s \to 0} s\,F(s) \qquad (5.1)$$

where

s = The Laplace domain Variable

F(s) = The Laplace transform of F(t).

Now, let F(t) "equal O(t), the response of the power to a step input,"

$$\lim_{t \to \infty} O(t) = \lim_{s \to 0} s\,O(s) \qquad (5.2)$$

$$= \lim_{s \to 0} s\,G(s)\,I(s). \qquad (5.3)$$

But for a step input,

$$I(s) = \frac{C}{S} \qquad (5.4)$$

where C is the magnitude of the step.

Therefore,

$$\lim_{t \to \infty} O(t) = \lim_{s \to 0} sG(s)\frac{C}{s} \qquad (5.5)$$

and,

$$\lim_{t \to \infty} O(t) = \lim_{s \to 0} G(s)C \qquad (5.6)$$

For frequency response calculations, $s=j\omega$, where ω is the frequency in radians per second. Therefore, as $s \to 0$, $\omega \to 0$, and it is apparent that at infinite time, step response is just equal to the product of the magnitude of the step and the frequency response gain at zero frequency. These steady state time responses will be discussed in more detail in Section 5.6.

The remainder of Figure 5.5 shows the simultaneous responses of the remainder of the system state variables to the 10 cent step. The response of the reactor inlet sodium temperature is of particular interest. Note that while most of the reactor region material temperatures appear to have almost stabilized, the temperatures of both the low and high pressure reactor inlet sodium are increasing at a rate of about two degrees per minute. This behavior can be traced to the primary sodium reservoir or "pot." One can see that while the temperature of the IHX primary sodium exhausting into the pot has almost stabilized at roughly 19.3°F above its original value, the temperature of the sodium within the pot is still increasing by roughly two degrees per minute. This behavior of the pot sodium temperature is due to the extremely long residence time of the sodium within the pot (approximately 553 seconds). The net physical effect of the sodium pot is to add thermal (and therefore reactivity) inertia to

the system. This behavior of the reactor inlet temperature following a reactivity perturbation should be considered a generic characteristic of pot type LMFBR's.

5.6 System Frequency Response for Reactivity Perturbations

The frequency response of the system state variables to reactivity perturbations at the 50 MW(t) power level is shown in Figures 5.6 and Appendix B, Figures B.1 through B.32. The zero power frequency response of the model is shown in Figure 5.7. Upon comparison of the zero power frequency response and the 50 MWt frequency response (Fig. 5.6), one sees that at lower frequencies ($\omega \leq .001$ rad/sec.), substantial negative feedback holds the system gain (percent change in power/cent reactivity) down substantially below the zero power gain. As the frequency increases, time constants of the various heat transfer processes are exceeded, and the amount of feedback being introduced into the reactor decreases. This effect can be seen in the 50 MWt frequency response (Fig. 5.6) over the 10^{-3} to 5×10^{-2} rad/sec. range. As the frequency increases from 10^{-3} rad/sec, the 50 MWt gain begins to approach that of the zero power gain due to decreased negative feedback. As the frequency continues to increase, the 50 MWt gain behaves like a zero power reactor, approaching a gain of unity at a frequency of 10 rad/sec. At some frequency greater than 70 rad/sec., the gain of the system would again break down and go asymptotically to zero, as the gain of all physical systems must do as the frequency increases towards infinity.

As previously described in Section 5.5, the steady state time response of the system to a given perturbation is equal to the

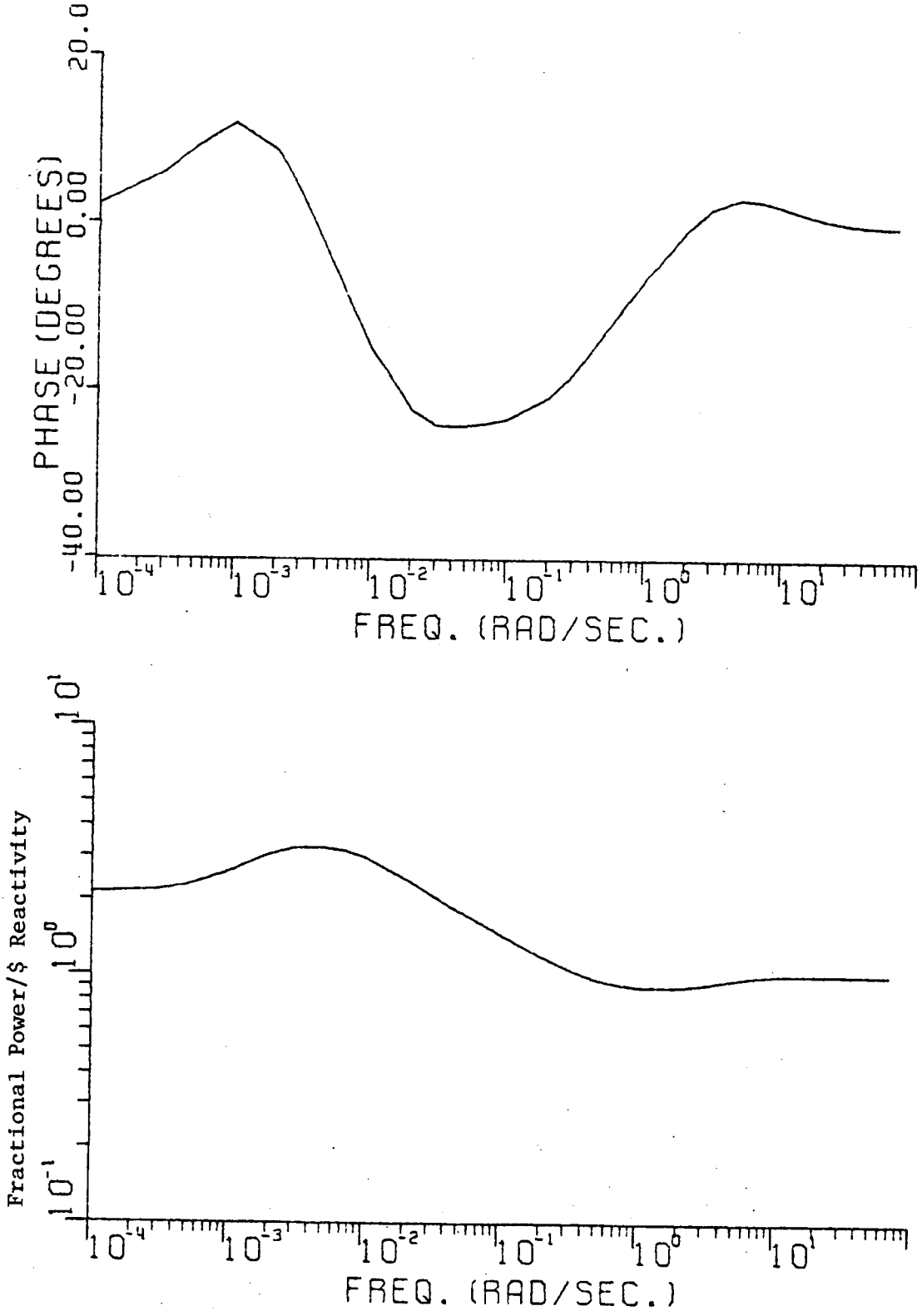


Figure 5.6 Frequency Response of Reactor Power for Reactivity Perturbation.

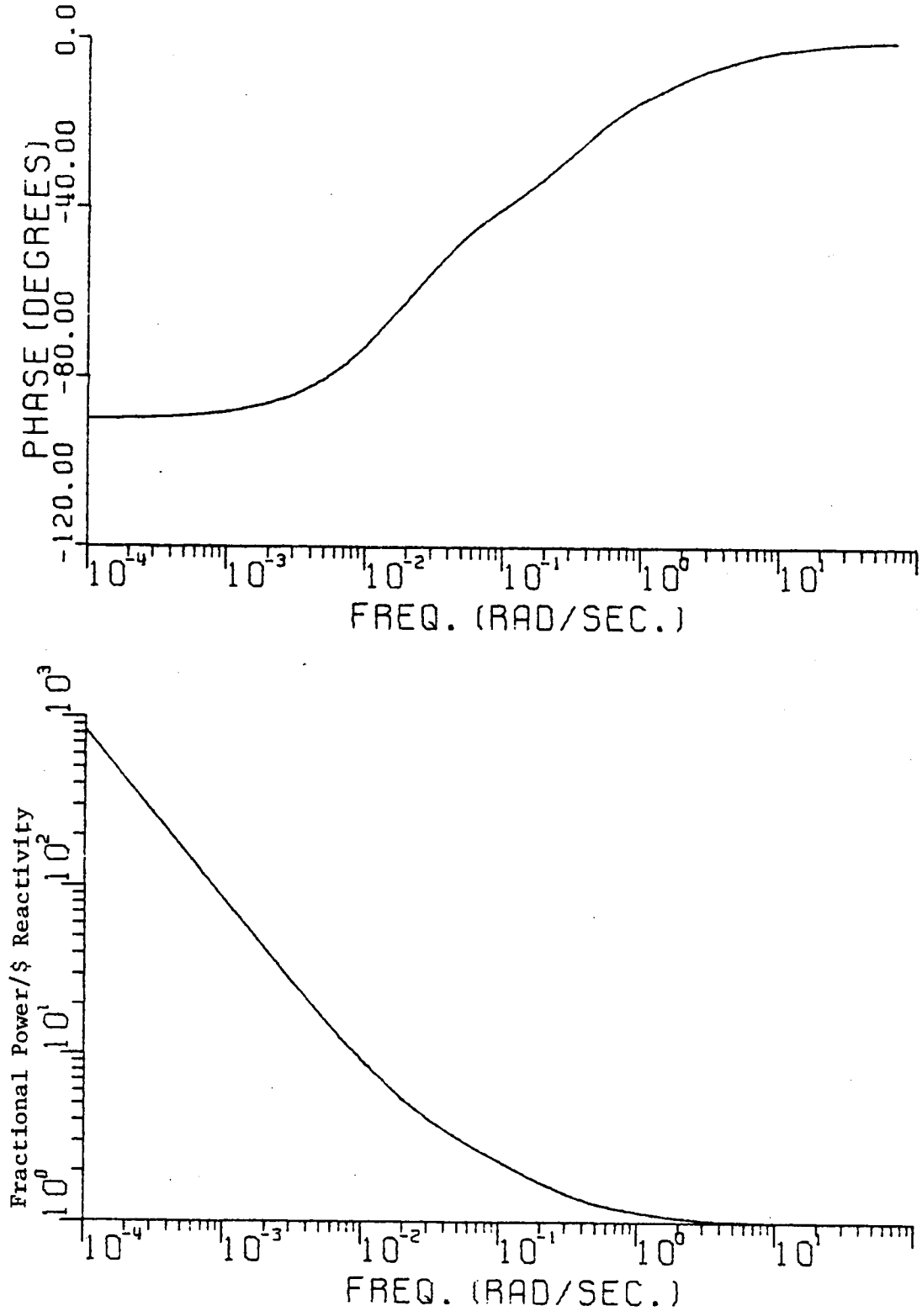


Figure 5.7 EBR-II Zero Power Frequency Response for Reactivity Perturbations.

product of the magnitude of the step and the frequency response gain at zero frequency. From Figure 5.8, it is seen that the steady state power level for the +10¢ reactivity perturbation will be a factor of 1.2098 times the original power level, rather than the 1.265 factor derived from the 200 sec. power time response. The steady state responses of the remainder of the system state variables are given in Table 5.3.

5.7 System Frequency Response for IHX Secondary Inlet Sodium Temperature Perturbations

The frequency response of the system state variables for IHX secondary inlet sodium temperature perturbations is shown in Figures 5.8, and Appendix C. Figure 5.8 shows that the low frequency power gain (fractional change in power per degree Fahrenheit) is 3×10^{-3}. The frequency response shown in this figure appears to approximate a first order lag, as do the remainder of the nodal responses. True first order lag behavior is not possible due to the heat transfer process within the intermediate heat exchanger. The results of this analysis reveal that the reactor power and core metal and coolant temperatures react very slowly to a change in IHX secondary inlet sodium temperature perturbations.

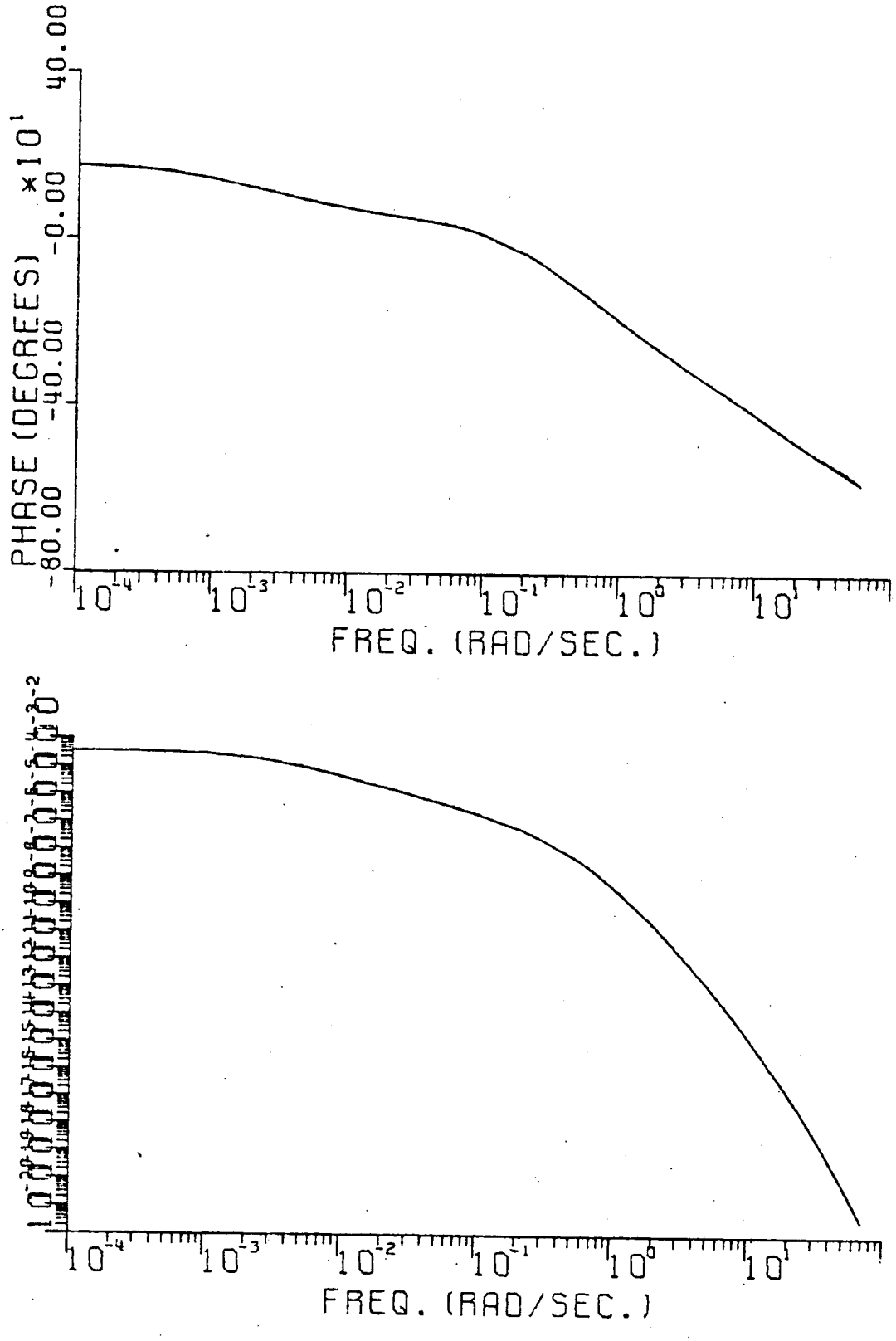


Figure 5.8 Frequency Response of Reactor Power for IHX Secondary Inlet Sodium Temperature Perturbations.

TABLE 5.3

38 NODE STEADY STATE MODEL RESPONSE TO $\delta\tau$ = +10 CENTS

Node	Response
1	.157 P/P_o
8	76.87°F
9	69.47°F
10	61.49°F
11	47.37°F
12	61.59°F
13	32.86°F
14	32.86°F
15	32.86°F
16	32.86°F
17	34.27°F
18	33.03°F
19	33.20°F
20	80.98°F
21	61.76°F
22	61.94°F
23	62.27°F
24	39.68°F
25	46.51°F
26	44.12°F
27	33.27°F
28	33.67°F
29	55.35°F
30	55.35°F
31	55.35°F
32	44.13°F
33	32.91°F
34	32.86°F
35	29.91°F
36	17.92°F
37	53.61°F
38	53.61°F

CHAPTER 6

PARAMETER IDENTIFICATION

6.1 Introduction

As stated in Section 1.2, one of the major benefits of dynamic testing is the use of test data in conjunction with a theoretical model to aid in the determination of various basic design parameters. Systematic parameter identification methods previously developed for PWR applications[12] can be applied to LMFBR's. One form of parameter estimation uses the experimental time or frequency response at N selected points and minimizes the error between theory and experiment. The error equation used for this purpose is:

$$E = \sum_{k=1}^{N} \left[\frac{X_e(k) - X_c(k)}{X_e(k)} \right]^2 \quad . \tag{6.1}$$

where

$X_e(k)$ is the experimental response at point k

$X_c(k)$ is the calculated response at point k.

Note that a zero value of the error requires that the error be zero at every observation point. The most common method of error minimization is the method of steepest descent. The change in error due to a change in a given parameter is expressed as a Taylor series:

$$E = E_o + \sum_{i=1}^{M} \frac{\partial E}{\partial P_i} \Delta P_i + \ldots . \tag{6.2}$$

Ignoring higher order terms,

$$E - E_o = \sum_{i=1}^{m} \frac{\partial E}{\partial P_i} \Delta P_i \,. \tag{6.3}$$

The greatest reduction in the error will therefore occur for

$$\Delta P_i \;\alpha\; (-\frac{\partial E}{\partial P_i}) \,. \tag{6.4}$$

This vector is explored by calculating the error at various points along the vector. When the best point is found, a new direction is determined and the process repeated. The sensitivity term is calculated as,

$$\frac{\partial E}{\partial P_i} = -2 \sum_{k=1}^{N} \frac{X_e(k) - X_c(k)}{X_e(k)} \quad \frac{\partial X_c(k)}{\partial P_i} \tag{6.5}$$

where the response sensitivity terms $\partial X_c(k)/\partial P_i$ are obtained from the model and the methods discussed in Chapter 4.

There are three aspects to the parameter identifiability problem: uniqueness, sensitivity, and separability.

6.2 Uniqueness

The uniqueness question deals with the mathematical possibility of determining parameters assuming perfectly accurate experimental data. For the case of a single input and output, the following uniqueness criteria have been developed[13].

1. Any (2n-1) coefficients can be determined uniquely if the initial guesses on these adjustable coefficients are close to the correct values.
2. Any two diagonal coefficients and (n-1) off diagonal coefficients from any single row or column can be determined uniquely, regardless of the error in the initial guesses on these adjustable coefficients.

According to the first criterion above, (2n-1) or 75 coefficients can be determined uniquely if the initial guesses on these parameters are close enough to the correct values. From the second criterion we know that any 2 diagonal elements and 37 off diagonal elements from any single row or column of the A matrix can be determined uniquely regardless of the error in the initial guesses on the parameters. The parameters of interest are listed in Table 6.1. Since only 13 coefficients are of interest, the first criterion is easily satisfied, if the original estimates are close enough to the true values. The five reactivity feedback coefficients are all off-diagonal elements in the reactor power equation. The core clad to coolant heat transfer coefficient-area product occurs both as diagonal and off-diagonal elements in the cladding temperature equation and the core coolant equations. The inner reflector and outer blanket heat transfer-area products occur both as diagonal and off-diagonal elements in their respective metal and coolant node equations. The IHX heat transfer coefficients occur both in diagonal and off-diagonal elements of the IHX primary coolant, tube wall temperature, and secondary coolant temperature equations. The sodium pot residence time occurs as a diagonal and off diagonal element in the pot sodium

TABLE 6.1

PARAMETERS OF INTEREST IN SENSITIVITY ANALYSIS

Parameter	Description
α_d	Doppler Reactivity Coefficient
α_{fe}	Fuel Expansion Reactivity Coefficient
α_s	Structural Steel Reactivity Coefficient
α_{cna}	Core Sodium Reactivity Coefficient
α_{ir}	Lower Reflector Sodium Reactivity Coefficient
α_{ur}	Upper Reflector Sodium Reactivity Coefficient
α_{ir}	Inner Reflector Sodium Reactivity Coefficient
UA_{core}	Core Fuel to Coolant Heat Transfer Coefficient
UA_{inner}	Inner Reflector Metal to Coolant Heat Transfer Coefficient
UA_{outer}	Outer Reflector Metal to Coolant Heat Transfer Coefficient
U_p	IHX Primary Side Heat Transfer Coefficient
U_s	IHX Secondary Side Heat Transfer Coefficient
τ_p	Primary Pot Sodium Residence Time

temperature. Since all of the coefficients do not appear in the same row or column, the second criterion can not be satisfied.

An additional aspect of the uniqueness question is that the established rules for examining the uniqueness of a set of parameters assume perfectly accurate data. The rules therefore, have limited usefulness for practical applications. The sensitivity and separability problems will be considered in the following sections.

6.3 Frequency Response Sensitivities

Sensitivity tests reveal whether the test response to be measured is sufficiently sensitive to the parameter of interest. The sensitivity of the system reactivity perturbation frequency response to parameter changes was calculated by the methods discussed in Chapter 4. The relative sensitivity level of each response is judged against the minimum desired sensitivity for analysis purposes. This minimum desired sensitivity was arbitrarily chosen as a .1 percent change in gain per percent change in the parameter value. The system reactivity perturbation frequency response sensitivities are shown in Appendix D. The reactor power frequency response is seen to be rather sensitive to the values of α_s, α_{cs}, α_{fe}, UA_c, U_p, $\forall_s$ and τ_p. Figure 6.1 summarizes the power frequency response sensitivity to each of these parameters.

The frequency response is seen to be extremely sensitive to the value of the structural steel reactivity feedback coefficient. This behavior might have been expected since this one coefficient is responsible for 28% of the total isothermal feedback coefficient, and is dependent on the temperature rise of the core fuel cladding. One

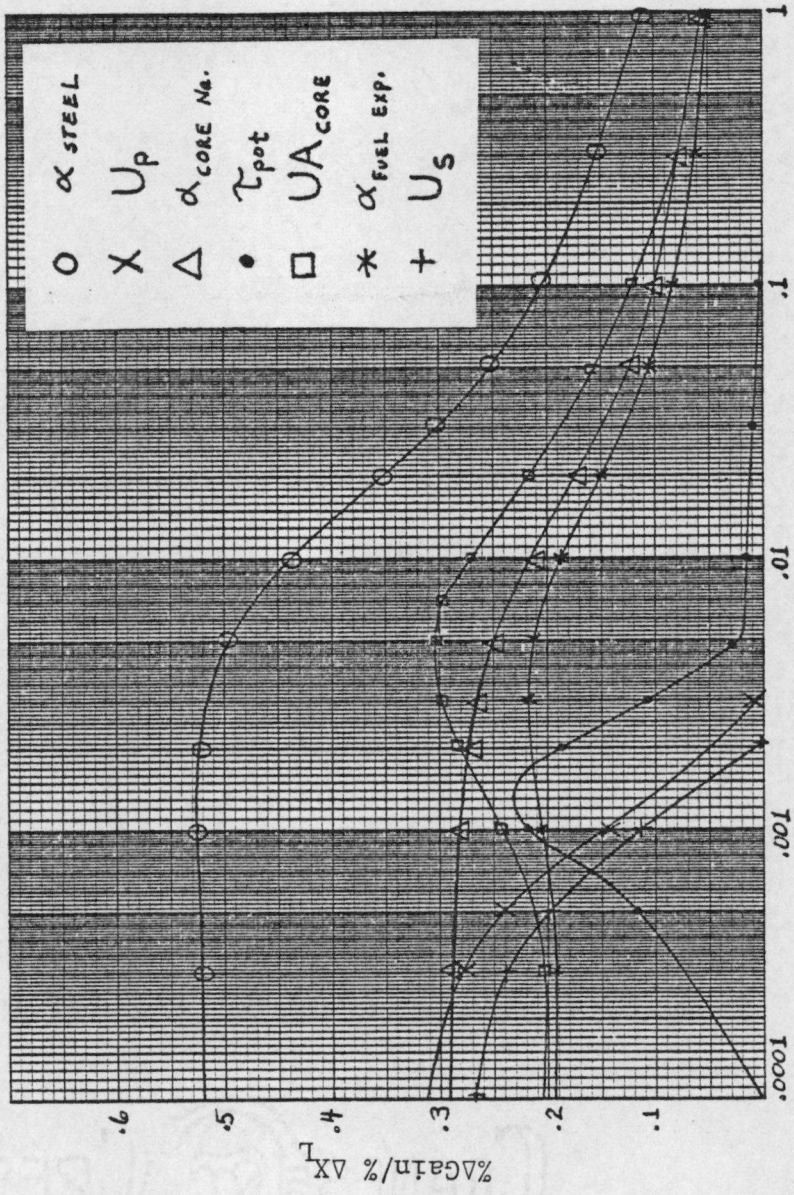


Figure 6.1 Power Frequency Response Sensitivity.

of the more outstanding features of Figure 6.1 is the abrupt peak in the plot of the gain sensitivity (percent change in power gain per percent change in τ_p) with respect to the sodium pot residence time. The center frequency of the spike is approximately .0018 rad/sec. In the time domain this corresponds to a time constant of 555 sec., or approximately the residence time of the sodium in the primary pot, τ_p. This sensitivity might also have been expected on physical grounds. At oscillation frequencies much greater than τ_p^{-1}, the temperature of the sodium in the pot cannot respond quickly enough to maintain pace with the oscillation. The behavior of the system is therefore not very sensitive to the value of τ_p at these high frequencies. At extremely low oscillation frequencies the sodium pot temperature has little trouble following the oscillation. However, at frequencies close to that corresponding to the pot residence time, small changes in the residence time value can have a significant effect on the system gain due to its primary effect on reactor inlet temperature. From Figure 6.1 it is clear that the frequency response sensitivities are of suitable magnitude to enable identification of system parameters with frequency response test data, if separability conditions can be satisfied.

6.4 Separability of Parameters

Separability considers the possibility of identifying all of the parameters of interest from the test results. The separability problem may be more clearly understood by considering two arbitrarily chosen parameters that satisfy all of the uniqueness and sensitivity criteria, but that have frequency response sensitivity curves which

are parallel over some given frequency range. At a given frequency, ω, a change in the error function $E(\omega)$, can be written as:

$$\Delta E(\omega) = \frac{\partial E(\omega)}{\partial P_1} \Delta P_1 + \frac{\partial E(\omega)}{\partial P_2} \Delta P_2 + \ldots \tag{6.6}$$

where

$\frac{\partial E(\omega)}{\partial P_i}$ = the value of the sensitivity of the response to parameter i at a frequency ω.

If $\frac{\partial E(\omega)}{\partial P_2}$ is proportional to $\frac{\partial E(\omega)}{\partial P_1}$, (slopes proportional on the sensitivity plot), then,

$$\frac{\partial E(\omega)}{\partial P_2} = C \frac{\partial E(\omega)}{\partial P_1} \tag{6.7}$$

and

$$\Delta E(\omega) = \frac{\partial E(\omega)}{\partial P_1} \Delta P_1 + C \frac{\partial E(\omega)}{\partial P_1} \Delta P_2 + \ldots \tag{6.8}$$

$$\Delta E(\omega) = \frac{\partial E(\omega)}{\partial P_1} [\Delta P_1 + C\Delta P_2] . \tag{6.9}$$

It is apparent from Eq. 6.9 that an infinite number of parameter value combinations can yield a given value of error. If the sensitivity curves are parallel over all frequencies, (C is constant) then any attempt to identify a unique set of parameters is doomed to failure. The separability criterion therefore requires that the gain sensitivity curves be nonparallel over at least some portion of the test frequency range.

Referring to Fig. 6.1, one observes that the three feedback

coefficient sensitivity curves are all roughly parallel throughout the entire analysis range. These three parameters would not therefore be identifiable from power frequency response test data. In the range .0013 to .005 rad/sec. the slope of the τ_p curve is not parallel to any of the other curves. The slope of the UA_{core} curve is also distinguishable over the same frequency range. The values of the sodium pot residence time and the core clad to coolant heat transfer coefficient should be identifiable from power frequency response test data. The slopes of the U_p and U_s curves are not distinguishable over this frequency range, and these parameters will therefore not be identifiable from power response data.

It is, of course, possible to make use of system frequency response data for outputs other than power, in parameter identification work. One might make use of any state variable for which frequency response data is experimentally obtainable. The frequency responses of various system temperatures are therefore likely candidates for application of parameter identification techniques. Figure 6.2 shows the reactivity perturbation frequency response sensitivity of the upper core coolant temperature to the same parameters shown in Figure 6.1.

One notes immediately the lack of frequency response sensitivity to the value of the sodium pot residence time and the primary IHX heat transfer coefficient. These parameters would not be identifiable from reactor coolant temperature frequency response data. The core heat transfer-area product coefficient, UA_c, would be identifiable from coolant temperature frequency response test data. The remaining curves in Figure 6.1 are nearly parallel over the total frequency range,

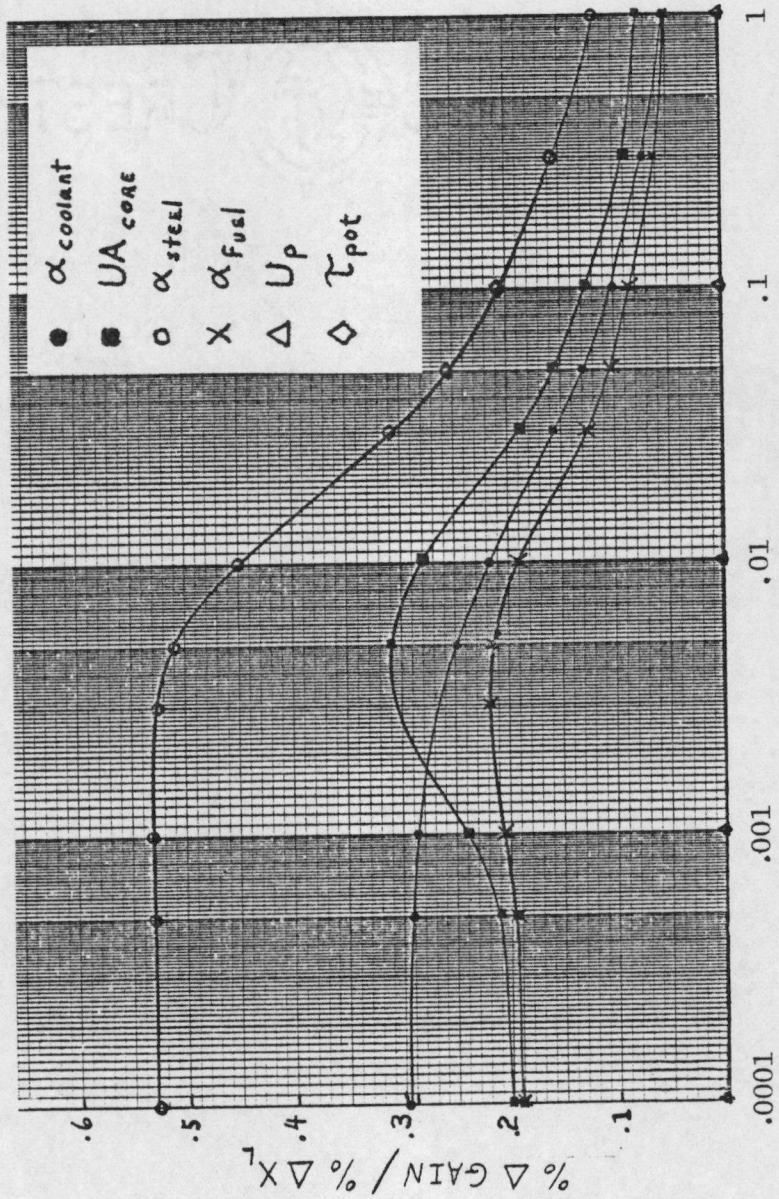


Figure 6.2 Upper Core Sodium Temperature Frequency Response Sensitivity.

and these parameters would not be identifiable from reactor coolant data.

Figures 6.3 and 6.4 show the frequency response sensitivity of the upper axial reflector upper coolant node and reactor upper plenum sodium temperatures to the value of the upper reflector sodium void coefficient. Both responses display such low sensitivity that their identification from nodal response data will not be possible. A similar situation is shown in Figures 6.5 and 6.6, where the sensitivity of the inner reflector upper coolant and reactor upper plenum sodium temperatures with respect to the value of the inner reflector sodium voiding coefficient are plotted. Figures 6.7 and 6.8 show the reactivity perturbation frequency response sensitivity of the inner reflector upper coolant and upper plenum sodium temperatures to the value of the inner reflector metal to coolant heat transfer coefficient-area product. The upper coolant nodal temperature displays significant sensitivity over all frequency ranges. The inner reflector heat transfer coefficient-area product should therefore be identifiable. The frequency response sensitivity of the outer blanket upper coolant and reactor upper plenum sodium temperatures to the value of the outer blanket heat transfer coefficient-area product is shown in Figures 6.9 and 6.10. The upper coolant node response displays very high sensitivity in the 7×10^{-2} through 3×10^{-1} rad/sec. range. This high sensitivity should make possible the identification of the UA_{outer} product. Figure 6.11 shows the sensitivity of the high pressure plenum sodium temperature to the values of both the IHX primary and secondary heat transfer coefficient, U_p, and U_s. Figures 6.12 through 6.13 show the sensitivity of the

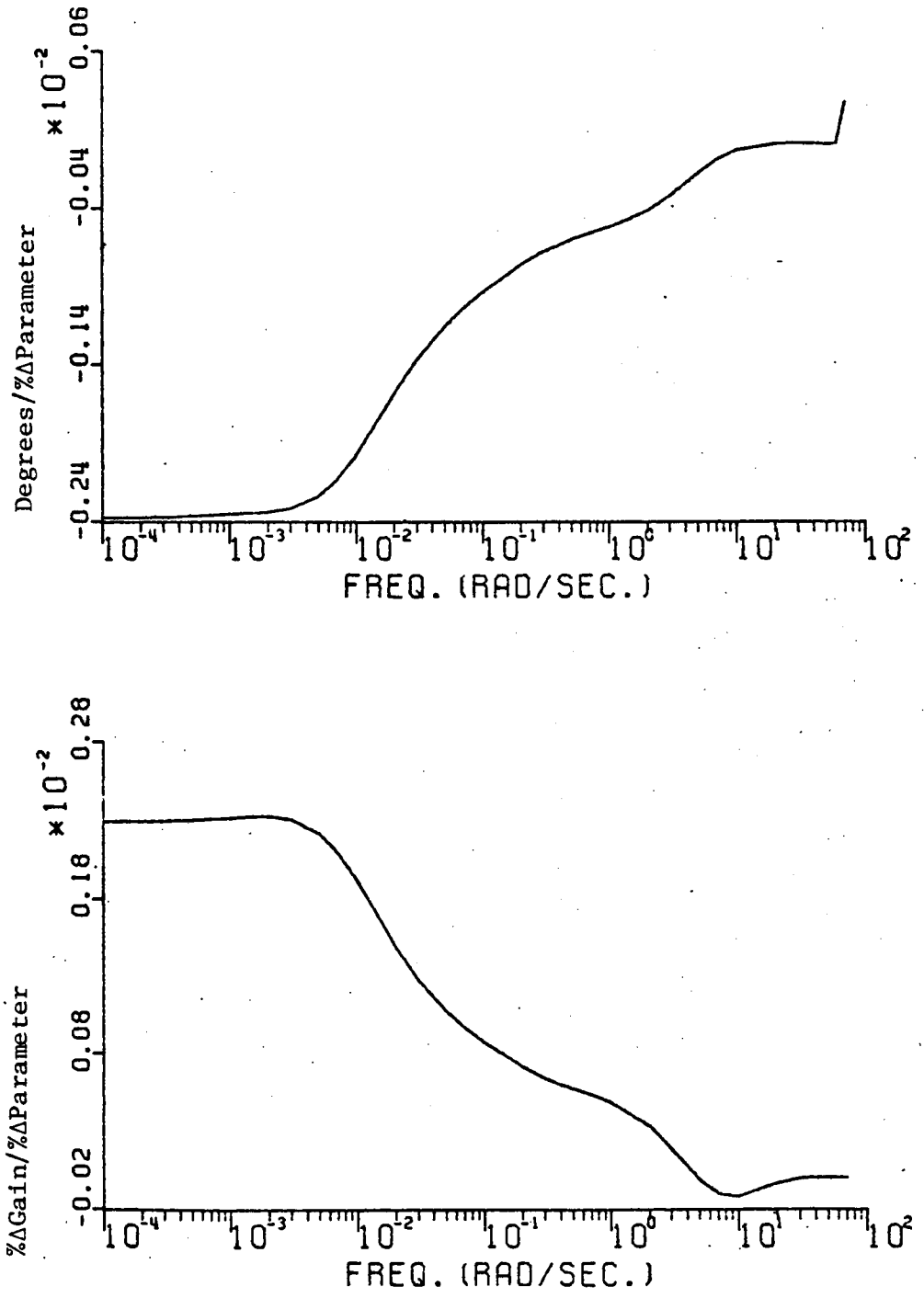


Figure 6.3 Sensitivity of the Upper Reflector Upper Sodium Temperature Frequency Response to the Upper Reflector Sodium Void Coefficient.

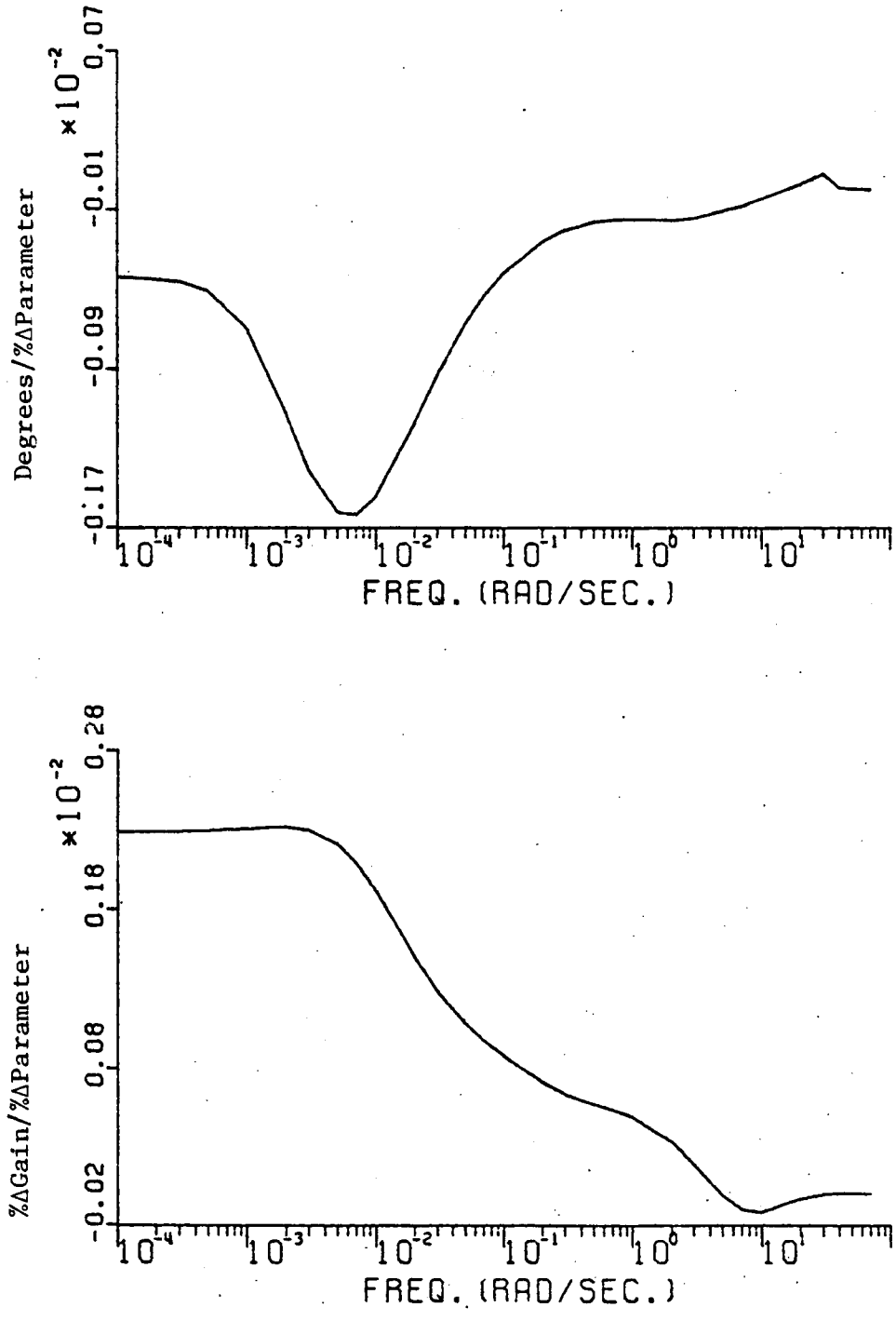


Figure 6.4 Sensitivity of Upper Plenum Sodium Temperature Frequency Response to the Upper Reflector Sodium Void Coefficient.

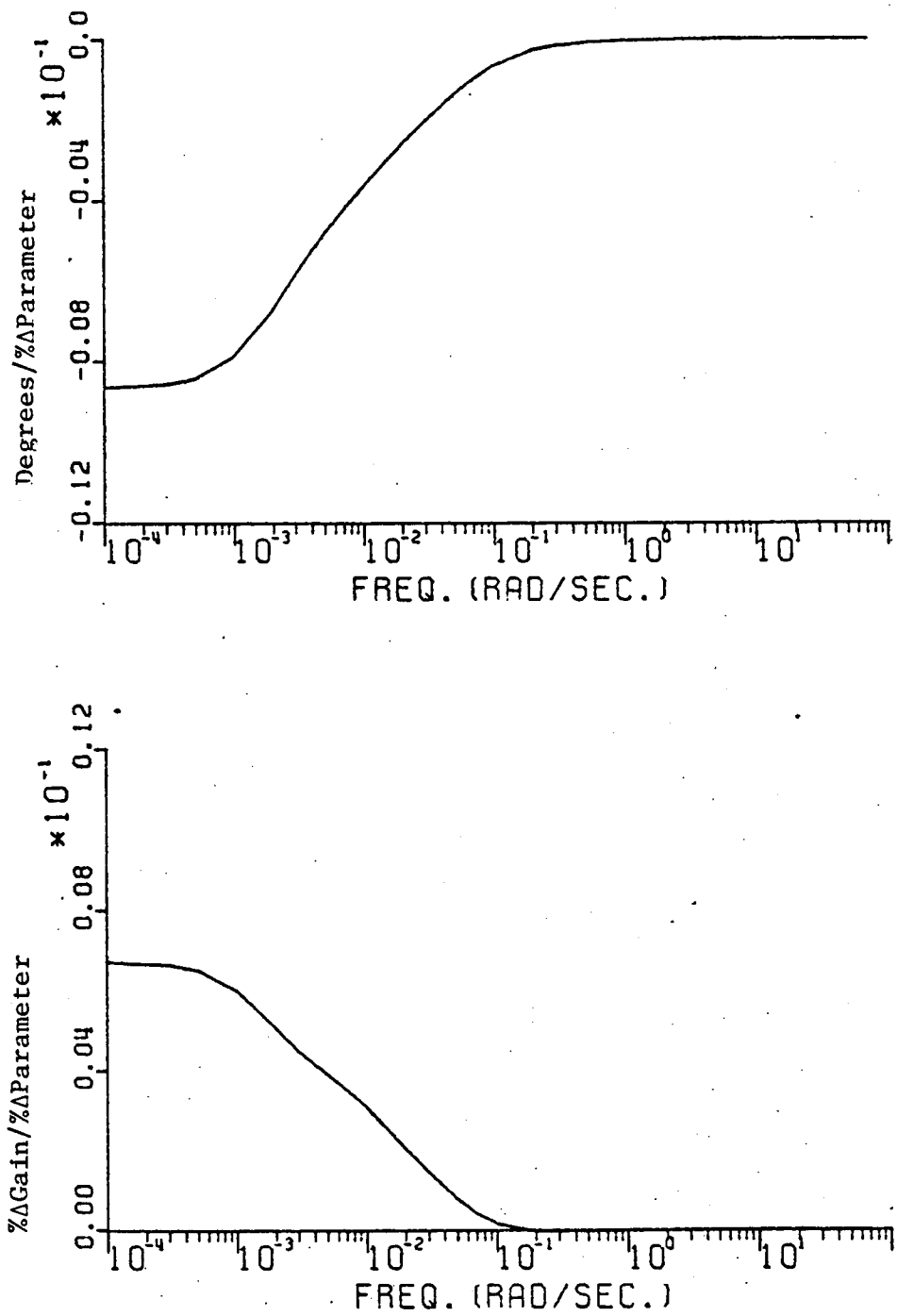


Figure 6.5 Sensitivity of Inner Reflector Upper Coolant Temperature Frequency Response to the Inner Reflector Sodium Void Coefficient.

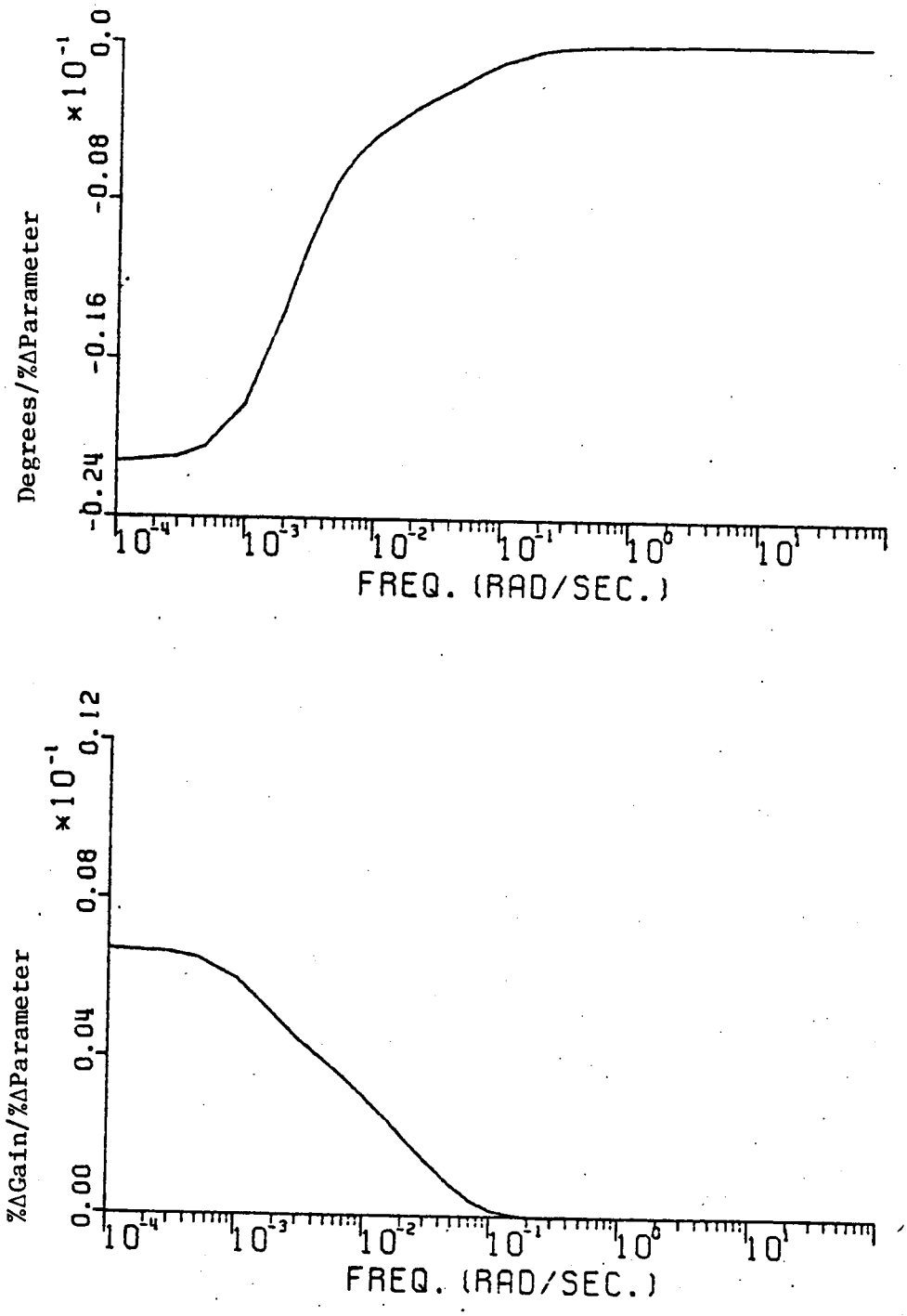


Figure 6.6 Sensitivity of the Upper Plenum Sodium Temperature Frequency Response to the Inner Reflector Sodium Void Coefficient.

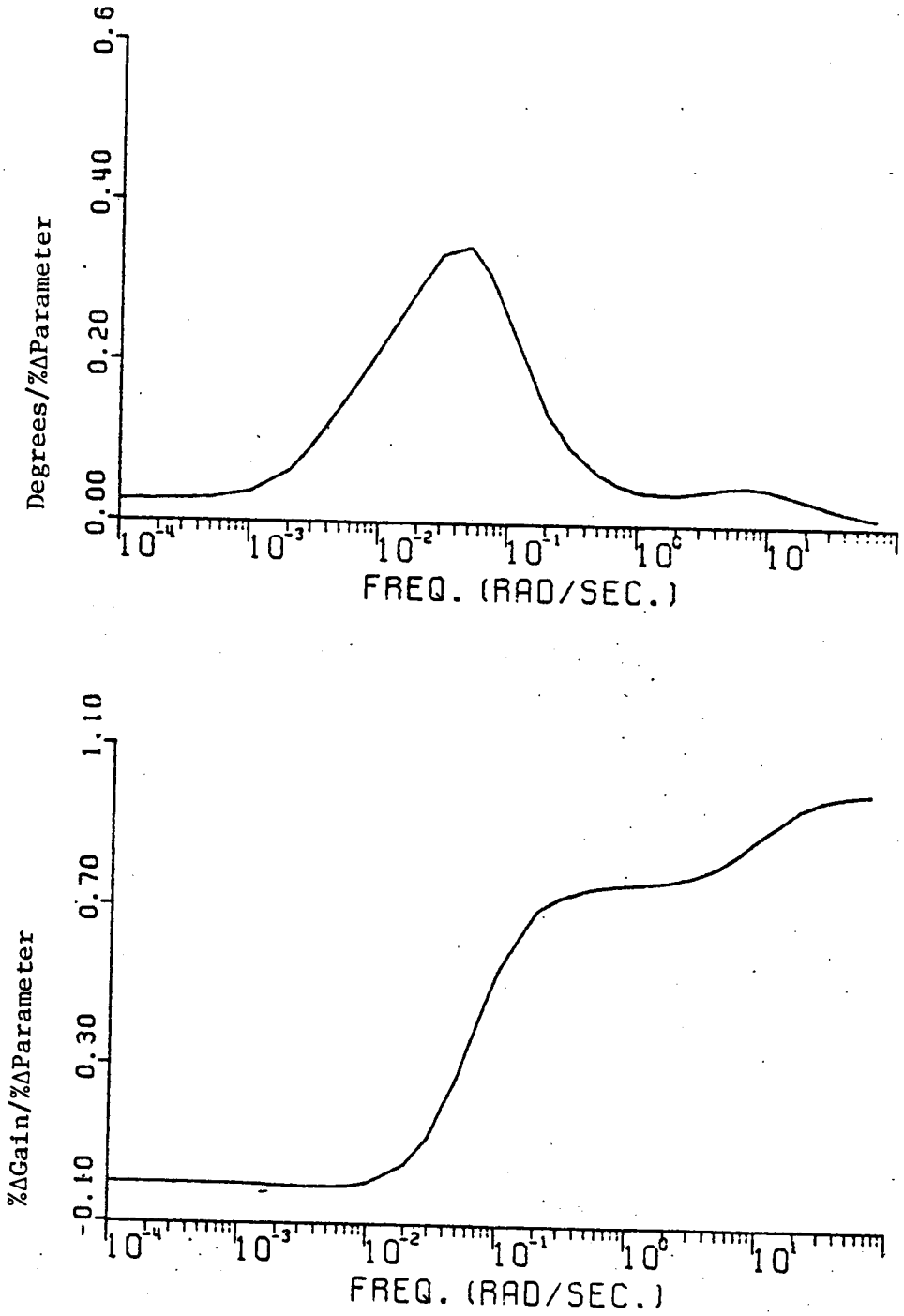


Figure 6.7 Sensitivity of the Inner Reflector Upper Sodium Temperature Frequency Response to UA_{inner}.

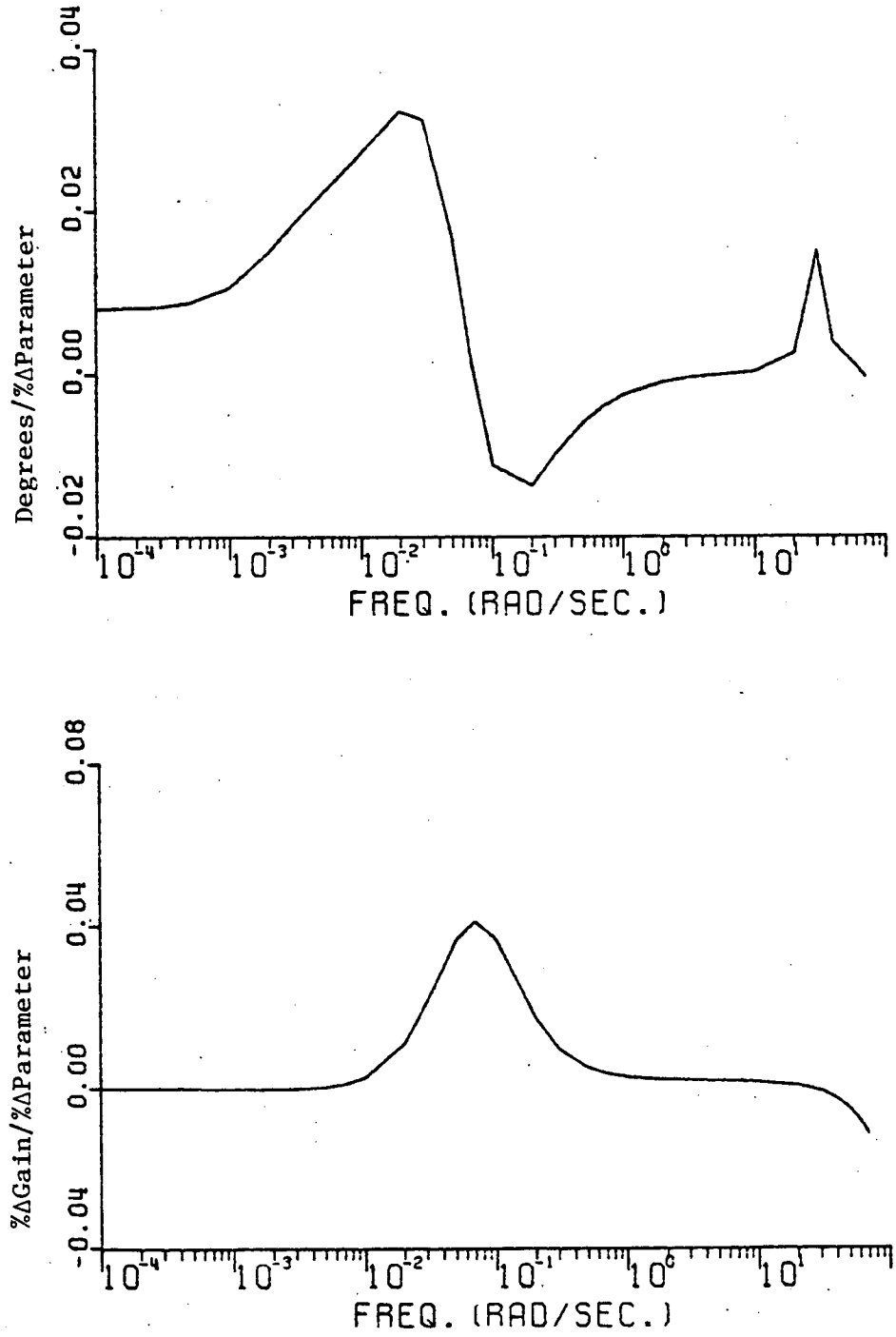


Figure 6.8 Sensitivity of the Upper Plenum Sodium Temperature Frequency Response to UA_{inner}.

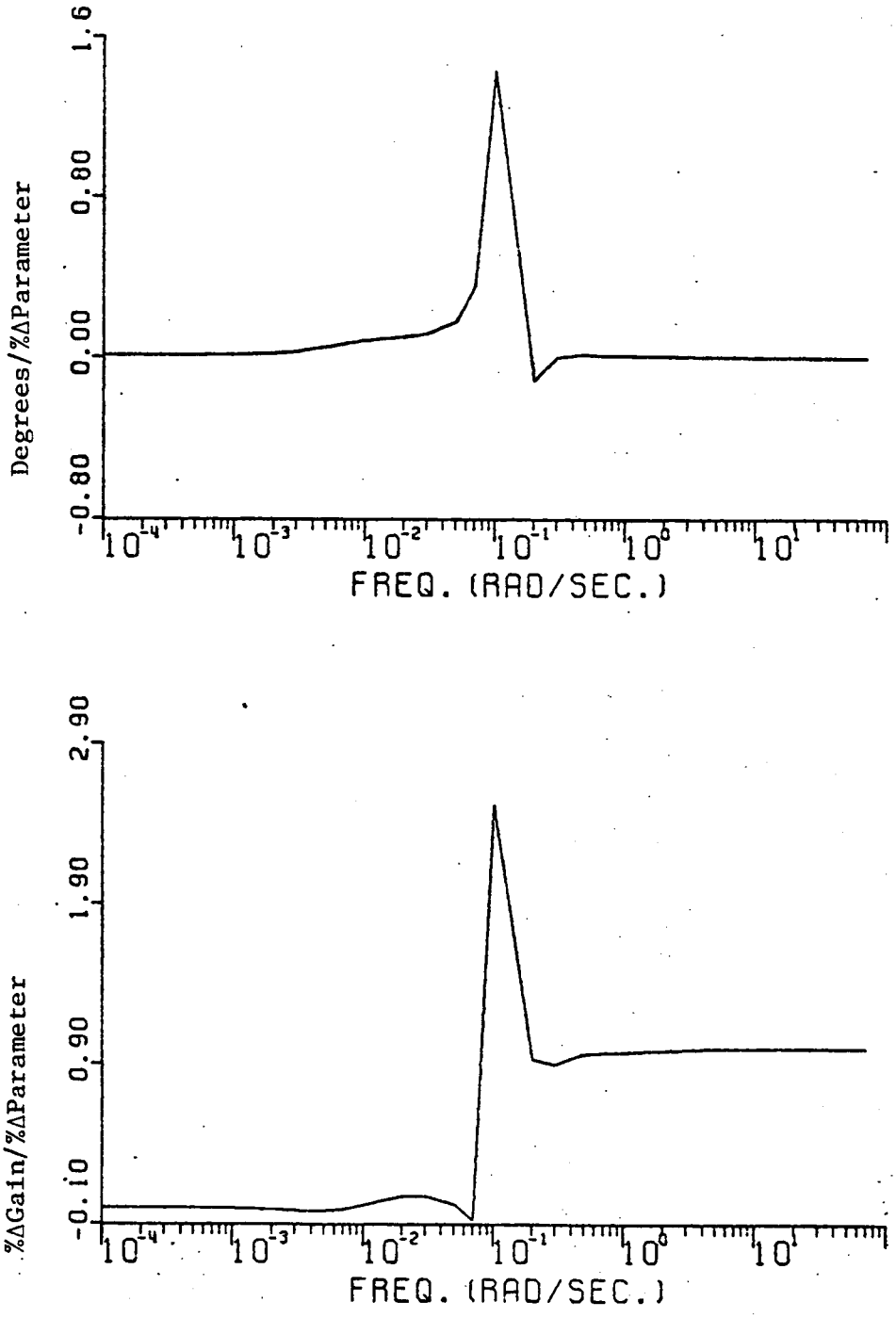


Figure 6.9 Sensitivity of Outer Blanket Upper Sodium Temperature Frequency Response to UA_{outer}.

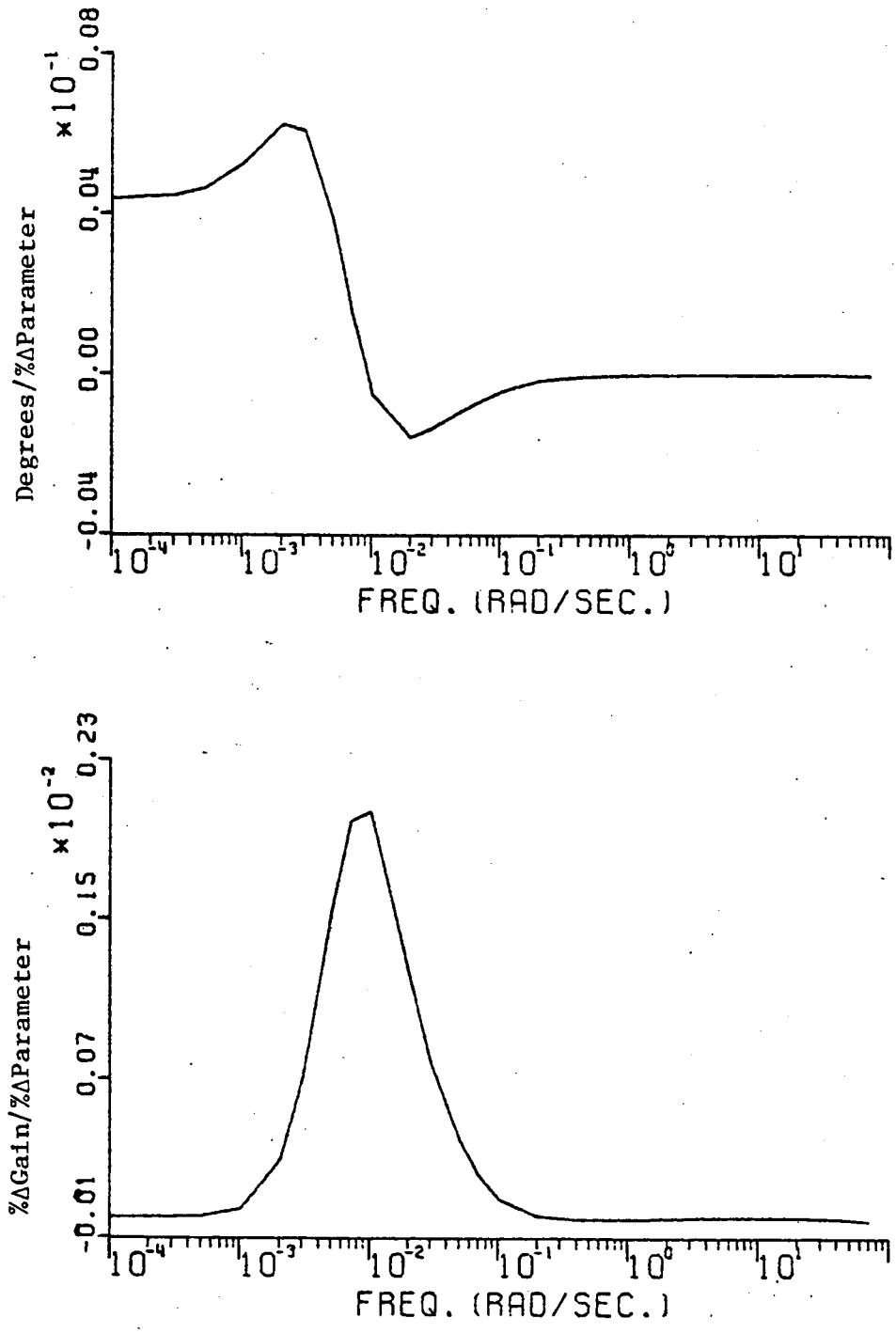


Figure 6.10 Sensitivity of the Upper Plenum Sodium Temperature Frequency to UA_{outer}.

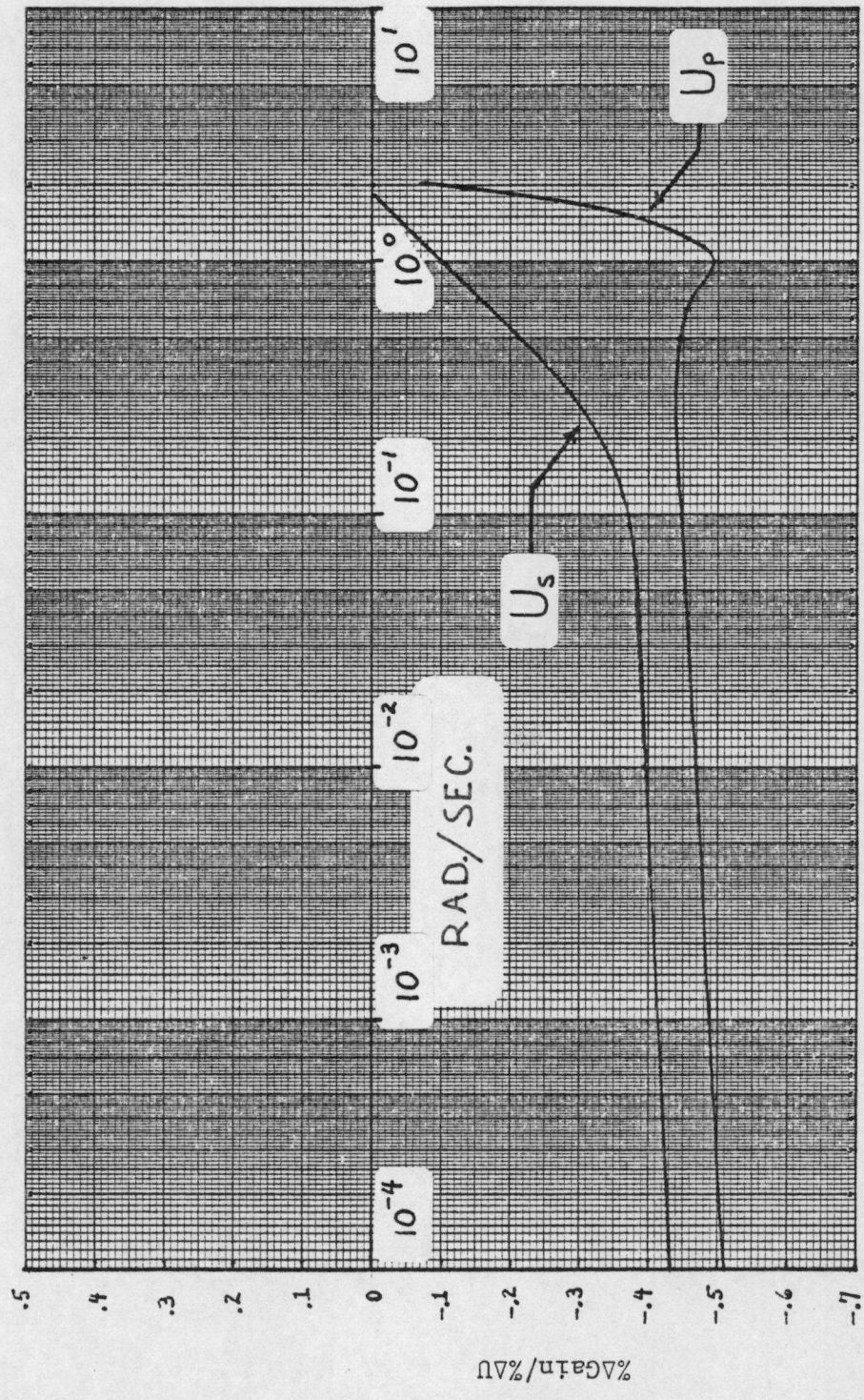


Figure 6.11 Sensitivity of the High Pressure Plenum Sodium Temperature Frequency Response to U_p and U_s.

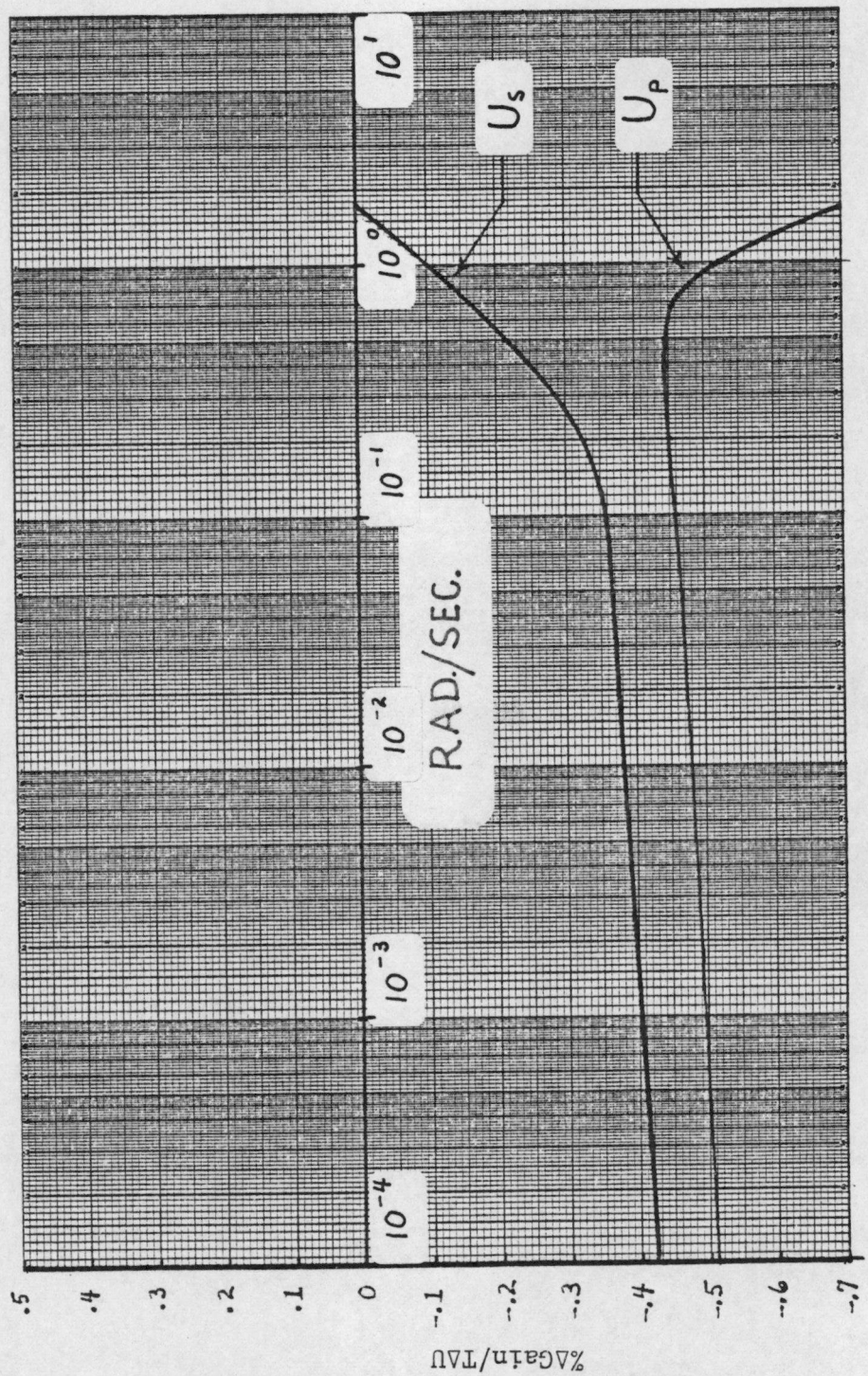


Figure 6.12 Sensitivity of the IHX Primary Outlet Sodium Temperature Frequency Response to U_p and U_s.

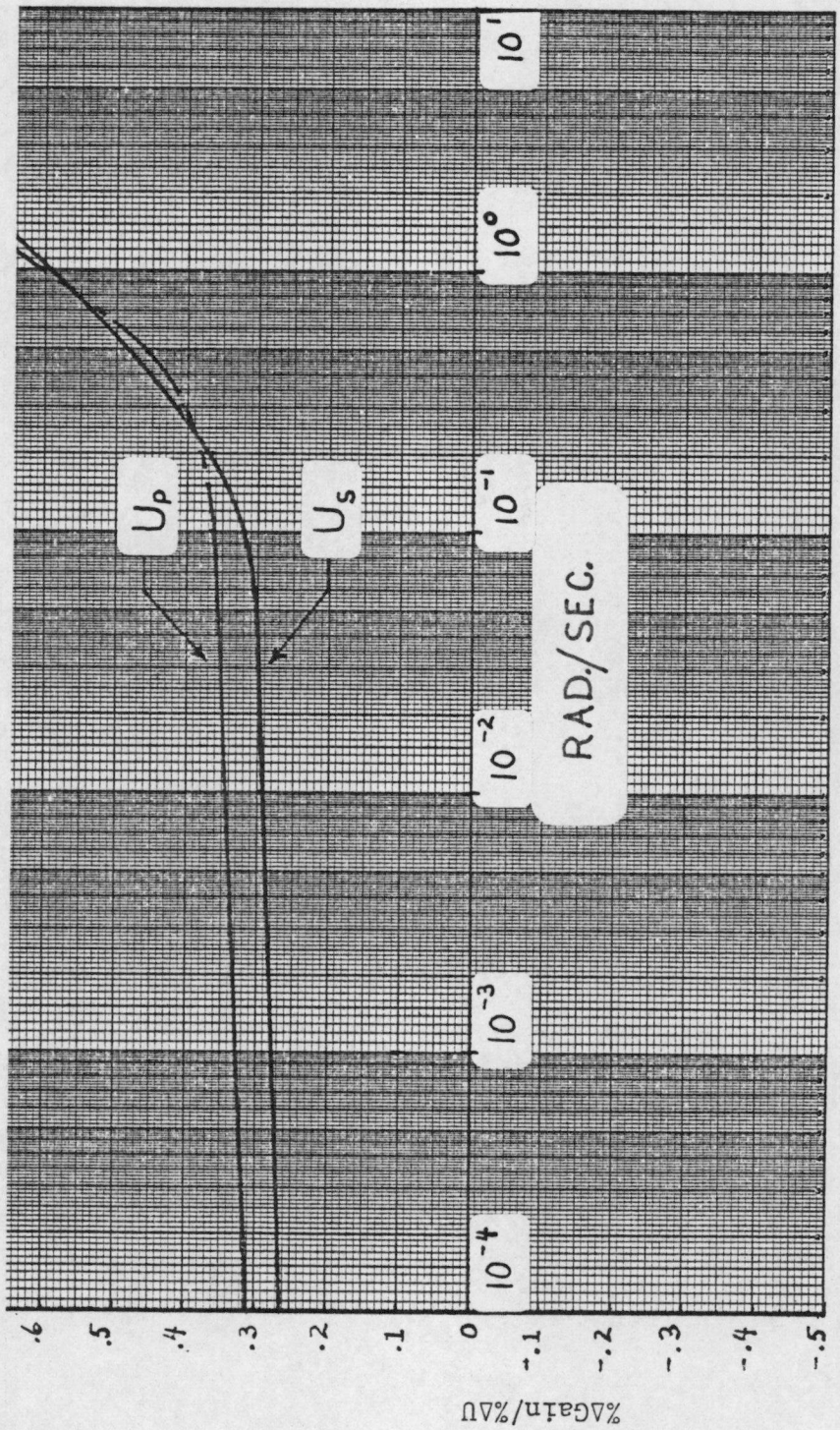


Figure 6.13 Sensitivity of the IHX Secondary Outlet Sodium Temperature Frequency Response to U_p and U_s.

IHX primary and secondary outlet sodium temperatures to the values of U_p and U_s. The plots of the gain sensitivity of the IHX high pressure plenum node to the IHX primary and secondary heat transfer coefficients are parallel over the 10^{-4} to 10^{-1} rad/sec. frequency range. The slopes of the two curves differ significantly in the .1 to 1 rad/sec. range, thus offering a possibility of identification of both the primary and secondary IHX heat transfer coefficients from high pressure plenum sodium temperature response data. Analysis of the IHX primary outlet sodium temperature gain sensitivity (Figure 6.12) also indicates a good possibility of identification of the IHX heat transfer coefficients in the .1 to 1 rad/sec. range. Figure 6.13 indicates that the IHX heat transfer coefficients probably could not be identified from IHX secondary outlet sodium temperature response data, since the plots are parallel or nearly parallel over the entire frequency range.

Table 6.2 summarizes the results of the identification feasibility study.

TABLE 6.2

EBR-II IDENTIFIABLE PARAMETERS

Parameter	Response to be Monitored	Freq. Range (Rad/sec)
p	Power	.001 - .01
UA_{core}	Power	.001 - .01
UA_{inner}	Inner Reflector Upper Coolant Temp.	.01 - .1
UA_{outer}	Blanket Upper Coolant Temp.	.07 - .9
U_p	High Press. Plenum Temp.	.1 - .9
	IHX Primary Outlet Temp.	.1 - .9
U_s	High Press. Plenum Temp.	.1 - .9
	IHX Primary Outlet Temp.	.1 - .9

CHAPTER 7

TEST DESIGN

7.1 Introduction

In previous chapters, the theoretical time and frequency response of the EBR-II was obtained using the theoretical model. The sensitivity of the system frequency response to various physical parameters was also investigated. In this chapter, these results are used to aid in the planning of a frequency response test for the EBR-II that will yield a maximum of information.

7.2 Planning the Test

The goal of dynamic test design is to formulate a testing procedure which will

1) Make use of existing plant equipment and instrumentation where at all feasible
2) Give the minimum interruption in normal plant operations
3) Yield the maximum amount of information for the least amount of test time
4) Minimize test costs.

It is apparent that these considerations are, to some degree, contradictory. In general, the investigator must be very familiar with the reactor control system (its interrelationship with other reactor systems and its physical capabilities), nuclear and thermal instrumentation equipment capabilities, methods of selection of input variables and controlling them during the test, methods of selection of input test signals and interfacing test equipment with inhouse instrumen-

tation in a safe and reliable manner. All of this work must be done well in advance of the actual test if one is to insure a minimal impact on normal plant operations.

7.3 Role of Theoretical Analysis

The most important use of the theoretical calculations is to identify the range of frequencies over which the test should be conducted. In Section 6.4 it was found that the low frequency range (.0001 to .01 rad/sec.) offers the best possibility for identification of the core heat transfer coefficient area product, and the sodium pot residence time. The power frequency response is very insensitive to the other design parameters of interest over all frequency ranges. The frequency response sensitivities with respect to the various reactivity feedback coefficients are parallel over all frequency ranges and are therefore not identifiable. The inner reflector heat transfer coefficient area product, and IHX primary and secondary heat transfer coefficients are identifiable from coolant nodal response data in the .01 to .8 rad/sec. range. From considerations discussed in Chapter 6, it will be necessary to monitor reactor power, inner reflector upper coolant temperature, outer blanket upper coolant temperature and either high pressure plenum coolant temperature or primary IHX exhaust coolant temperatures during the test. The frequency range of interest will be the .001 to .8 rad/sec.

7.4 Evaluation of Input Equipment Capabilities

The suitability of existant plant control hardware for dynamic

test purposes is determined by whether it is capable of introducing perturbations of suitable magnitude in the frequency range of interest. The pertinent question is therefore, whether the control rods are capable of moving quickly enough to introduce the necessary perturbations.

The highest frequency that one is likely to be able to produce can be determined with the use of the simplest binary signal, a square wave. Eighty-one percent of the total signal energy in a square wave is located in the first harmonic, therefore, the dominant frequency is the fundamental frequency, ω_o, where

$$\omega_o = \frac{2\pi}{T} \quad \frac{\text{rad}}{\text{sec}} \tag{7.1}$$

and T is the period of the square wave. Consideration must be given to the fact that the actual waveform of the signal produced by the control rods will not be a square wave, but a trapizodal form (Figure 7.1). It was shown in Section 2.10 that the maximum reactivity insertion rate, M, for one control rod is .52¢/second. Therefore,

$$T = \frac{2\rho_T}{M} \tag{7.2}$$

and

$$\omega_{MAX} = \frac{2\pi}{\frac{2\rho_T}{M}} = \frac{\pi M}{\rho_T} \quad \frac{\text{rad}}{\text{sec}} \tag{7.3}$$

$$\omega_{MAX} = \frac{1.634}{\rho_T} \quad \frac{\text{rad}}{\text{sec}}$$

where ρ_T is the desired reactivity test perturbation amplitude in cents.

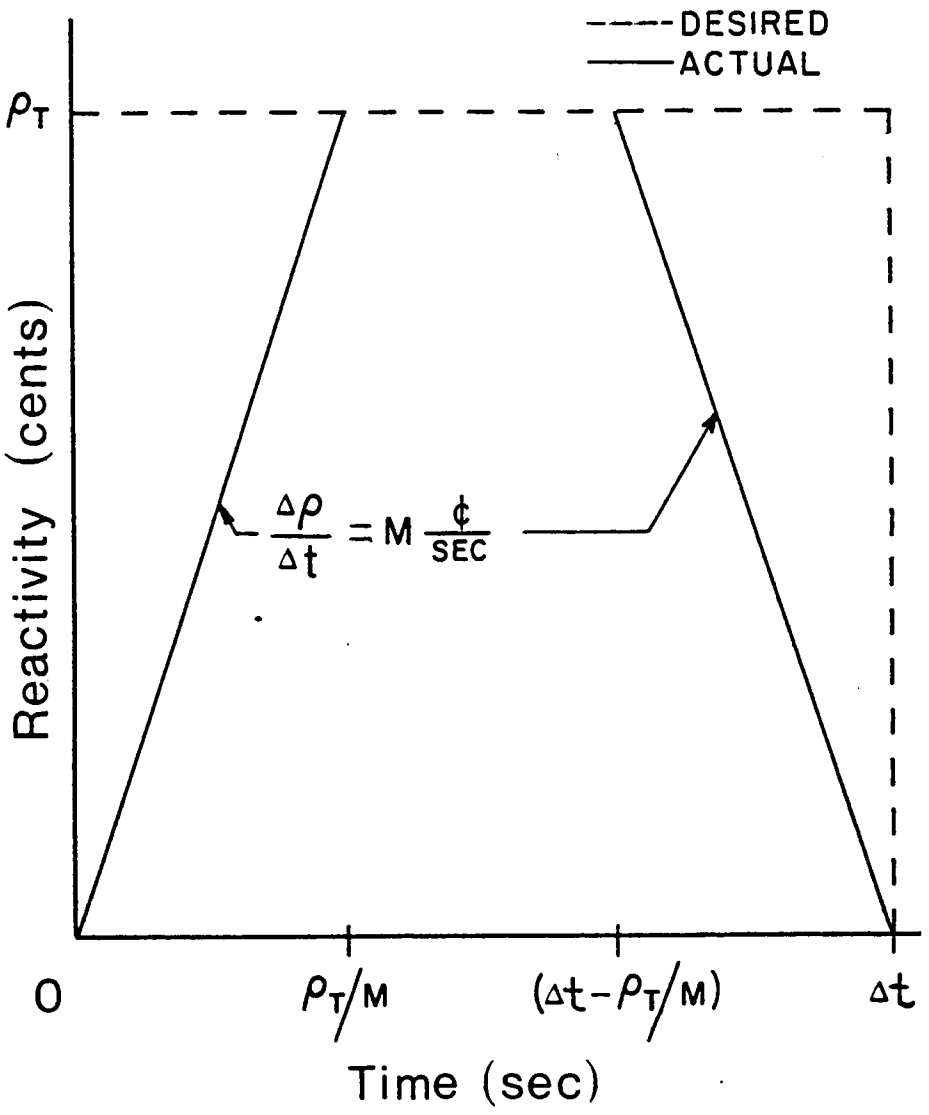


Figure 7.1 Desired and Actual Input Test Signals.

7.5 Effects of Imperfect Test Signals on Test Planning

The ramifications of the limitations of the plant control hardware can now be examined. In the previous section, it was found that the highest frequency at which one could expect to obtain usable results is

$$\omega_{MAX} = \frac{1.634}{\rho_T(\text{¢})} \ \frac{\text{rad}}{\text{sec}} . \tag{7.5}$$

In order to identify all the parameters listed in Table 6.1, it will be necessary to test at frequencies up to .9 rad/sec. From equation 6.1, this would require the use of reactivity perturbations of approximately 1.6 cents. The next step in the planning of the test is to determine whether these small signal perturbations will produce power and temperature perturbations of sufficient amplitude to be distinguished by the data acquisition system.

7.6 Evaluation of Sensor Capabilities

The necessary system response data must be acquired via fission chambers and thermocouples. The suitability of a sensor for test purposes is determined by its frequency response and sensitivity. The time constant of the sensor must be smaller than the inverse of the highest test frequency, ω_m. For ω_m = .9 rad/sec., this time constant must be less than 1.1 seconds.

Table 7.1 lists the appropriate system response as well as the instrumentation identification number of the sensors which may be used to monitor the response in each case, and the associated time constants of the sensors. From Table 7.1 it appears that it may be necessary to limit the upper cut-off frequency to ω_m = 1/1.5, or .67

TABLE 7.1

TEST SENSORS

Response	Reference #	I.D. #	Time Constant
Inner Reflector Upper Coolant Temp.	7F4	R1 TC 503 AE	
	7D4	AD	1.5 sec.
	6C4	N	
	7A3	AB	
Outer Blanket Upper Coolant Temp.	9E4	R1 TC 503 R	
	12E6	X	1.5 sec.
	16E9	W	
IHX Primary Outlet Coolant Temp.	14	R1 TC 507 BT	
	15	BM	1.5 sec.
	16	BR	
	17	BP	
Power	-	P1 NPR 580	0.5 msec.

rad/sec. Since the time constants of individual thermocouples may vary somewhat, it is possible that a sensor may be found in each group which meets the test requirements. If necessary, in-situ response time testing of the sensors can be used to determine if they meet the desired response characteristics. If it does become necessary to limit the upper test frequency to .67 rad/sec., it appears from Figure 6.3, 6.4 and 6.9 that all the parameters listed in Table 6.2 will still be identifiable.

7.7 Selection of Test Signal

After the frequency range of interest has been chosen, and the input/output capabilities of the system hardware evaluated, the system input perturbation signal must be chosen. If a non sinusoidal input signal is employed, the system frequency response at multiple frequencies can be obtained from a single test. Fourier analysis of the system response to non sinusoidal periodic and non periodic signals may be applied to yield the system frequency response at these frequencies. Discrete level periodic sequences are a subclass of non sinusoidal, periodic sequences. There are five types of discrete-level periodic sequences[3]: pseudo-random binary sequence (PRBS), n sequences, pseudo-random ternary sequences (PRTS), multi-frequency binary sequences (MFBS), and the square waves. The PRBS has been used in previous LWR dynamic tests and will be the sole test signal considered here. This choice of the PRBS as the test signal to be employed is mandated by previous test experience and the fact that PRBS generation equipment is commercially available. The pertinent characteristics of a PRBS are:

1) Number of bits in sequence. The number of bits in the sequence, Z, is determined by

$$Z = 2^n - 1 \tag{7.7}$$

where n is an integer.

2) Useful frequency range. The useful frequency range of a PRBS is

$$\frac{2\pi}{T} < \omega \leq \frac{0.88\pi}{T} \quad \frac{\text{rad}}{\text{sec}} \tag{7.8}$$

or

$$\frac{1}{T} \leq f \leq \frac{0.44}{\Delta t} \text{ Hz.} \tag{7.9}$$

where T is the period and Δt is the bit duration in seconds. The upper limit of this frequency range is the harmonic which has half the power of the fundamental[3],

$$K^1/2 = 0.44\ Z\ . \tag{7.10}$$

3) Power Spectrum

$$P_K = \frac{A^2}{Z^2} \quad \text{for } K = 0 \tag{7.11}$$

$$P_K = \frac{2(Z+1)}{Z^2} A^2 \left[\frac{\sin(k\pi/Z)}{k\pi/Z}\right]^2 \quad \text{for } K \neq 0 \tag{7.12}$$

where P_k = power in the k^{th} harmonic

A = signal amplitude.

4) Auto Correlation Function

$$C_{11}(\tau) = 1 - [(Z+1)/T]\tau \qquad 0 \leq \tau \leq \frac{T}{Z} \tag{7.13}$$

$$= -1/Z \qquad T \leq \tau \leq \frac{Z-1}{Z} T \tag{7.14}$$

$$= -Z + [\frac{Z+1}{T}]\tau \qquad \frac{(Z-1)T}{Z} \leq \tau \leq T \tag{7.15}$$

where C_{11} is the auto correlation function and τ is the lag time of the signal.

With these signal characteristics known, it is possible to design the test signal. The procedure is as follows:

The lower limit of the frequency range of interest is .001 rad/sec (from Table 6.1, page 116),

$$\omega_o = .001 = \frac{2\pi}{T} \ \frac{\text{rad}}{\text{sec}} . \tag{7.16}$$

The period, T, of the PRBS must be,

$$T = \frac{2\pi}{.001} = 6283 \text{ sec} . \tag{7.17}$$

The upper limit of the frequency range .9 rad/sec., or

$$\omega_m = .9 \text{ rad/sec} \tag{7.18}$$

and

$$\omega_m \leq \frac{.88\pi}{\Delta t} \leq .9 \ \frac{\text{rad}}{\text{sec}} \tag{7.19}$$

but $T = Z\,\Delta t$ or, $\Delta t = T/Z$, therefore

$$\omega_m \leq .9 \ \frac{\text{rad}}{\text{sec}} \leq \frac{.88\pi Z}{T} \tag{7.20}$$

$$.9 \leq \frac{.88\pi Z}{6283} \tag{7.21}$$

$$Z \geq (6283)(.9)/.88\pi \text{ bits} \tag{7.22}$$

$$Z \geq 2045.39 \text{ bits} . \tag{7.23}$$

From Equation 7.7,

$$2^n - 1 \leq 2045.39 \text{ bits} \tag{7.24}$$

The closest available PRBS signal is

$$n = 11,\ Z = 2047 \text{ bits} \tag{7.25}$$

and

$$\Delta t = \frac{T}{Z} = 6283/2047 = 3.07 \text{ Sec.} \tag{7.26}$$

The PRBS signal necessary to cover the frequency range of interest must therefore have 2047 bits in the sequence, with a bit length of 3.07 seconds.

Two problems are immediately evident upon examination of the selected test signal:

1) Since the EBR-II has no automatic control system, all test signals must be manually input. A 2047 bit signal will require an extremely large number of engagements of the CRDM's, at less than 2 second intervals. This procedure would represent severe demands upon reactor operational personnel.

2) The spectrum of a PRBS signal is completely determined once the number of bits in the sequence is chosen, and its harmonics are evenly spaced on a linear scale. Most frequency response results are interpreted with Bode plots which employ a logarithmic frequency scale. The practical implications of this is that the harmonics of a PRBS will fall closer and closer on a logarithmic scale as the frequency increases. For a signal with a bandwidth of 3 decades, there are 999 harmonics in the frequency range. The harmonics distributed as follows:

1st Decade	9 Harmonics
2nd Decade	90 Harmonics
3rd Decade	900 Harmonics.

An excessive amount of signal energy is placed in the higher, more closely spaced harmonics, where it is used to identify frequency response points which are only slightly different than each other. The test procedure is influenced by the fact that the test must be run long enough to build up sufficient energy in these high frequency harmonics.

Because of the above mentioned problems, it is desirable to use multiple test signals with frequencies that cover different portions of the frequency band of interest $.001 \leq \omega \leq .9$ rad/sec. The signal specification procedure for a set of two, 127 bit signals is discussed in the next section.

7.8 An Alternate Test Procedure

Consider two 127 bit PRBS signals. The first signal is chosen to have the same period as the 2047 bit signal,

$$T_1 = 6283 \text{ seconds} \tag{7.27}$$

and $T = Z\Delta t$,

$$\Delta t = T/Z = 6283/127 \tag{7.28}$$

$$\Delta t_1 = 49.47 \text{ seconds} . \tag{7.29}$$

The upper limit on the useful range of this first signal would be the $.44Z^{th}$ harmonic, or

$$K^1/2 = .44(127) = 55.9 \tag{7.30}$$

and

$$\omega_{m_1} = .055 \text{ rad/sec.} \tag{7.31}$$

The second test signal would use a period equal to one-fifteenth of the first or,

$$T_2 = \frac{6283}{15} = 418.87 \text{ sec} \tag{7.32}$$

and

$$T_2 = Z_2 \, \Delta t_2$$

$$\Delta t_2 = \frac{418.87}{127} = 3.29 \text{ sec.} \tag{7.33}$$

The upper limit on the useful frequency of this test signal will also be the 55^{th} harmonic, or

$$\omega_{m2} = 55 \ (2\pi)/418.87 \tag{7.34}$$

$$\omega_{m2} = .825 \text{ rad/sec} . \tag{7.35}$$

Figure 7.2 shows the bandwidth of the original 2047 bit signal and that of the two 127 bit replacement signals. The two test signals provide results at 110 frequencies, (127 x 0.44 x 2), compared to 999 frequencies for the original 2047 bit signal. If the two signal test procedure resolution is suitable, the test would require only 110/999, or approximately one tenth as much time to produce the same energy in the useful harmonics.

During the design of the PRBS test signal, the designer must be conscious of the effect of signal runs on the reactor response. A signal run is defined as a successive occurrence of a signal state[3]. In practical terms, the maximum run length of a signal dictates the maximum time which a control rod can remain in a given position. It has been shown that the length of the longest run in a PRBS with a

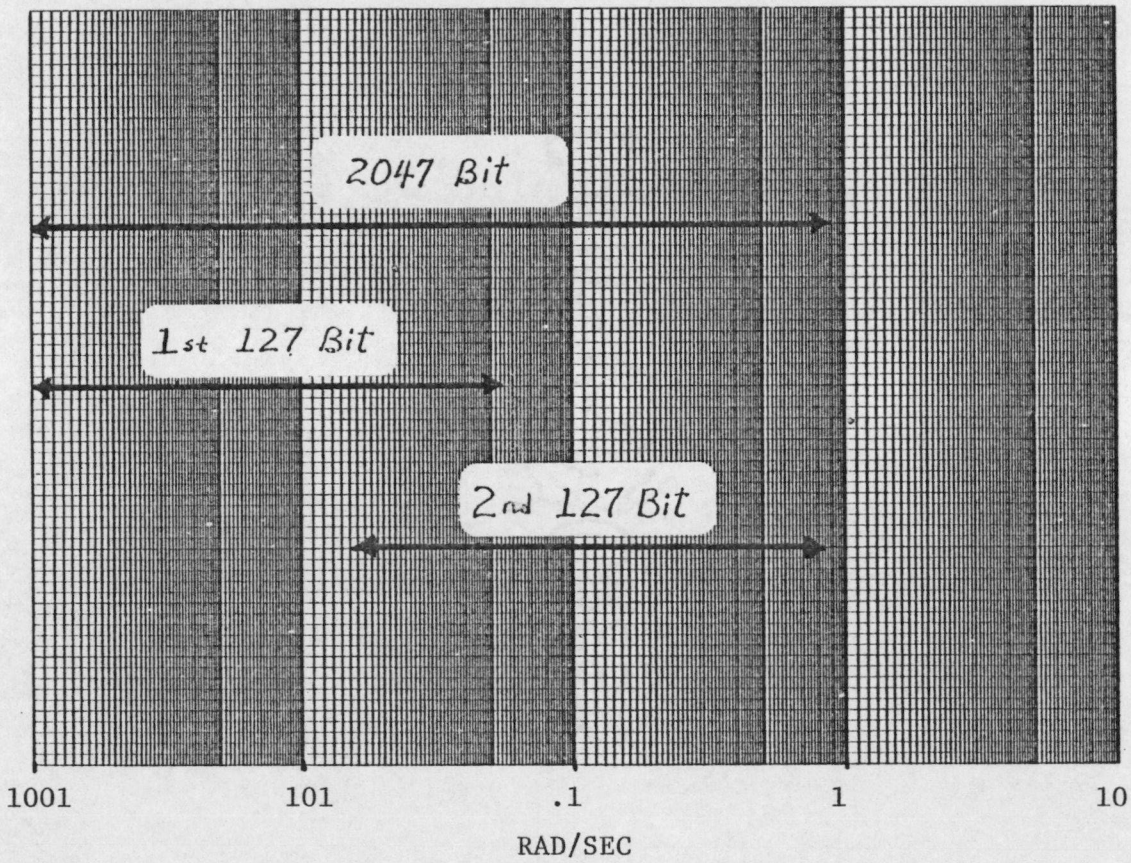


Figure 7.2 Bandwidth of 2047 Bit and Two 127 Bit Test Signals.

given period decreases as the number of bits increases[3]. The duration of the longest run is $n\Delta t$, where n is the integer in Equation 7.7, and Δt the bit width. For the case of the 2047 bit signal, the maximum run length is 33.8 seconds. The two 127 bit signals would have run lengths of 346.3 seconds, and 36.2 seconds respectively. These run lengths are of sufficient duration to warrant further consideration. In Section 7.5, it was determined that the maximum amplitude of the test signal will be on the order of 1.6 cents. In Section 5.3 it was shown that the system response to a 10 cent reactivity step perturbation is a 20.9% increase in power, with an accompanied 82°F rise in fuel temperature. Since these results were obtained with a linearized model, the sytem response to a 1.6 cent step would be 16% of the response to a 10¢ step. The reactor power would therefore, increase by 3.3% and fuel temperature by 13.1°F. The actual system response to the test signal would be somewhat lower in magnitude than the response to a step, due to the periodic nature of the test signal. The system response to the maximum theoretical run length of the test signal would therefore fall well within the limits for normal plant operation.

Another, parallel problem, is the question of whether the data acquisition system will be capable of resolving the relatively small response signal perturbations which will be produced by the 1.6¢ test signal. Table 7.2 lists the maximum response signal amplitudes which can be expected with the 1.6¢ test signal. It is clear from Table 7.2 that significant signal to noise ratio problems may be enountered if one attempts to use this low amplitude test signal. It has been

TABLE 7.2

PREDICTED NODAL RESPONSE TO 1.6 CENT TEST SIGNAL

Temperature	Response(Deg. F)
Inner Ref Upper Coolant	7.4
Outer Blanket Upper Coolant	5.4
IHX Primary Outlet	5.3

shown[14] that the error in the system response, E, is inversely proportional to the amplitude of the test signal, A, and inversely proportional to the square root of the test duration, T,

$$E \propto \frac{1}{A\sqrt{T}}$$

If one hopes to obtain the same response signal accuracy with the 1.6¢ signal as would be possible with the 10¢ signal, the 1.6¢ test duration must be,

$$\frac{T_{1.6}}{T_{10}} = \left[\frac{A_{10}}{A_{1.6}}\right]^2 = \left[\frac{10}{1.6}\right]^2 = 39.06$$

or approximately 39 times longer than that required if the system hardware were capable of producing binary input signals with a 10¢ amplitude. The conclusion is that any signal to noise ratio problems encountered can probably be eliminated by simply increasing the duration of the test signal sequence (number of times the periodic signal is repeated).

CHAPTER 8

TEST IMPLEMENTATION

8.1 Introduction

The first step in the test implementation program is the preparation of a detailed test proposal or procedure. This test procedure should include a thorough specification of any special test equipment, an identification of the plant sensors whose output will be monitored during the test, specification of any necessary modifications in the plant control or safety system operation during the test, some indication of the number of personnel and man hours required for test implementation, an analysis of the impact of the testing program on normal plant operation and safety and detailed plant operator instructions for test implementation. The operator instructions should include a listing of operator actions to be taken in case of test equipment failure during the test.

8.2 Method of Inputting Test Signal

As discussed in Section 2.11, the EBR-II has no form of automatic control. It will therefore be necessary to input the test signal sequence manually from the reactor control console. This process has been successfully used in the H. B. Robinson reactor[15]. The method consists of placing a set of marks on a roll of stripchart paper, which correspond to either control rod insertion or withdrawal. This record is run through the recorder at the appropriate speed needed to produce the desired signal pattern. The reactor operator need only watch the stripchart recorder and perform the necessary rod movement upon

visual cue from the recorder. The necessary PRBS may be generated with a digital shift register with Modulo-2 adder feedback[3]. The 127 bit PRBS may be generated with a 7 stage Modulo-2 shift register with feedback from stages one and seven. Figure 8.1 shows the necessary shift register configuration for generation of the signal. The rules for Modulo-2 addition are shown in Table 8.1. Table 8.2 shows the generation of the first 27 bits of the test signal. Column one of Table 8.2 is arbitrarily chosen as the signal control column. The signal represented by column one is shown in Figure 8.2 along with the actual EBR-II input signal produced by the control rods.

8.3 Data Acquisition and Analysis

The basic data analysis technique consists of Fourier analysis of the sensor time response signals to obtain the frequency response of the system. The data acquisition/analysis method to be used during the test is shown schematically in Figure 8.3. The signals from the sensors are preconditioned by the equipment in Figure 8.3, prior to being recorded and analyzed. Amplifier number one is an isolation amplifier, which serves as an inpedence matching device and thereby insures that data collection equipment does not disrupt the operation of the regular plant instrumentation. Amplifier number two is a differential amplifier which subtracts the sensor's ground signal from the live signal. This subtraction process removes any random noise component which is common to both leads from the live signal. The signal is next high pass filtered to remove the unwanted D.C. signal component. Amplifier number three is used to gain (or attenuate) the sensor signal as may be necessary for recording and analysis purposes.

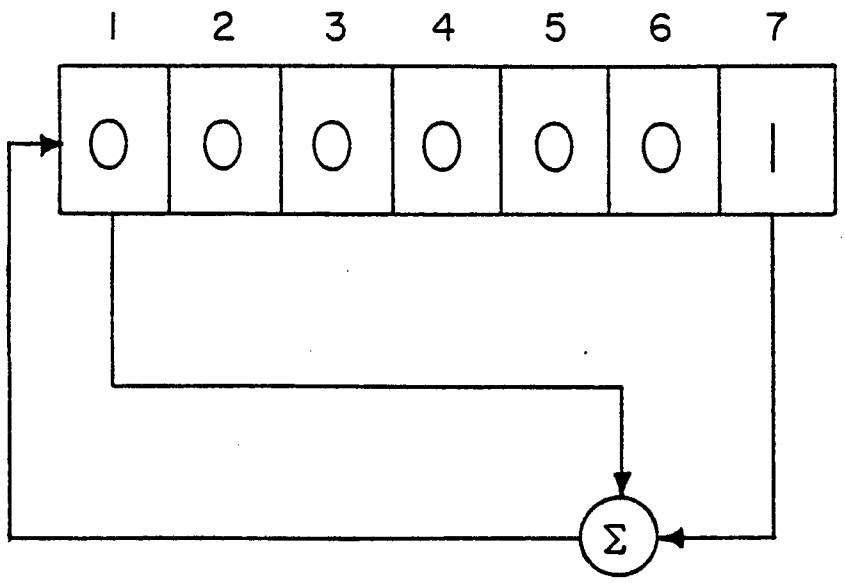


Figure 8.1 Seven Stage Modulo-2 Shift Register With Feedback From Stages One and Seven.

TABLE 8.1

MODULO-2 ADDITION RULES

m	n	(m+n) mod 2
0	1	1
1	0	1
1	1	0
0	0	0

TABLE 8.2

TEST SIGNAL GENERATION

0	0 0 0 0 0 1
1	0 0 0 0 0 0
1	1 0 0 0 0 0
1	1 1 0 0 0 0
1	1 1 1 0 0 0
1	1 1 1 1 0 0
1	1 1 1 1 1 0
1	1 1 1 1 1 1
0	1 1 1 1 1 1
1	0 1 1 1 1 1
0	1 0 1 1 1 1
1	0 1 0 1 1 1
0	1 0 1 0 1 1
1	0 1 0 1 0 1
0	1 0 1 0 1 0
0	0 1 0 1 0 1
1	0 0 1 0 1 0
1	1 0 0 1 0 1
0	1 1 0 0 1 0
0	0 1 1 0 0 1

TABLE 8.2 (continued)

1	1 0 0 1 1 0
1	1 1 0 0 1 1
0	1 1 1 0 0 1
1	0 1 1 1 0 0
1	1 0 1 1 1 0
1	1 1 0 1 1 1

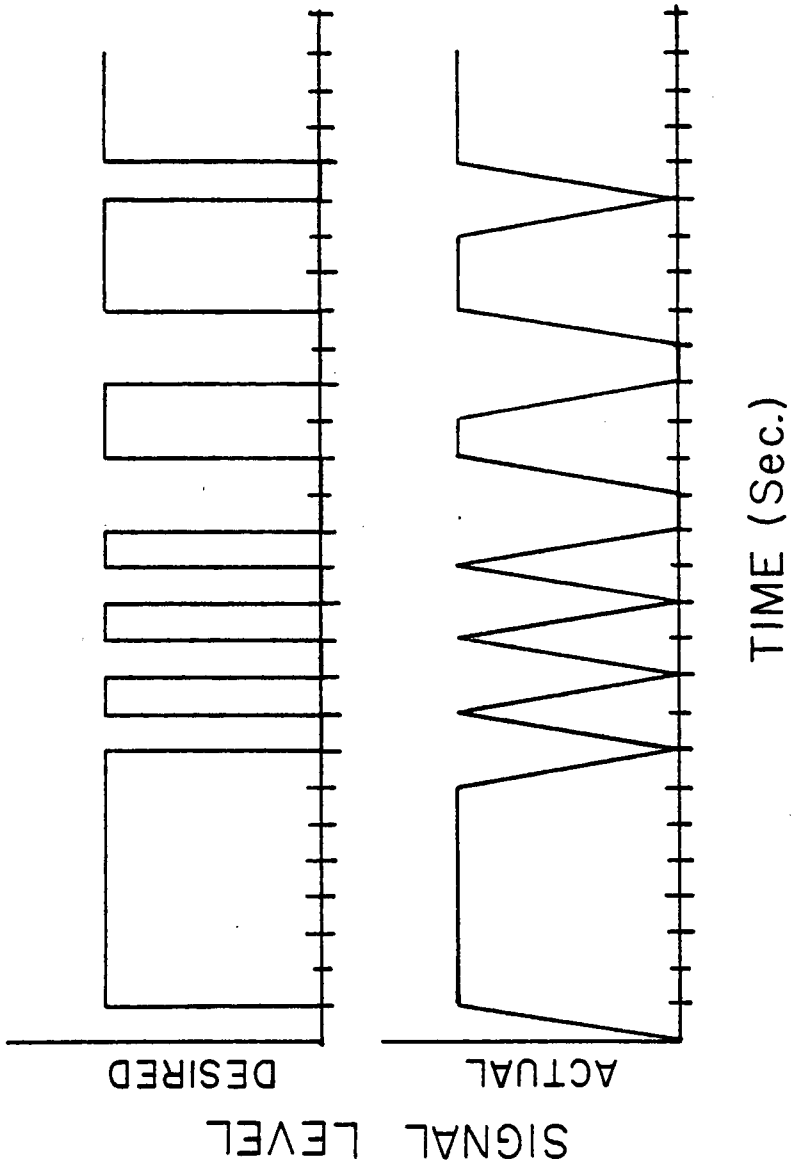


Figure 8.2 EBR-II Input Test Signal.

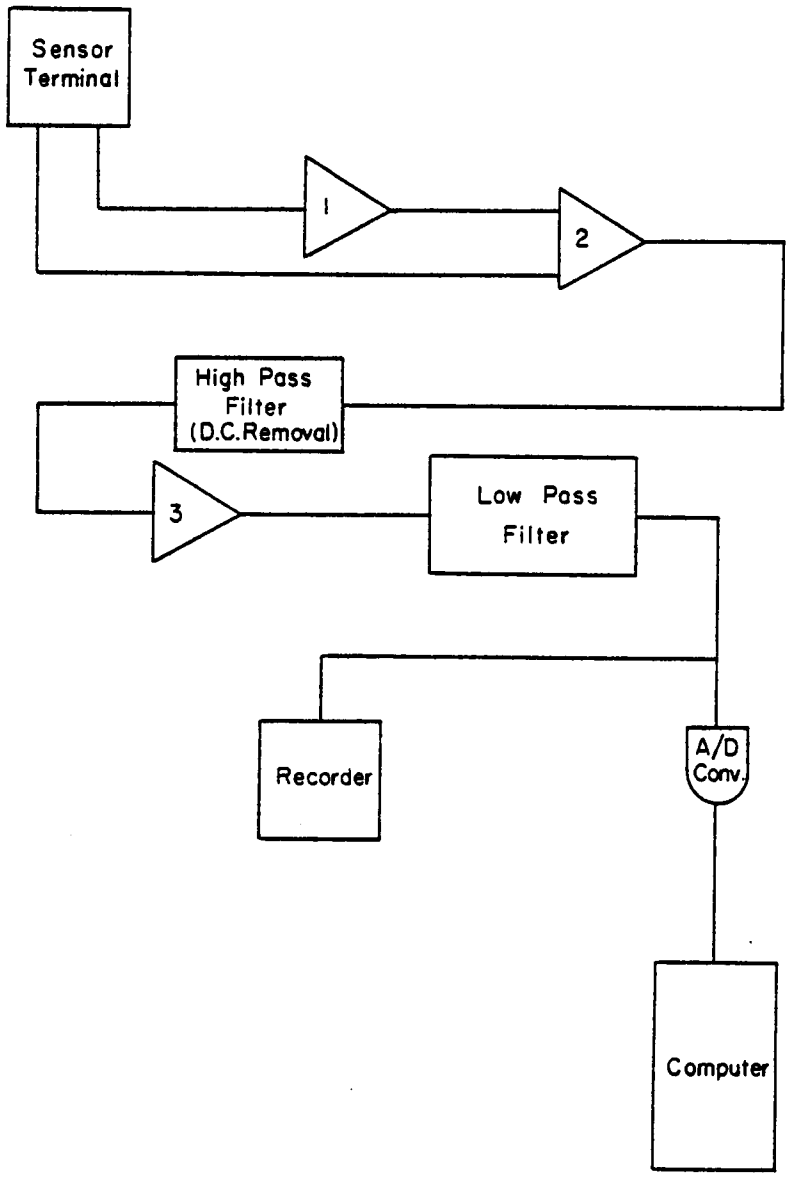


Figure 8.3 Data Acquisition Equipment Arrangement.

Prior to being processed by the on-line A/D converter and analysis system, the signals are low pass filtered to remove any high frequency contamination. At this point in the signal flow, the sensor signals are recorded on a multichannel FM recorder. Recording the signals at this point provides for retention of test data in case of analyzer failure and provides the experimenter the option of analyzing the data at a later time. The signals are then digitized and fed to a minicomputer, which performs the Fourier analysis. The on-line analysis process does not begin until the initial signal transients have died out, and the sytem response in two adjacent periods of the periodic waveform have been acquired.

8.4 Interpreting Results

As soon as the test is complete, the frequency response of a system will be available for immediate examination. The occurrence of resonance peaks or any other anomaly in the plant frequency response should be evident at this time. This plant closed loop frequency response, G_c, can be used in conjunction with the methods discussed in Section 4.5 to determine the plant stability margin. The other main area of data interpretation is in plant parameters and model verification. The parameter identification process makes use of the techniques discussed in Chapter 6 i.e., minimization of the difference between experimental and model frequency response by systematic adjustment of model parameters. The computer code PARAPE[16] would be used for this purpose. Upon completion of this parameter adjustment process, these optimized parameters will be employed in the 38 node

model, to give accurate prediction of the actual EBR-II systems response to any reactivity or IHX secondary sodium inlet temperature perturbation of interest.

CHAPTER 9

COST/BENEFIT ANALYSIS

9.1 Introduction

A detailed cost/benefit analysis of dynamic testing in the EBR-II will be presented in this chapter. An effort will then be made to examine the cost/benefit ratio of dynamic testing in LMFBR's on a generic basis. Finally, an attempt will be made to quantify the benefits of dynamic testing to LMFBR power plant owners and operators in light of current Nuclear Regulatory Commission (NRC) safety and licensing practices.

9.2 Costs of Testing in EBR-II

In previous chapters, it was concluded that frequency response tests of high accuracy can be performed in EBR-II. Since these testing procedures require no modification of standard plant hardware, the costs of test implementation can be categorized primarily as those costs associated with procurement of the necessary test equipment, test equipment installation and data analysis (both manpower costs and computer time costs).

Referring to Figure 8.3, one sees that a signal conditioning unit will be needed for each channel of data to be recorded. This conditioning unit would include amplifiers 1 through 3, and the low and high pass filters. The estimated hardware costs of the testing program in LMFBR's in general are shown in Table 9.1. It is important to note that $50,000 or 85% of the test equipment costs is associated with the recorder and computer analyzer, items which can be used in

TABLE 9.1

TEST HARDWARE COSTS

Signal Conditioner ($1000.00/channel)	6000.00
Strip Chart Recorder	2500.00
Tape Recorder	20000.00
Mini Computer based Fourier Analyzer and Terminal*	30000.00
Misc.	200.00
	$58700.00**

*Does not apply to EBR-II (See Text)

**$28700.00 in EBR-II

many other applications. It is also important to note that if a plant computer of the type currently being installed in commercial LWR plants were available, the equipment costs would be reduced to $28700.00. This fact is a significant consideration in the cost/benefit analysis of dynamic testing in future commercial LMFBR plants, which most certainly will include a minicomputer in their basic plant design for data acquisition, analysis and plant control purposes. In the particular case of EBR-II, the minicomputer is already in place, and will not have to be purchased for the project. The actual cost of test hardware in EBR-II will be on the order of $28,700.

9.3 Approximate Man Power Costs

The man power costs associated with a dynamic testing program in EBR-II can be divided into those costs associated with initial equipment installation, and those associated with routine testing and data analysis.

The initial hardware installation process will require the services of a plant instrument mechanic and the experimenter. Together, they would decide upon the best points for coupling the various test instruments to the plant instrumentation and the physical locations of the test hardware. These costs are summarized in Table 9.2.

Those manpower costs associated with the routine tests must now be considered. The testing procedure will require three people - the experimenter, the analyst and a plant operator. From Section 7.8, one test sequence will involve inputing two test signals. The time required for this procedure will be (6283 + 418 = 6701 seconds) or approximately 2 hours. As mentioned in Section 8.8, due to low signal

TABLE 9.2

HARDWARE INSTALLATION MANPOWER COSTS

Personnel	Number	Number Hrs. Required	Cost Hr	Individual Cost
Instrument Mechanic	1	80	$25	$2000
Experimenter	1	120	$25	$3000
		Total		$5000

to noise ratios on some of the channels, it will probably be necessary to take data during multiple test input sequences. It is therefore reasonable to assume that an entire eight hour shift might be dedicated to each regularly scheduled test. Each test would, therefore, require the presence of the analyst and instrument mechanic for an eight hour period. If one makes the assumption that the plant would be operating in the normal mode were the test not being conducted, the presence of the operator during the test period represents no additional man power cost. In addition to these costs, the analyst must spend a substantial amount of time running the parameter optimization/identification program PARAPE (Section 8.4) after the frequency response has been obtained. This parameter identification work must be performed with the aid of a much larger computer such as the IBM 360/370 series. It is estimated that this work will require approximately 30 man hours of the analyst's time after each test. The costs associated with each test are summarized in Table 9.3.

It is highly likely that in many cases, the investigator will wish only to examine the stability margin for changes that may have occurred since the last test. In these cases, the investigator would spend only approximately 3 hours working with the raw Fourier analyzer data, and no additional computer time. For tests of this nature, the actual incremented test cost would be ((8x25) + (8x25)) or $475, rather than the $1900 value derived for a complete parameter identification analysis.

9.4 Summary of EBR-II Test Costs

Table 9.4 summarizes the test cost analysis results. It is

TABLE 9.3

INCREMENTAL TEST COSTS

Man Power

Worker	# Hours	Rate	Cost
Analyst	38	$25/hr	$950
Inst. Mech.	8	$25/hr	$200
		Total Manpower	$1150

Computer Time*

# hrs CPU	Rate	Cost
3**	$250/hr	$750
	Total Single Test Cost	$1900

*Parameter Identification Work

**IB3 360/65

TABLE 9.4

EBR-II TESTING PROGRAM COSTS

Hardware Costs	$28,700.00*
Hardware Installation Costs	5,000.00
Total One-Time Costs	$33,700.00**
Total Incremental Testing & Analysis Costs	$ 1,900.00

*$58,700.00 for a plant not having a mini computer available for test data analysis

**$63,700.00 for a plant not having a mini computer available for test data analysis

apparent that the capital cost of hardware procurement and installation far overshadows the cost of the routine testing procedure. It is also now evident that the capital cost of the computer based Fourier analyzer system represents the dominant cost in any moderately aggressive testing program in future LMFBR's. It is obvious that the availability of a plant computer for analysis work would result in a great reduction in the cost/benefit ratio for the dynamic testing program. However, it is nearsighted to imagine that any computer system purchased for the testing program would not be useful for routine operational parameter data acquisition and analysis and other plant projects. When viewed in this fashion, it is clear that designating the total computer system cost as a testing program cost is, in most cases unrealistic, due to cost sharing with other projects.

9.5 Costs of Rod Drop Testing

Sections 9.2 and 9.3 discussed the costs of implementing a PRBS dynamic testing program in EBR-II. As mentioned in Section 1.3, both rod drop and oscillator rod tests have been employed for many years in dynamic testing of nuclear reactors. Tests of this nature have been performed in EBR-II on a continual basis since plant startup in the early 1960's.

The rod drop method employed in EBR-II allows determination of the time-dependent, linear, feedback transfer function. Typically three to five rod drop tests are conducted for a given set of power and coolant-flow conditions, and the results are averaged. The drop rod is first released at 500 KWt, a power level low enough that feedback effects are unimportant. The power trace from these data are

digitized and analyzed by inverse kinetics to yield the reactivity without feedback. In the remaining tests, the drop rod is released at the desired power level, the data is digitized and the reactivity is determined. This reactivity is subtracted point by point from that found at 500KWt, yielding the feedback results. This analysis is performed by an on-line IBM-1620 computer. Drop-rod worths of 1.5 to 4.5 cents have been employed in the tests.

While the rod-drop technique is easily implemented, it is accompanied by several disadvantages. Since the rod drop (step) perturbation's energy is concentrated in the d.c. region, signal-to-noise ratio problems are often encountered when wideband information is desired. Wideband frequency response results of the type needed for parameter identification work are, therefore, difficult to obtain and the results from several tests must be averaged together to obtain useful wideband data. Perturbations of the magnitude needed to overcome signal-to-noise problems can easily disrupt EBR-II irradiation experiments and would be highly undesirable in any commercial LMFBR facility. Another factor to be considered in an evaluation of the EBR-II rod drop program is that the procedure employed in EBR-II requires that the reactor be brought to very low power for the first run of each test sequence. In the EBR-II, this procedure could interfere with the in-core experiments. In a commercial LMFBR, this type of test procedure would be highly undesirable, since it would result in a decrease in power production.

In summary, it is felt that although the rod-drop test is easily implemented, it represents a substantial disruption to the normal plant operating procedure, requires more analytical or mathematical

manipulation to obtain the information experimentally than does either the oscillator rod or PRBS test, and would in the final analysis, be a more costly method of testing than the PRBS method.

9.6 Costs of Oscillator Rod Testing

The original equipment consisted of a reciprocating oscillator rod with a frequency range of 0.001 to 1.1 Hz (.0063 - 6.9 rad/sec). This unit failed during run 2. Three other oscillator rods have since been employed. The second rod suffered a premature mechanical failure which forced its removal after a short period of time during run 24. The third rod also suffered mechanical problems which resulted in limitation of its useful frequency range to the region 0.1 through 8.8 Hz (.628 - 55 rad/sec) at power levels of 30 MWt. The latest oscillator rod consists of two adjacent cylinders rotated axially about a line on the radius of each and on their radial centers.[17] This unit has yielded results over the frequency range 0.001 through 10 Hz (.0063 - 62.8 rad/sec). The hardware costs associated with the installation of this most recent oscillator rod were on the order of a half million dollars. It is apparent that dynamic tests of the type described in this thesis can result in a considerable economic savings when compared to the costs associated with the implementation of a testing program employing the oscillator rod technique.

9.7 The Economic Impact of Dynamic Testing on LMFBR Design and Operation

Dynamic testing in general, and PRBS testing in particular, can significantly influence the design and operational economics of future

LMFBRs. This impact can occur in three separate areas: (1) Reducing unnecessary plant design conservatisms (2) Reducing unnecessary plant operational conservatisms and (3) Providing a less expensive method of obtaining the stability margin and safety related performance data required of reactor owners by the Nuclear Regulatory Commission.

A reduction in plant operational conservatisms could be brought about via identification of the reactor heat transfer coefficients. In a operational plant, the power distribution and core coolant temperatures are normally known. The core fuel to coolant heat transfer coefficient identified by methods discussed in this thesis can therefore be used in local heat balance equations to determine spatial fuel temperatures. If it could be shown that the fuel temperatures are significantly lower than some current operational limit, the reactor owner might be allowed to raise the operation power level of the reactor. If the reactor were a power production unit, the income produced by the sale of the additional energy could easily approach several hundred thousand dollars annually.

For the plant designer's viewpoint, a precise determination of the spatial fuel temperature distribution during a transient would identify the amount of stored energy in the system. Reactor emergency core coolant systems (ECCS) and residual heat removal systems (RHRS) are designed on the basis of their ability to safety handle this stored energy. If it could be shown that for a given size plant, the actual fuel temperatures were significantly lower than the ECCS and RHRS design base temperatures, the ECCS and RHRS of future plants could be "downsized." This reduction in the necessary heat removal capacity of these sytems and the subsequent reduction in the physical

size of the components could result in a substantial savings to those companies purchasing future LMFBR's.

Finally, it is very probable that the NRC (Nuclear Regulatory Commission) will require that frequency response tests be conducted in all future LMFBR's in order to verify their stability margins. One must examine the relative costs involved in performing these tests with the methods discussed in this thesis, versus the costs of conducting oscillator rod tests. In Section 9.4 it was shown that the total costs of implementing a PRBS testing program in the EBR-II are $33,700, plus $1900 per test (if one wishes to obtain the maximum amount of information from each test). Even a superficial comparison of these costs to those associated with oscillator rod tests, (Section 9.6), reveals the tremendous economical incentive to implement a PRBS testing program in those cases where the NRC requires such stability margin data. The PRBS method would also be superior to the rod-drop test, since a commercial plant could remain on-line while the tests are conducted.

CHAPTER 10

CONCLUSIONS AND RECOMMENDATIONS FOR FUTURE WORK

10.1 Conclusions

This thesis has discussed the development and implementation of a dynamic testing program in the EBR-II. In Chapter 5, it was concluded that the primary system responds so slowly to IHX secondary inlet sodium temperature changes that these perturbations are not suitable for test purposes. In Chapter 6, it was determined that accurate frequency response tests can be performed in the EBR-II with reactivity perturbation signals. In addition to the plant stability margin, the tests should yield accurate values for the sodium pot residence time and the heat transfer coefficient-area products of the core, inner reflector and outer blanket regions. Accurate values for both the primary and secondary IHX heat transfer coefficients should also be obtainable.

Chapter 7 discusses the design of the test signal. The test procedure chosen involves the use to two different 127 bit PRBS signals - the first with a 49.47 second bit width, and the second having a 3.29 second bit width. Due to the lack of any form of automatic control system, these test signals will be input manually from the control console.

Chapter 8 discussed the implementation of the testing program and concluded that standard plant control rods and sensors may be utilized in the test. This fact eliminates the need for any expensive plant hardware purchase or modification.

In Chapter 9 the costs of implementing a dynamic testing program in EBR-II was analyzed. It was concluded that the implementation program would involve a maximum one-time cost of $33700.00, with an associated incremental or single test cost of $1900.00. The figures indicate the maximum probable test cost, assuming a complete parameter identification analysis is performed after each test. Since it is highly unlikely that a complete analysis would be performed after each test, the actual incremental test cost would be approximately $475.00. To be viewed in perspective, the costs must be compared to the several hundred thousand dollar cost of implementing a comparable oscillator rod testing program. It was also shown that real possibilities exist for reducing plant construction costs and/or increasing plant power (and therefore revenue via sales of the increased electricity production) through the use of plant operational parameter identification methods discussed in this thesis.

10.2 Future Work and Study

It is recommended that the frequency response tests described in this thesis be performed in EBR-II. The results of these tests should be used to augment and verify the data previously obtained in the oscillator rod program. The parameter identification techniques can provide useful and hitherto unavailable information about plant operational parameters.

The plant model employed in this analysis could be improved. Some form of core bowing and control drive expansion reactivity feedback could be incorporated. If parameter identification work is to be performed, care must be taken to ensure that this modification does

not disturb the physical integrity of the model. A more accurate representation of the sodium temperature within the primary vessel (pot) could be employed. Temperature stratification is known to occur within the sodium, but the current model represents the entire sodium mass as a single node. It is also believed that significant heat losses occur through the upper plenum wall[18]. This phenomenon occurs due to the fact that the plenum wall is in contact with the hot core sodium on one side, and the much lower temperature pot sodium on the other. A representation of this process should be included in any future EBR-II model modifications.

In addition to the modifications mentioned above, the model could be expanded to include the entire plant, i.e., the reactor core through the utility grid connections. This expanded model would be useful for general LMFBR electric power plant control system studies. This model expansion could be of particular significance, since the EBR-II is the United States' sole LMFBR power productional facility.

LIST OF REFERENCES

LIST OF REFERENCES

1. Huynh, Quang An, "A Cost/Benefit Analysis for Dynamic Testing in the Fast Flux Test Facility," M.S. Thesis, Nuclear Engineering Department, The University, Knoxville (March 1979).

2. Foltman, A. J., "Limitations of EBR-II Rod-Drop Tests and Proposed Improvements Using Frequency Response Testing," Contribution Paper, Proceedings of the Second Power Plant Dynamics, Control and Testing Symposium, Knoxville, Tennessee (September 1975).

3. Kerlin, T. W., Frequency Response Testing in Nuclear Reactors, Academic Press, New York (1974).

4. Katz, E. M., "Planning, Performing, and Interpreting Dynamic Measurements in Pressurized Water Reactors," Ph.D. Dissertation, Nuclear Engineering Department, The University of Tennessee (June 1975).

5. Argonne National Laboratory, EBR-II System Description (June 1971).

6. Madell, J. T., and Jarka, R. E., "Analysis of the Linear Components of the Power-Reactivity Decrement (PRD) in EBR-II," (ANL-7539), Argonne National Laboratory (October 1969).

7. Ball, S. J., "Approximate Models for Distributed Parameter Heat Transfer Systems," ISA Trans., 3,38 (January 1964).

8. Ball, S. J. and Adams, R. K., "MATEXP: A General Purpose Digital Computer Program for Solving Ordinary Differential Equations by the Matrix Exponential Method," ORNL-TM-1933, Oak Ridge National Laboratory (August 1967).

9. Saphier, D., Kirsch, L. W. and Mulcahey, T. P., "A Reactor Core Model for a Fast Breeder Power Plant Simulator," Contributed Paper, Proceedings of the Second Power Plant Dynamics, Control and Testing Symposium (September 1975).

10. Kerlin, T. W. and Lucius, J. L., "The SFR-3 Code - A Fortran Program for Calculating the Frequency Response of a Multivariable System and its Sensitivity to Parameter Changes," ORNL-TM-1575, Oak Ridge National Laboratory (October 1975).

11. Campise, A. V., "Dynamic Simulation and Analysis of EBR-II Rod-Drop Experiments," (ANL-7664), Argonne National Laboratory (March 1970).

12. Chang, S. I. and Kerlin, T. W., "Identification of Nuclear Plant Parameters Using Experimental Data and High-Order Dynamic Models," Nuclear Science and Engineering 64, 673-683 (1977).

13. Buckner, M. R., "A Study of the Application of System Identification Techniques in the Analysis of Nuclear Reactor Dynamics," M.S. Thesis, Nuclear Engineering Department, The University of Tennessee, Knoxville (1968).

14. Hennig, T., "Testing for Plant Transfer Functions in the Pressure of Noise and Nonlinearity, Part II," Control Engineering 10, 119-124 (1963).

15. Thakkar, J. G., "Correlation of Theory and Experiment for the Dynamics of a Pressurized Water Reactor," M.S. Thesis, Nuclear Engineering Department, The University of Tennessee, Knoxville (March 1975).

16. Chang, Sen-I, "A Method for Systematic Interpretation of Dynamic Measurements in a High Temperature Gas-Cooled Reactor," M.S. Thesis, Nuclear Engineering Department, The University of Tennessee, Knoxville (March 1976).

17. Hyndmar, R. W. and Tuck, M. R., "An On-line Method of Transfer Function Analysis at EBR-II," Nucl. Appl. 16, 137 (February 1969).

18. Feldman, E., Mohr, D. and Gillette, J., Personal Communication, (August 1978).

APPENDIXES

APPENDIX A

FORMULAS FOR HEAT TRANSFER RESISTANCES IN CYLINDRICAL RODS

The formulas given here were used in the calculation of fuel pin thermal resistances and derived in Reference 1.

1. No internal heat generation

$$R = \frac{\ln r_o/r_i}{4\pi kL}$$

2. Annular rings with same thermal conductivity, Q''' = Constant:

$$R_{i,i+1} = \frac{(r_{i+1}^2 - r_{i-1}^2)/r_i^2}{8\pi kL}$$

3. Annular rings with different thermal conductivity, Q''' = Constant:

$$R_{i,i+1} = \frac{1}{8\pi L}\left[\frac{r_{i+1}^2 + r_i^2}{k_{i+1} r_i^2} - \frac{r_{i+}^2 r_{i-1}^2}{k_i r_i^2}\right]$$

4. Annular ring closest to the surface of the cylinder, Q''' = Constant:

$$R_{SO} = \frac{(r_s^2 - r_{s-1}^2)/r_s^2}{8\pi kL}$$

5. Clad node average-to-clad surface:

$$R_{CAS} = \frac{\ln(r_o/r_i)}{r\pi kL}$$

6. Fluid film resistance:

$$R_f = \frac{1}{h2\pi r_o L}$$

APPENDIX B

The frequency response of the 38 node EBR-II model for reactivity perturbations is shown in the following figures.

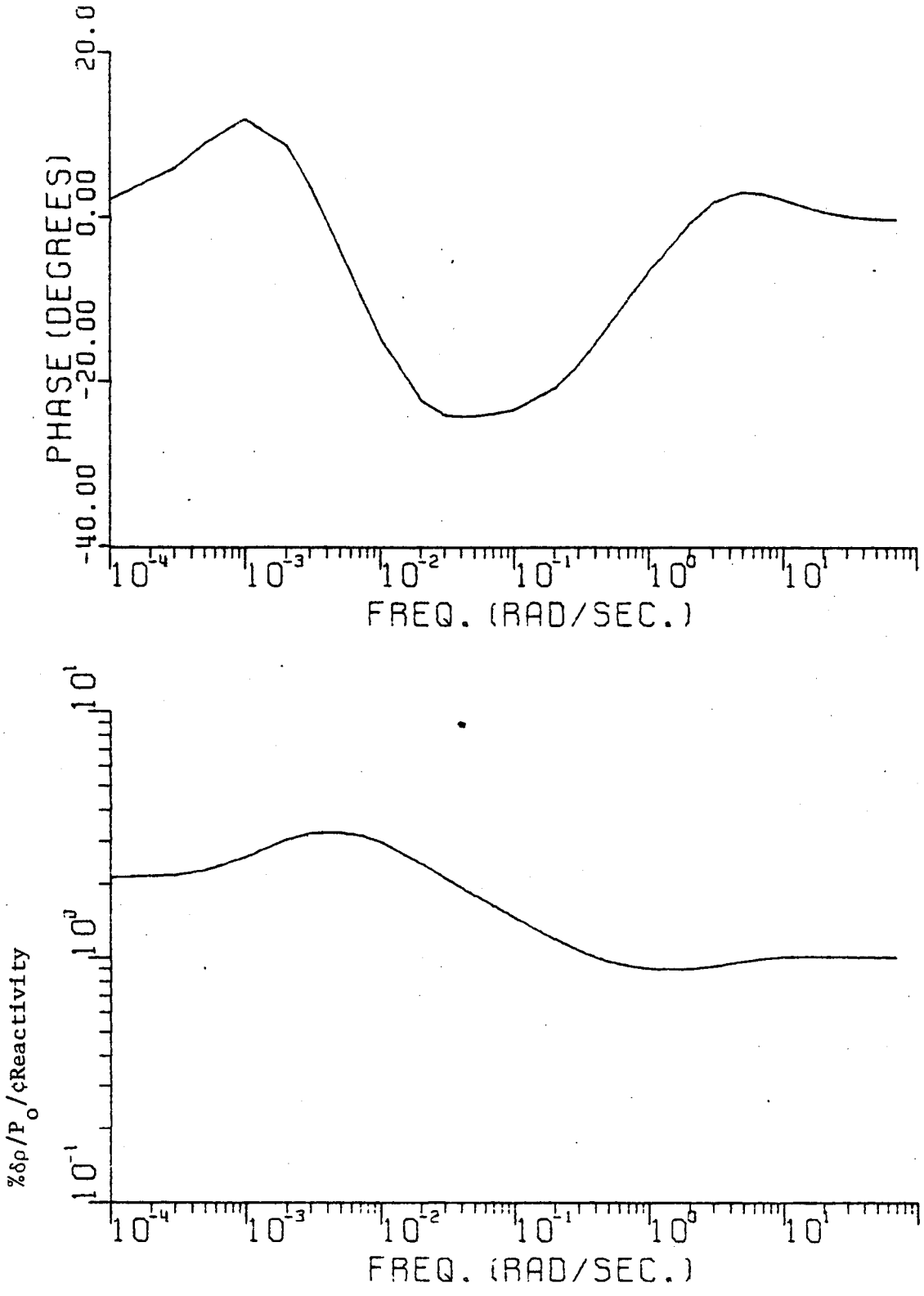


Figure B.1 Frequency Response of Reactor Power for Reactivity Perturbations.

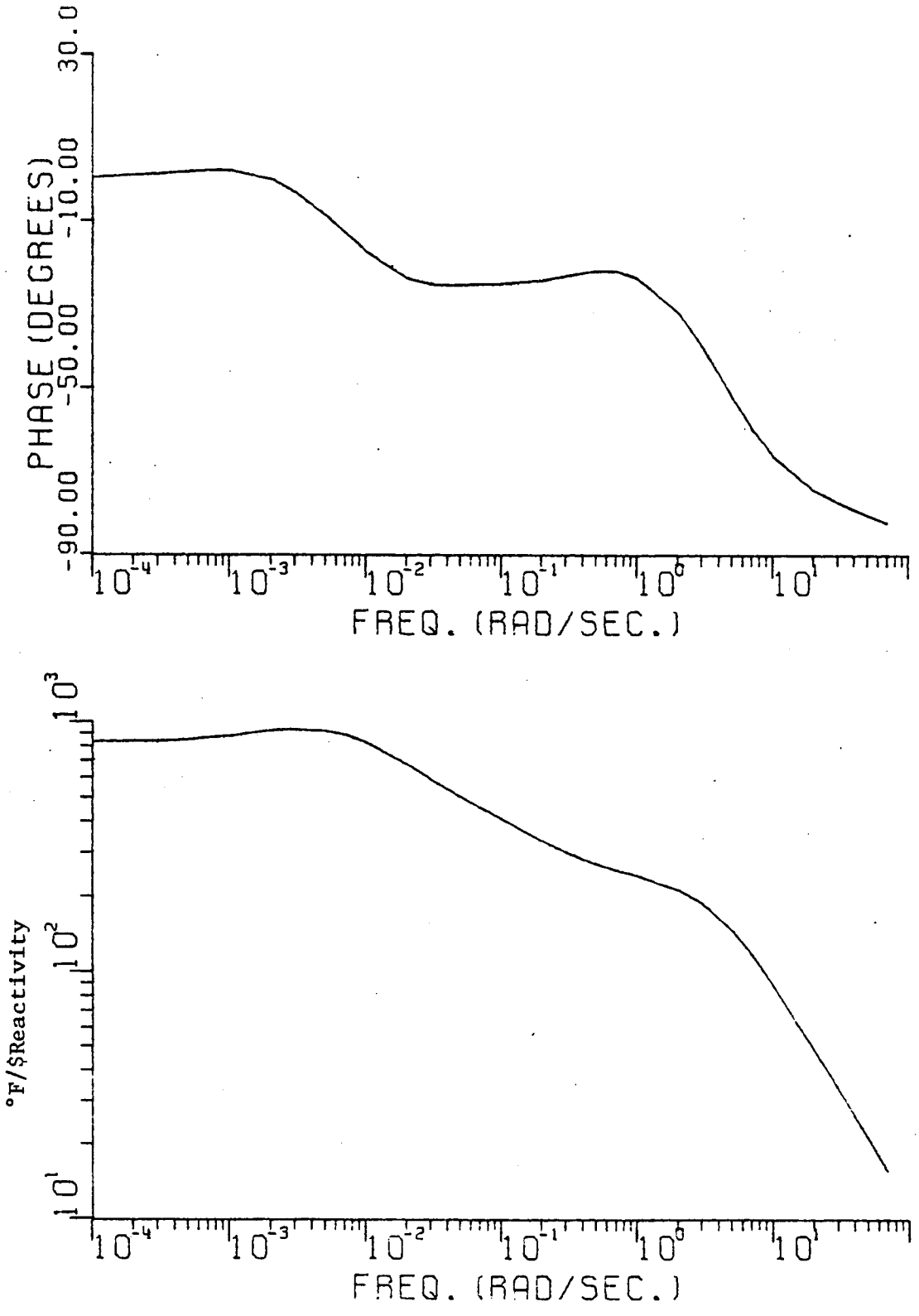


Figure B.2 Frequency Response of Fuel Temperature for Reactivity Perturbations.

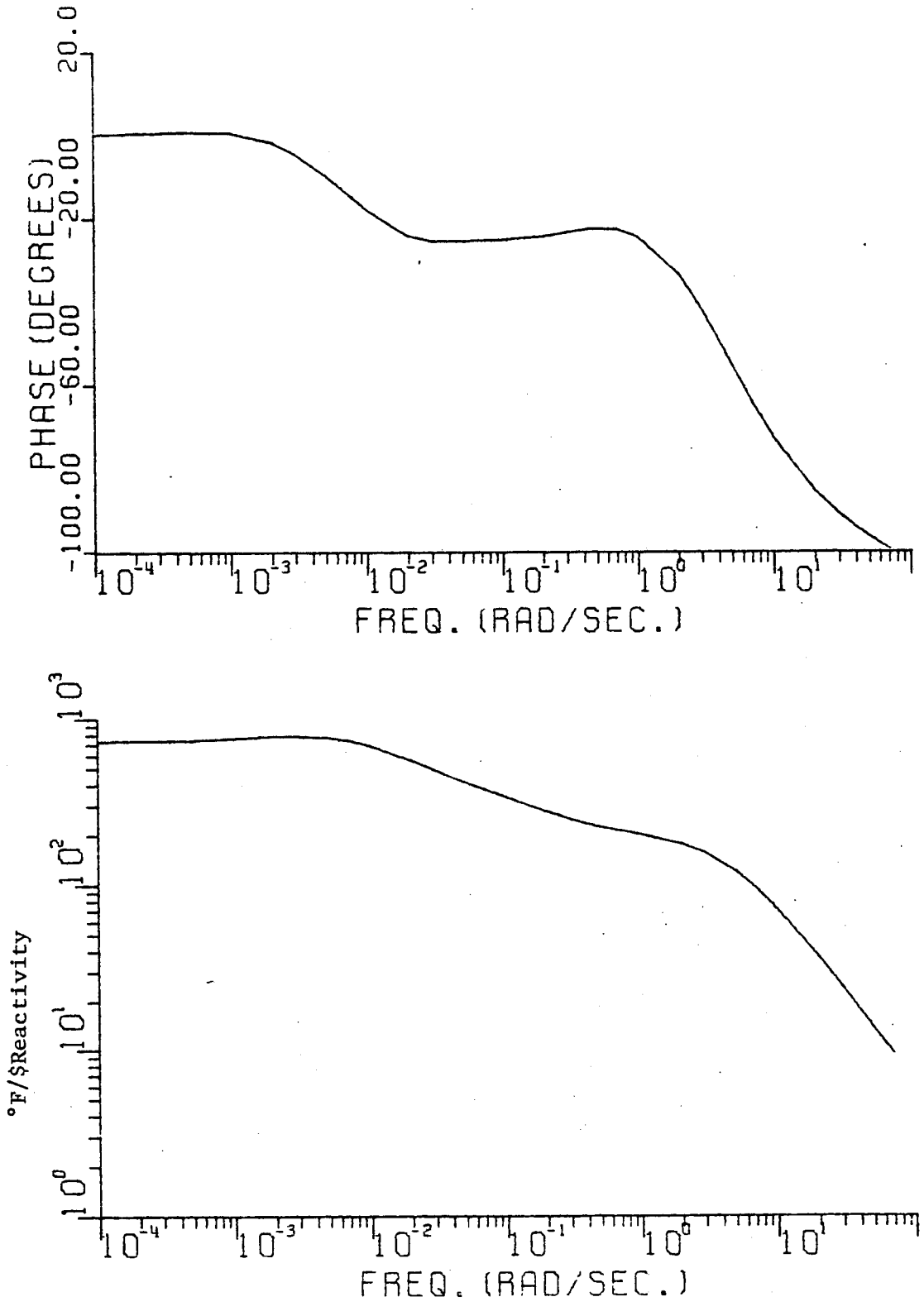


Figure B.3 Frequency Response of Fuel Pin Sodium Bond Temperature for Reactivity Perturbations.

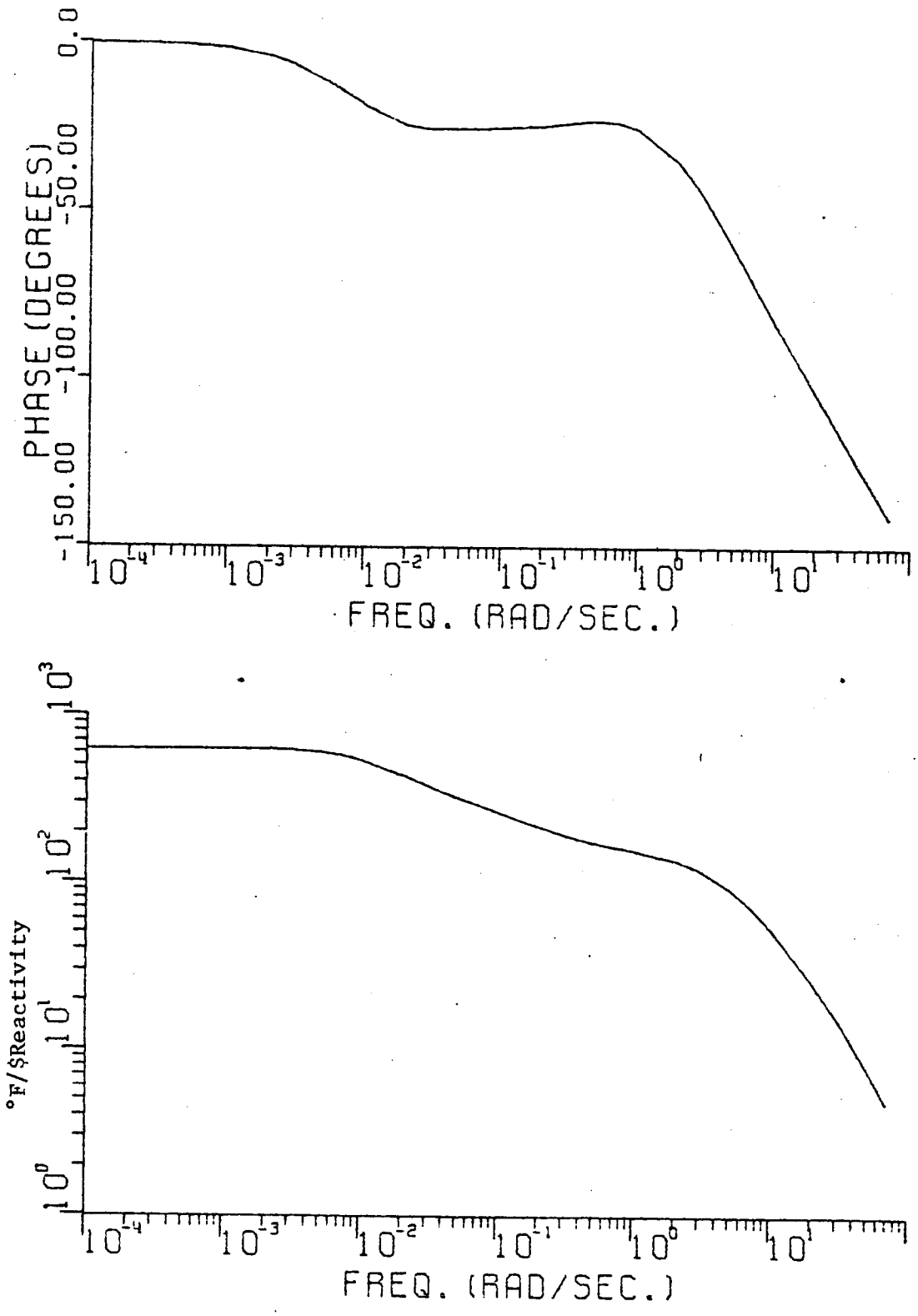


Figure B.4 Frequency Response of Fuel Cladding Temperature for Reactivity Perturbations.

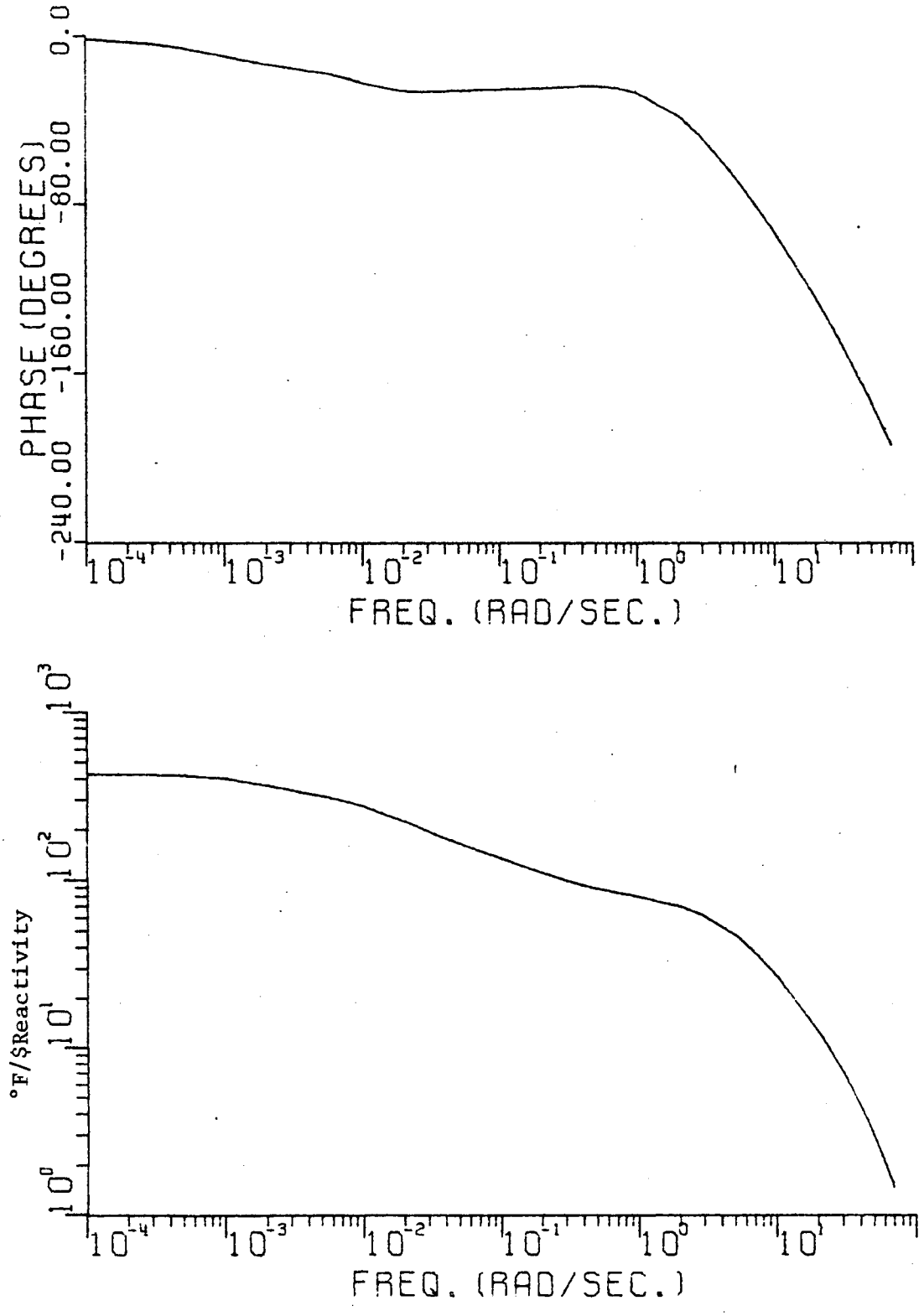


Figure B.5 Frequency Response of Lower Core Sodium Temperature for Reactivity Perturbations.

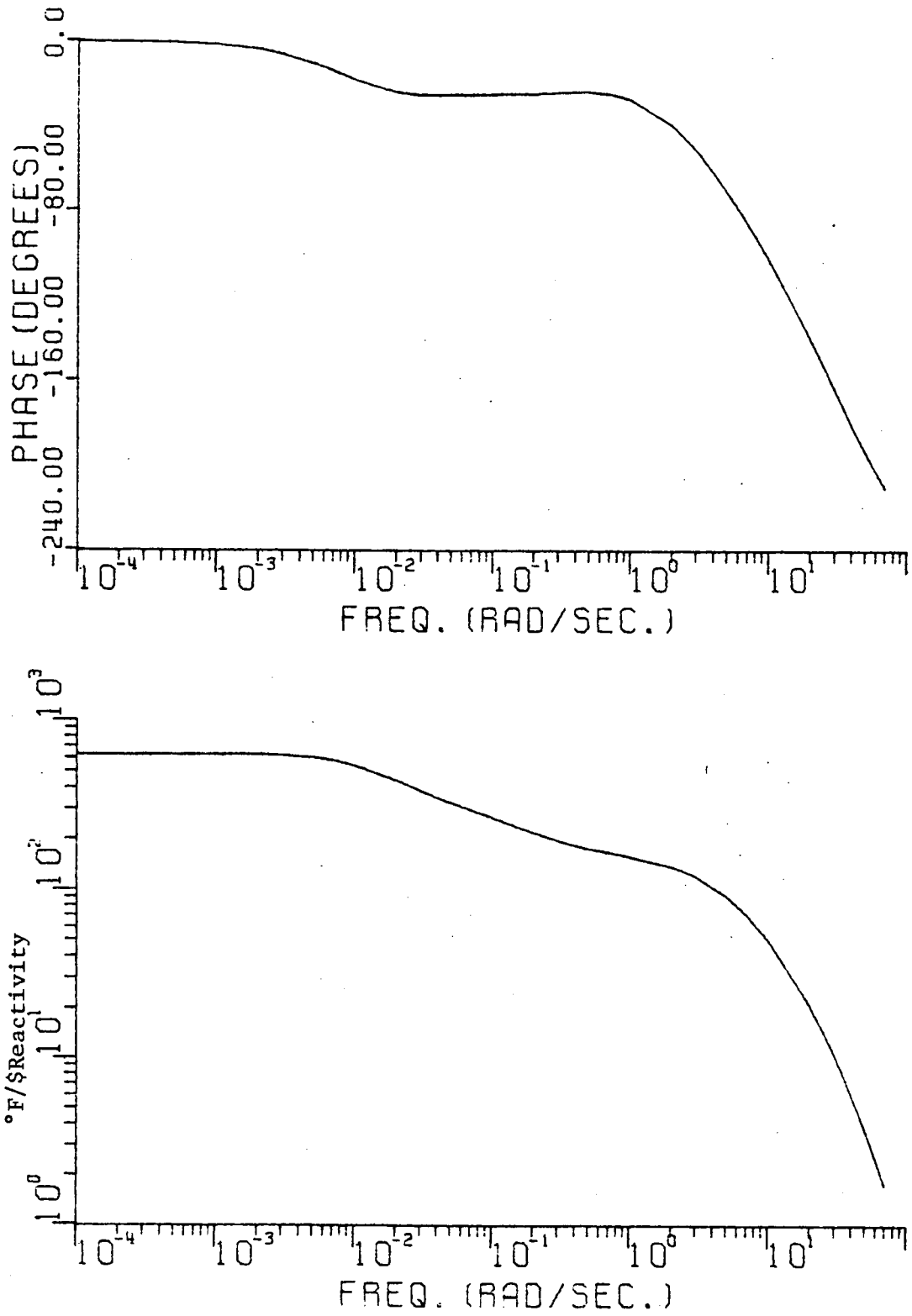


Figure B.6 Frequency Response of Upper Core Sodium Temperature for Reactivity Perturbations.

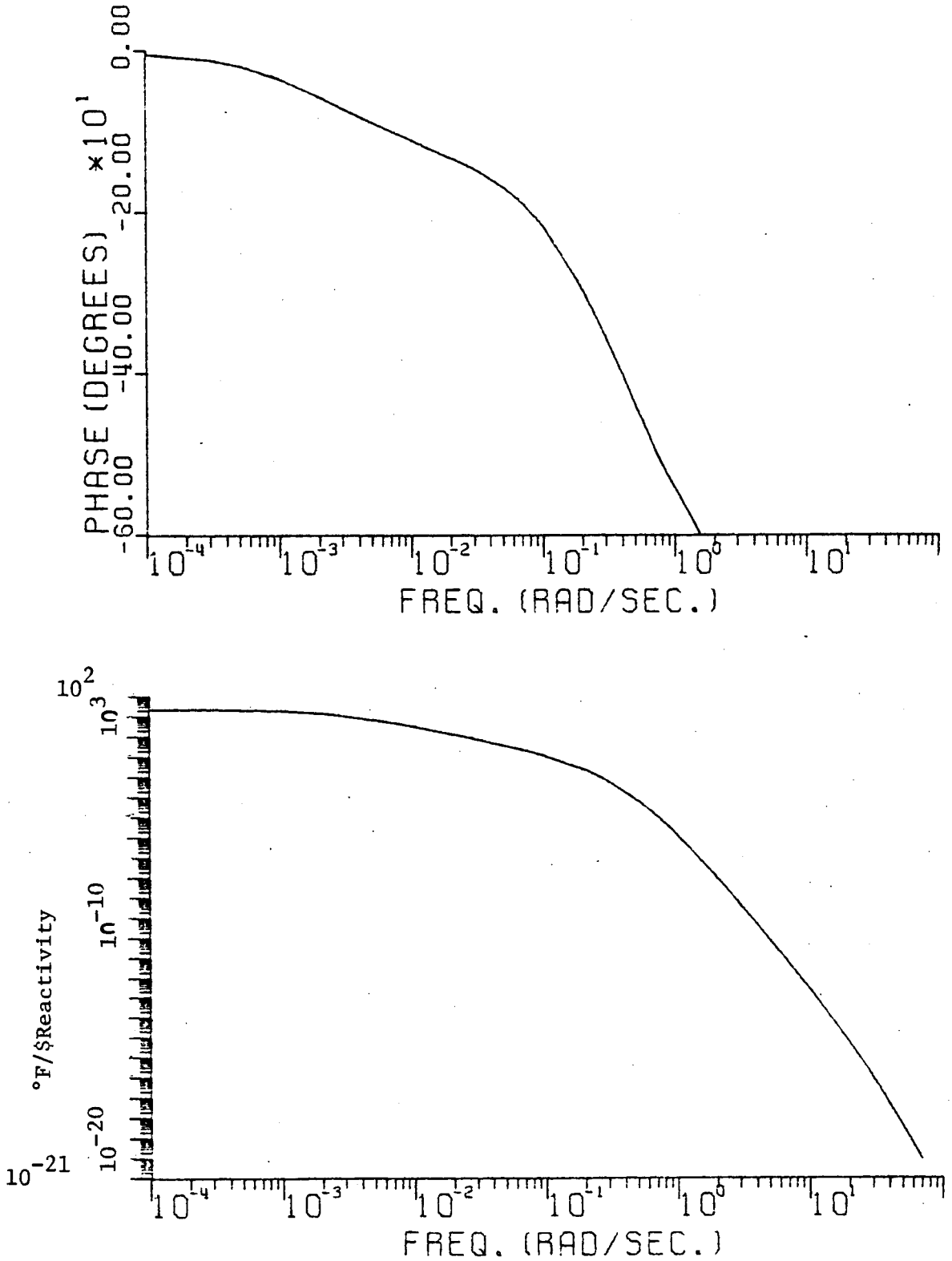


Figure B.7 Frequency Response of Low Pressure Inlet Sodium Temperature for Reactivity Perturbations.

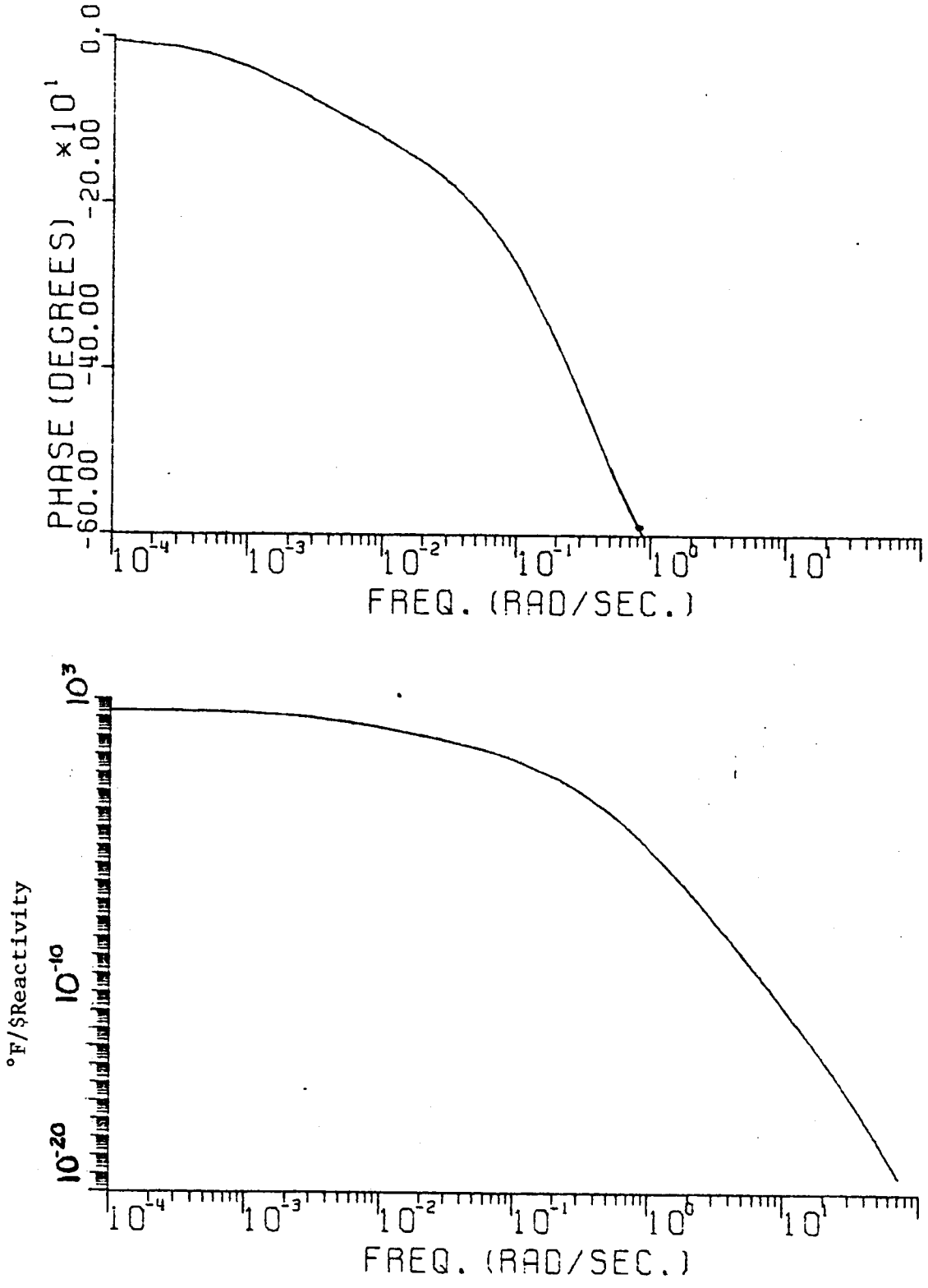


Figure B.8 Frequency Response of Low Pressure Plenum Sodium Temperature for Reactivity Perturbations.

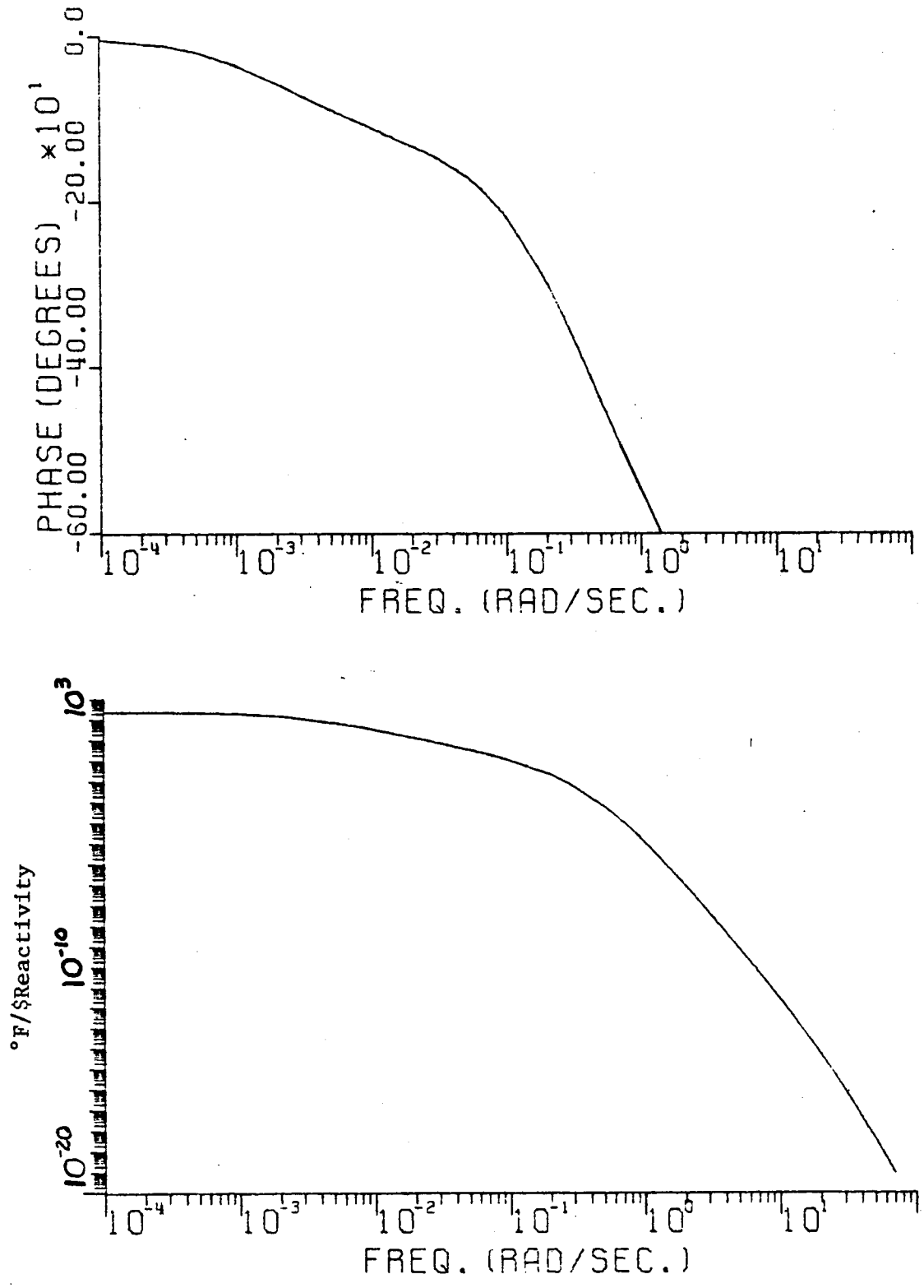


Figure B.9 Frequency Response of High Pressure Inlet Sodium Temperature for Reactivity Perturbations.

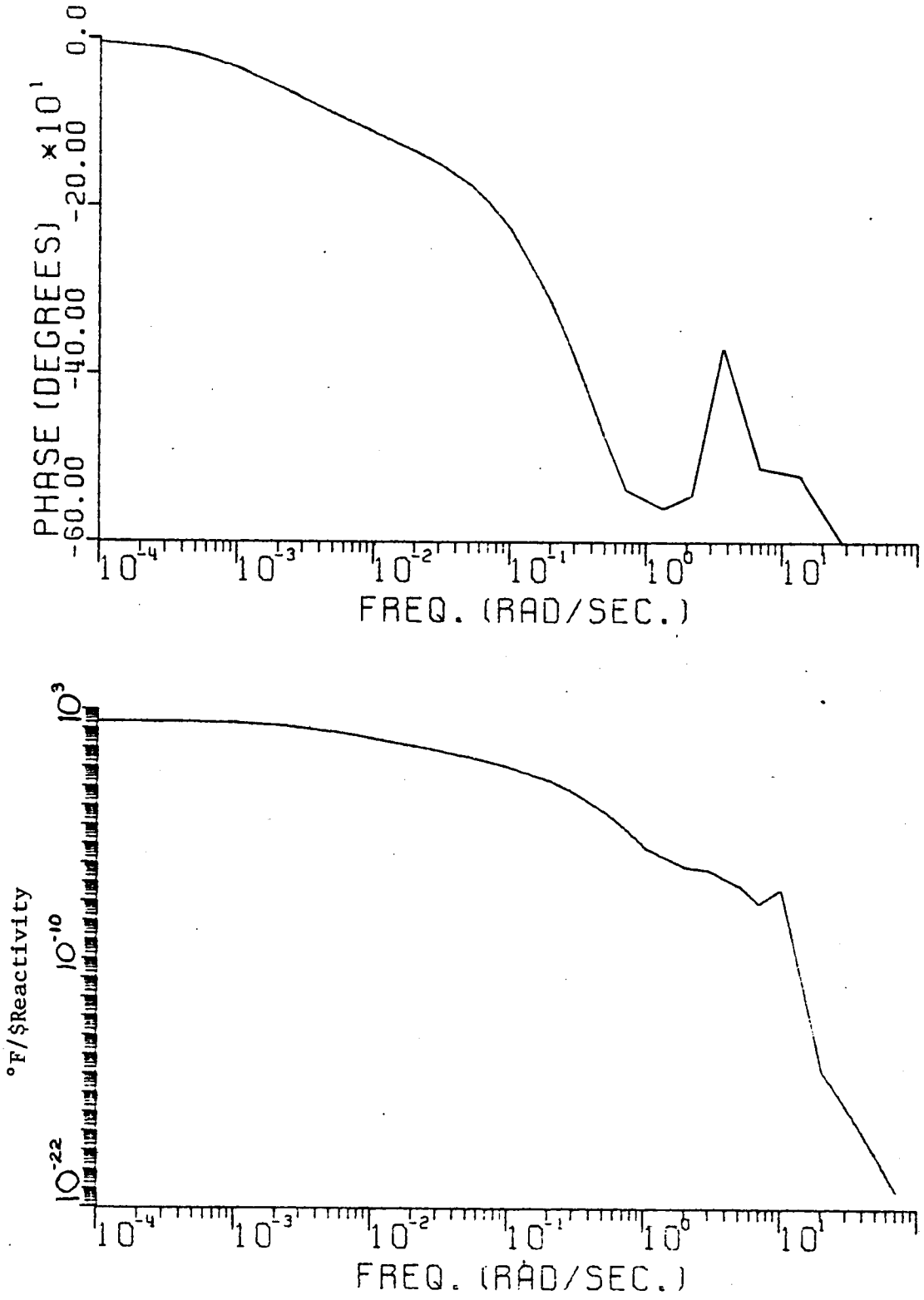


Figure B.10 Frequence Response of High Pressure Plenum Sodium Temperature for Reactivity Perturbations.

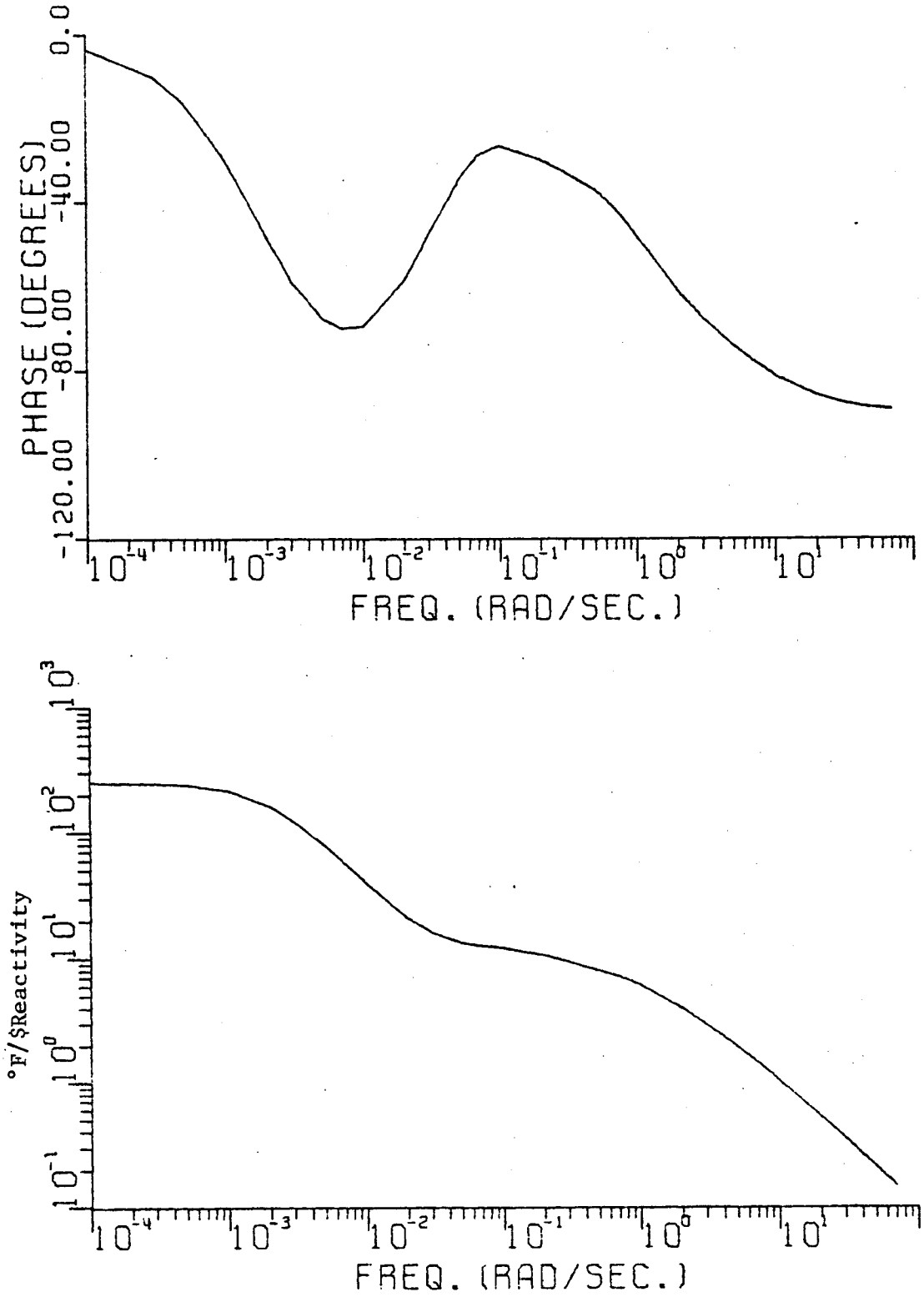


Figure B.11 Frequency Response of Lower Reflector Metal Temperature for Reactivity Perturbations.

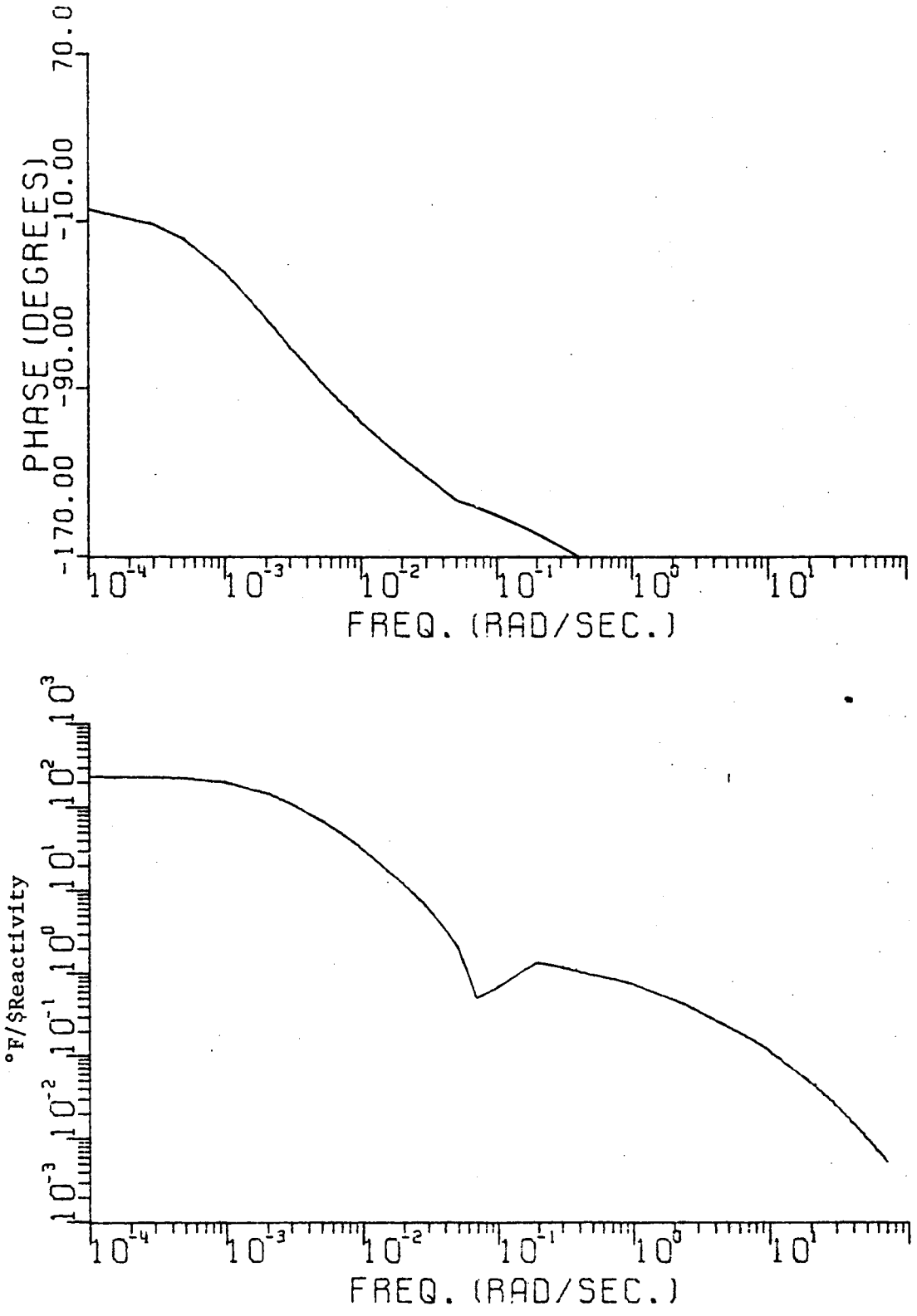


Figure B.12 Frequency Response of Lower Reflector Lower Sodium Temperature for Reactivity Perturbations.

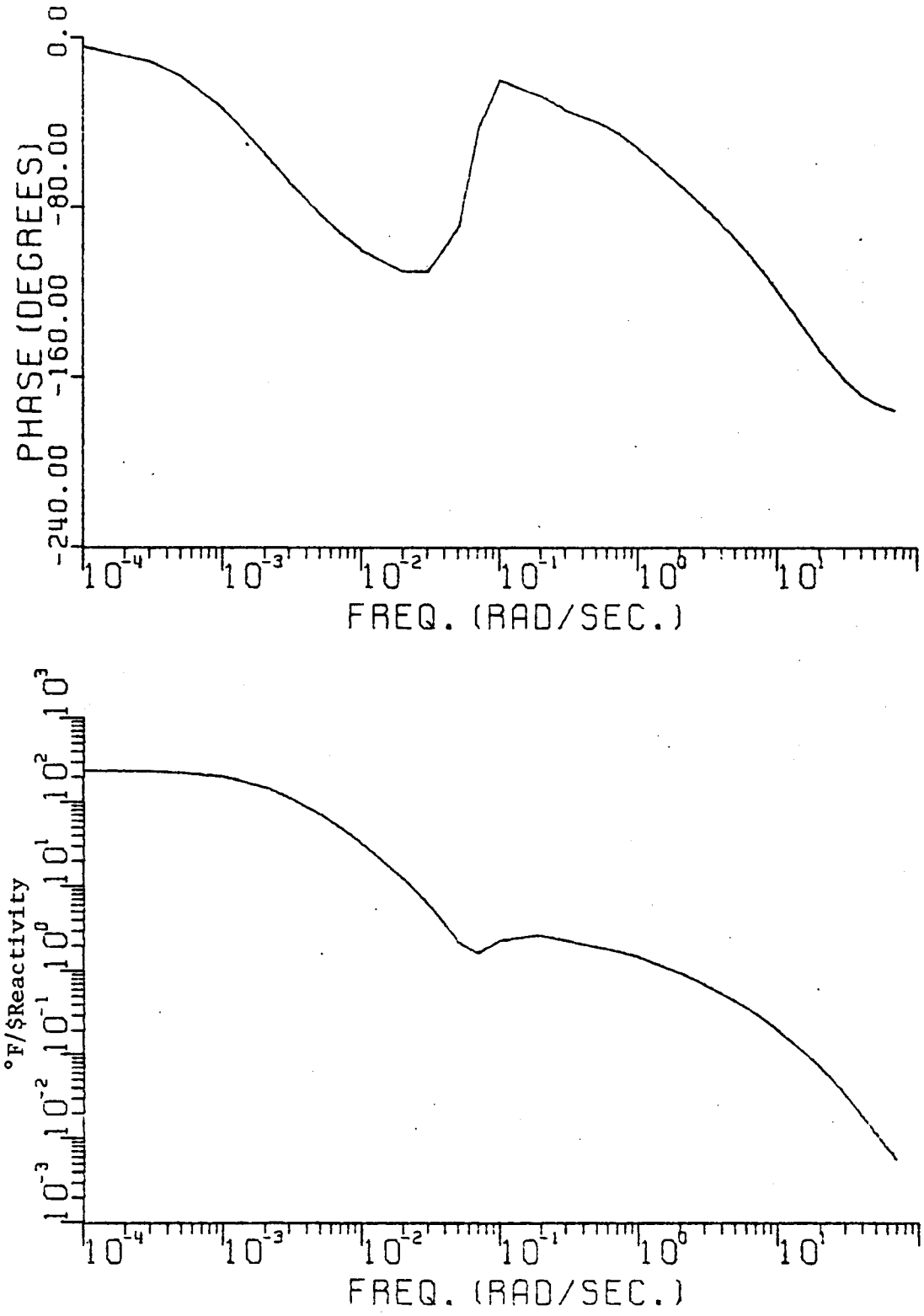


Figure B.13 Frequency Response of Lower Reflector Upper Sodium Temperature for Reactivity Perturbations.

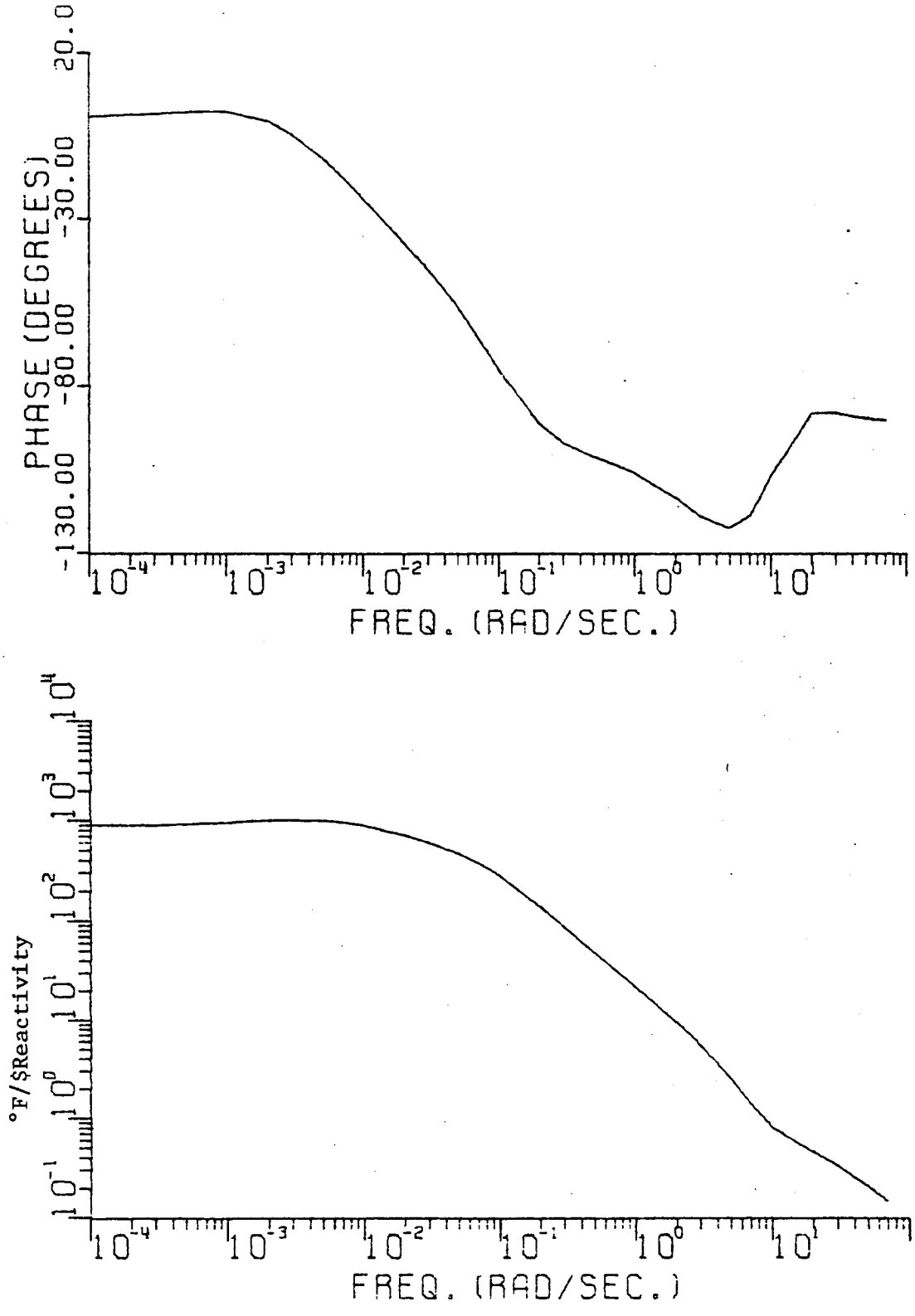


Figure B.14 Frequency Response of Upper Reflector Metal Temperature for Reactivity Perturbations.

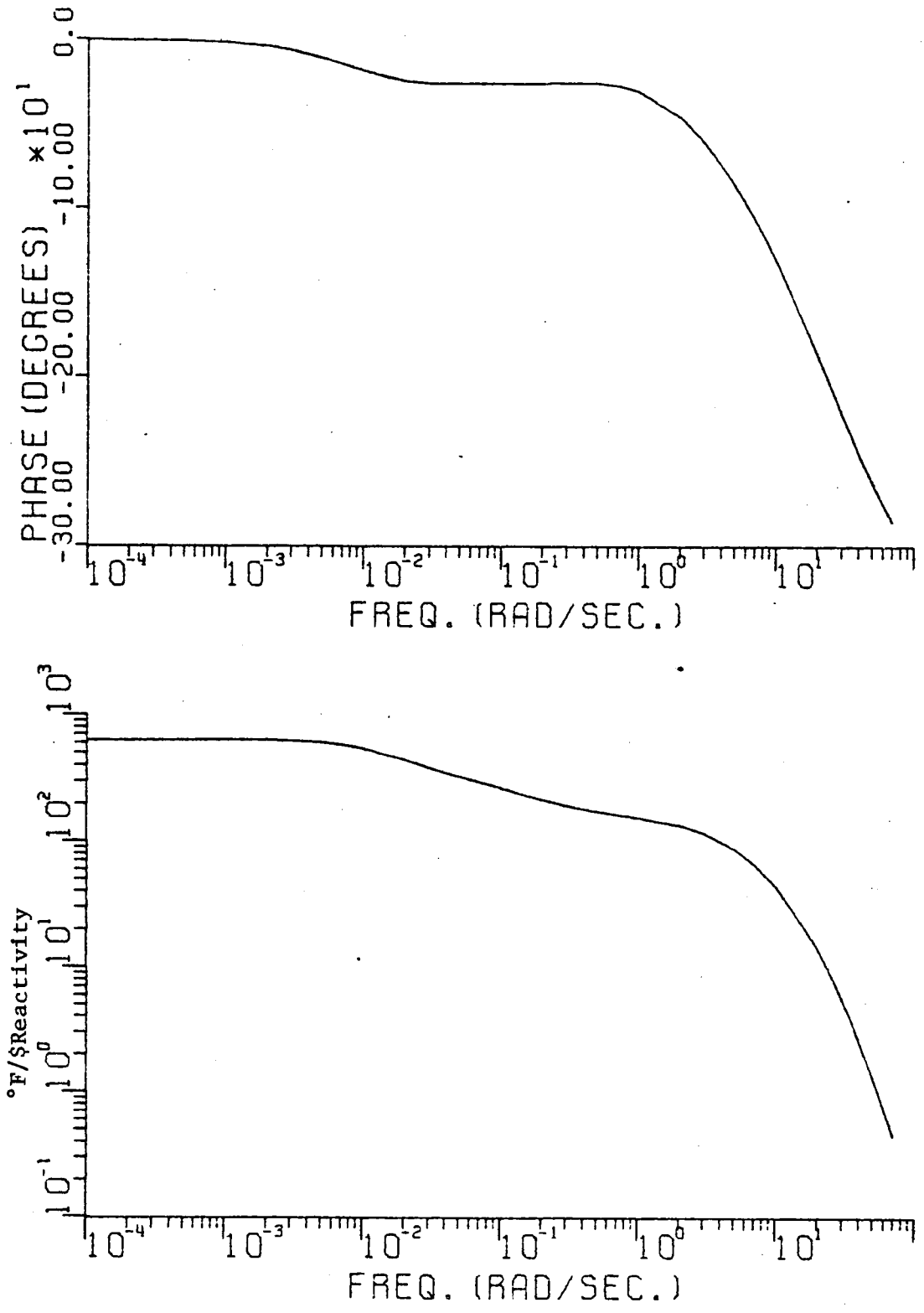


Figure B.15 Frequency Response of Upper Reflector Lower Sodium Temperature for Reactivity Perturbations.

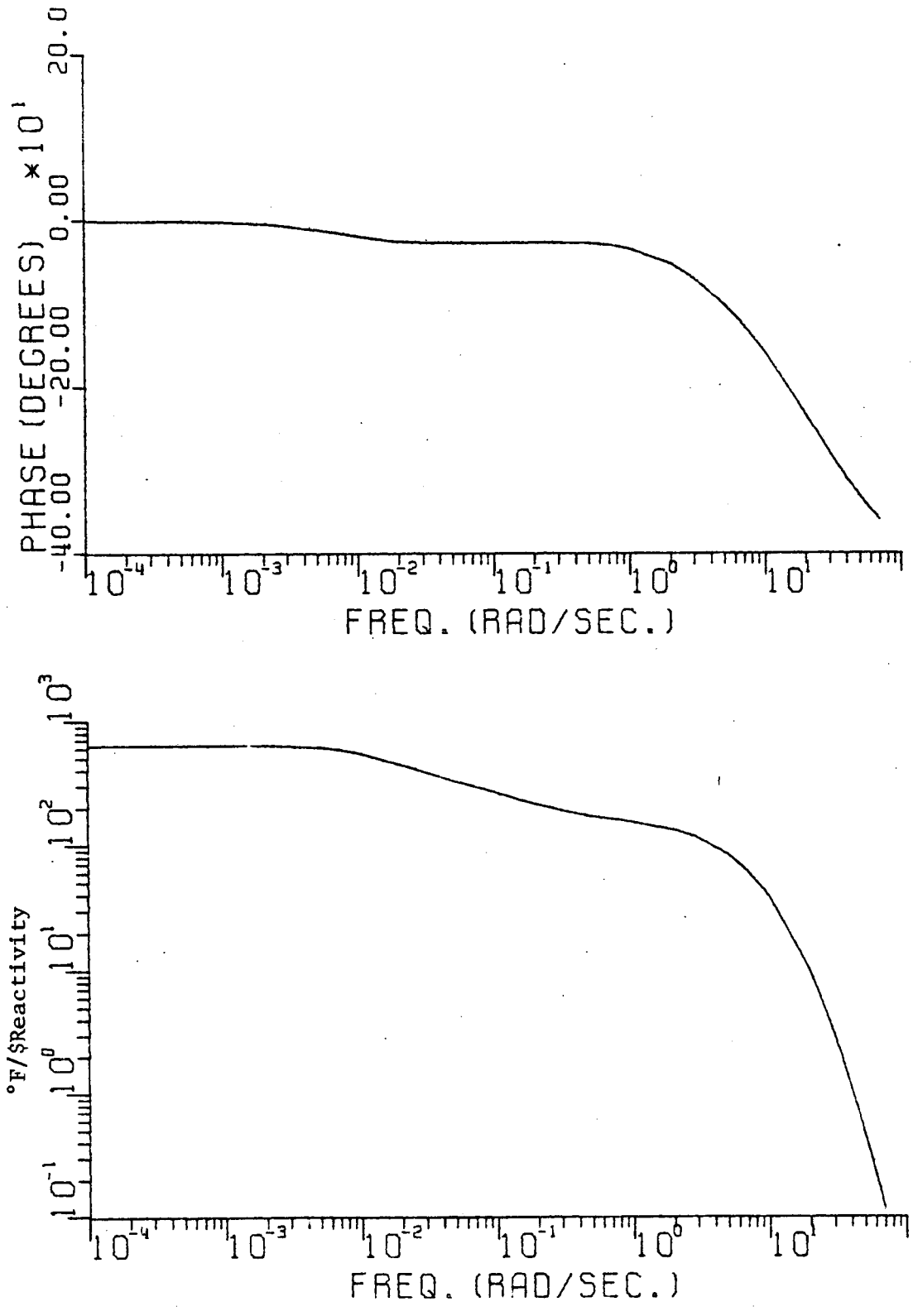


Figure B.16 Frequency Response of Upper Reflector Upper Sodium Temperature for Reactivity Perturbations.

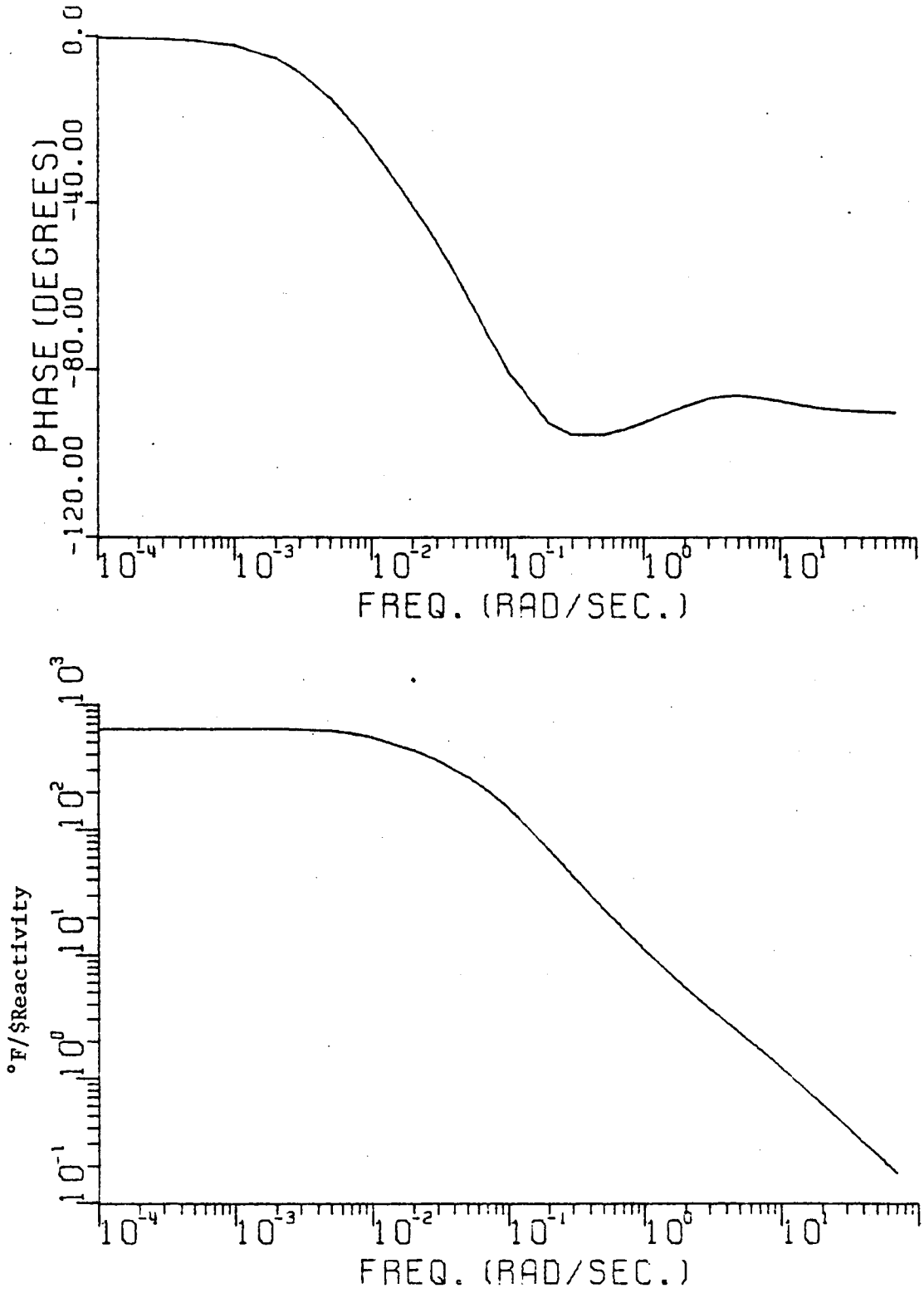


Figure B.17 Frequency Response of Inner Reflector Metal Temperature for Reactivity Perturbations.

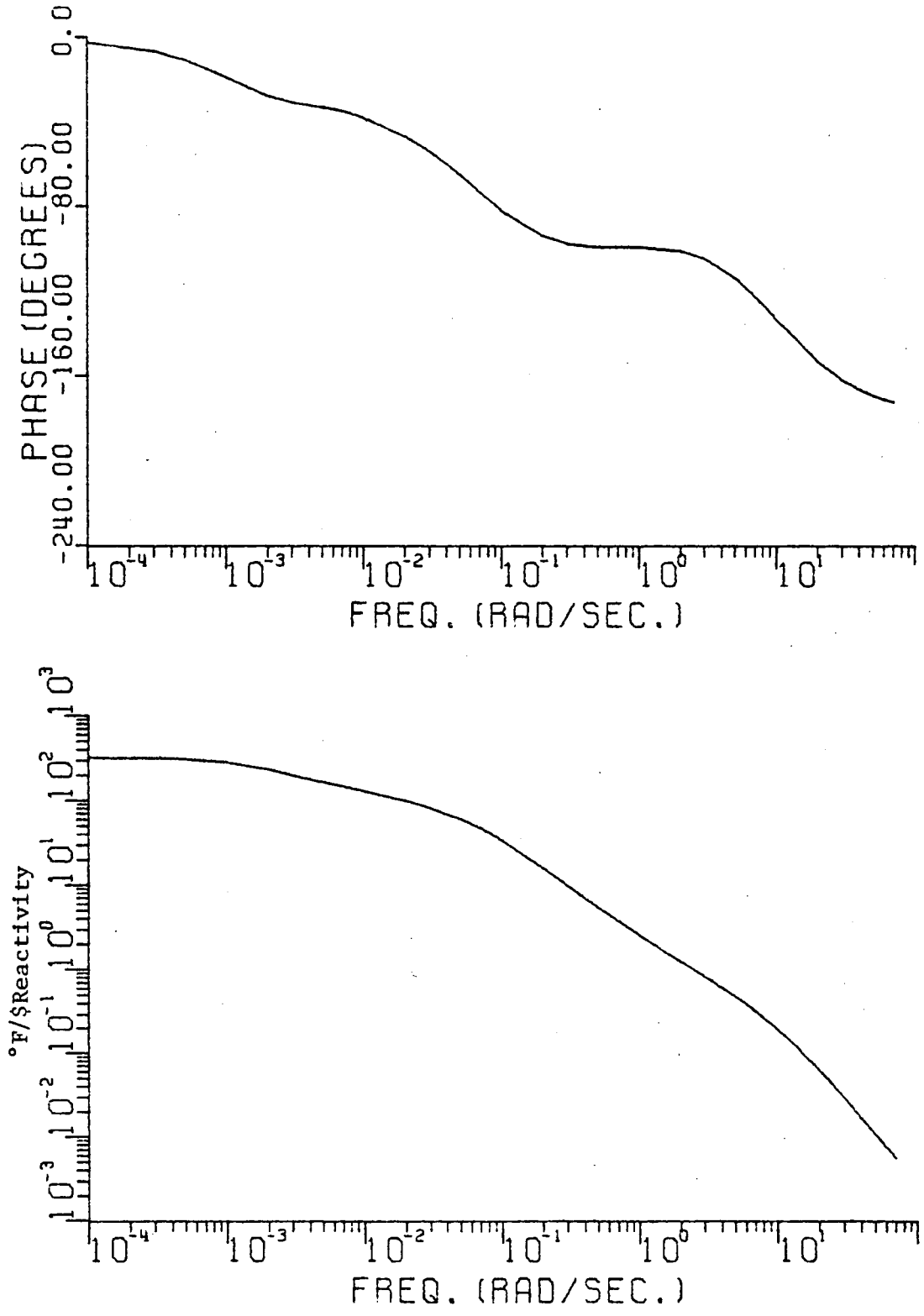


Figure B.18 Frequency Response of Inner Reflector Lower Sodium Temperature for Reactivity Perturbations.

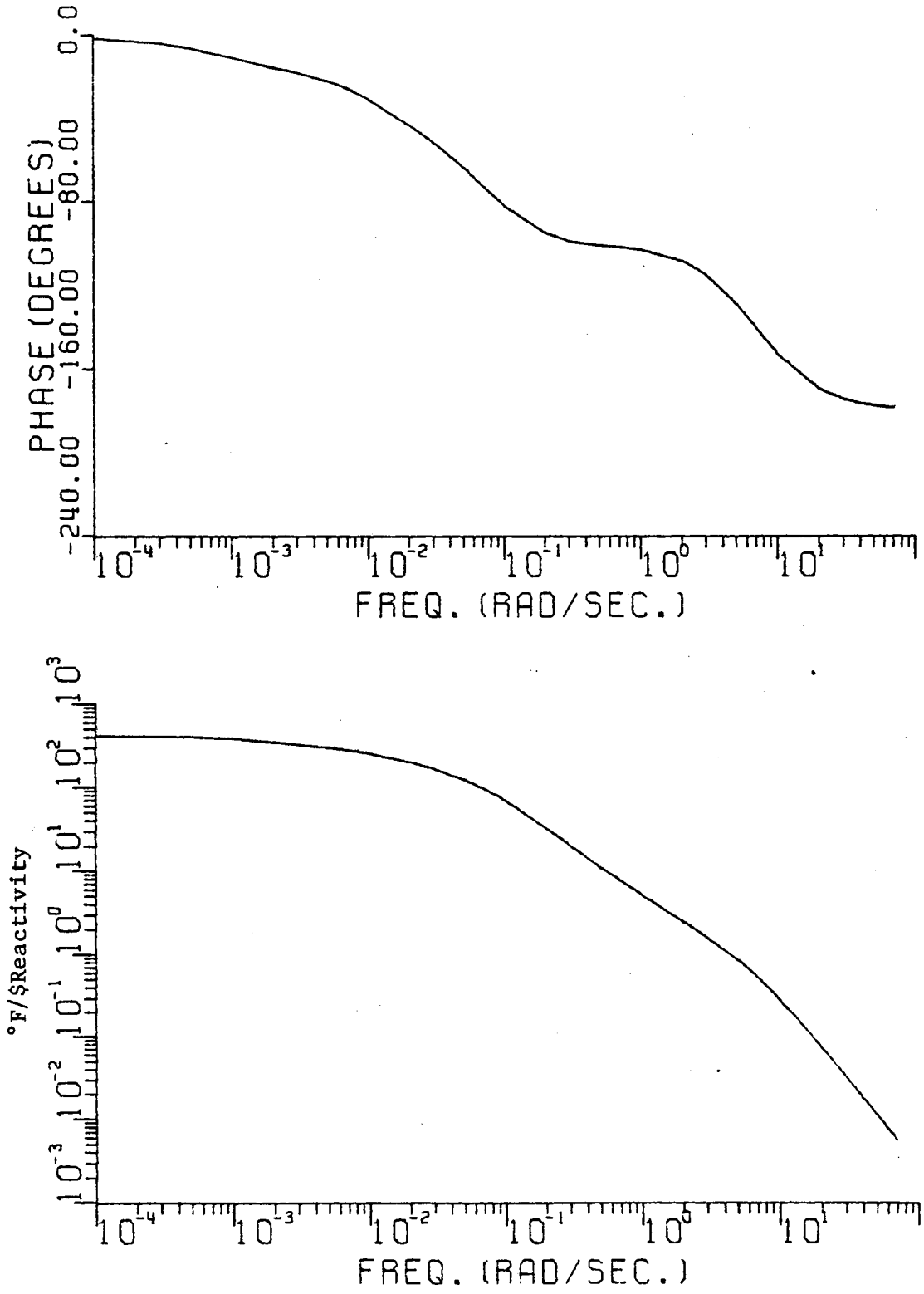


Figure B.19 Frequency Response of Inner Reflector Upper Sodium Temperature for Reactivity Perturbations.

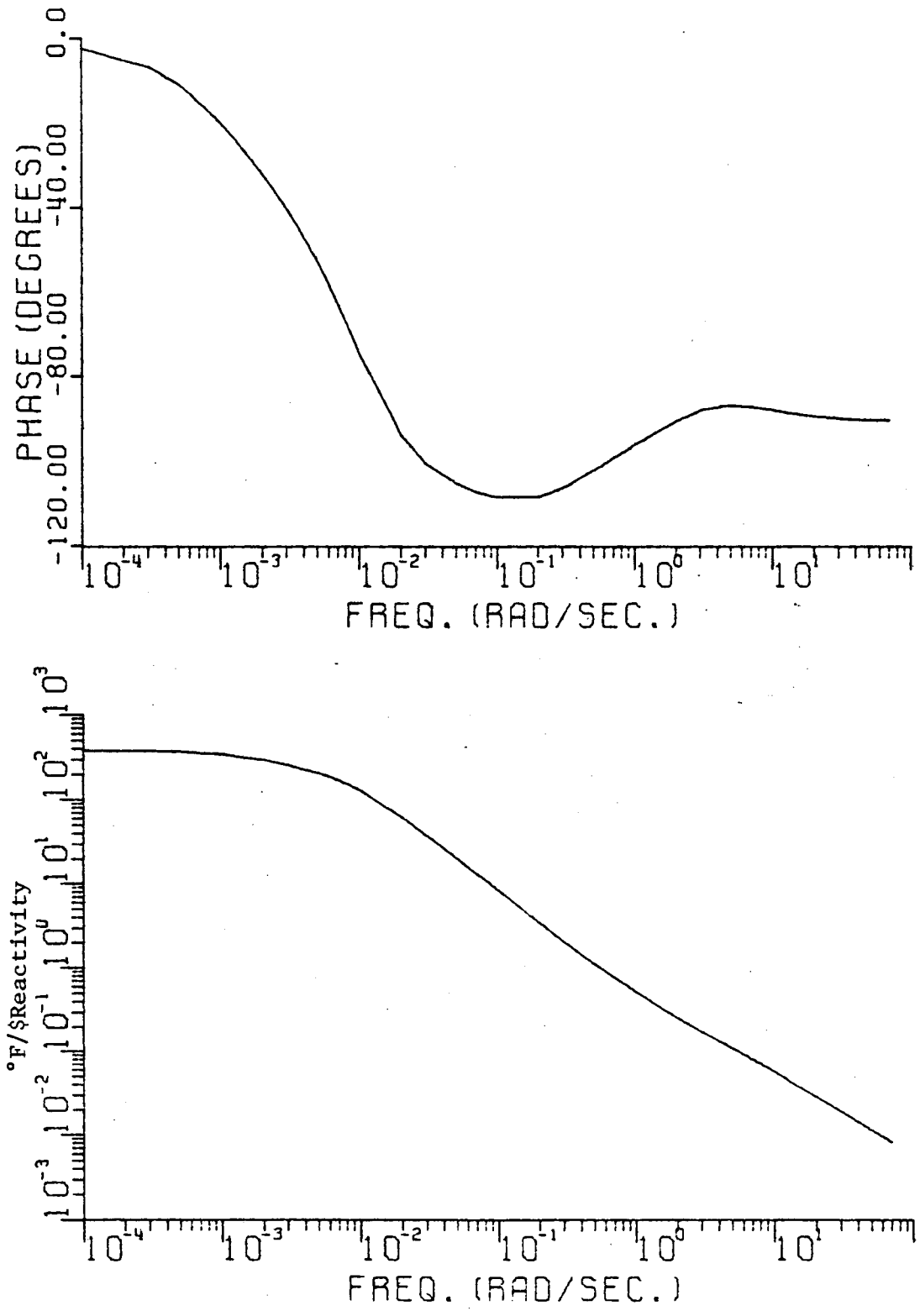


Figure B.20 Frequency Response of Blanket Metal Temperature for Reactivity Perturbations.

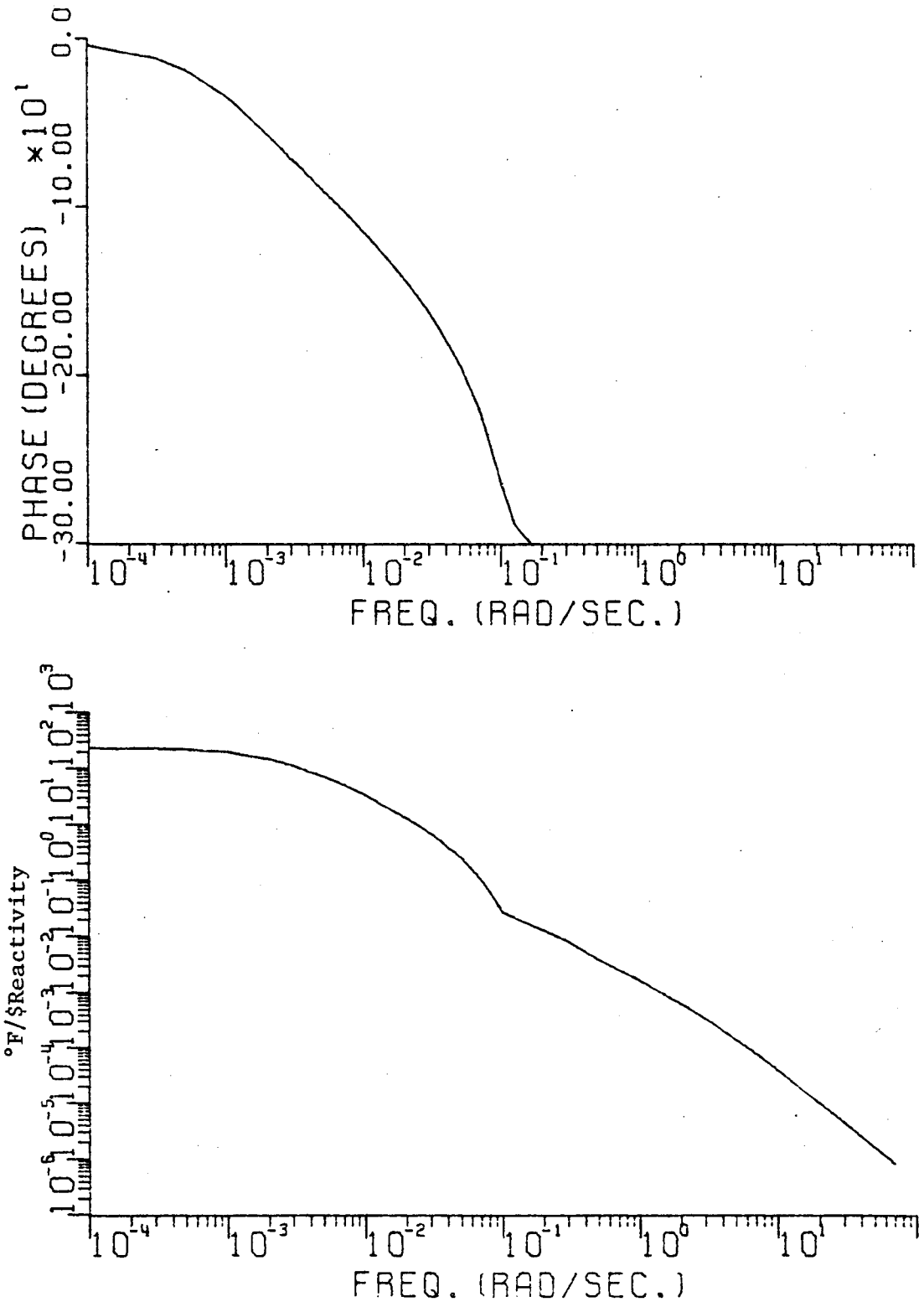


Figure B.21 Frequency Response of Blanket Lower Sodium Temperature for Reactivity Perturbations.

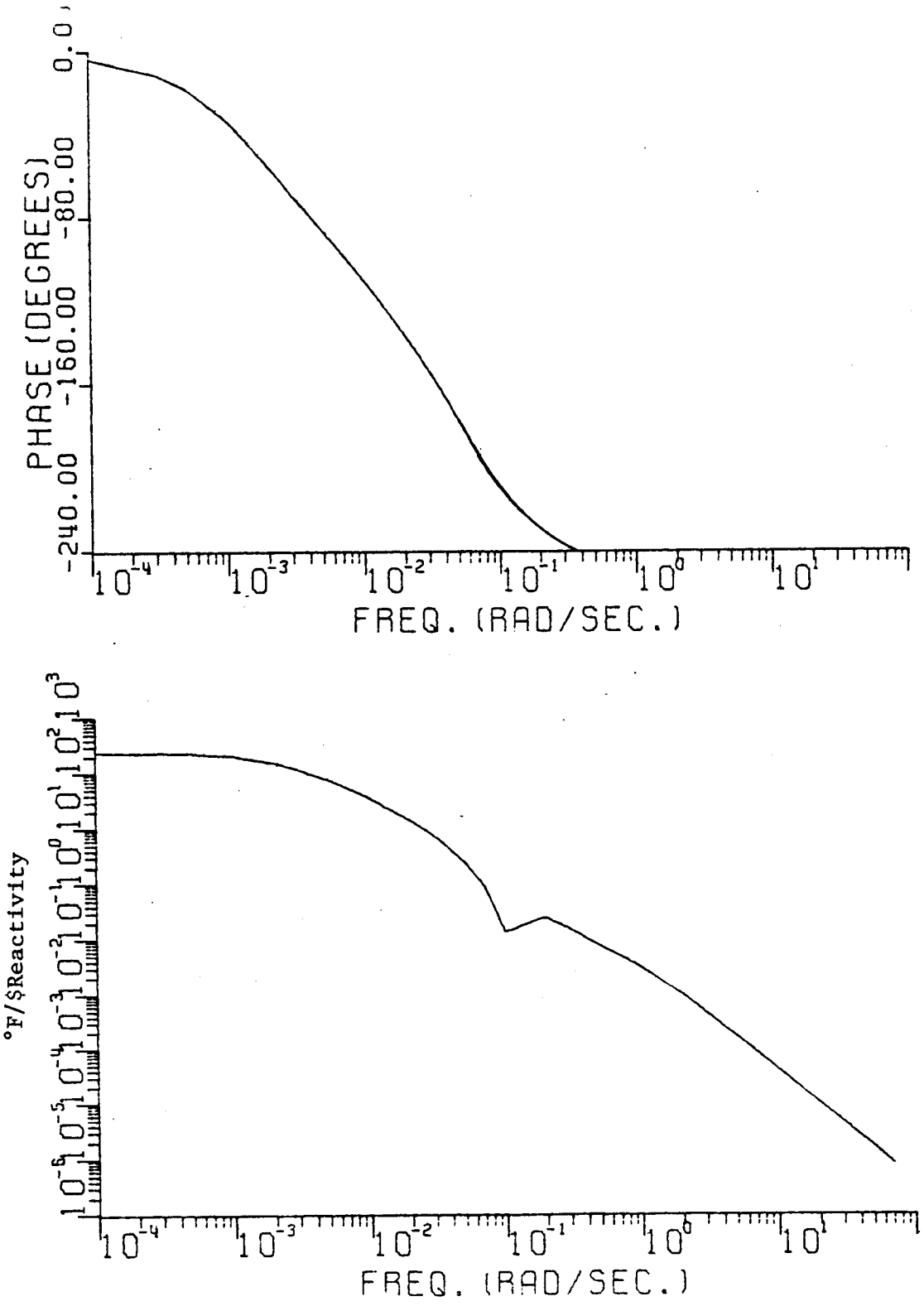


Figure B.22 Frequency Response of Blanket Upper Sodium Temperature for Reactivity Perturbations.

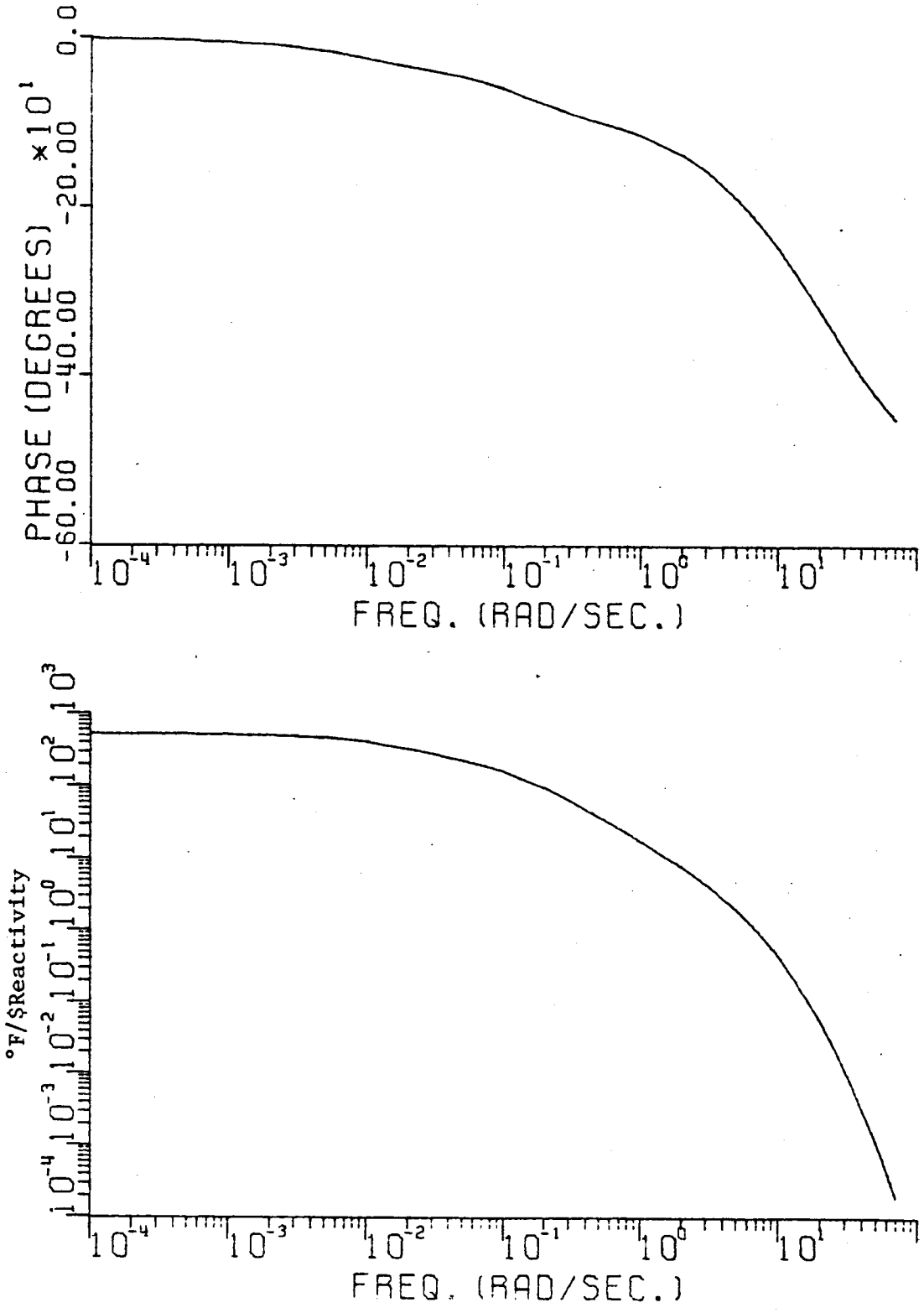


Figure B.23 Frequency Response of Upper Plenum Sodium Temperature for Reactivity Perturbations.

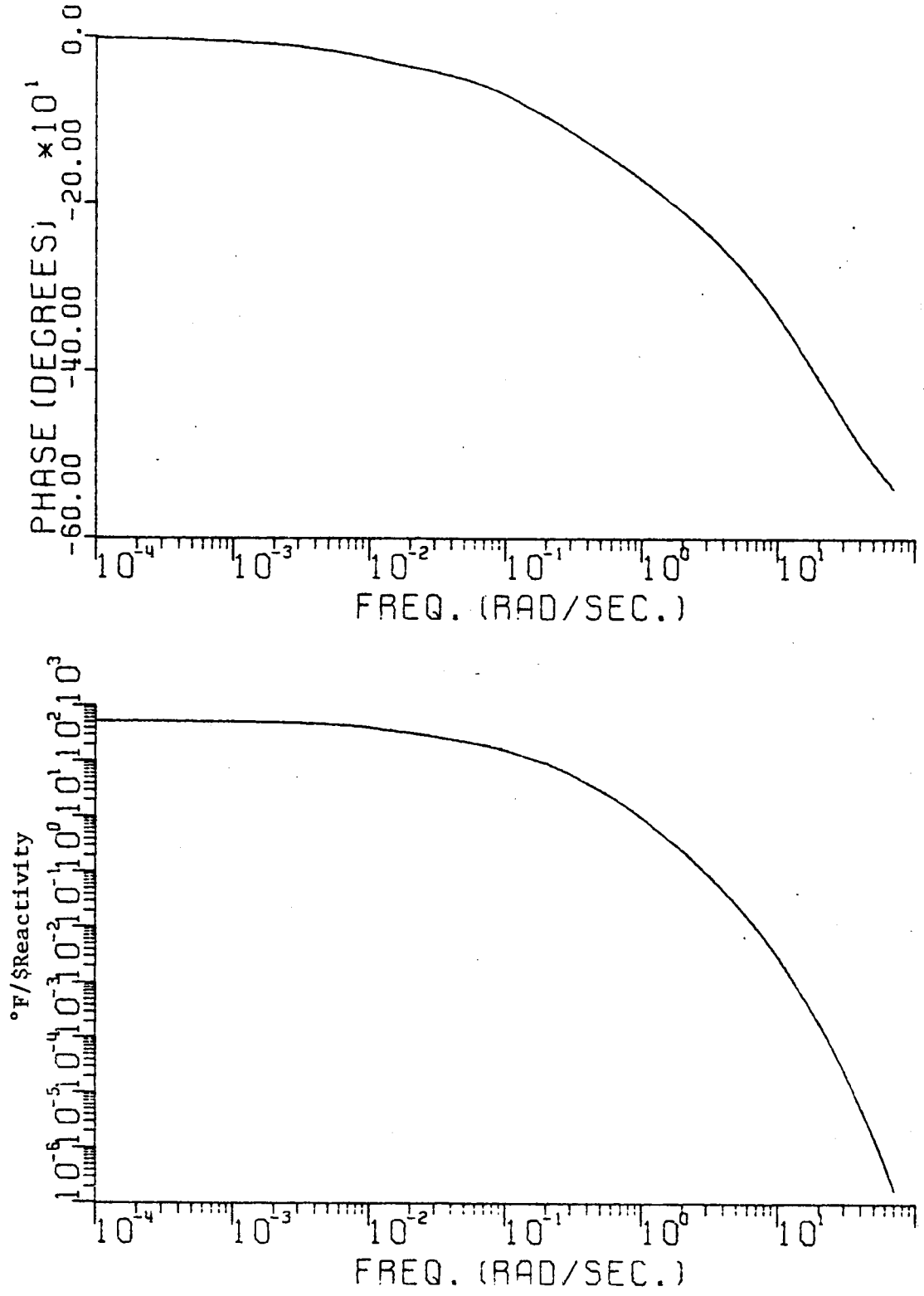


Figure B.24 Frequency Response of Reactor Outlet Sodium Temperature for Reactivity Perturbations.

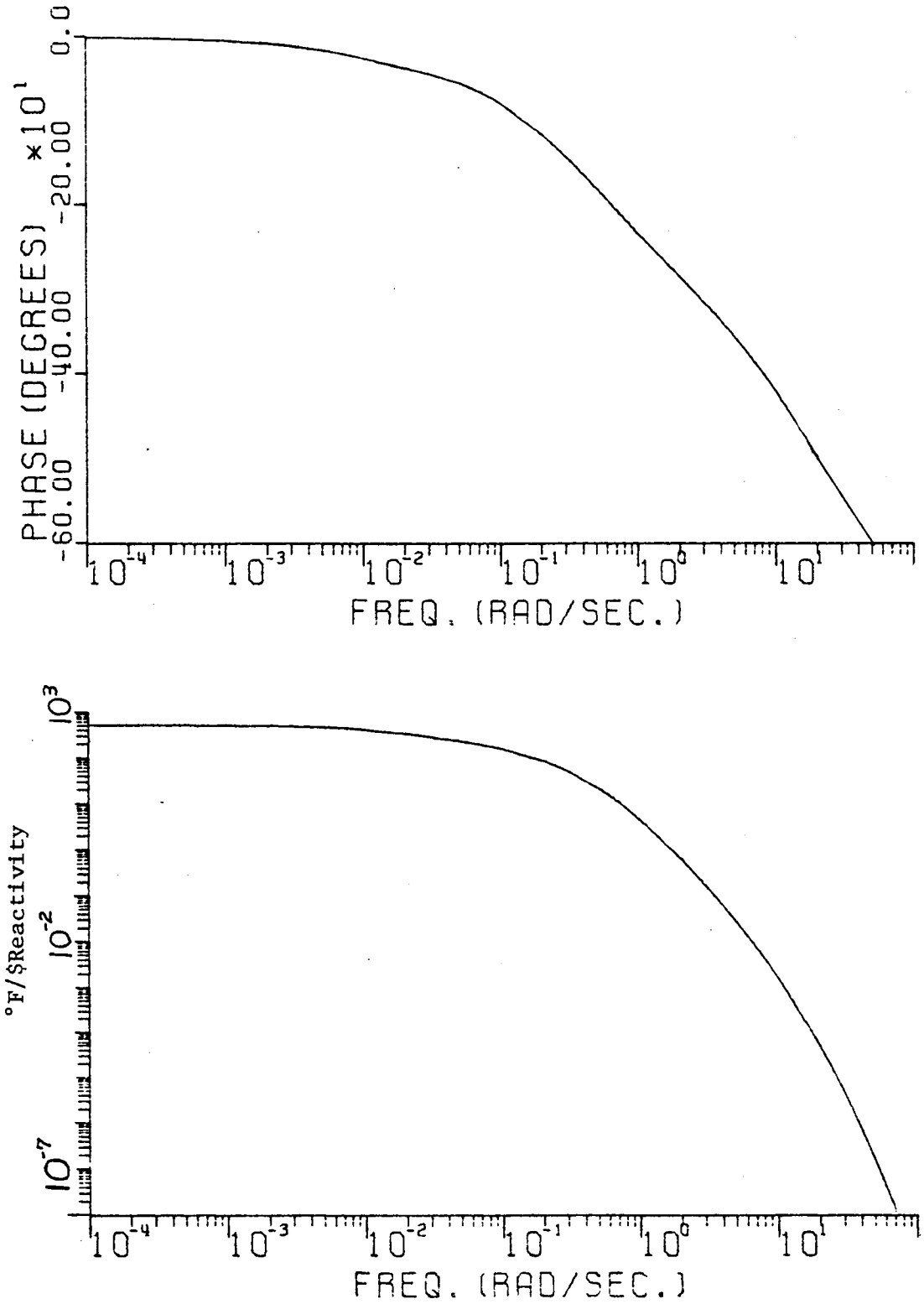


Figure B.25 Frequency Response of IHX Inlet Sodium Temperature for Reactivity Perturbations.

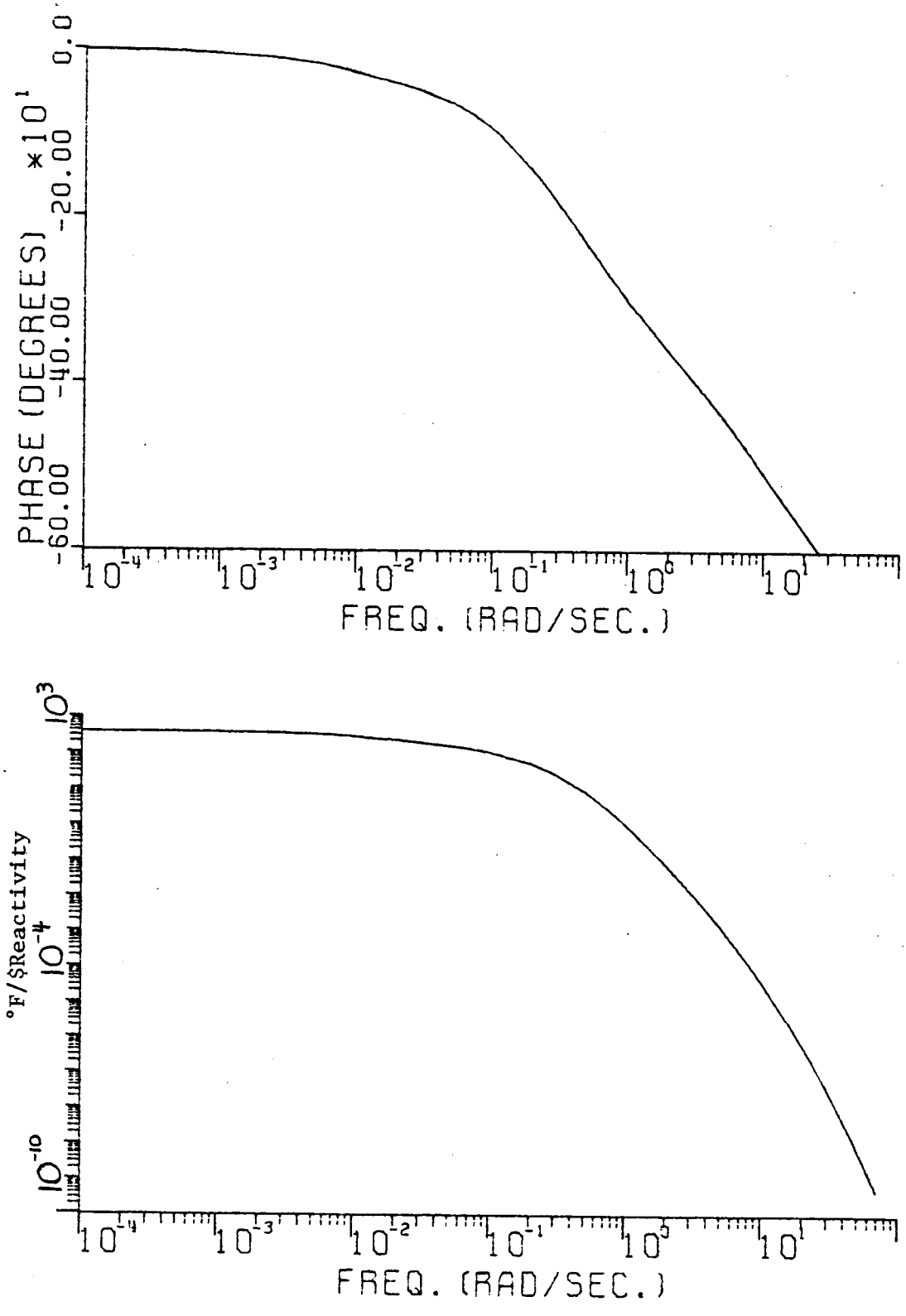


Figure B.26 Frequency Response of IHX Primary Node 1 Sodium Temperature for Reactivity Perturbations.

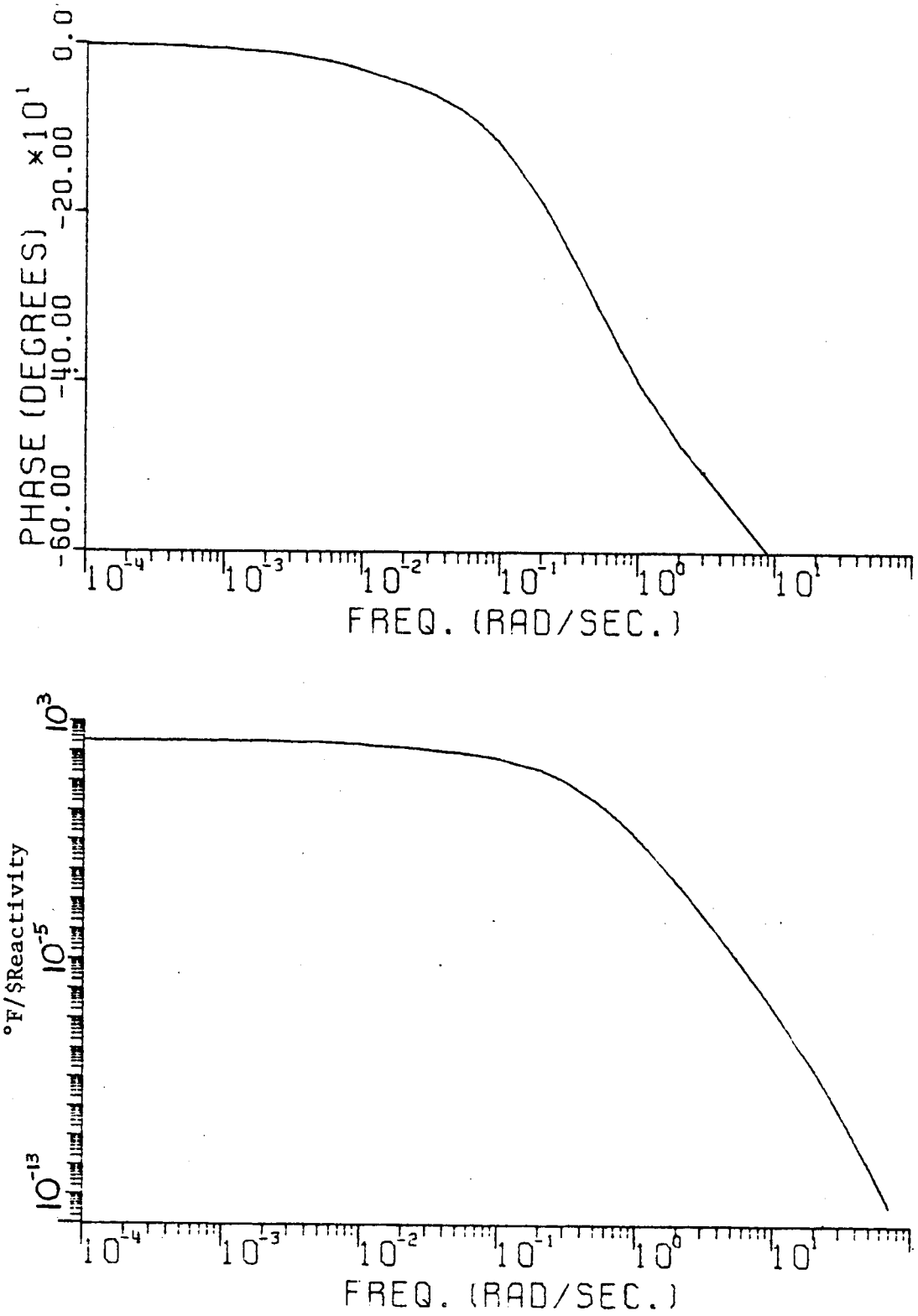


Figure B.27 Frequency Response of IHX Primary Node 2 Sodium Temperature for Reactivity Perturbations.

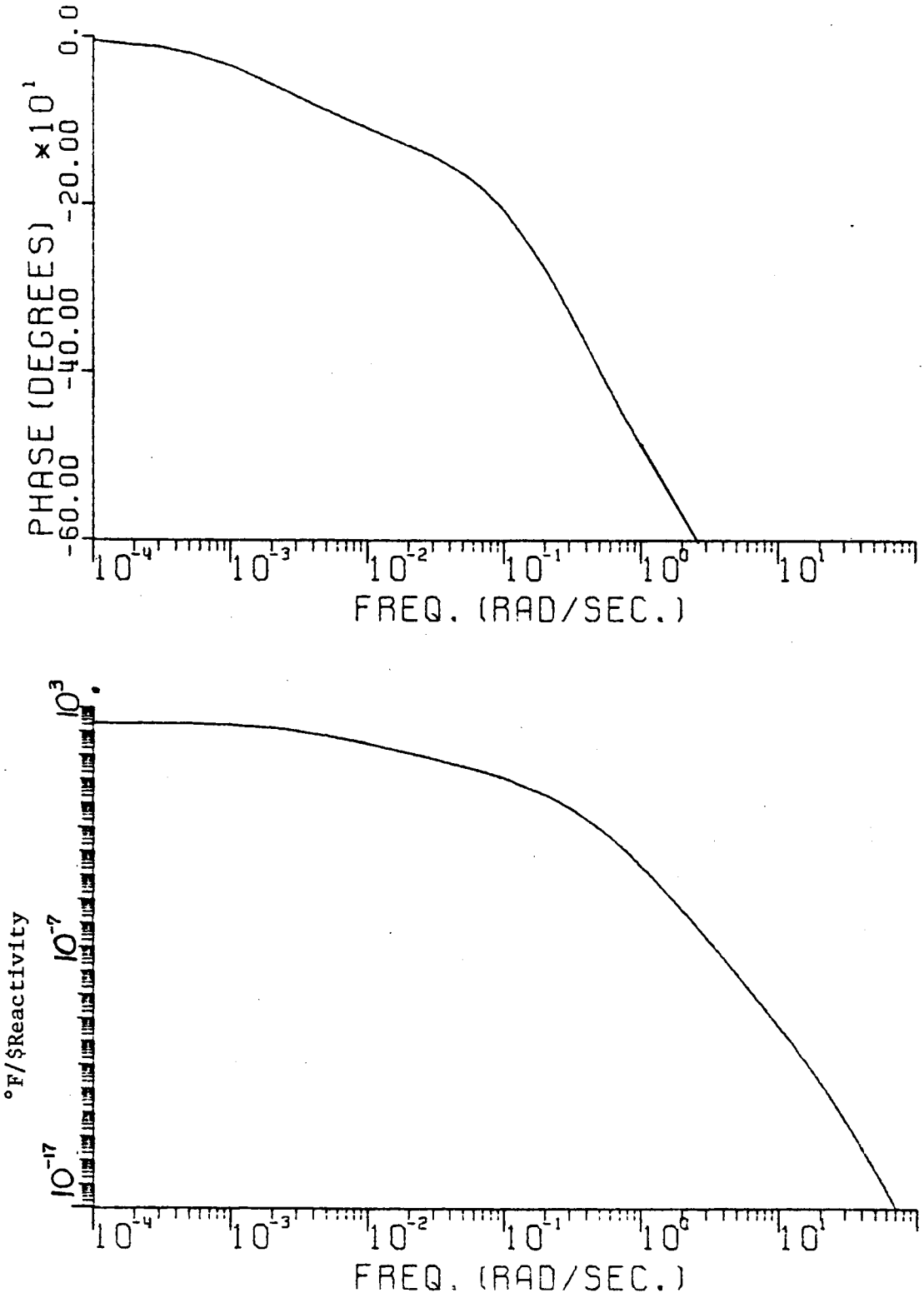


Figure B.28 Frequency Response of Pot Sodium Temperature for Reactivity Perturbations.

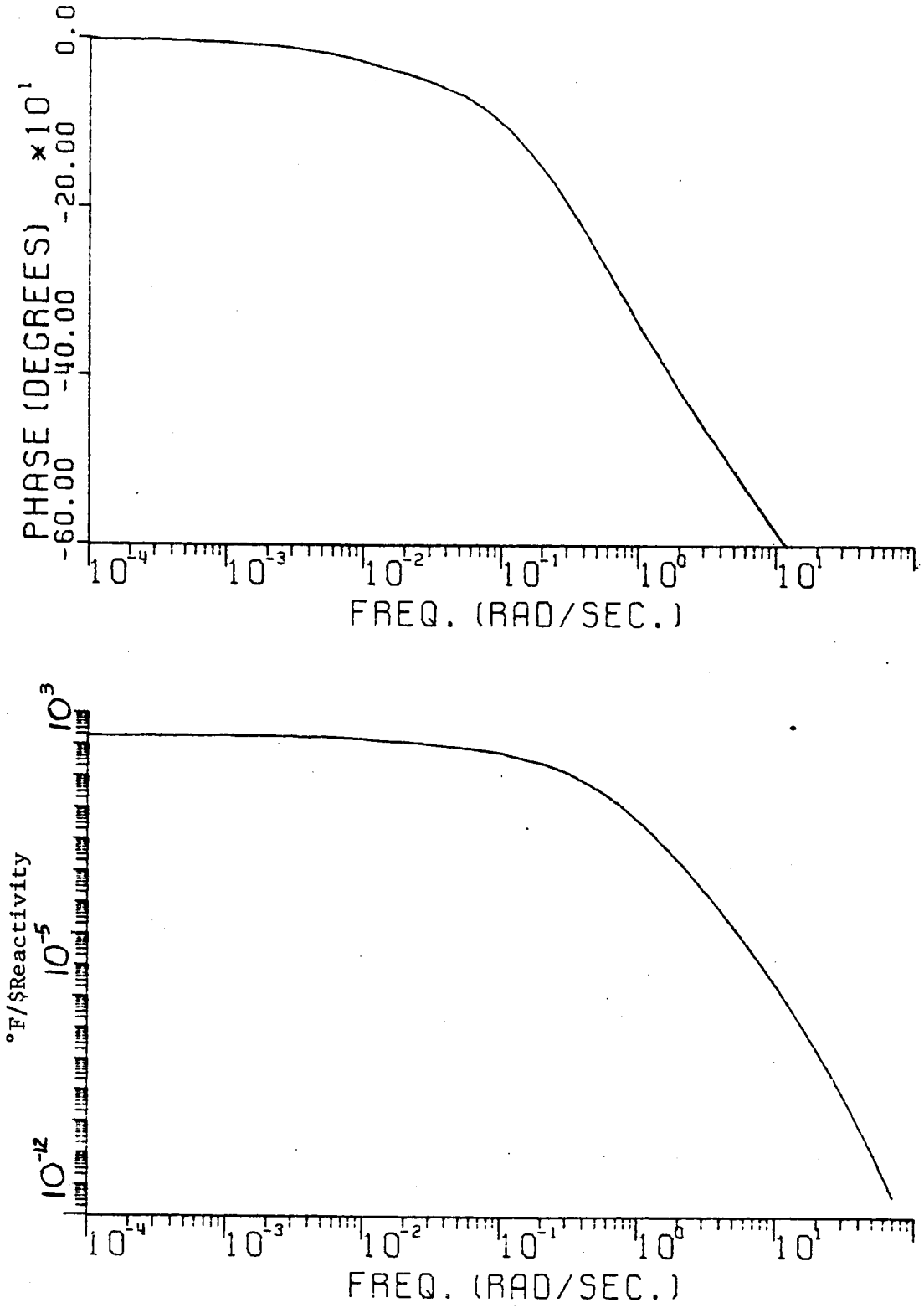


Figure B.29 Frequency Response of IHX Tube Bundle Temperature for Reactivity Perturbations.

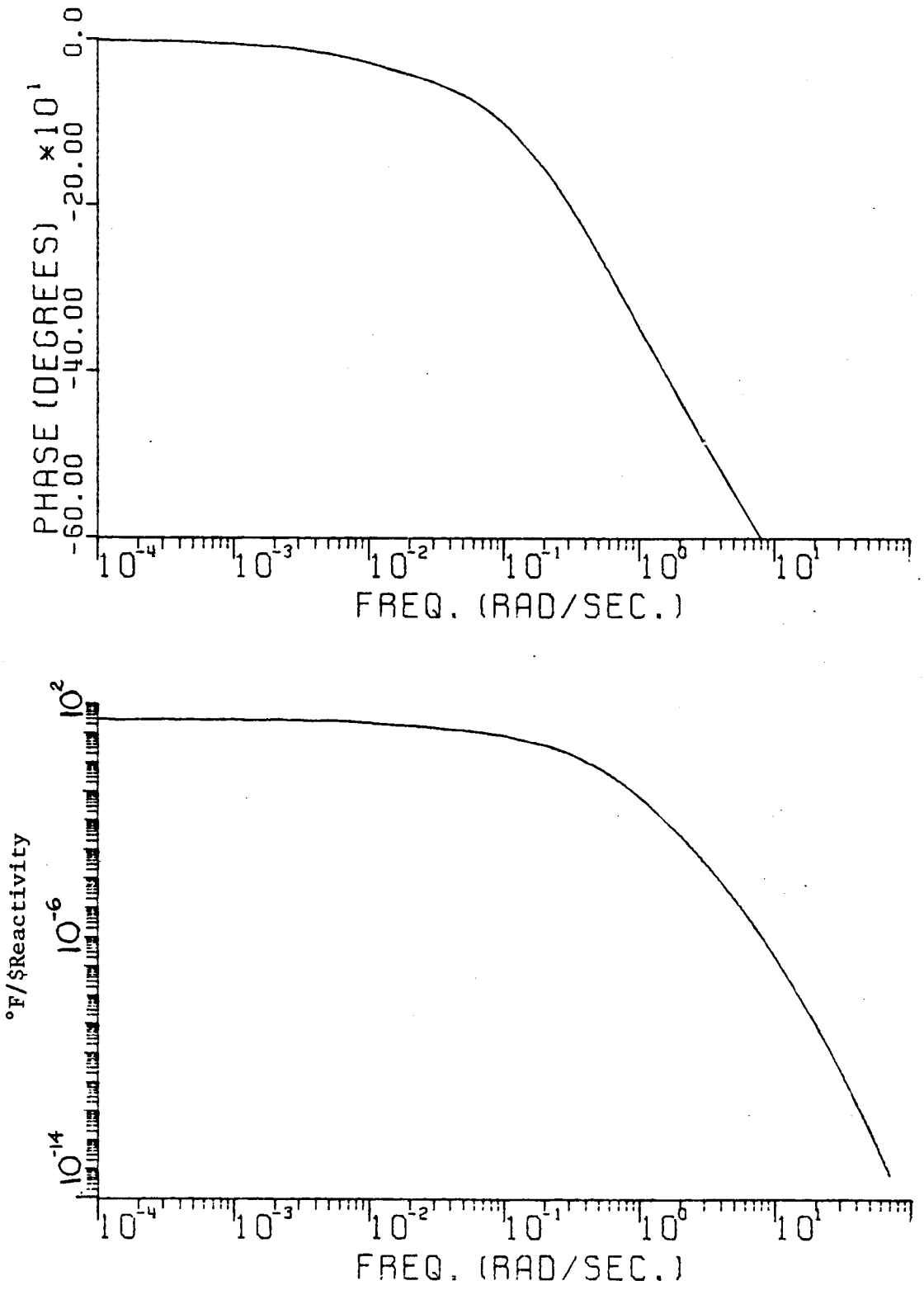


Figure B.30 Frequency Response of IHX Secondary Node 1 Sodium Temperature for Reactivity Perturbations.

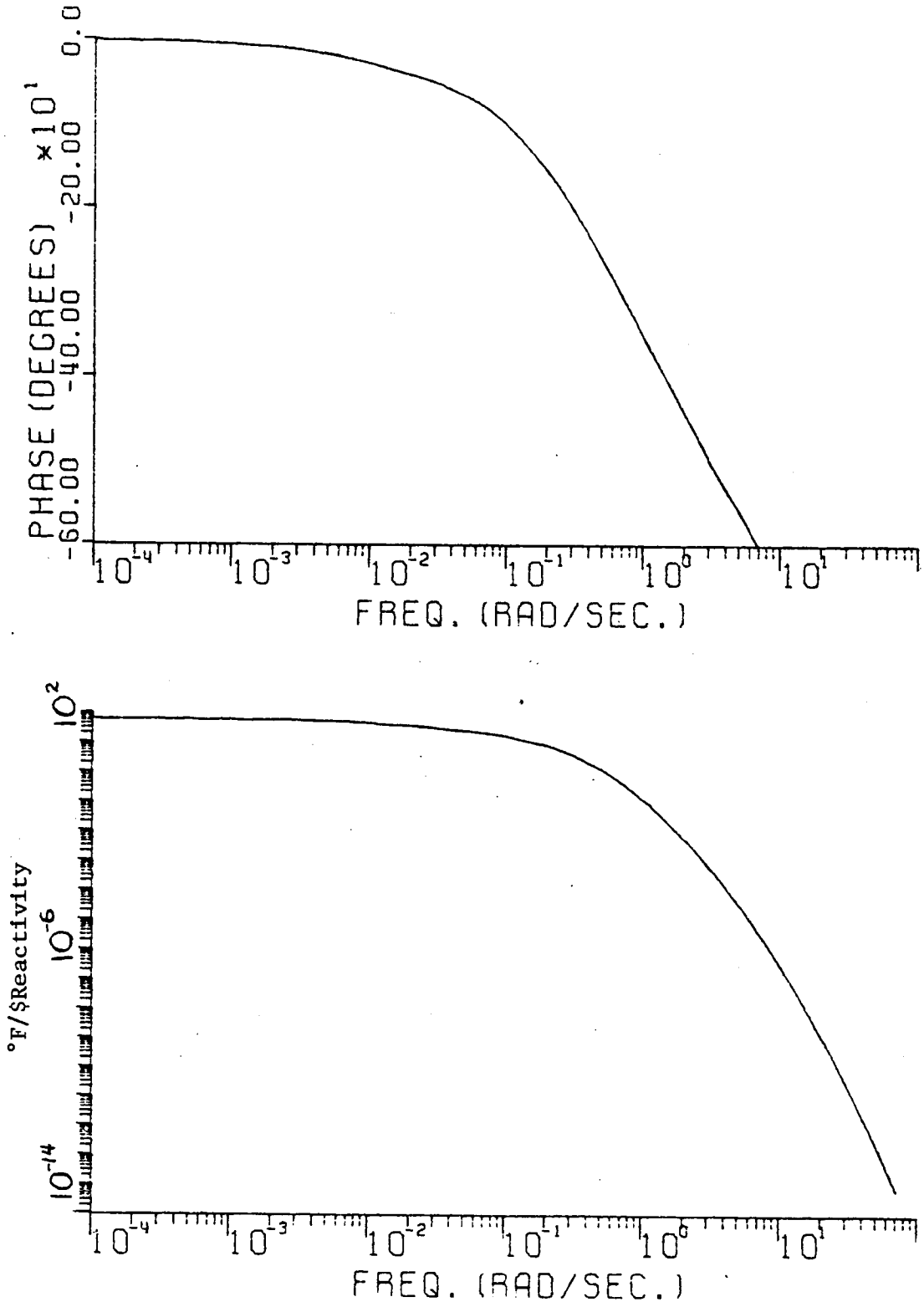


Figure B.31 Frequency Response of IHX Secondary Node 2 Sodium Temperature for Reactivity Perturbations.

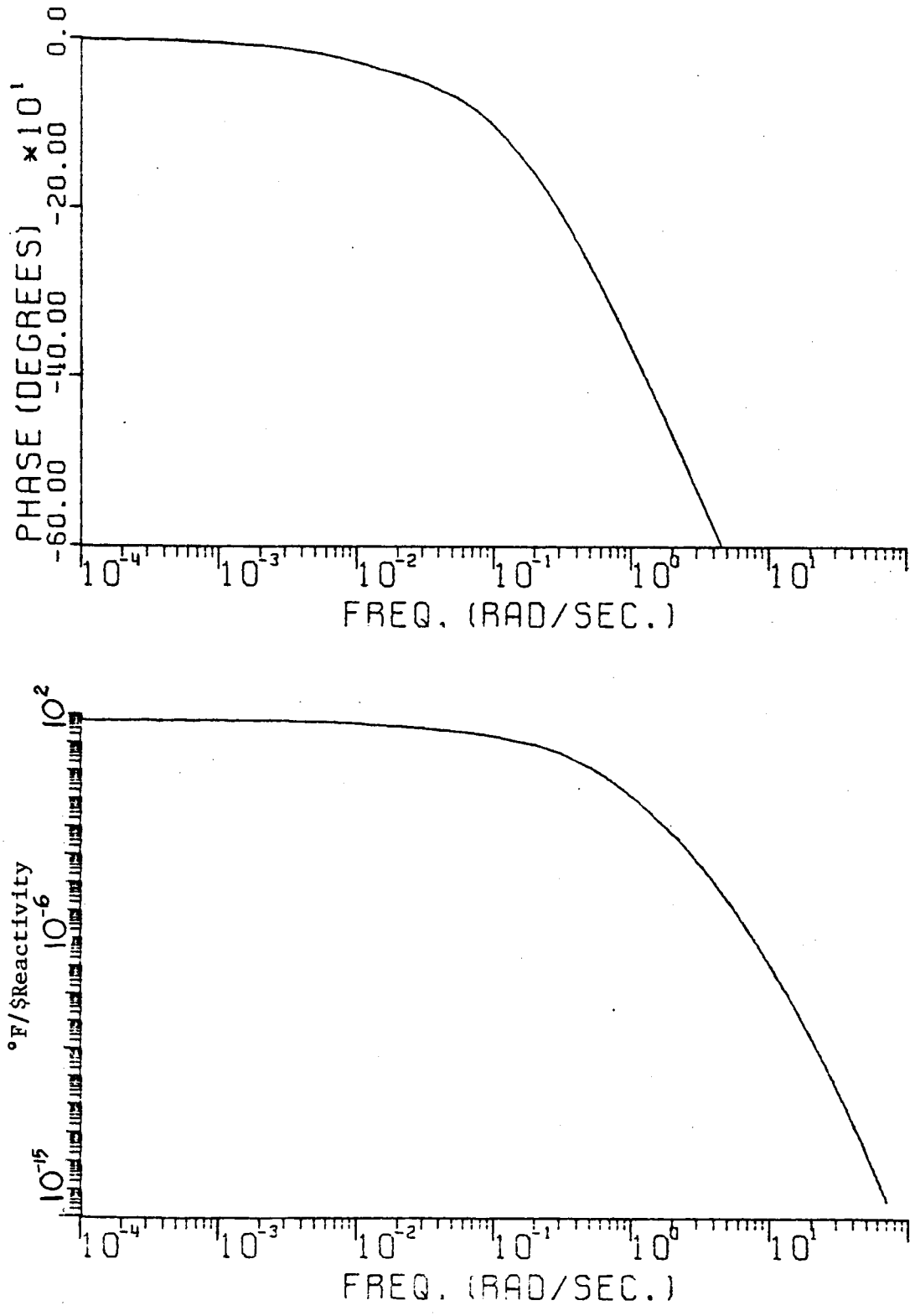


Figure B.32 Frequency Response of IHX Secondary Outlet Sodium Temperature for Reactivity Perturbations.

APPENDIX C

This appendix shows the frequency response of the 38 node EBR-II model for intermediate heat exchanger (IHX) secondary inlet temperature perturbations.

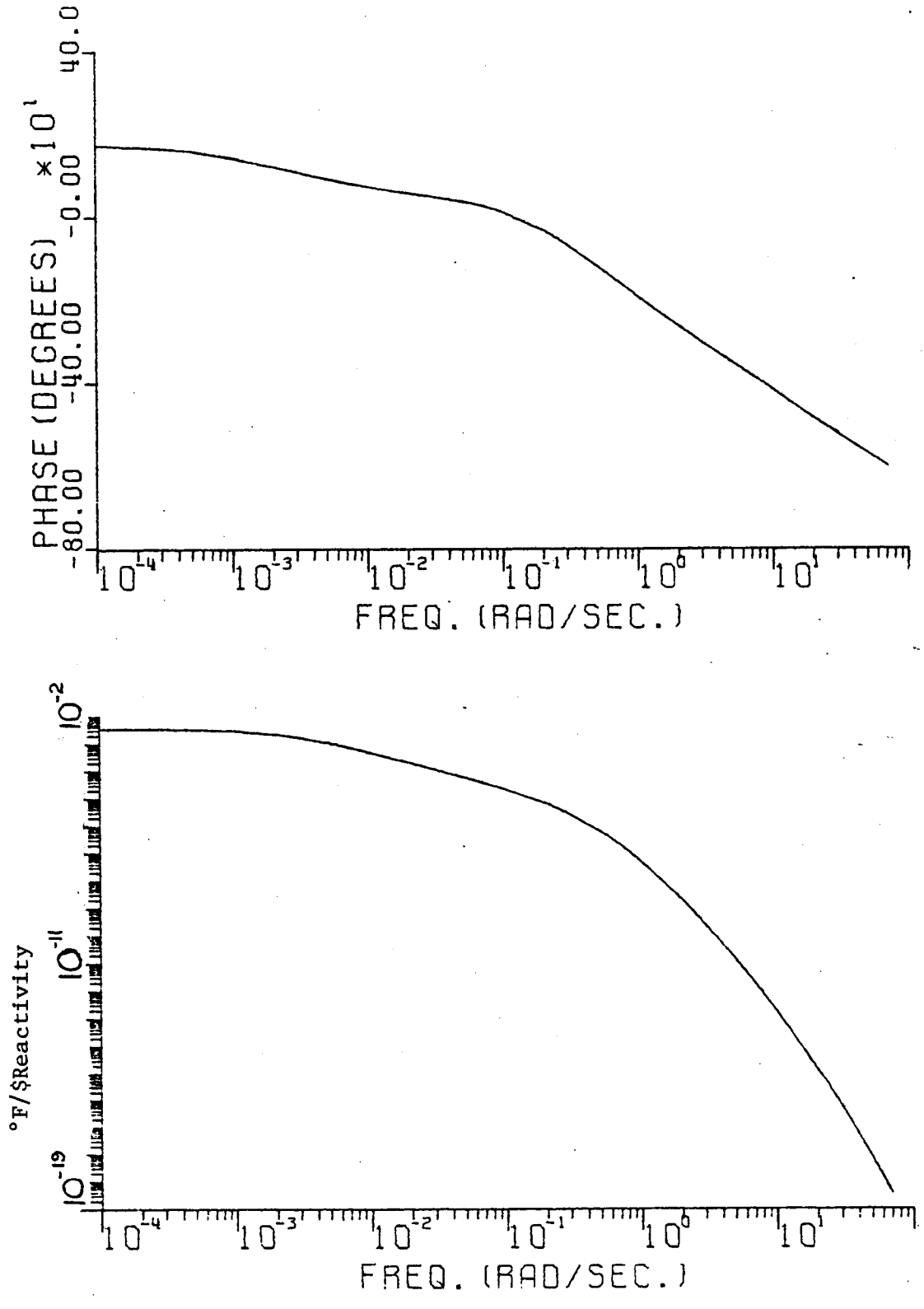


Figure C.1 Frequency Response of Reactor Power for IHX Secondary Inlet Sodium Temperature Perturbations.

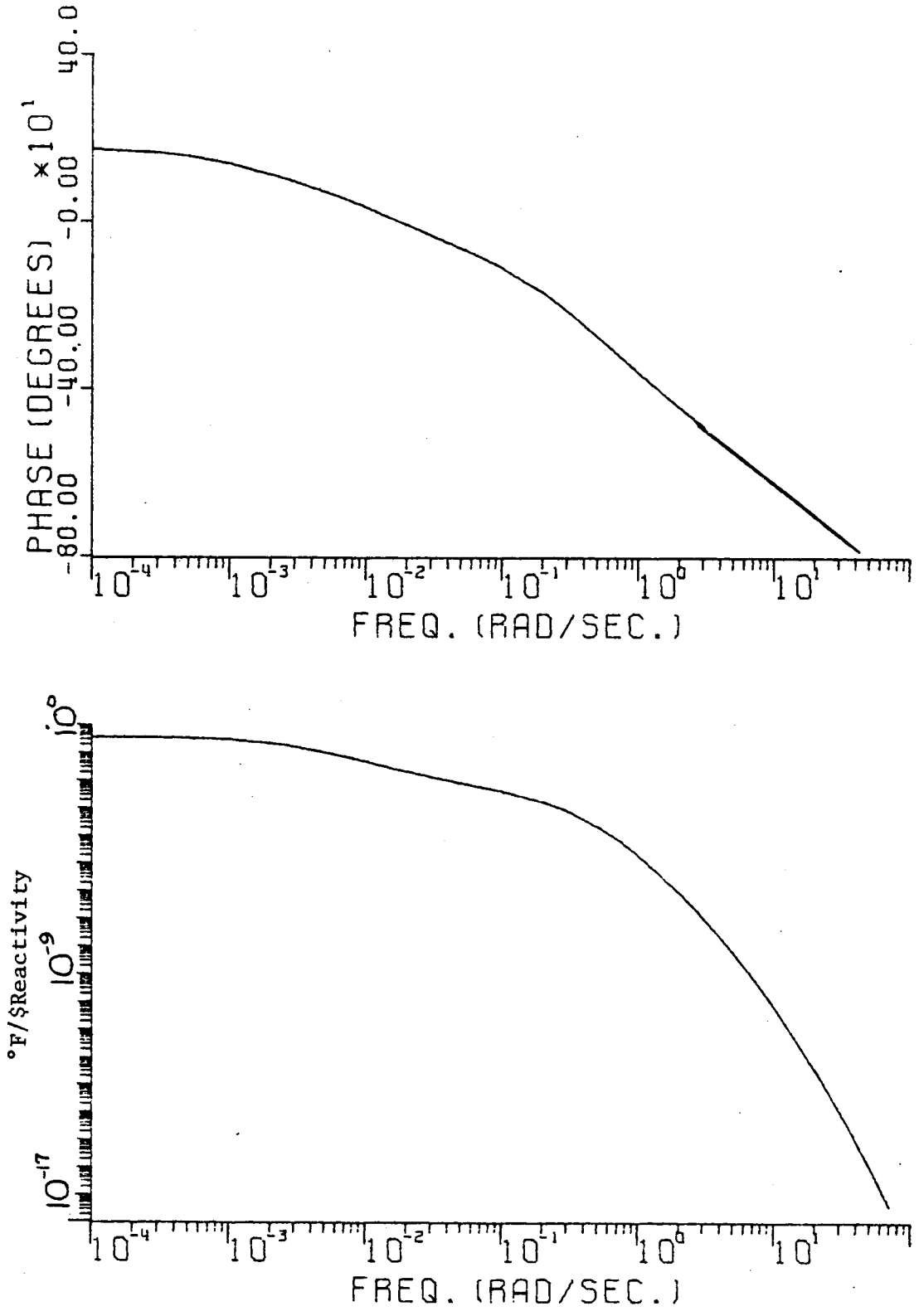


Figure C.2 Frequency Response of Fuel Temperature for IHX Secondary Inlet Sodium Temperature Perturbations.

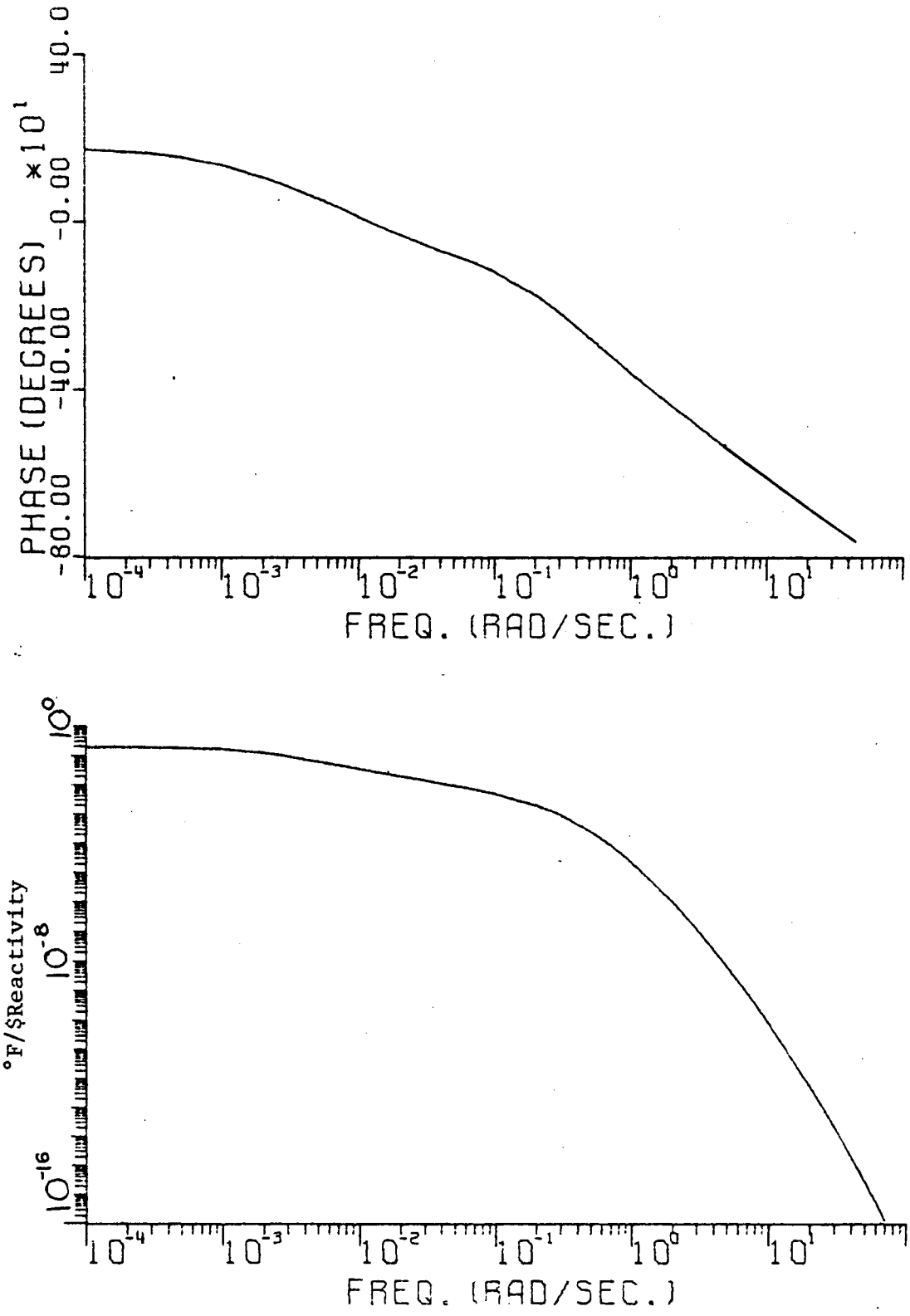


Figure C.3 Frequency Response of Sodium Bond Temperature for IHX Secondary Inlet Sodium Temperature Perturbations.

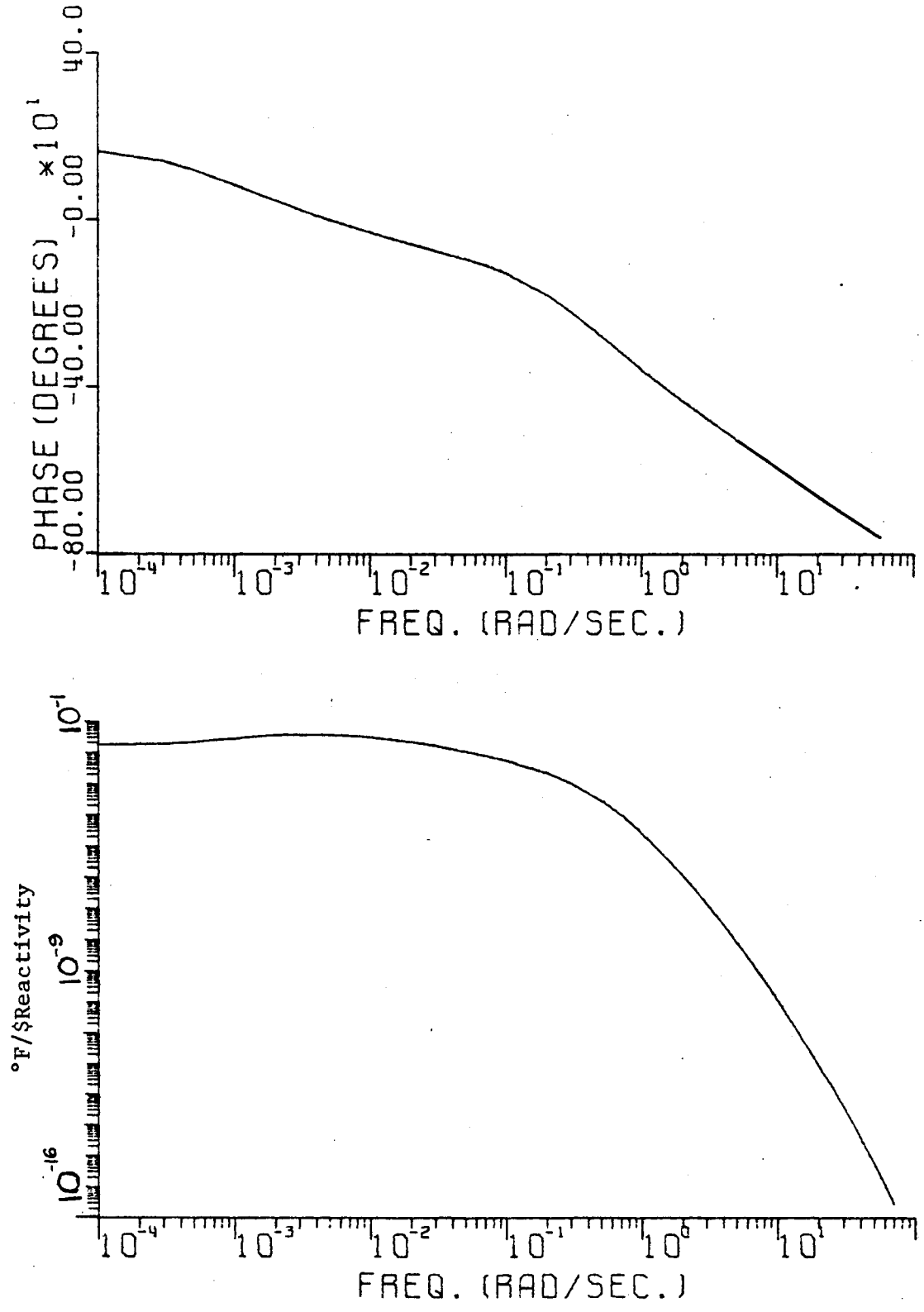


Figure C.4 Frequency Response of Clad Temperature for IHX Secondary Inlet Sodium Temperature Perturbations.

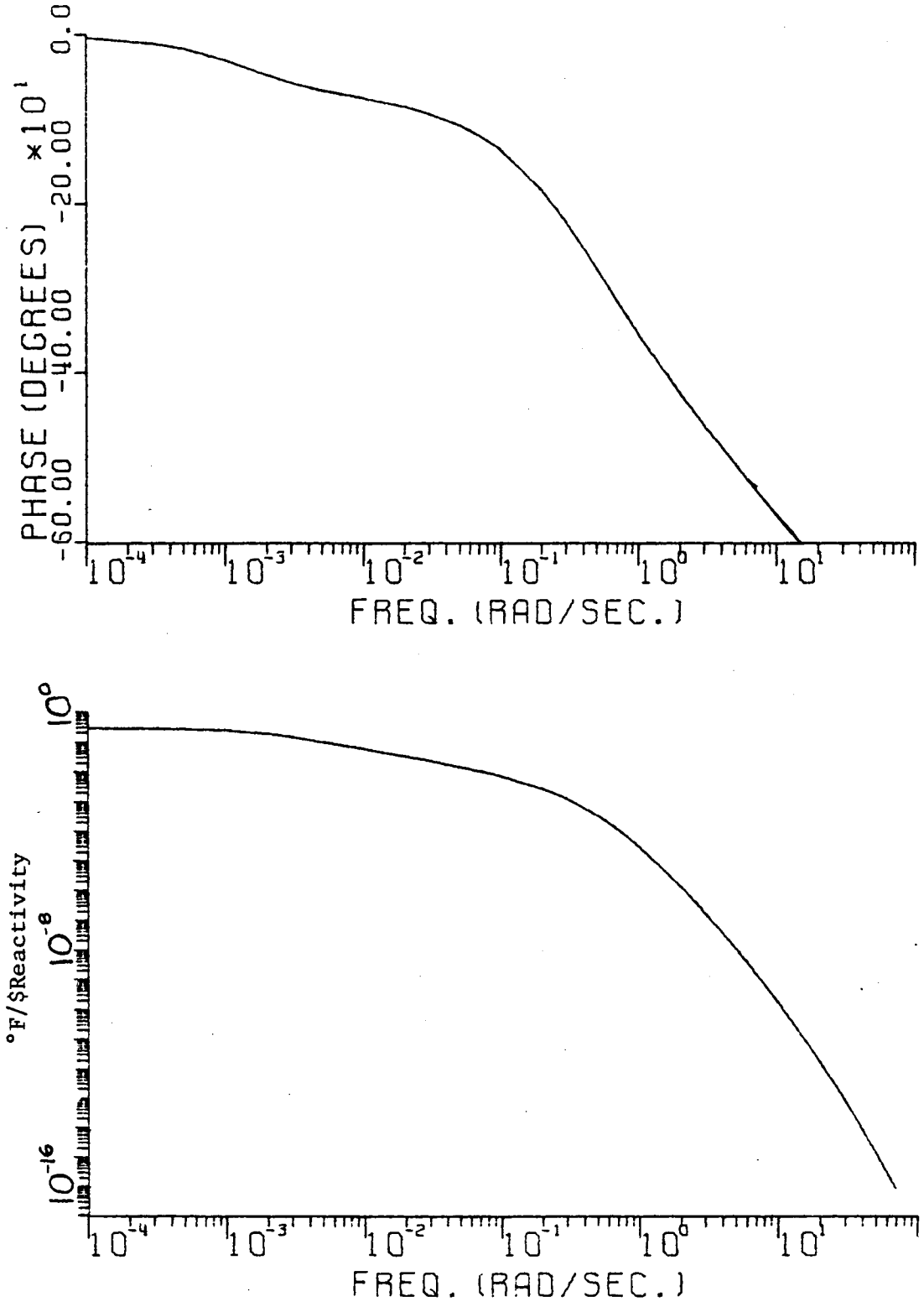


Figure C.5 Frequency Response of Lower Core Sodium Temperature for IHX Secondary Inlet Sodium Temperature Perturbations.

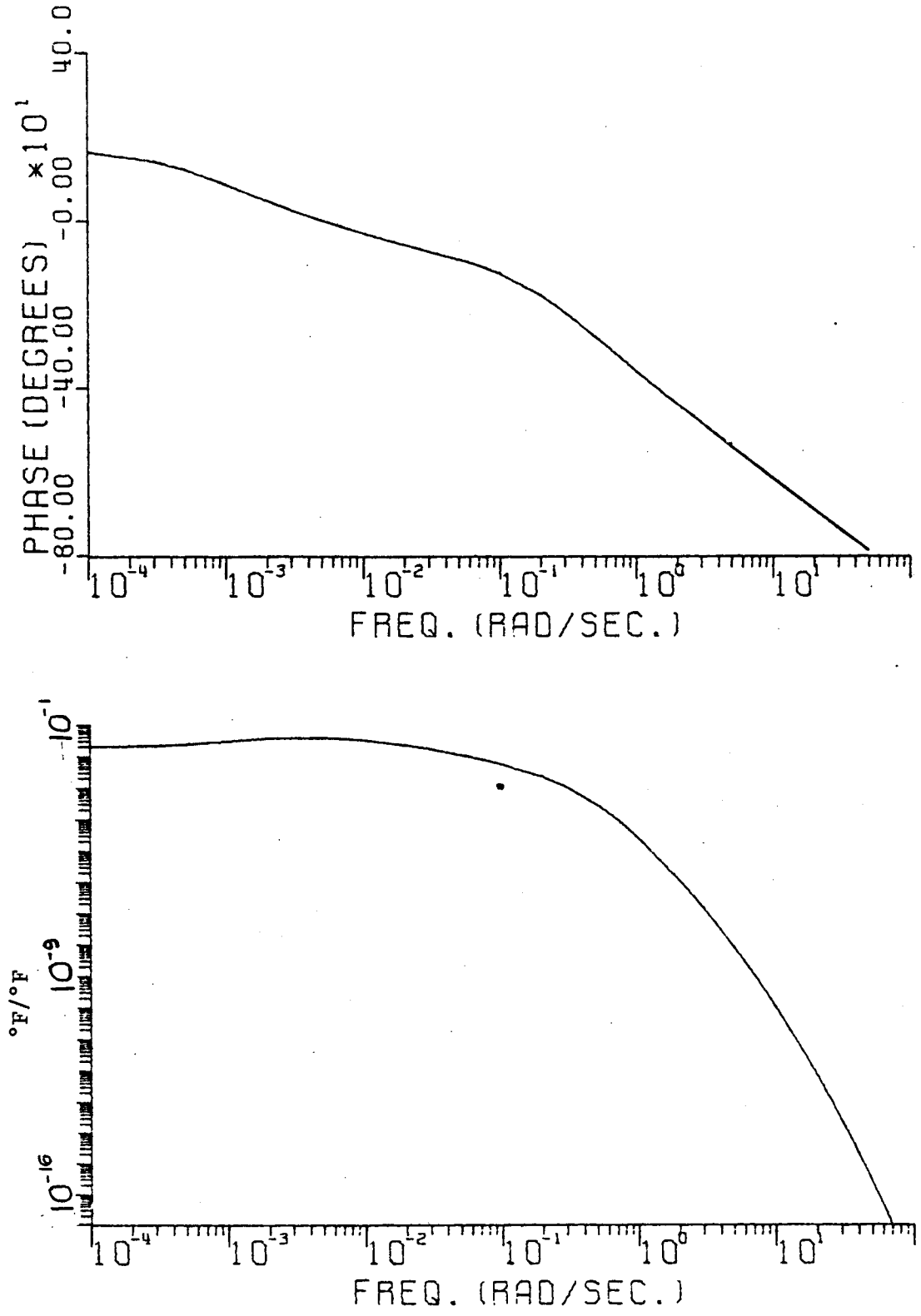


Figure C.6 Frequency Response of Upper Core Sodium Temperature for IHX Secondary Inlet Sodium Temperature Perturbations.

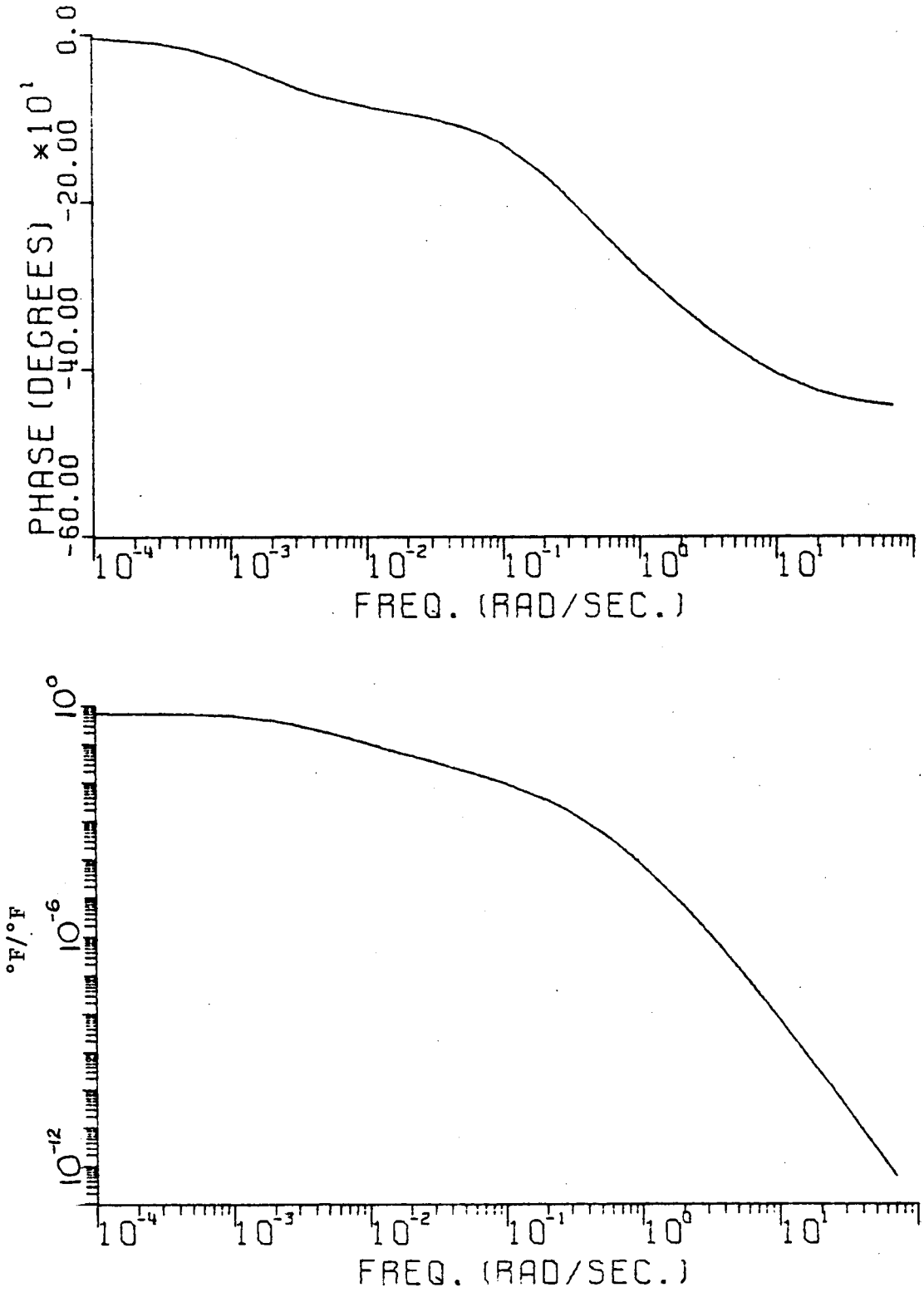


Figure C.7 Frequency Response of Low Pressure Inlet Sodium Temperature for IHX Secondary Inlet Sodium Temperature Perturbations.

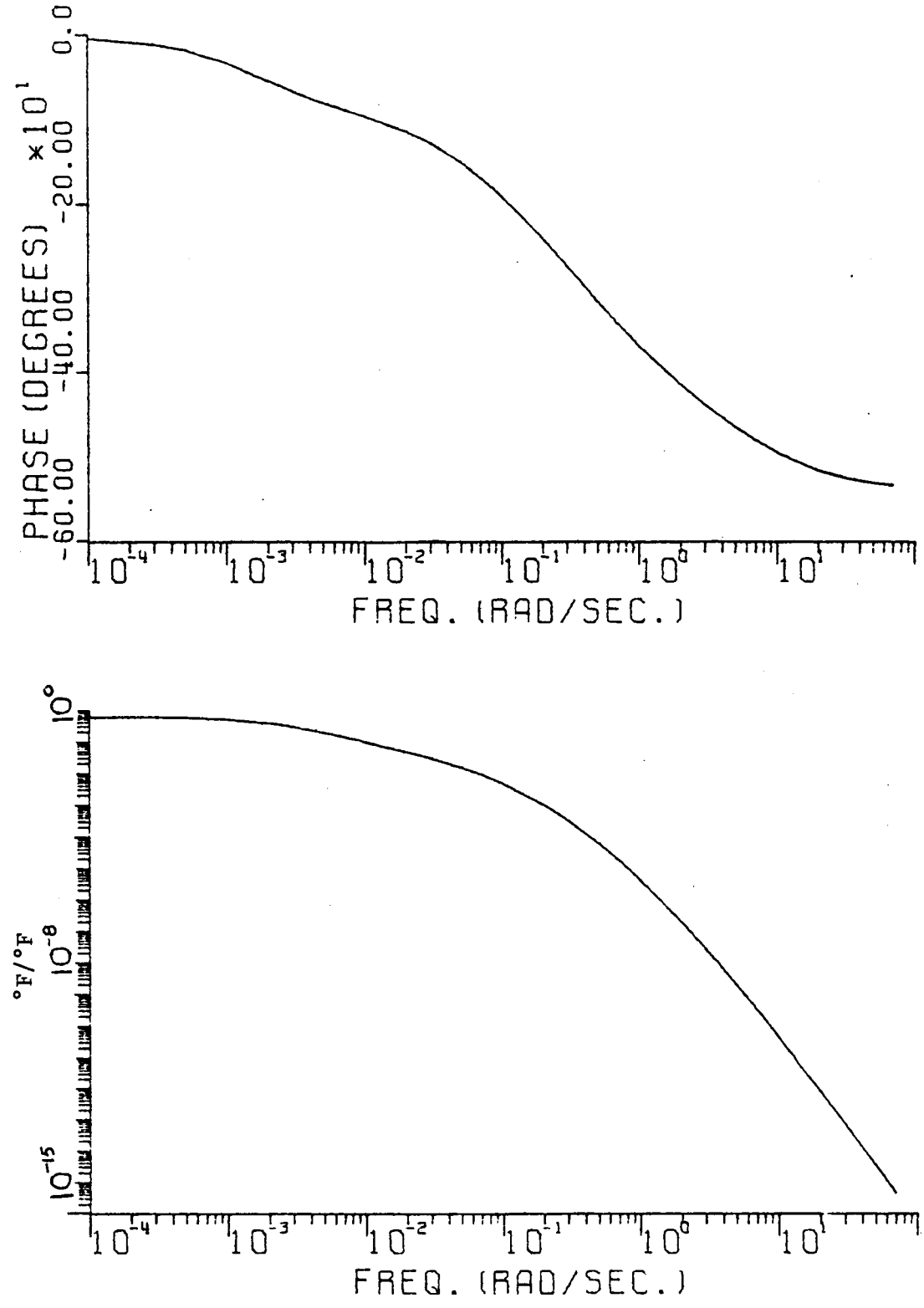


Figure C.8 Frequency Response of Low Pressure Plenum Sodium Temperature for IHX Secondary Inlet Sodium Temperature Perturbations.

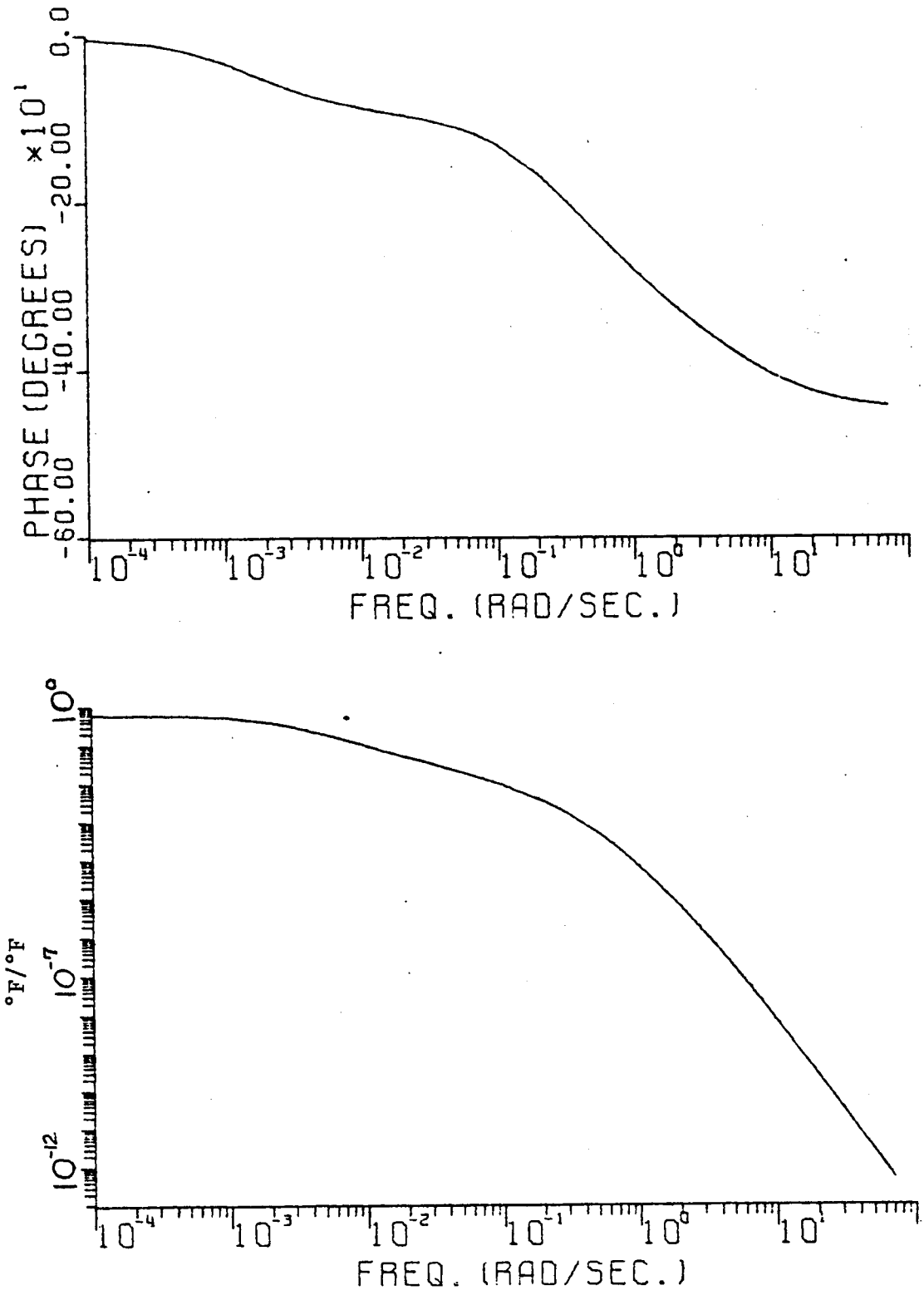


Figure C.9 Frequency Response of High Pressure Inlet Sodium Temperature for IHX Secondary Inlet Sodium Temperature Perturbations.

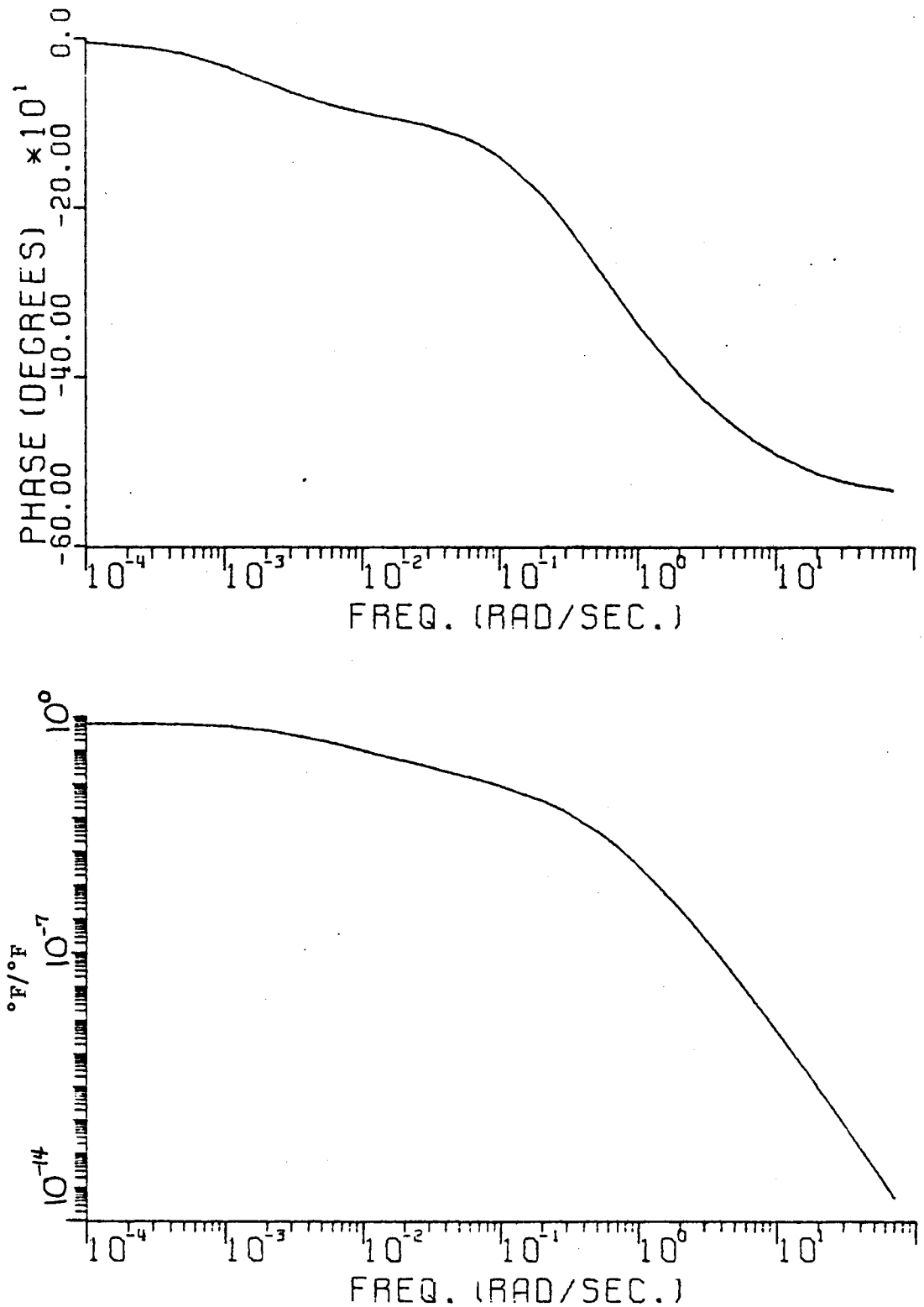


Figure C.10 Frequency Response of High Pressure Plenum Sodium Temperature for IHX Secondary Inlet Sodium Temperature Perturbations.

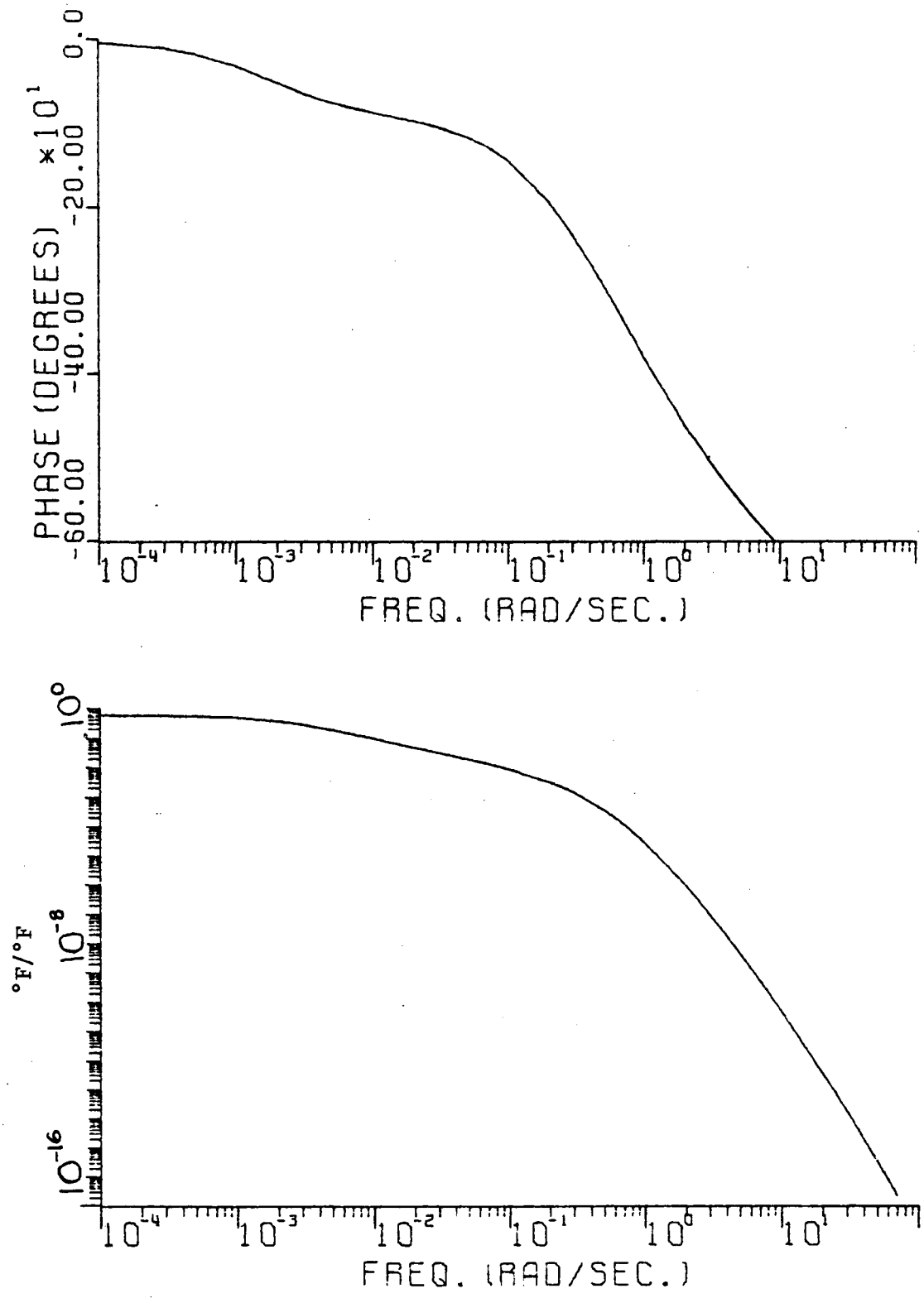


Figure C.11 Frequency Response of Lower Reflector Metal Temperature for IHX Secondary Inlet Sodium Temperature Perturbations.

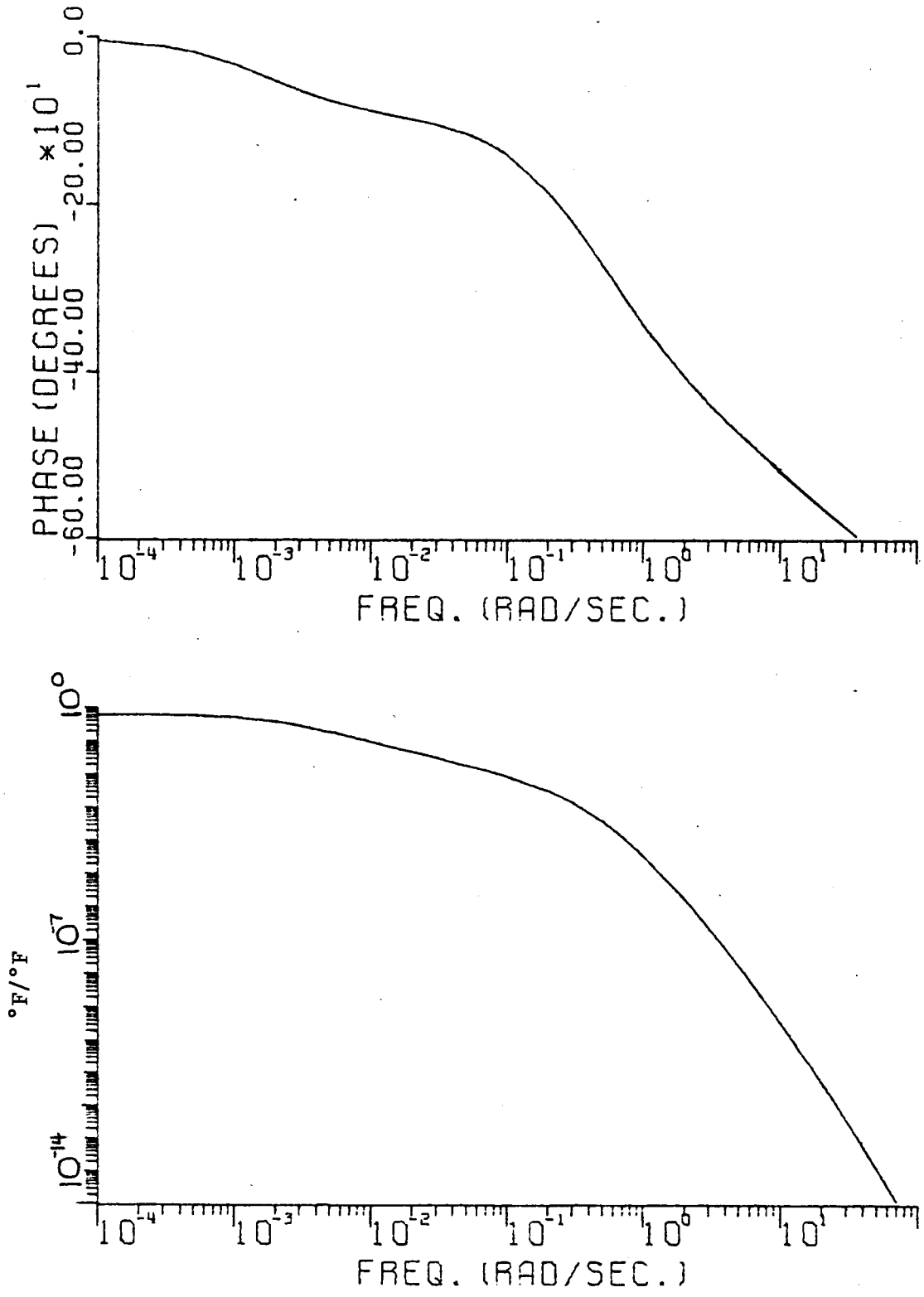


Figure C.12 Frequency Response of Lower Reflector Lower Sodium Temperature for IHX Secondary Inlet Sodium Temperature Perturbations.

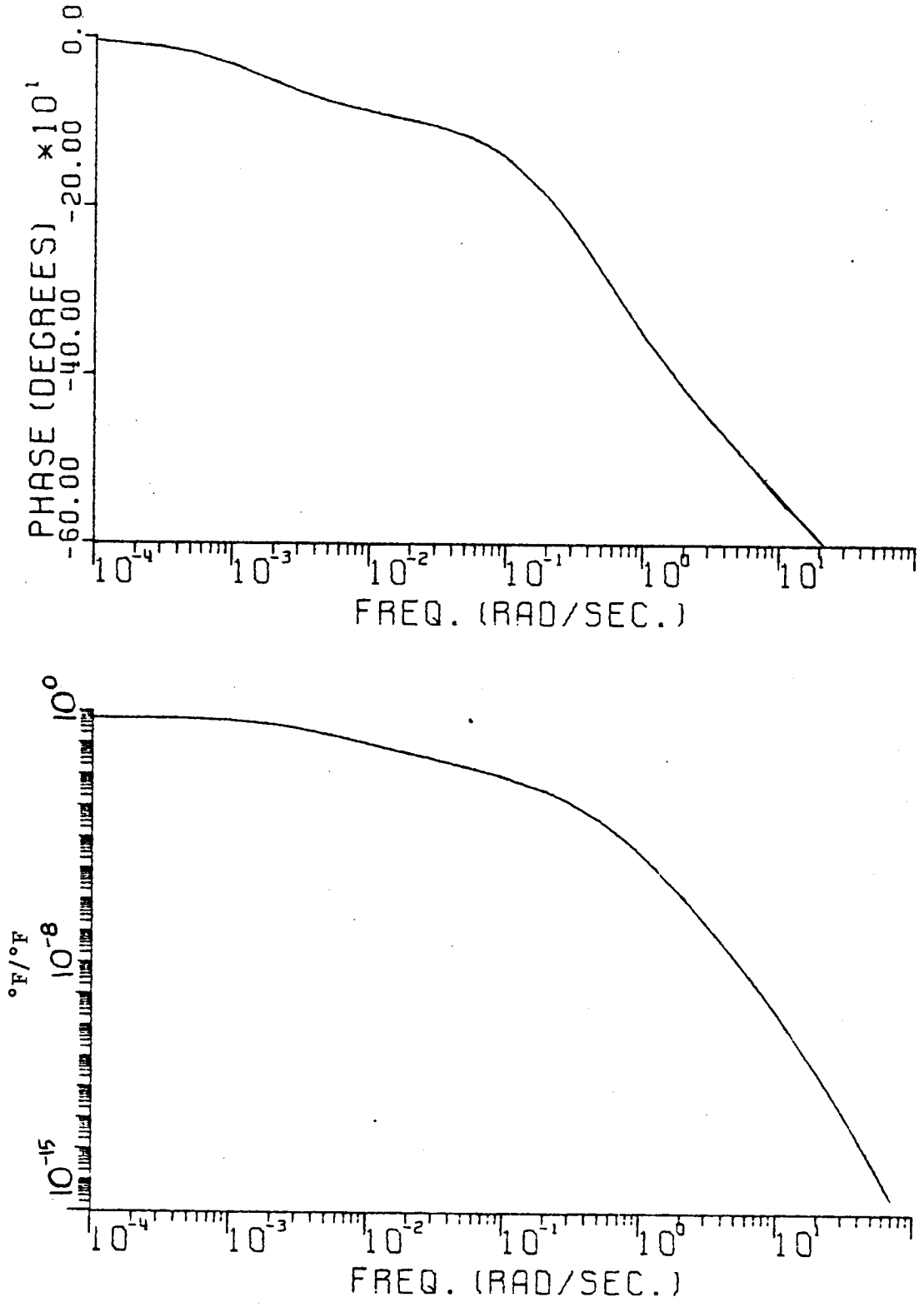


Figure C.13 Frequency Response of Lower Reflector Upper Sodium Temperature for IHX Secondary Inlet Sodium Temperature Perturbations.

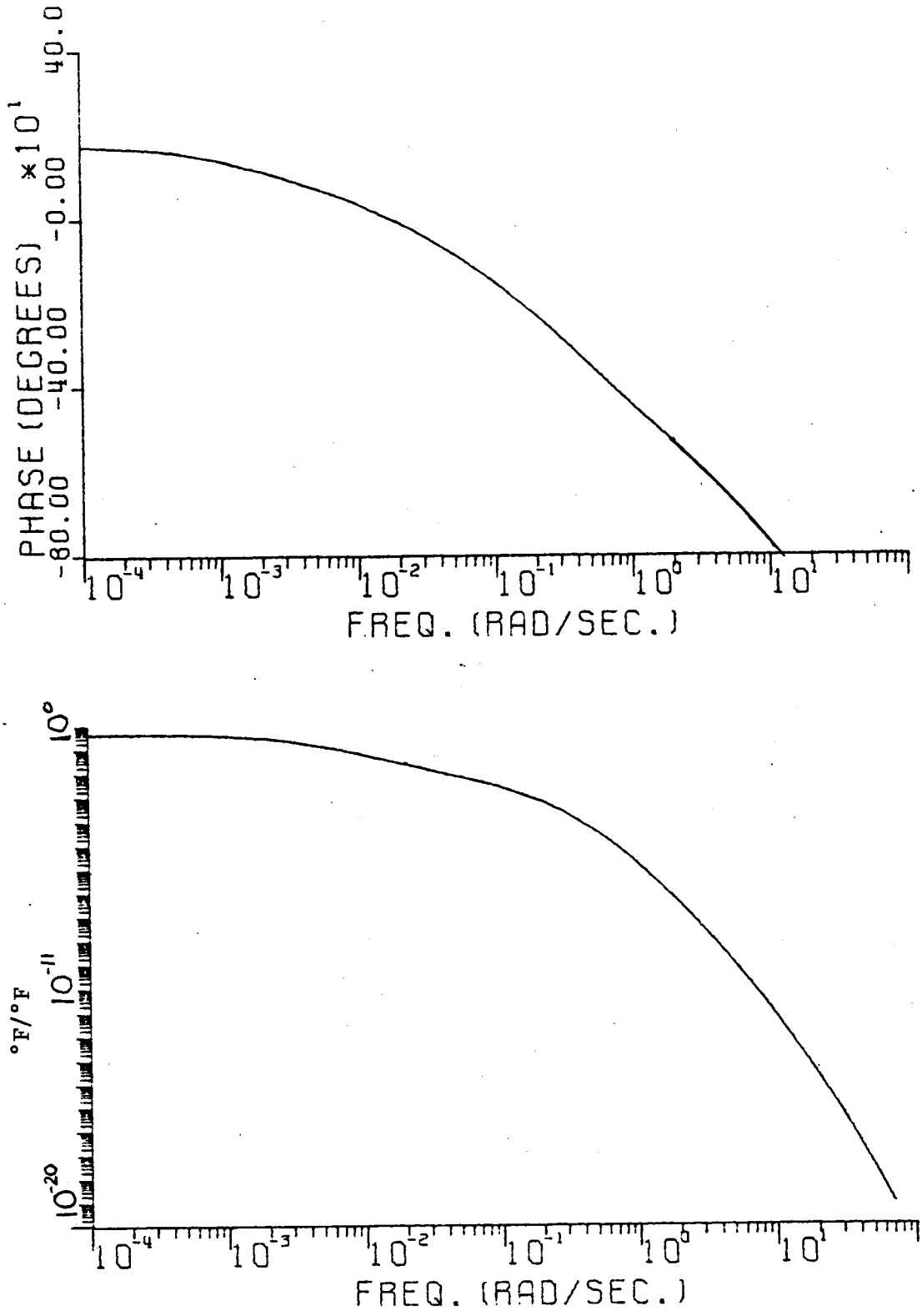


Figure C.14 Frequency Response of Upper Reflector Metal Temperature for IHX Secondary Inlet Sodium Temperature Perturbations.

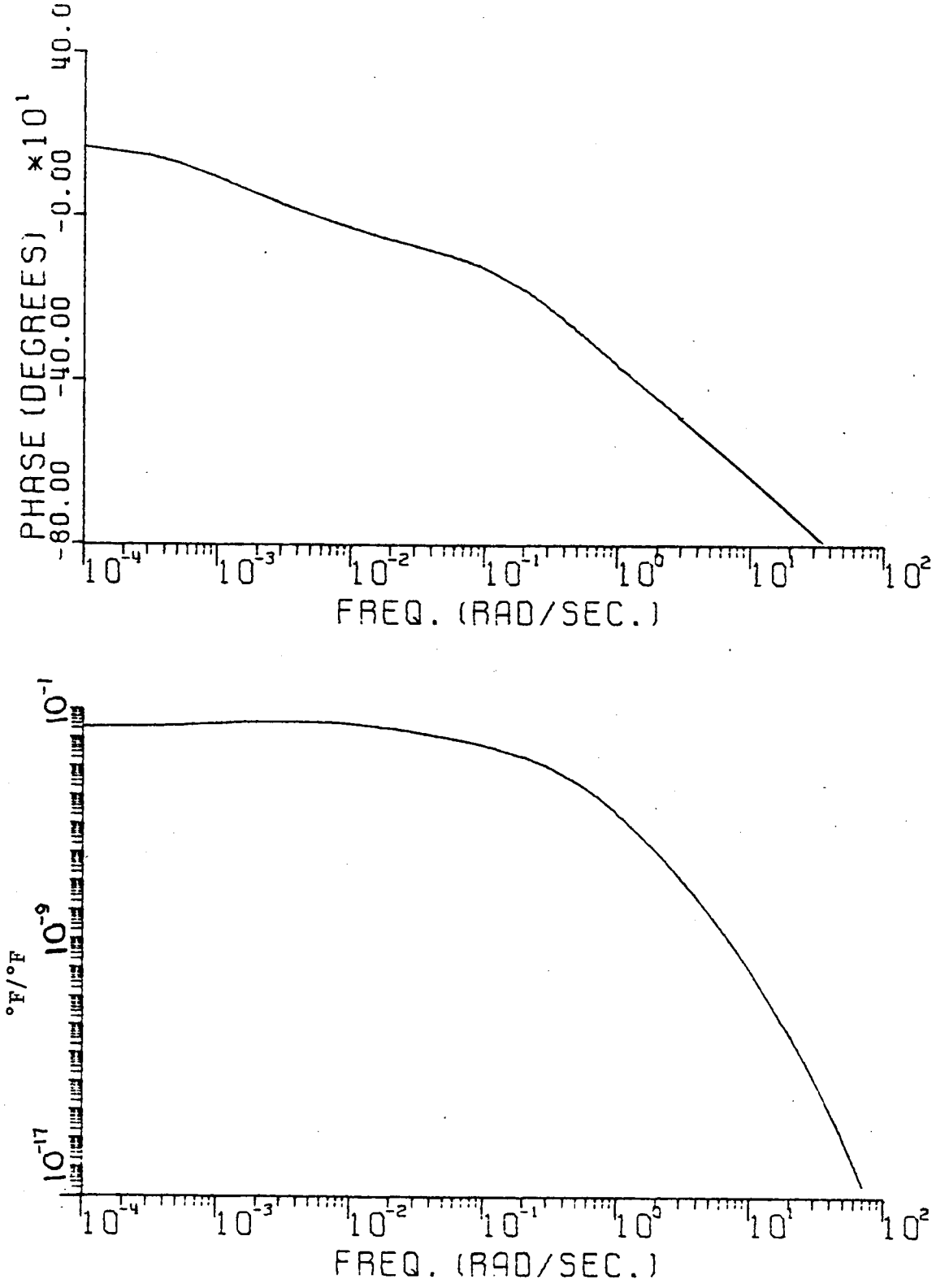


Figure C.15 Frequency Response of Upper Reflector Lower Sodium Temperature for IHX Secondary Inlet Sodium Temperature Perturbations.

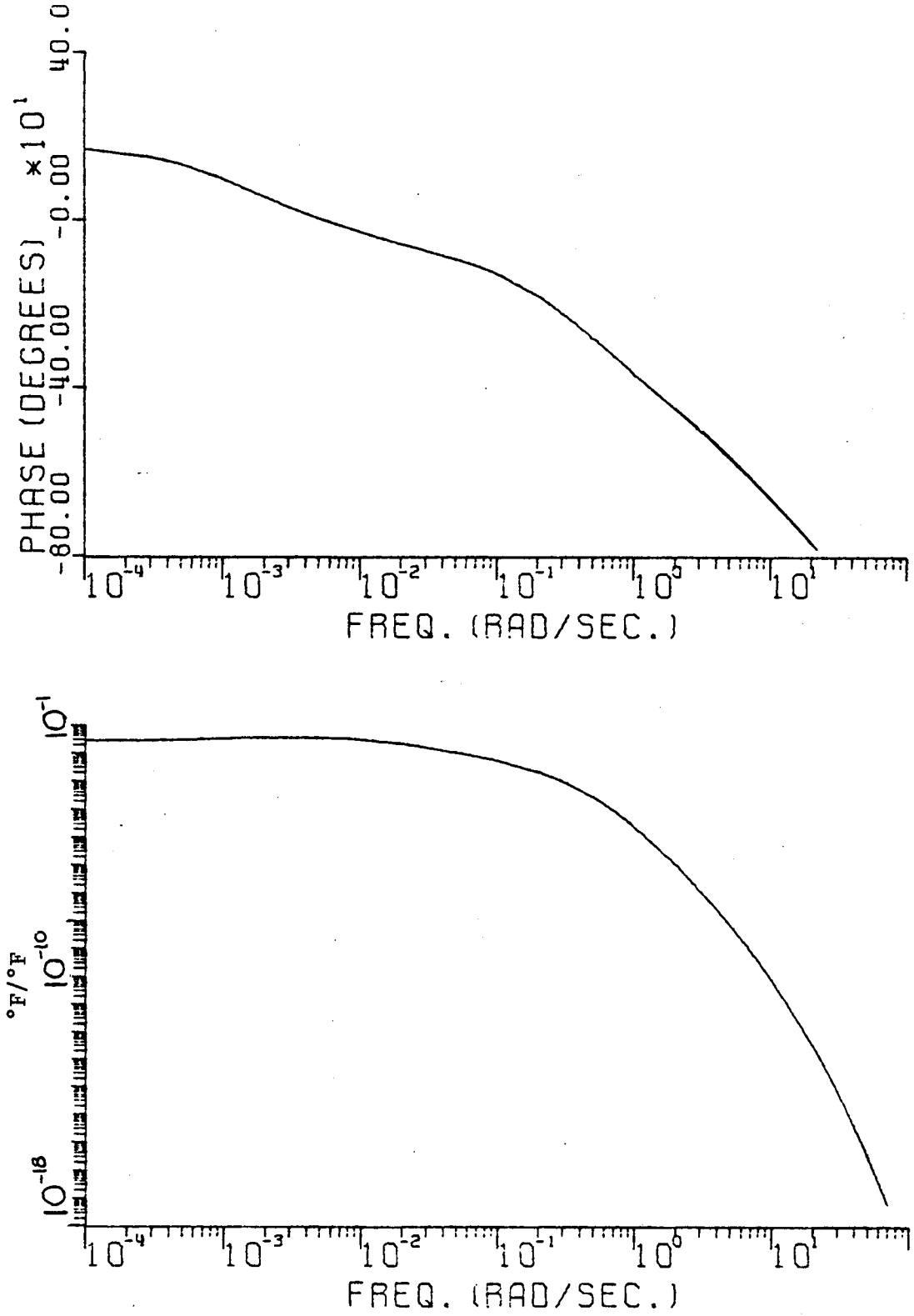


Figure C.16 Frequency Response of Upper Reflector Upper Sodium Temperature for IHX Secondary Inlet Sodium Temperature Perturbations.

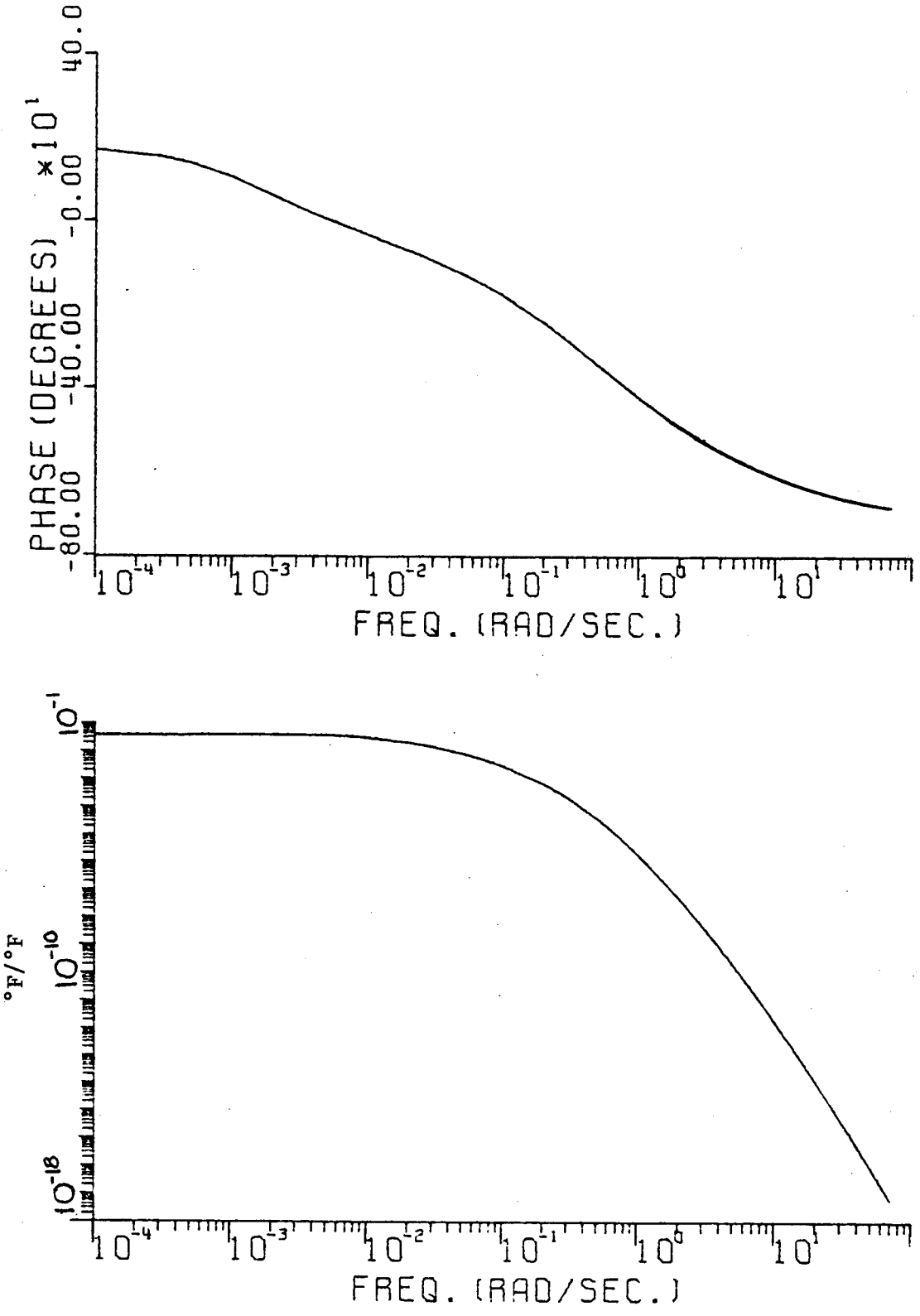


Figure C.17 Frequency Response of Inner Reflector Metal Temperature for IHX Secondary Inlet Sodium Temperature Perturbations.

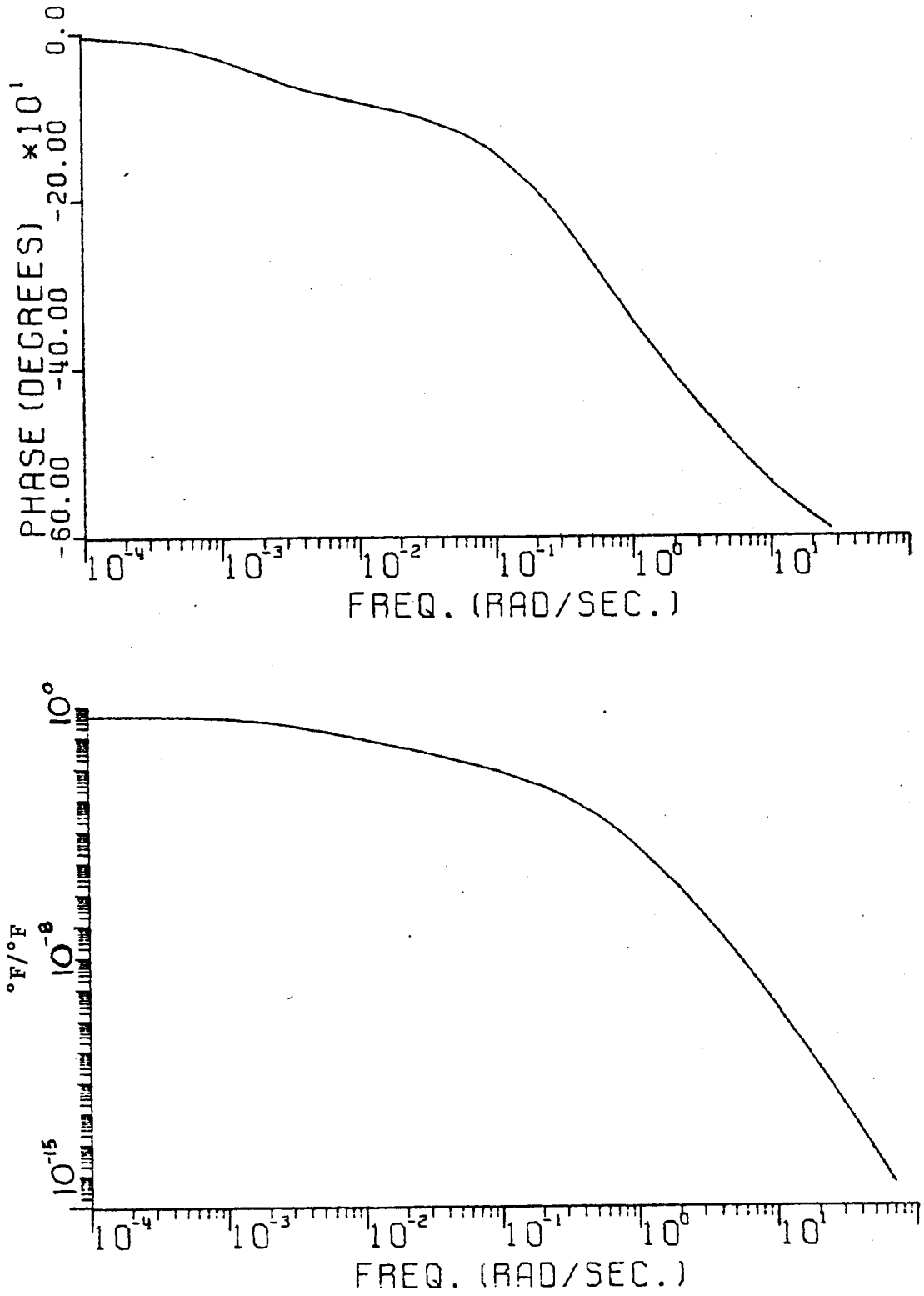


Figure C.18 Frequency Response of Inner Reflector Lower Sodium Temperature for IHX Secondary Inlet Sodium Temperature Perturbations.

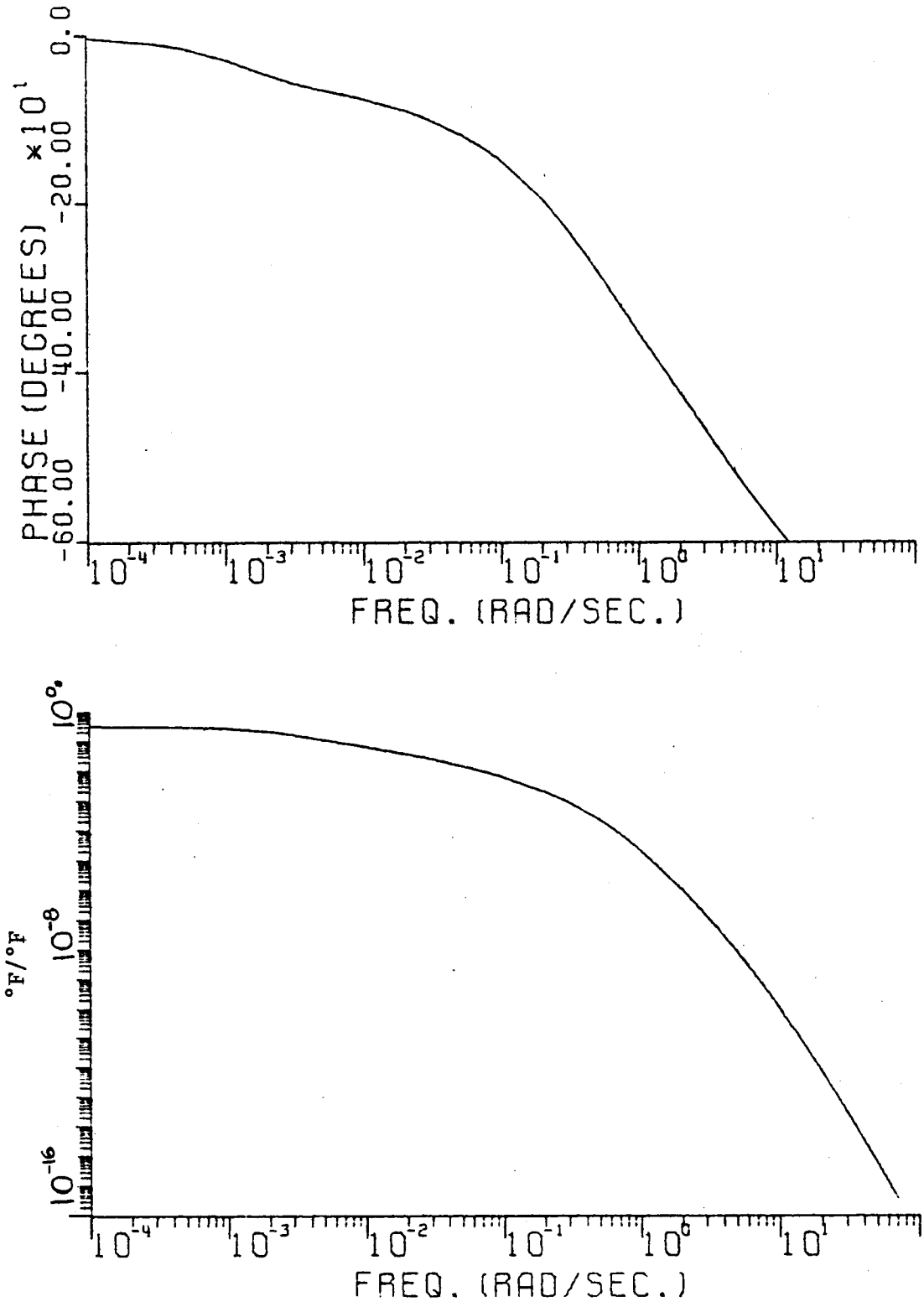


Figure C.19 Frequency Response of Inner Reflector Upper Sodium Temperature for IHX Secondary Inlet Sodium Temperature Perturbations.

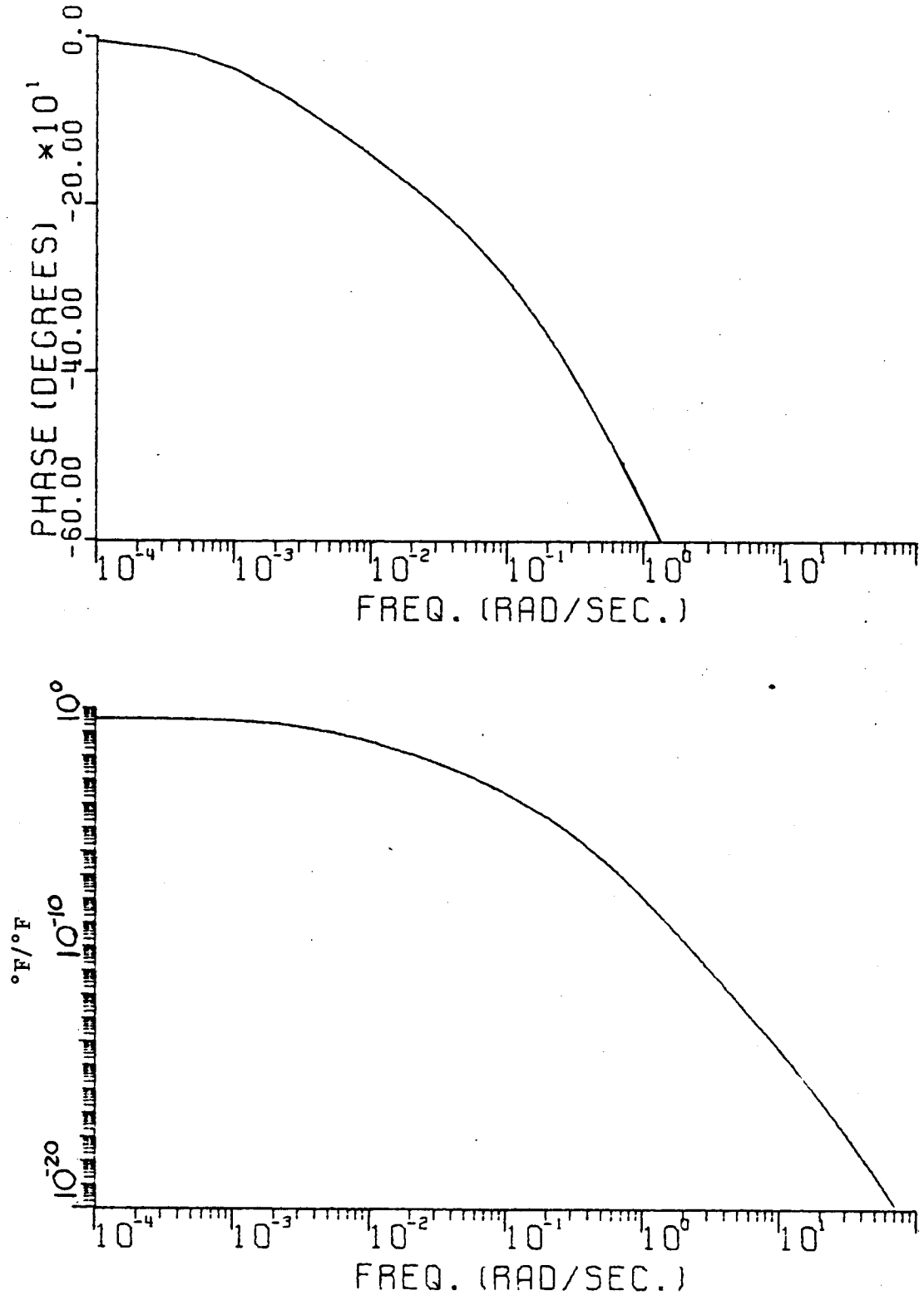


Figure C.20 Frequency Response of Blanket Metal Temperature for IHX Secondary Inlet Sodium Temperature Perturbations.

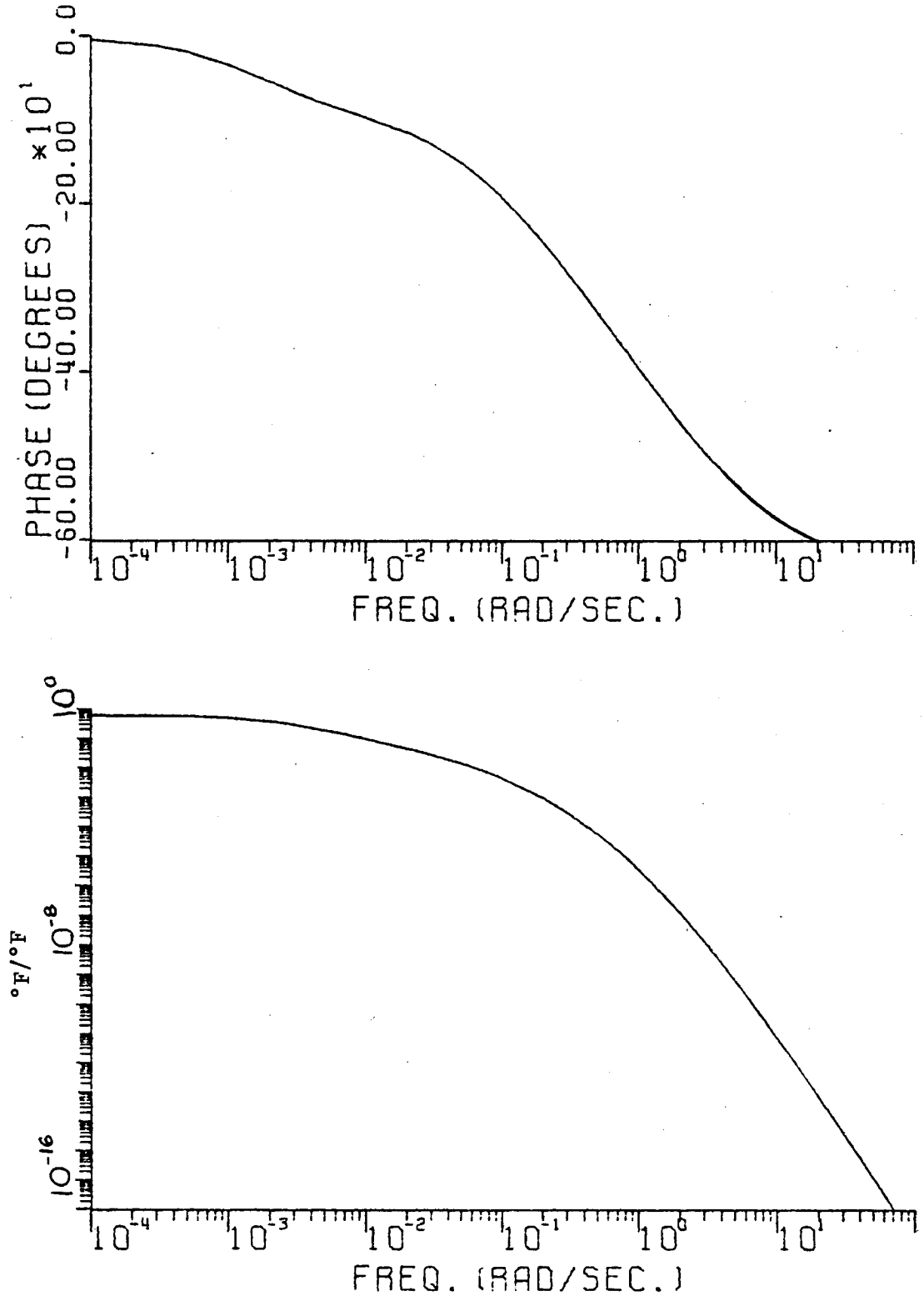


Figure C.21 Frequency Response of Blanket Lower Sodium Temperature for IHX Secondary Inlet Sodium Temperature Perturbations.

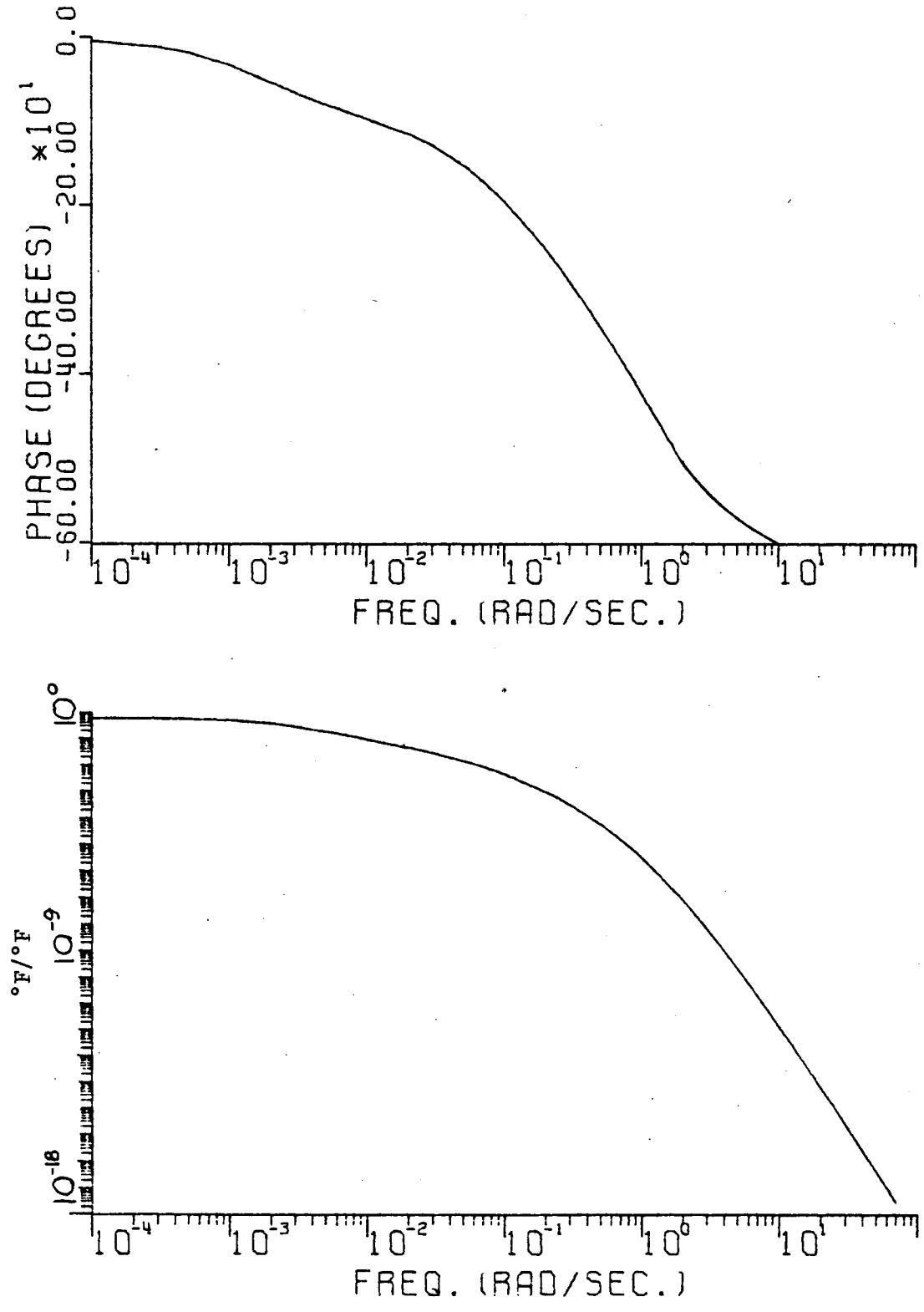


Figure C.22 Frequency Response of Blanket Upper Sodium Temperature for IHX Secondary Inlet Sodium Temperature Perturbations.

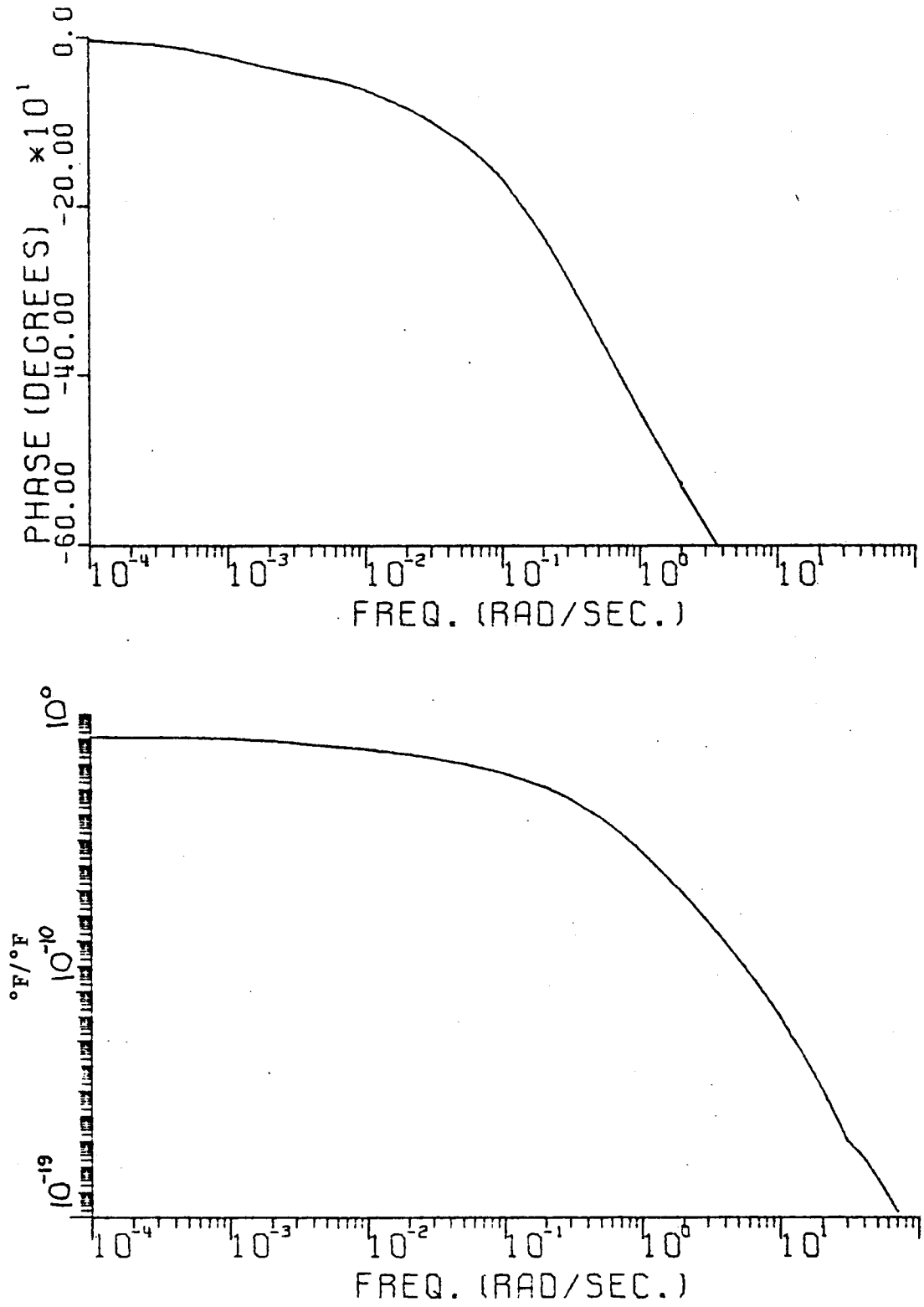


Figure C.23 Frequency Response of Upper Plenum Sodium Temperature for IHX Secondary Inlet Sodium Temperature Perturbations.

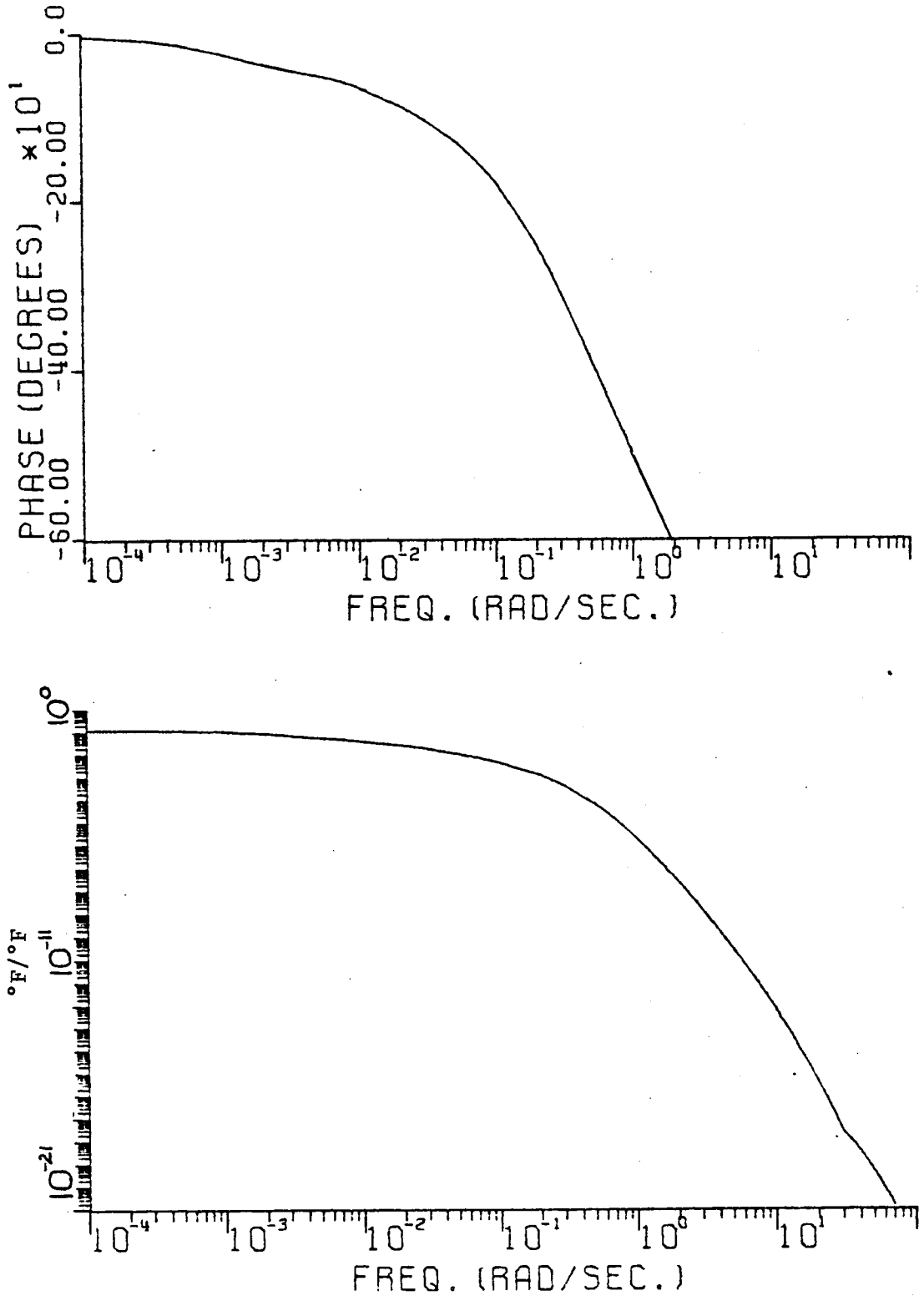


Figure C.24 Frequency Response of Reactor Outlet Sodium Temperature for IHX Secondary Inlet Sodium Temperature Perturbations.

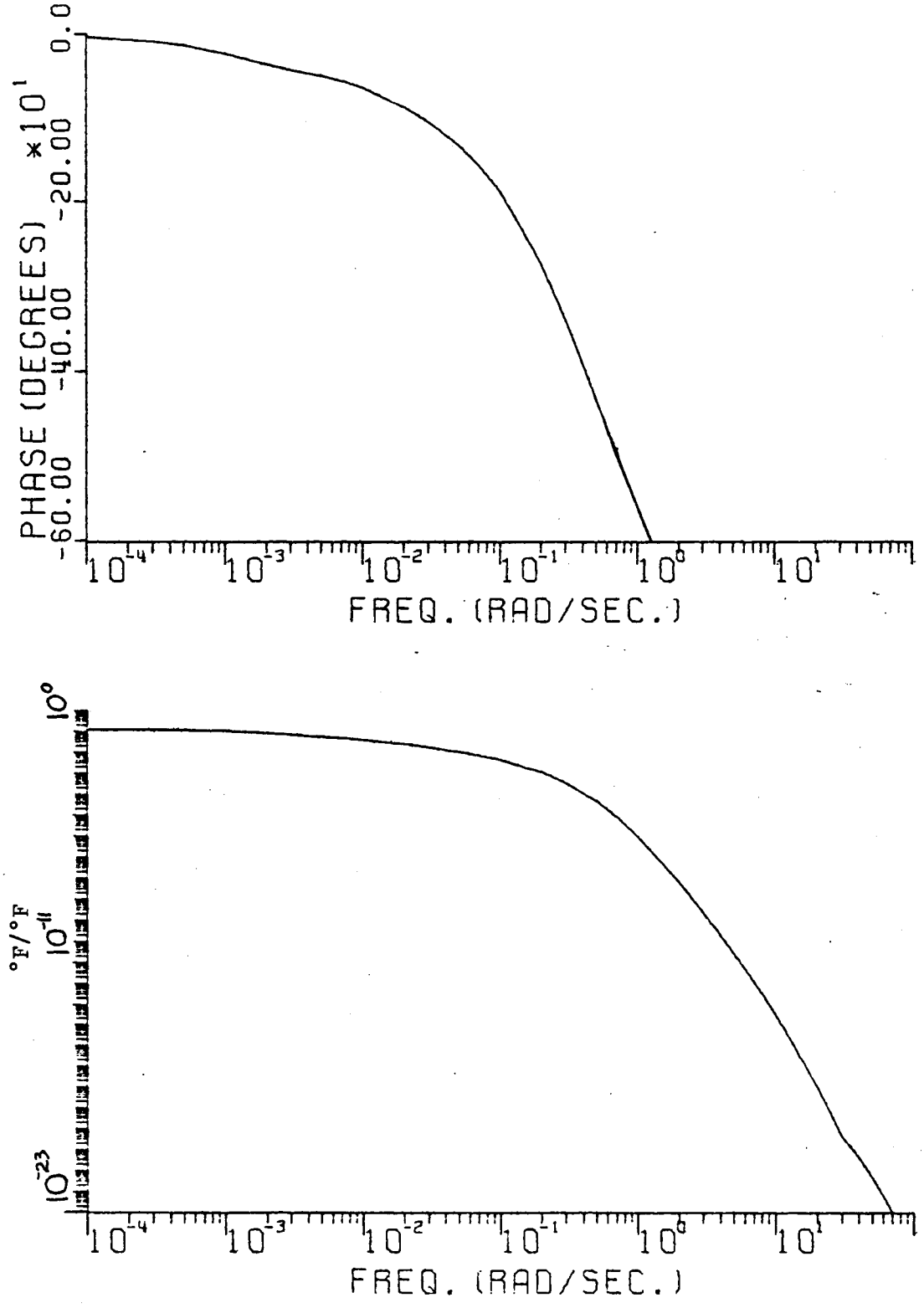


Figure C.25 Frequency Response of IHX Primary Inlet Sodium Temperature for IHX Secondary Inlet Sodium Temperature Perturbations.

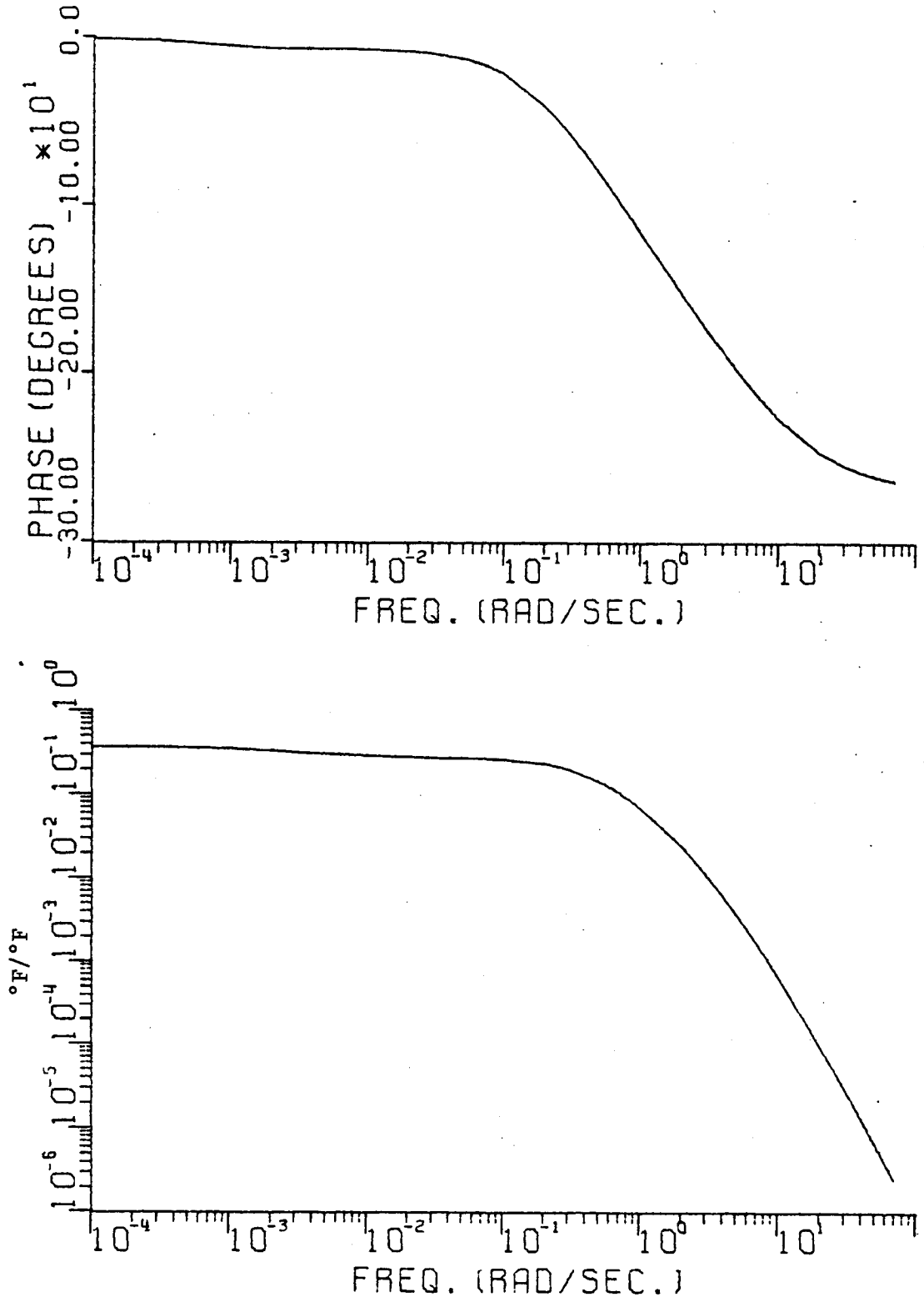


Figure C.26 Frequency Response of IHX Primary Node 1 Sodium Temperature for IHX Secondary Inlet Sodium Temperature Perturbations.

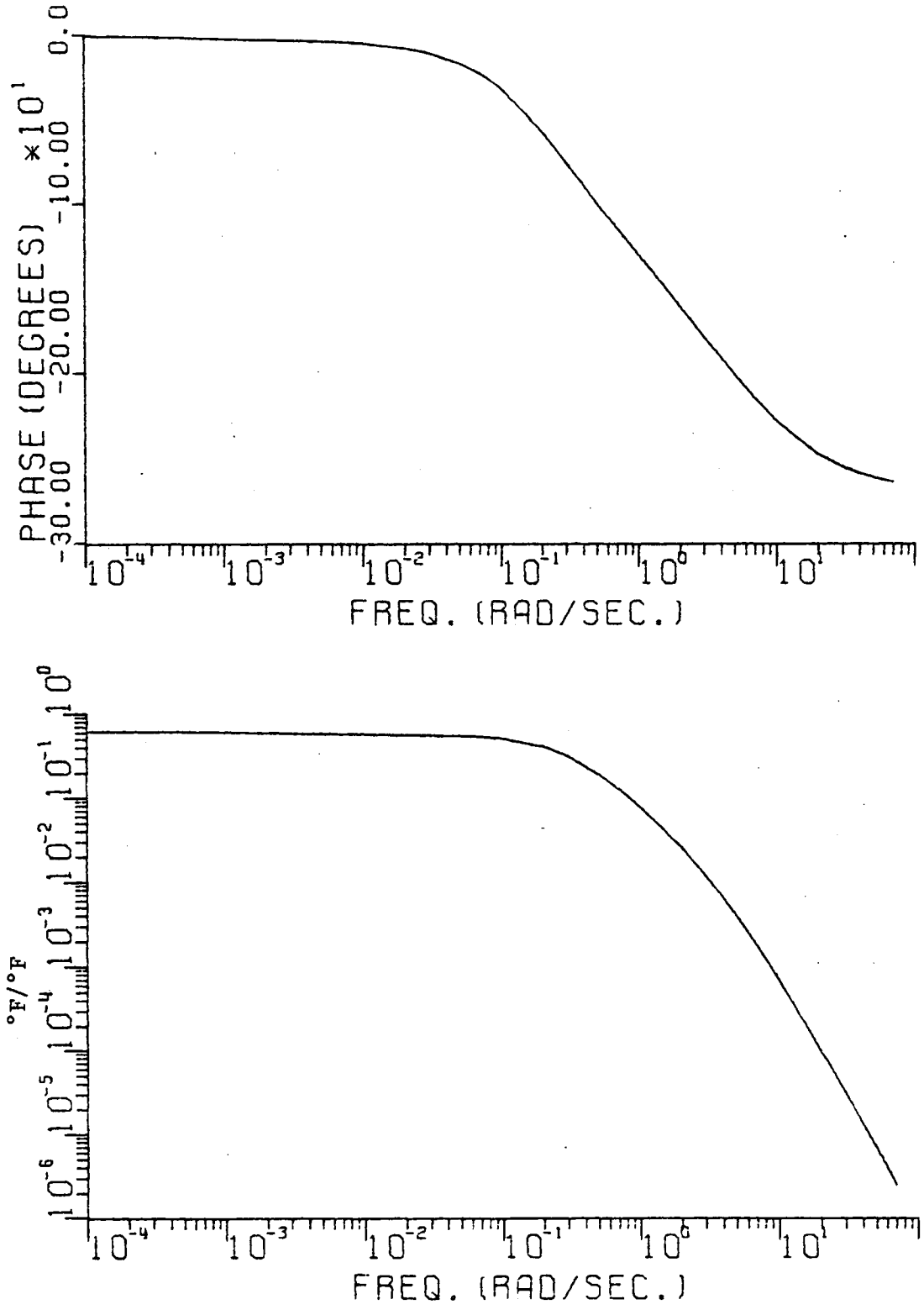


Figure C.27 Frequency Response of IHX Primary Node 2 Sodium Temperature for IHX Secondary Inlet Sodium Temperature Perturbations.

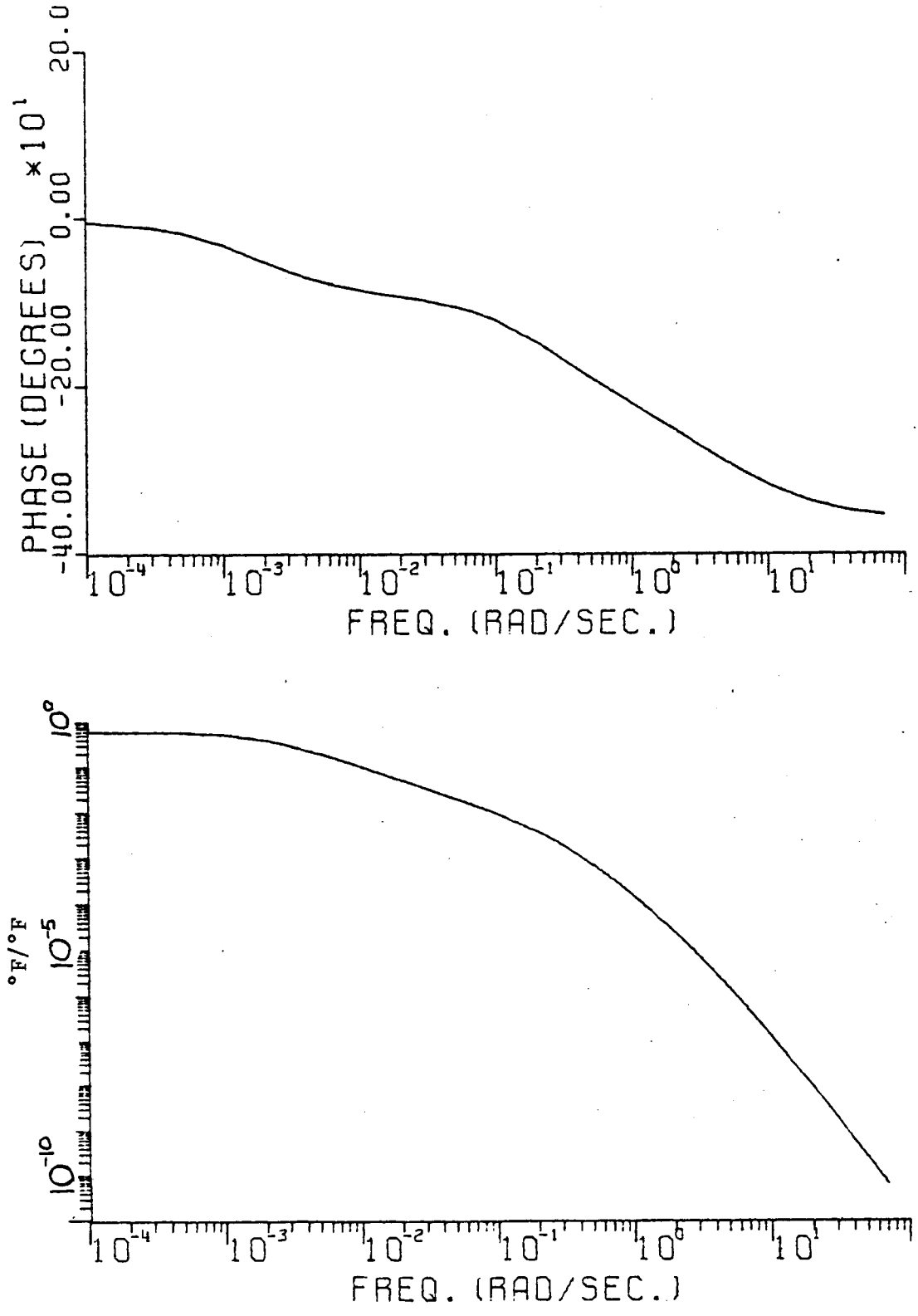


Figure C.28 Frequency Response of Primary Pot Sodium Temperature for IHX Secondary Inlet Sodium Temperature Perturbations.

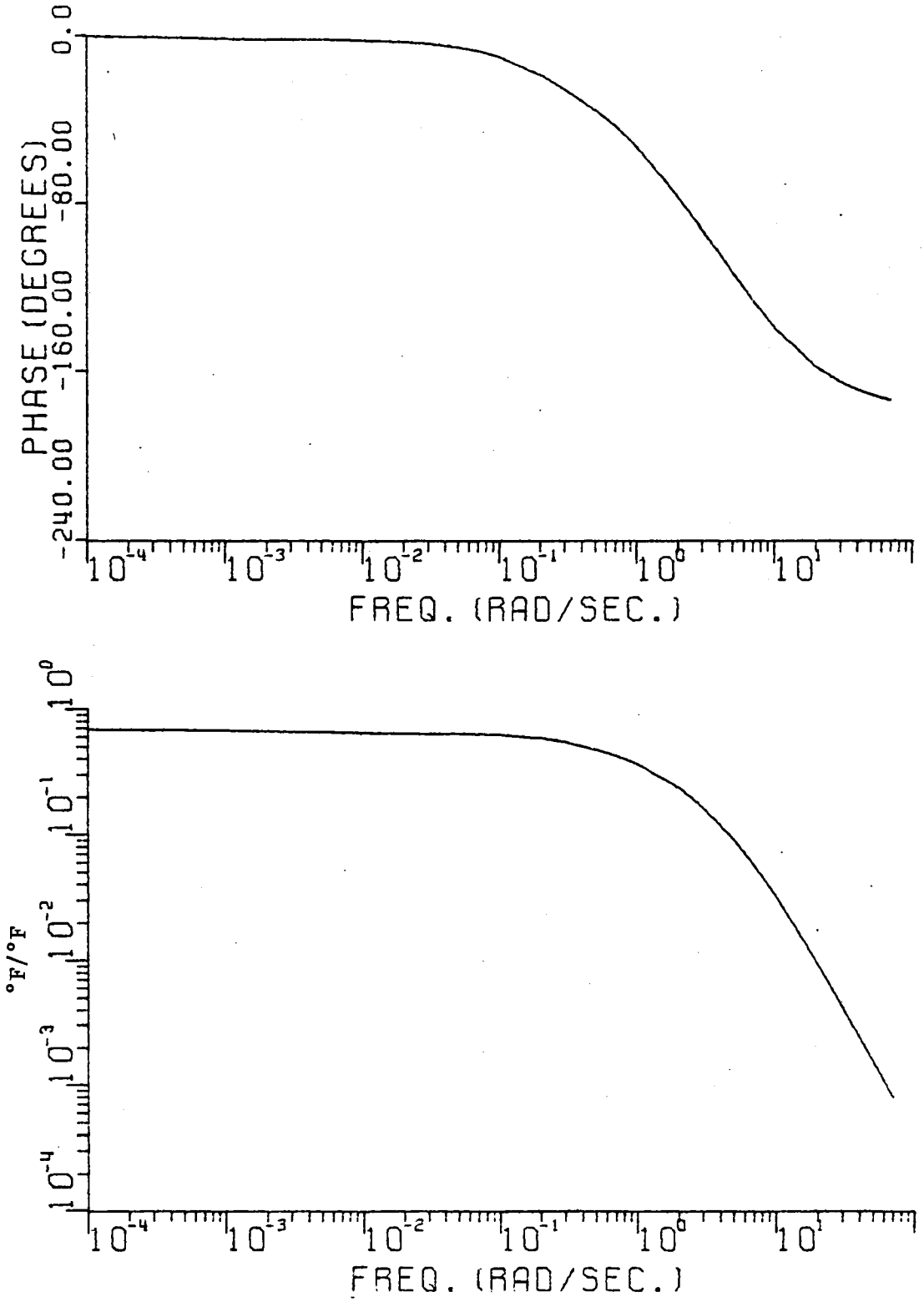


Figure C.29 Frequency Response of IHX Tube Bundle Temperature for IHX Secondary Inlet Sodium Temperature Perturbations.

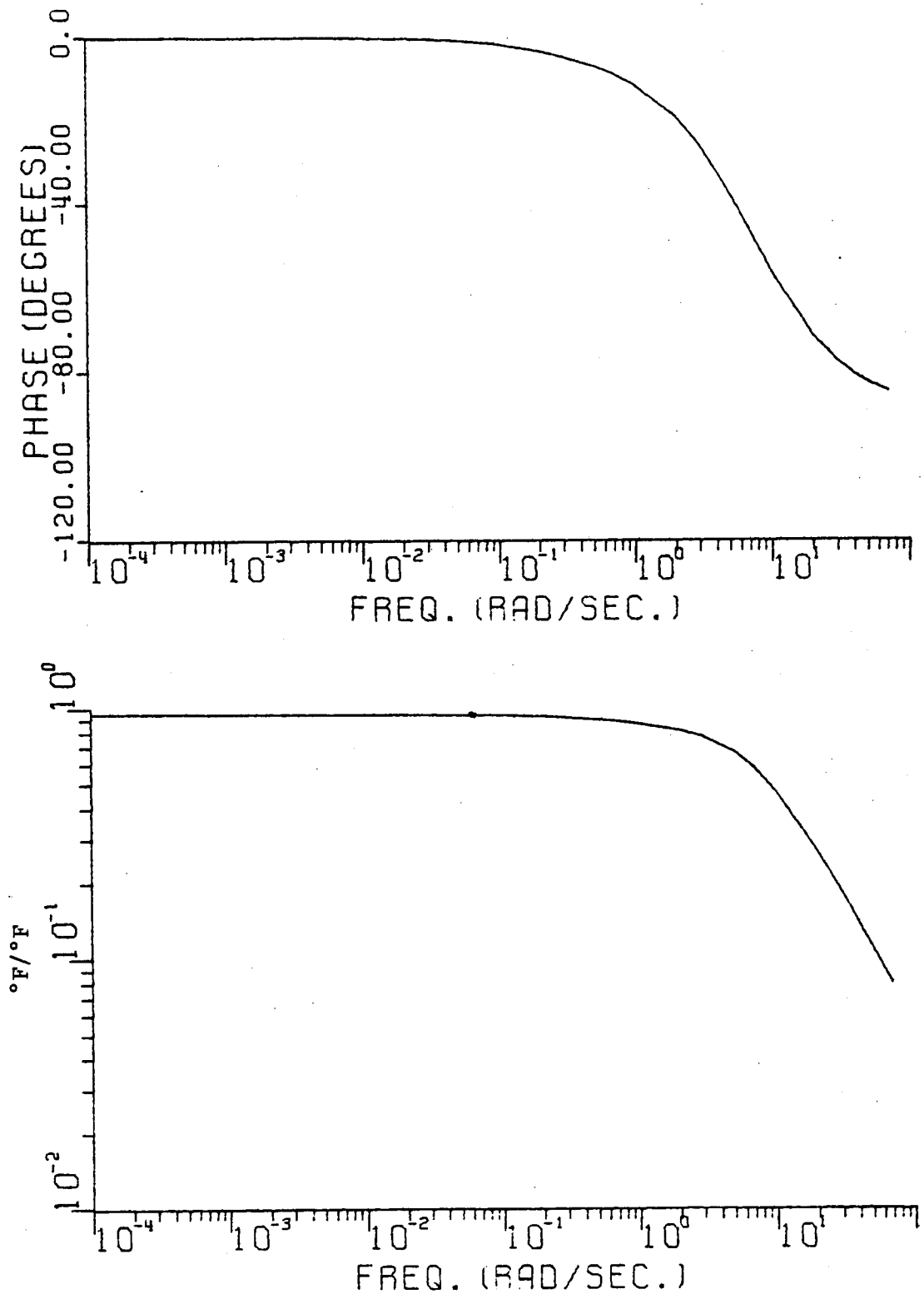


Figure C.30 Frequency Response of IHX Secondary Node 1 Temperature for IHX Secondary Inlet Sodium Temperature Perturbations.

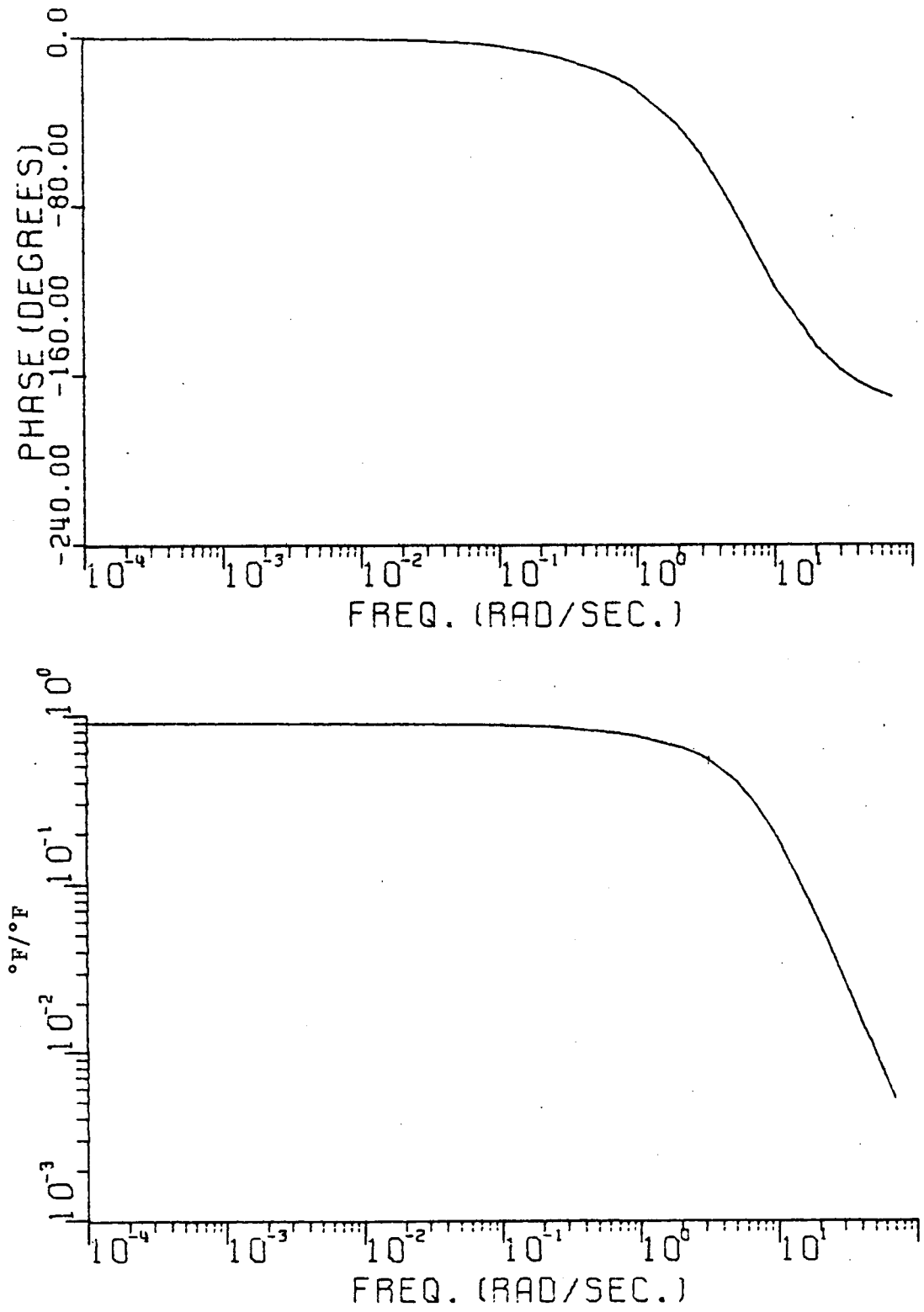


Figure C.31 Frequency Response of IHX Secondary Node 2 Sodium Temperature for IHX Secondary Inlet Sodium Temperature Perturbations.

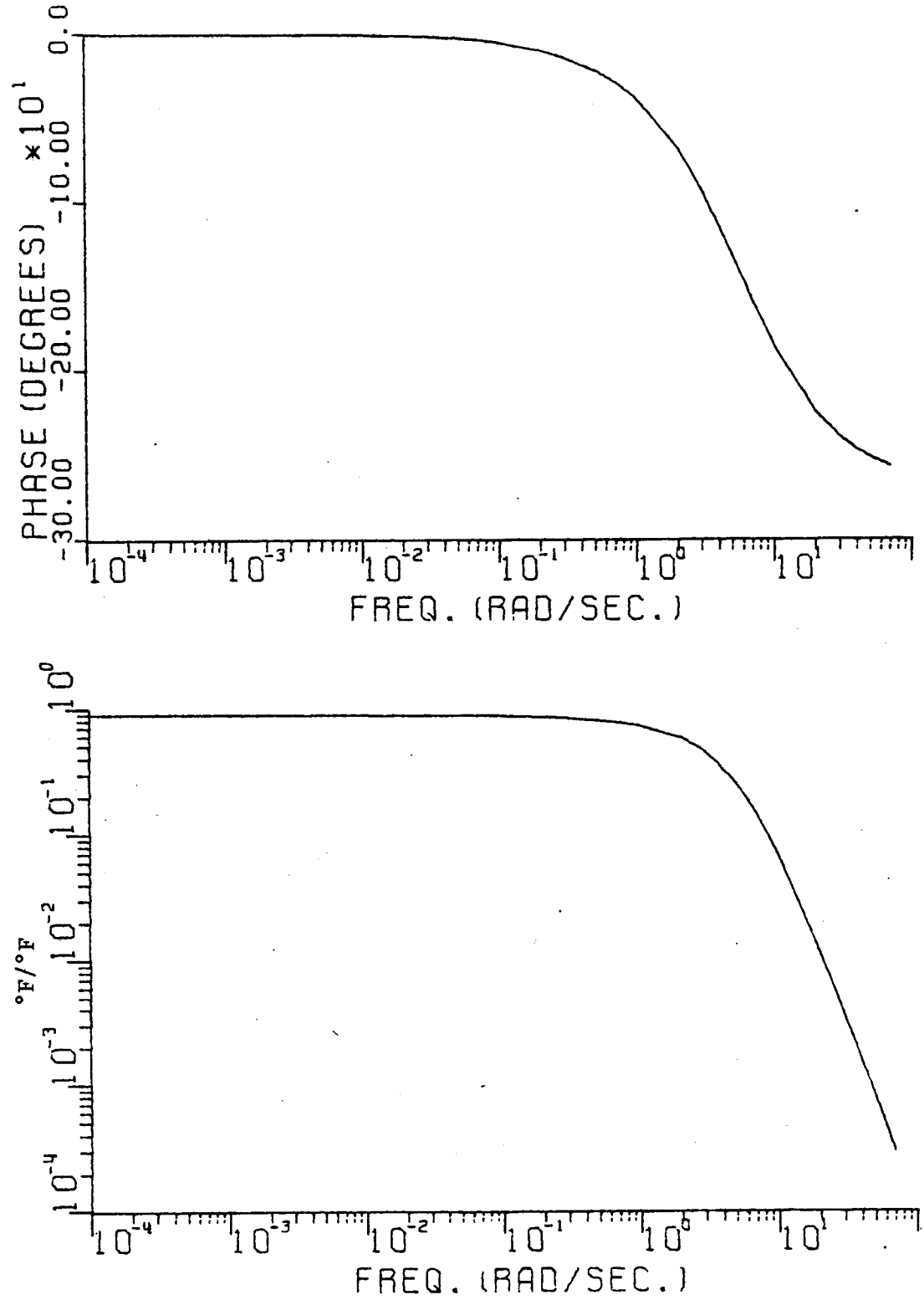


Figure C.32 Frequency Response of IHX Secondary Outlet Sodium Temperature for IHX Secondary Inlet Sodium Temperature Perturbations.

APPENDIX D

Some of the more important system, reactivity perturbation, frequency response sensitivities are given in the following figures.

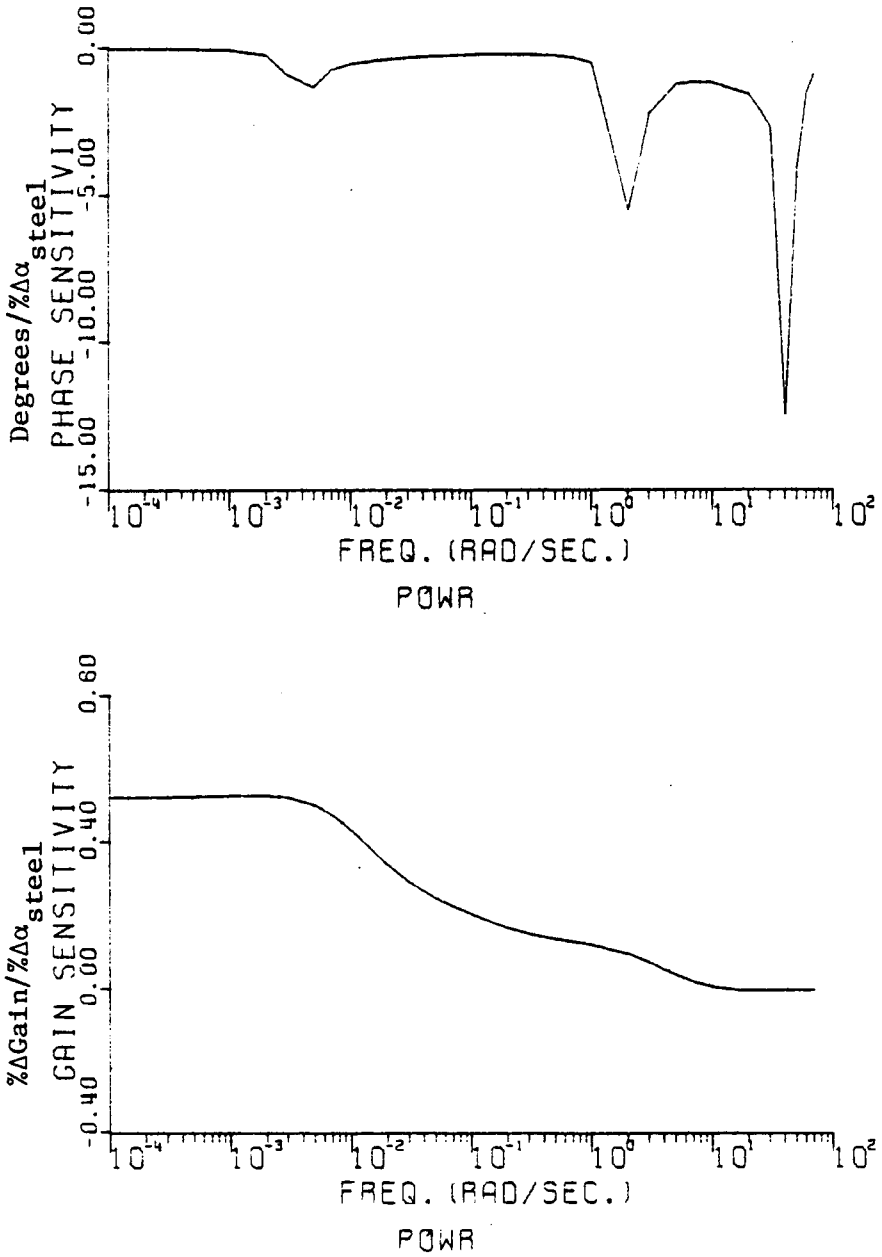


Figure D.1 Reactor Power Frequency Response Sensitivity to α_{steel}.

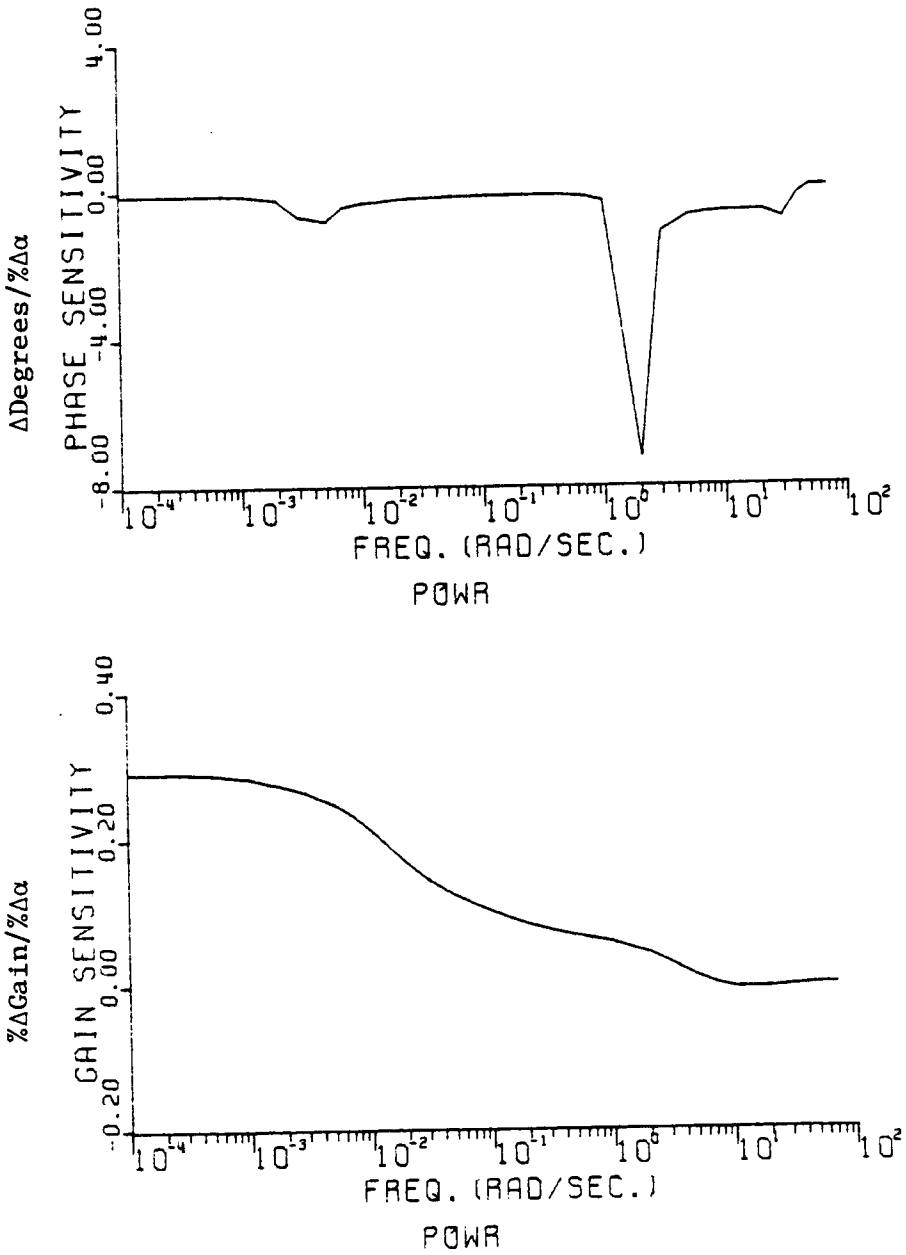


Figure D.2 Reactor Power Frequency Response Sensitivity To $\alpha_{\text{core sodium}}$.

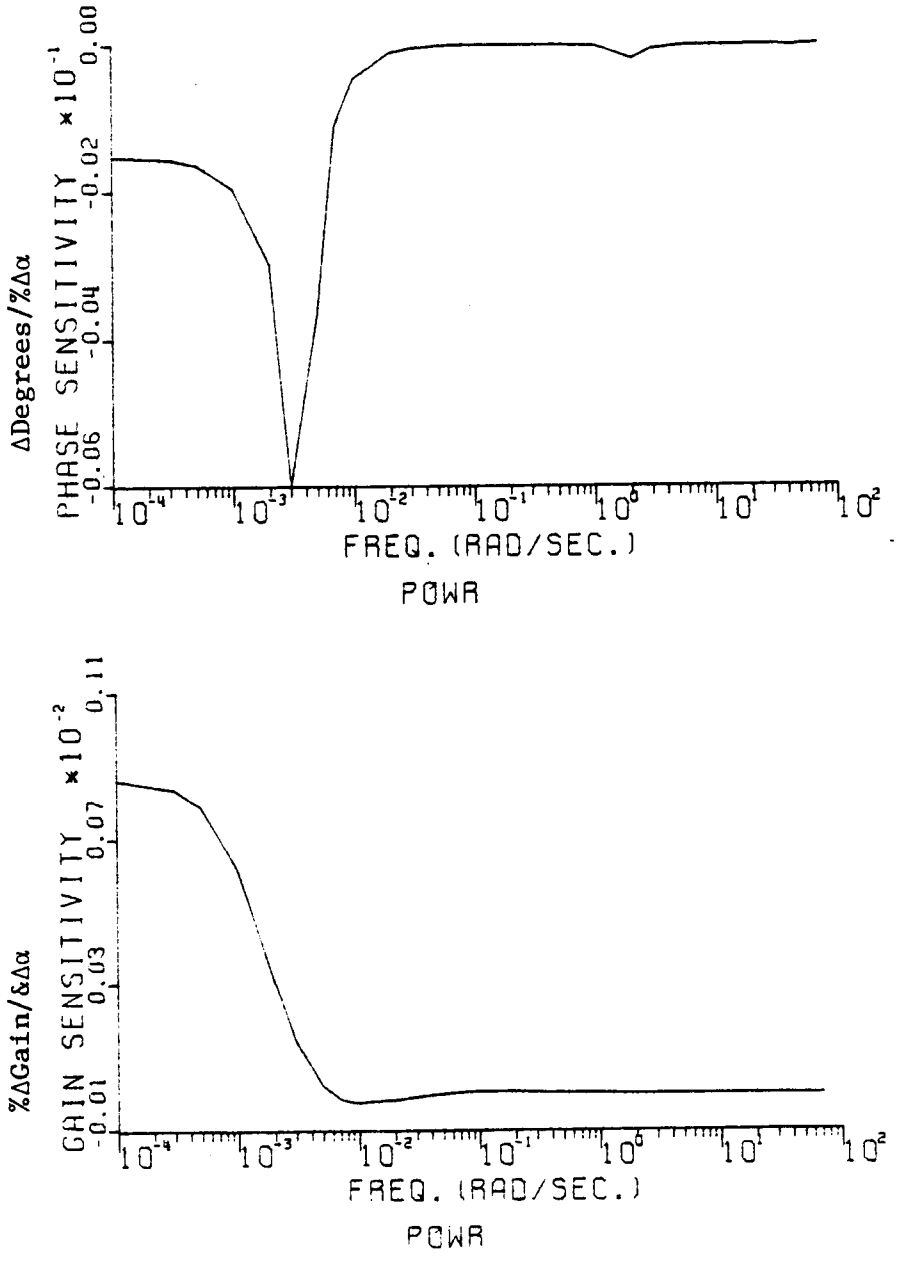


Figure D.3 Reactor Power Frequency Response Sensitivity To $\alpha_{\text{Lower Ref. Sodium}}$

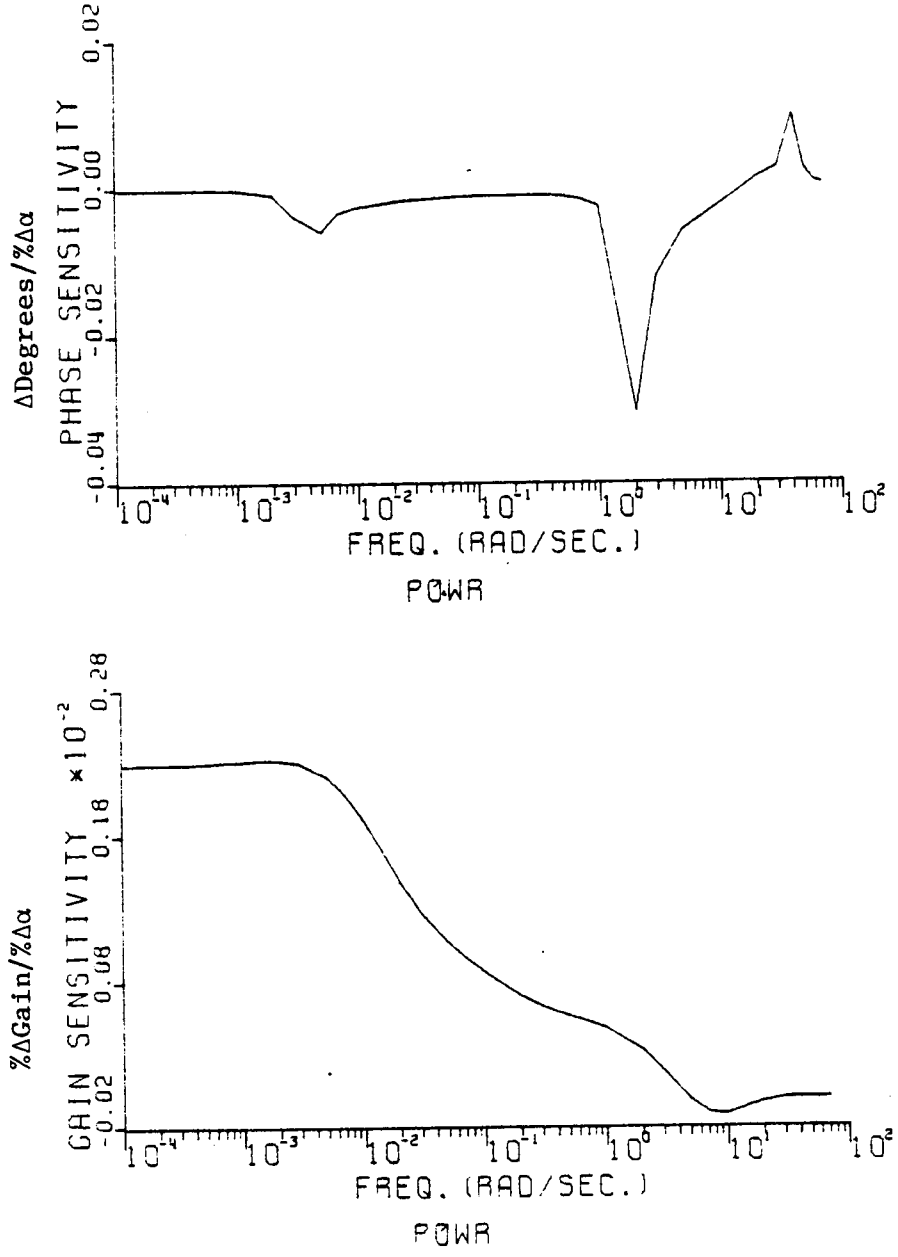


Figure D.4 Reactor Power Frequency Response Sensitivity To $\alpha_{\text{Upper Ref. Sodium.}}$

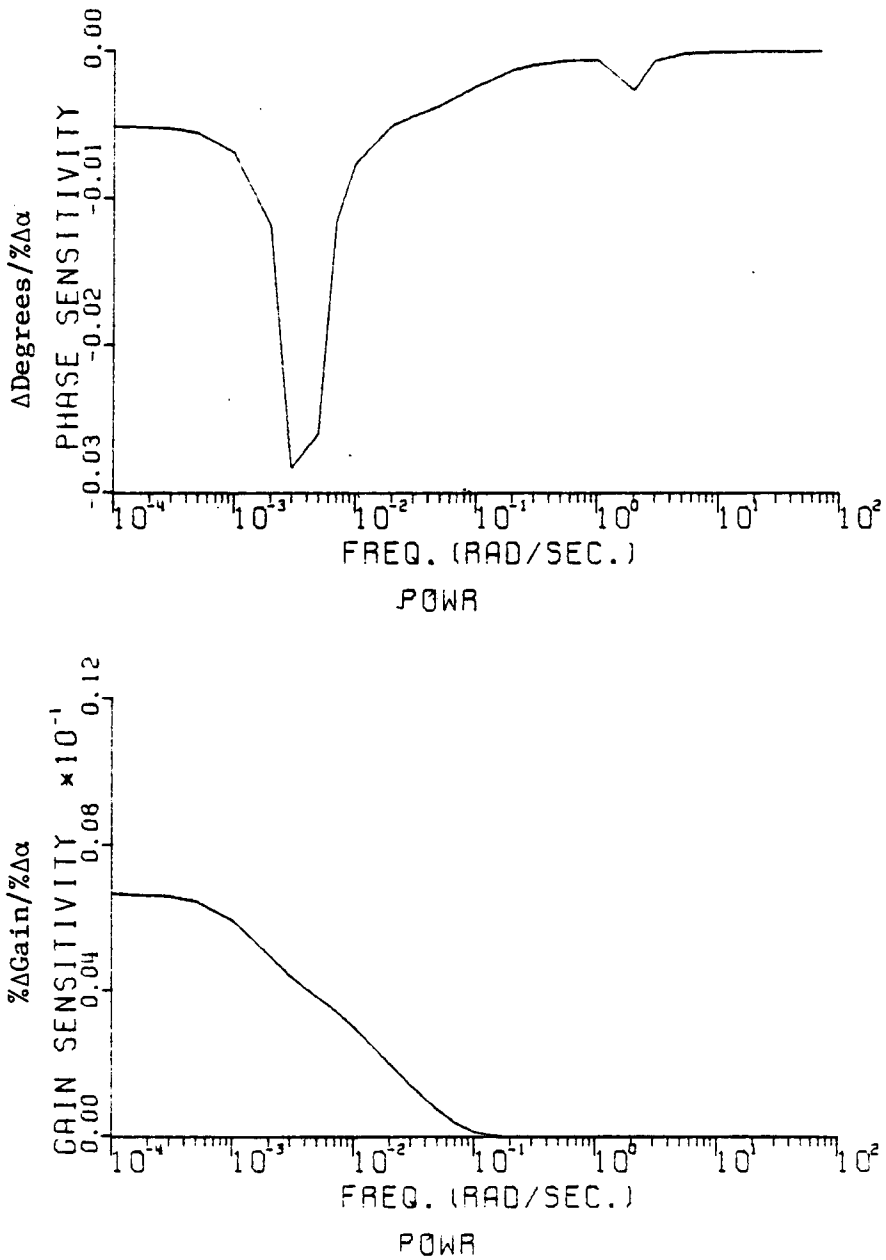


Figure D.5 Reactor Power Frequency Response Sensitivity To $\alpha_{\text{Inner Ref. Sodium}}$

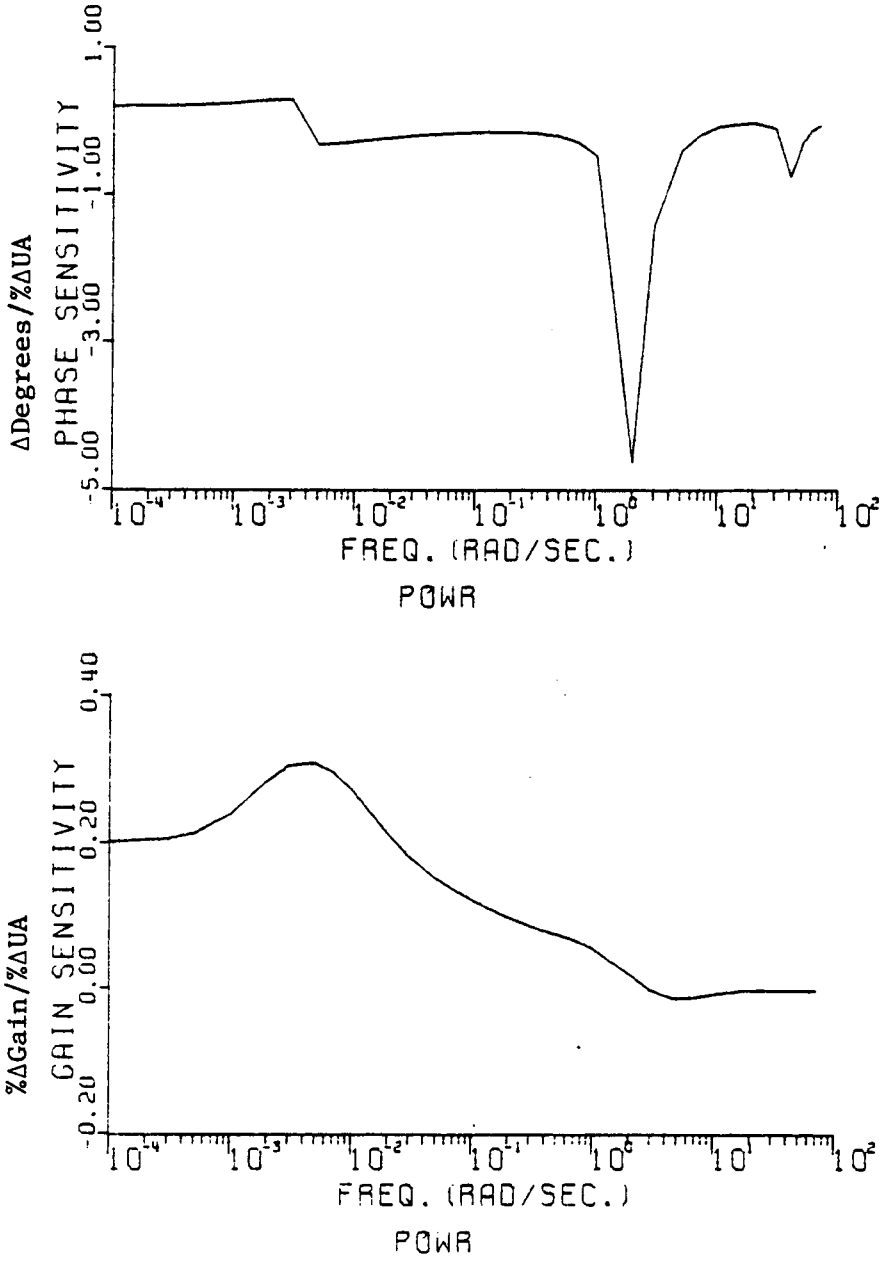


Figure D.6 Reactor Power Frequency Response Sensitivity to UA_{core}.

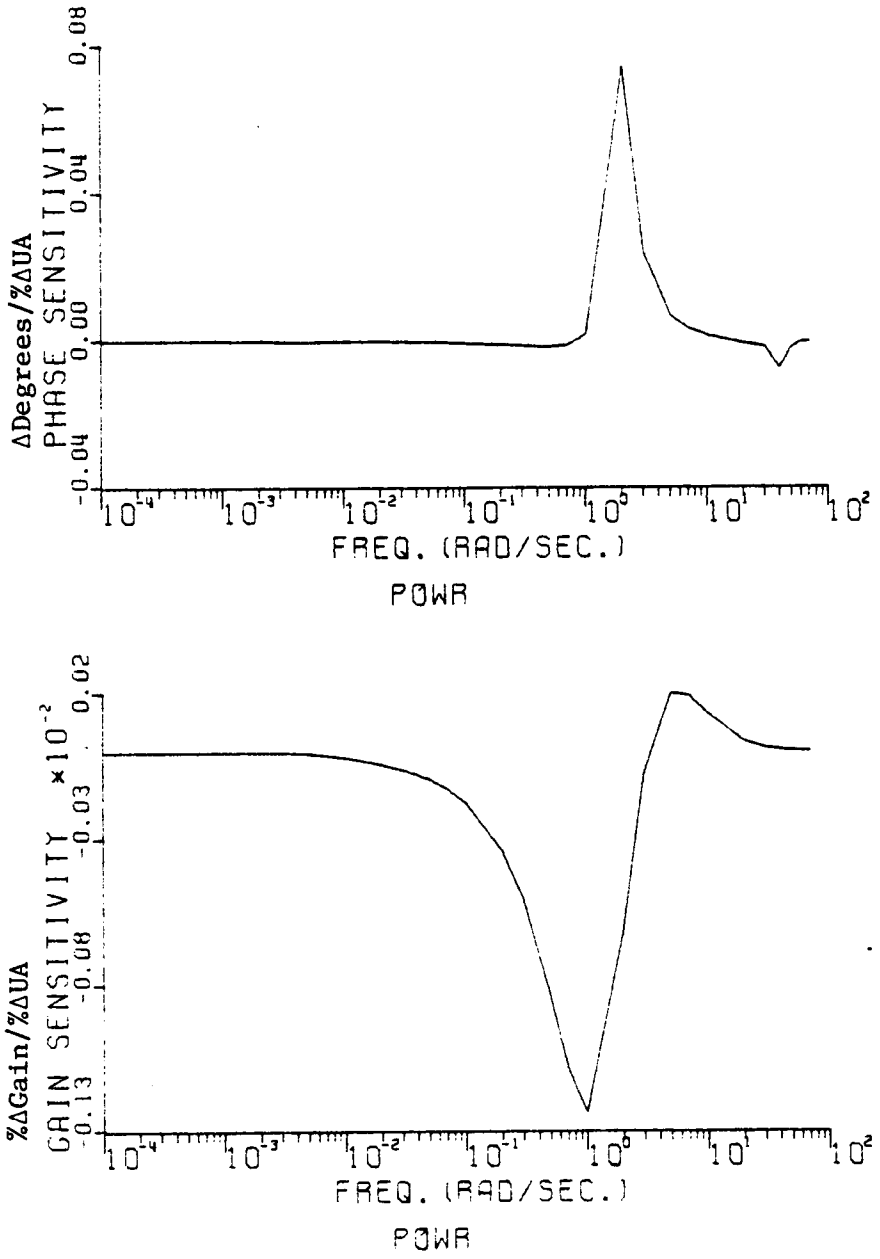


Figure D.7 Reactor Power Frequency Response Sensitivity to UA_{lower}.

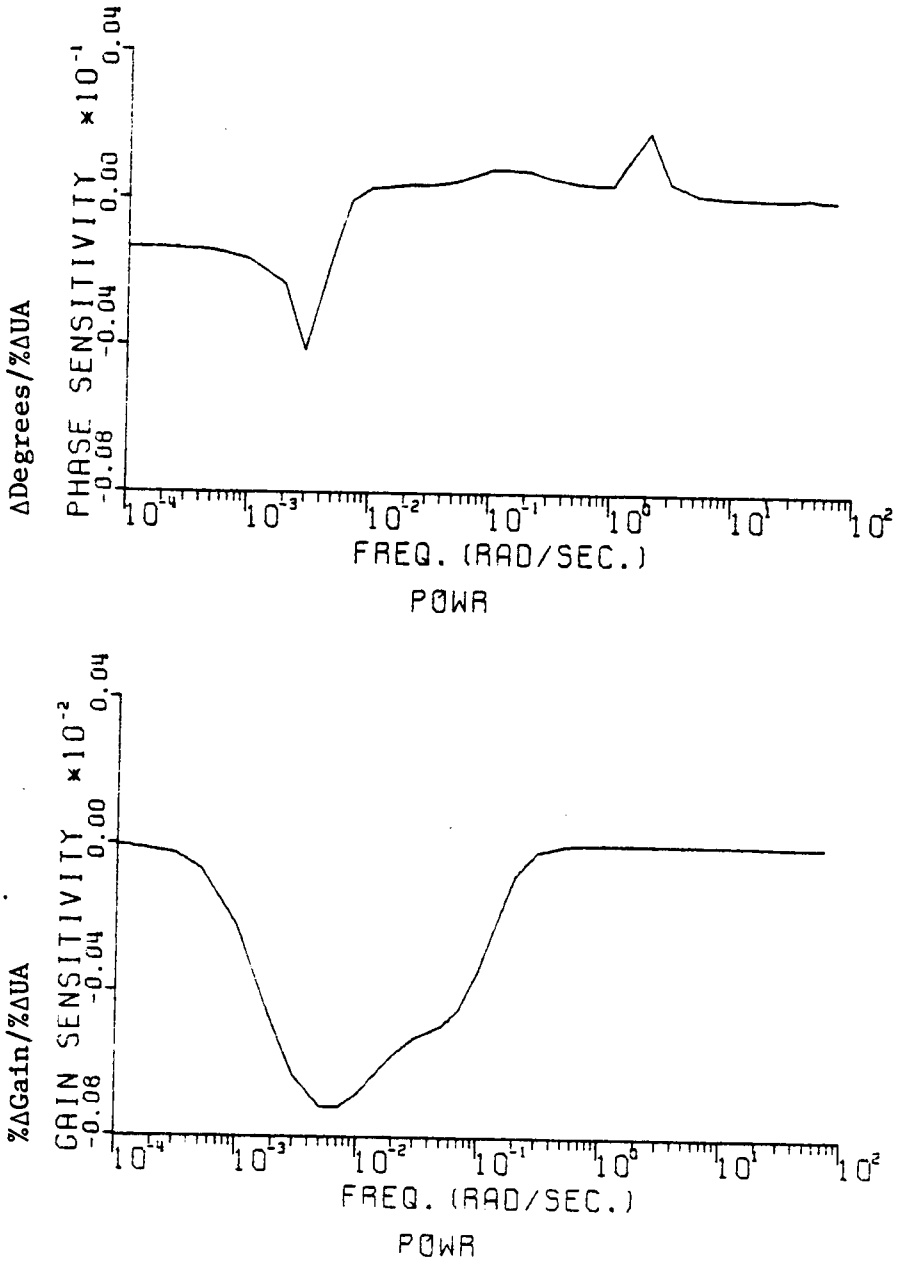


Figure D.8 Reactor Power Frequency Response Sensitivity To $UA_{inner\ reflector}$

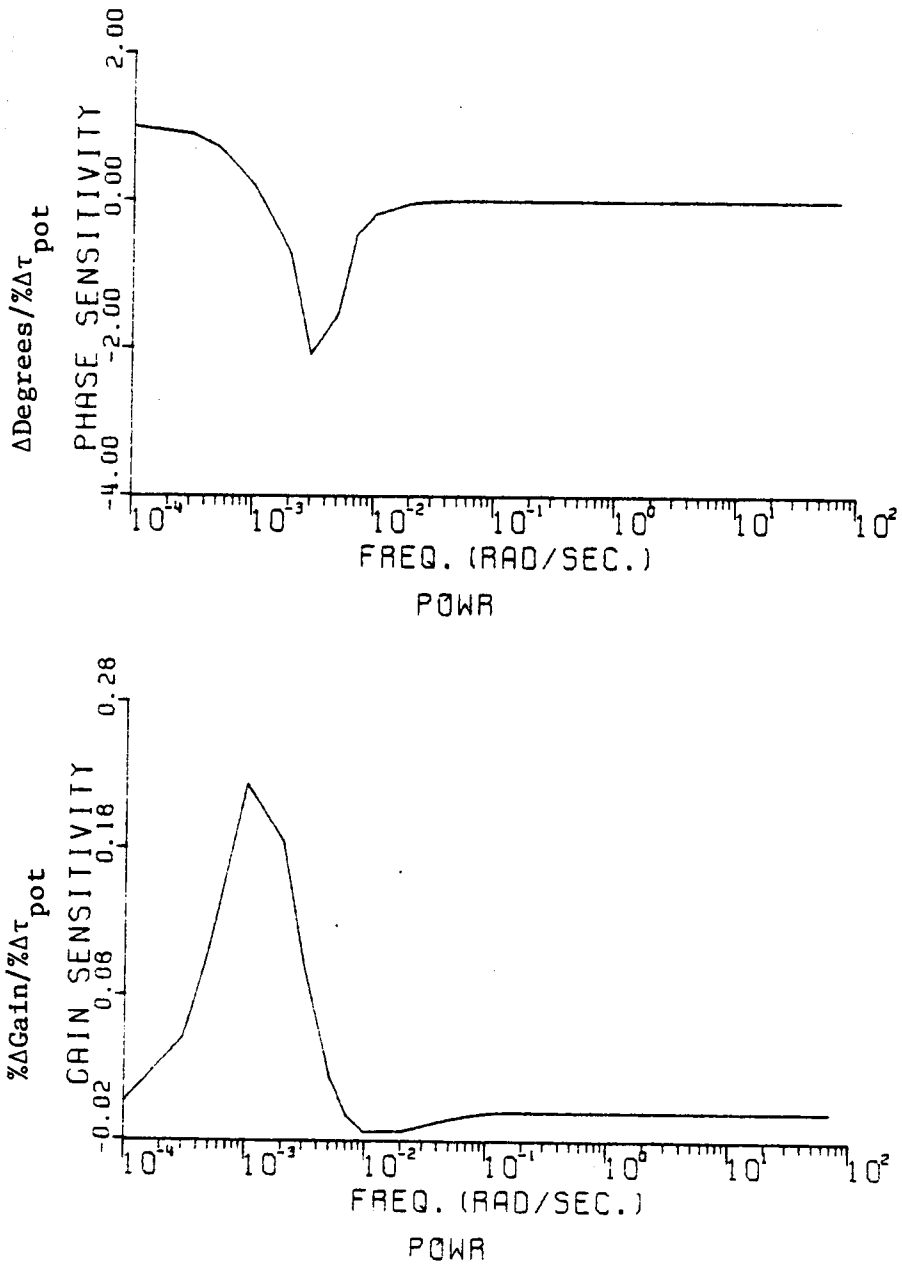


Figure D.9 Reactor Power Frequency Response Sensitivity To τ_{pot}.

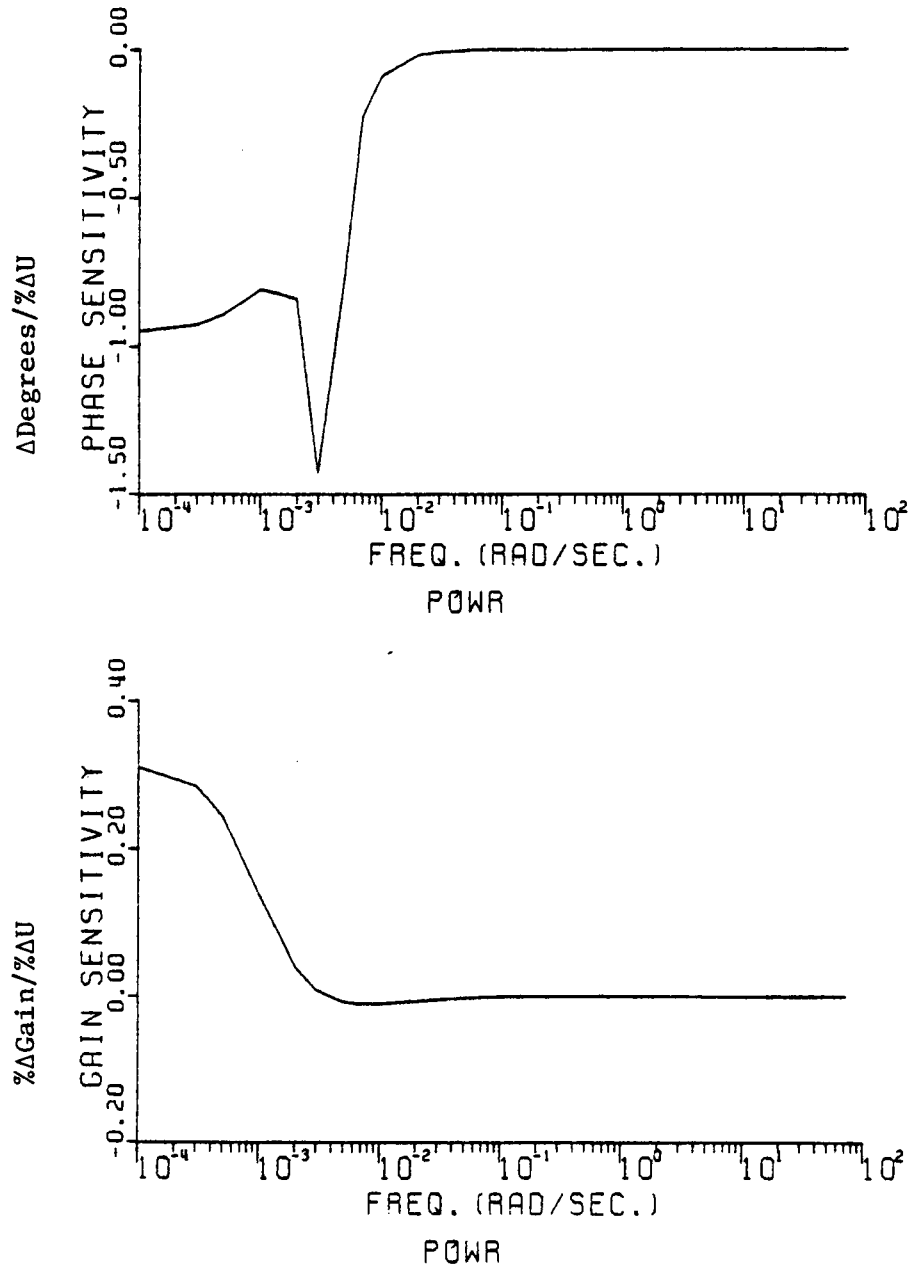


Figure D.10 Reactor Power Frequency Response Sensitivity To U_p.

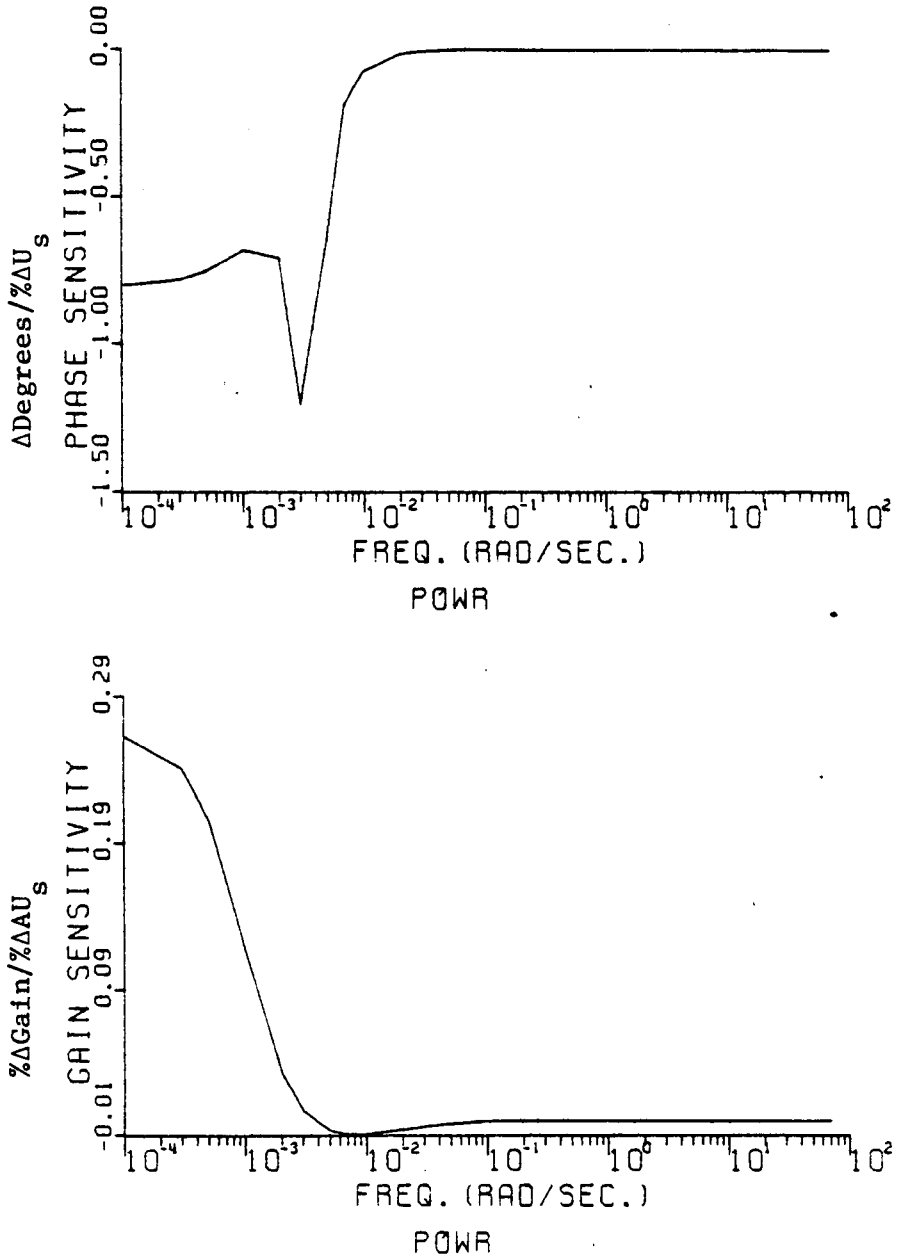


Figure D.11 Reactor Power Frequency Response Sensitivity To U_s.

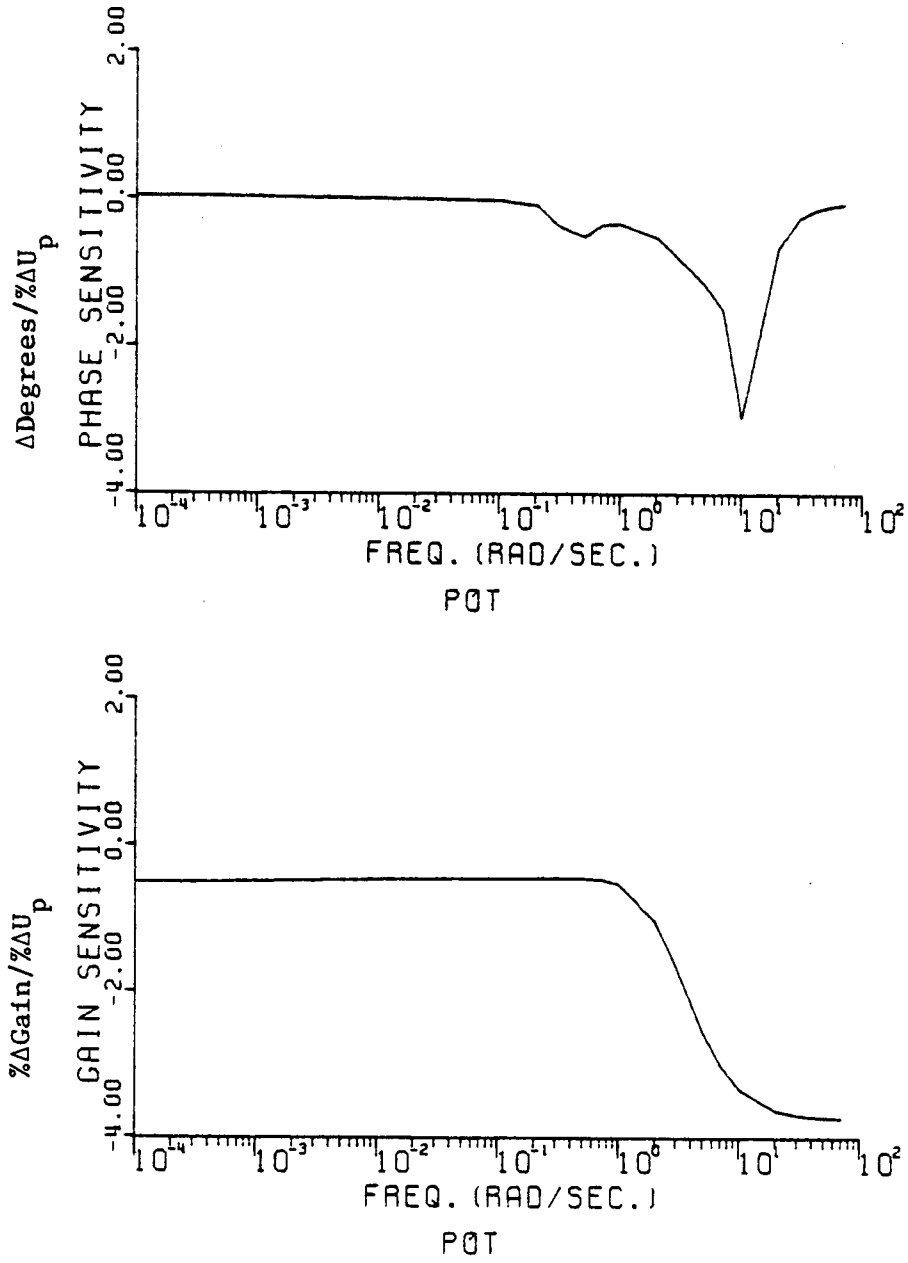


Figure D.12 Pot Sodium Temperature Frequency Response Sensitivity To U_p.

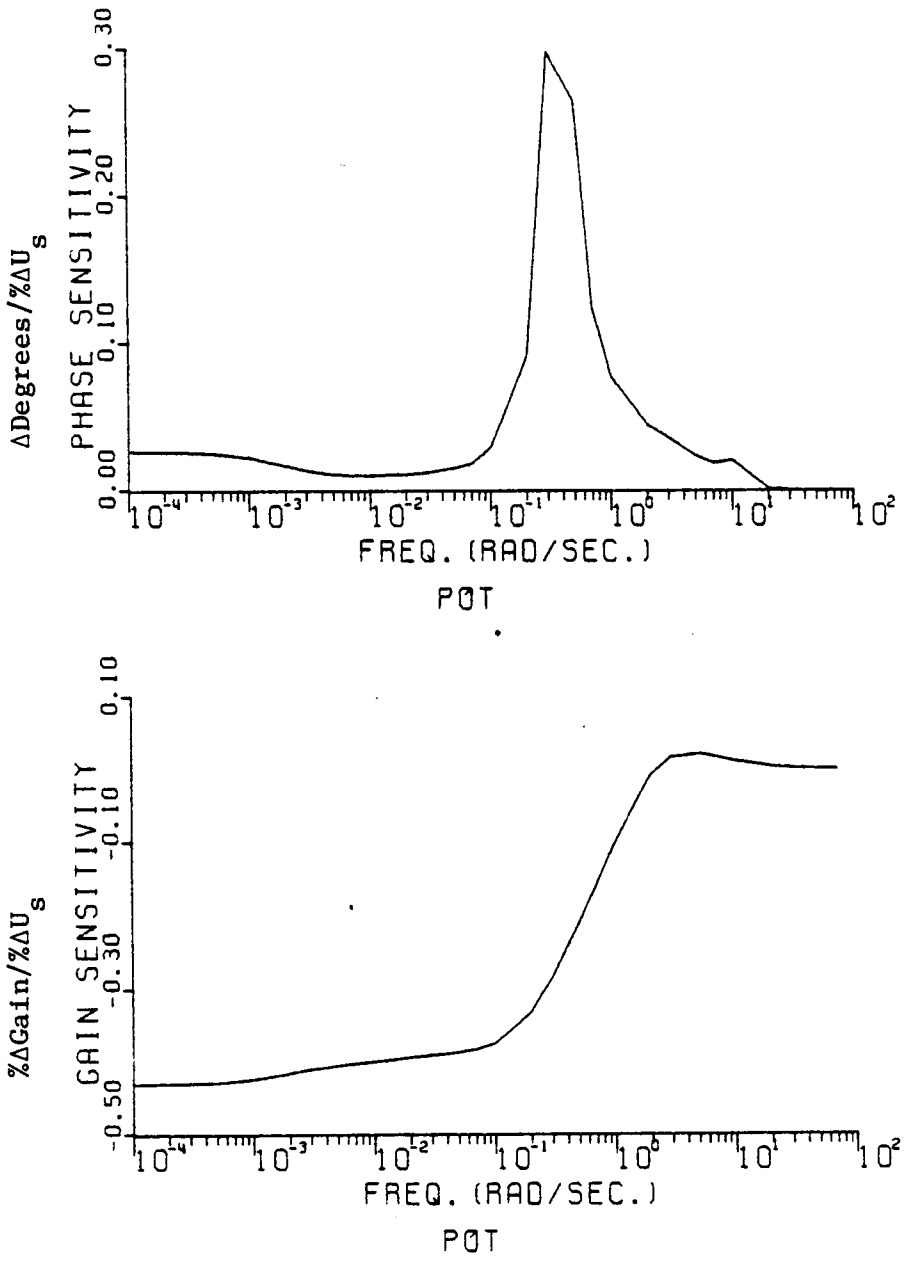


Figure D.13 Pot Sodium Temperature Frequency Response Sensitivity To U_s.

VITA

Sherrell Ray Greene was born in Jefferson City, Tennessee, on March 13, 1954. He attended Plainview Elementary School near Luttrell, Tennessee, and was graduated from Gibbs High School in June 1972. The following September he entered The University of Tennessee, and received a Bachelor of Science degree in Nuclear Engineering in June 1977. While an undergraduate, he participated in The University of Tennessee Co-op Engineering Program.

In the fall of 1977 he accepted a graduate research assistantship at The University of Tennessee and began to study toward a Master of Science degree in Nuclear Engineering. The degree was granted in March 1979.

The author is a member of the American Nuclear Society, the American Society of Heating, Refrigerating and Air-Conditioning Engineers and is a certified Engineer-In-Training in the state of Tennessee. Mr. Greene is currently employed with Oak Ridge National Laboratory.

He is married to the former Rebecca Harvey of Chattanooga, Tennessee.